Fall 12-21-2018

The Influence of Age, Gender, and Thiol Repletion in an In Vivo Model of Lewy Body Disorders

DANIEL MASON

THE INFLUENCE OF AGE, GENDER, AND THIOL REPLETION IN AN *IN VIVO* MODEL OF LEWY BODY DISORDERS

A Dissertation

Submitted to the Graduate School of Pharmacy

Duquesne University

In partial fulfillment of the requirements for

the degree of Doctor of Philosophy

By

Daniel M. Mason

December 2018

THE INFLUENCE OF AGE, GENDER, AND THIOL REPLETION IN AN *IN VIVO* MODEL OF LEWY BODY DISORDERS

By

Daniel M. Mason

Approved July 31, 2018

_____
Rehana K. Leak, Ph.D.
Associate Professor of Pharmacology
Graduate School Pharmaceutical Sciences
Duquesne University, Pittsburgh, PA

_____
John Stolz, Ph.D.
Director, Center for Environmental Research and Education
Professor, Environmental Microbiology
Department of Biological Sciences
Duquesne University, Pittsburgh, PA

_____
David A. Johnson, Ph.D
Associate Professor of
Pharmacology and Toxicology
Graduate School Pharmaceutical Science
Duquesne University, Pittsburgh, PA

_____
Dr. Wilson Meng Ph.D.
Associate Professor of Pharmaceutics
Graduate School Pharmaceutical Sciences
Duquesne University, Pittsburgh, PA

_____
Paula A. Witt-Enderby, Ph.D.
Professor of Pharmacology
Graduate School Pharmaceutical Sciences
Duquesne University, Pittsburgh, PA

_____
James K. Drennen, III, Ph.D.
Associate Dean and Associate Professor of Pharmaceutics
Graduate School of Pharmaceutical Sciences
Duquesne University, Pittsburgh, PA

_____
Jane E. Cavanaugh, Ph.D.
Associate Professor of Pharmacology
Graduate School Pharmaceutical Sciences
Duquesne University, Pittsburgh, PA

_____
J. Douglas Bricker, PhD, Dean
Duquesne School of Pharmacy and
Graduate School Pharmaceutical Sciences
Duquesne University, Pittsburgh, PA

ABSTRACT

THE INFLUENCE OF AGE, GENDER, AND THIOL REPLETION IN AN *IN VIVO* MODEL OF LEWY BODY DISORDERS

By

Daniel M. Mason

July 2018

Dissertation supervised by Dr. Rehana K. Leak

Lewy body disorders are a family of neurological brain disorders associated with olfactory, motor, and cognitive deficits and are collectively defined as α-synucleinopathies, as they are characterized by hallmark "Lewy bodies" composed of aggregated, fibrillar α-synuclein. It is not certain but often posited that fibrillar α-synuclein seeds the progressive, self-propagating spread of Lewy pathology through neuroanatomical circuitry. Furthermore, the site of disease induction is still debated. In Aim I, we developed a novel protocol for generating reproducible and robust α-synucleinopathy in the limbic temporal lobe of the mouse brain following infusions of preformed α-synuclein fibrils into the olfactory bulb, which is often the first brain region to display Lewy pathology in humans. Our tract-tracer studies revealed that all areas displaying dense Lewy-like pathology were indeed connected to the induction site. However, the specific pattern of α-synucleinopathy resembled that of Stage IIb of Beach's unified staging theory rather than

Parkinson's disease as it remained confined to the limbic system and did not enter motor brain regions. In Aim 2, we further observed that α-synucleinopathy remained confined to the limbic connectome regardless of gender, age, or incubation period. Any Lewy pathology that developed in the ventral mesencephalon was confined to the ventral tegmental area, which is associated with limbic rather than motor functions. Furthermore, our studies are the first to show that females are more resistant to the development of α-synucleinopathy and neurodegeneration than males, and that fibril infusions hasten mortality in aged mice. In Aim 3, N-acetyl cysteine protected primary neuron cultures against proteotoxicity, including that of α-synuclein fibrils, and the mechanism appeared to be partly dependent on the chaperone activity of heat shock protein 70. These findings were expanded to an *in vivo* study, in which mice were fed N-acetyl cysteine for 90 days after induction of olfactory α-synucleinopathy. Oral N-acetyl cysteine reduced Lewy-like pathology, but only in the anterior olfactory nucleus, the area of densest α-synucleinopathy in this model. In conclusion, we have developed a robust model of early-stage limbic-predominant Lewy body disorders that appears to mimic the higher risk of Lewy body disorders in men and the acceleration of mortality in these conditions.

DEDICATION

This dissertation is dedicated to my parents, Brian and Lisa Mason as well as my wife, Erin Mason, who have provided ceaseless encouragement, love, and support.

ACKNOWLEDGEMENT

I acknowledge and thank my advisor, Dr. Rehana Leak, for encouraging me to pursue my Ph.D. and for continuously supporting me throughout my time here at Duquesne University. I would also like to thank my committee members, Dr. Jane Cavanaugh, Dr. David Johnson, Dr. Paula Witt-Enderby, and Dr. John Stolz for their guidance and advice.

I would like to thank Dr. Virginia Lee and Dr. Kelvin Luk from the University of Pennsylvania for generating the synuclein fibrils used in my project. I also thank Dr. Peter Wipf and Dr. Jeffrey Brodsky from the University of Pittsburgh for their generosity in providing the Hsp70 inhibitors for my studies. I thank Dr. John Stolz for help with electron and confocal microscopy. I would also like to acknowledge the assistance of Denise Butler-Buccilli and Christine Close in maintaining the animal colonies.

I thank all of the graduate students, faculty, and administrative staff in the Graduate School of Pharmaceutical Sciences.

Finally, I thank my family and friends, especially my wife, Erin Mason, whose love and support made all of this possible.

TABLE OF CONTENTS

LIST OF FIGURES

Page

Introduction

The impact of Lewy body disorders

The term "Lewy body disorders" is used to encompass several related diseases characterized by the progressive accumulation of protein aggregates known as Lewy bodies and Lewy neurites. Parkinson's disease (PD) is the most common clinically diagnosed Lewy body disorder and affects 1-3% of people over 50 (Dehay et al., 2015) and 2-3% of the population over 65 year of age (Poewe et al., 2017). Within the United States, the financial burden of PD is estimated to be on average $22,800 (in 2010 dollars) per patient per year, and this number substantially increases with age (Kowal et al., 2013). Beyond the well characterized motor symptoms associated with PD, 75% of PD patients who survive for more than 10 years will develop Parkinson's disease dementia (PDD) (Aarsland & Kurz, 2010a), and this percentage increases to 83% if they survive for more than 20 years (Aarsland et al., 2001; Hely et al., 2008). Dementia with Lewy bodies (DLB) is another common Lewy body disorder and represents approximately 15% of dementia cases (Rahkonen et al., 2003; Stevens et al., 2002). DLB is diagnosed when dementia symptoms appear before or within a year of motor symptoms (McKeith et al., 2005). Individuals with PD, PDD, and DLB all have an increased risk of dying younger than the general population (Savica et al., 2017).

Asymptomatic and cognitively normal people may also present with Lewy pathology upon postmortem examination, suggesting that incidental Lewy body disease (ILBD) represents the earliest stages of Lewy body disorders (Beach, Adler, et al., 2009). Approximately 10-30% of cognitively normal elderly people present with Lewy bodies at autopsy, which is a greater

prevalence than those diagnosed with PD (Beach, Adler, et al., 2009; de Rijk et al., 1997), suggesting that ILBD is the most common Lewy Body disorder. The prevalence of Lewy bodies in the brains of otherwise healthy elderly people increases from 3.8% in the 6th decade to 12.8% in the 9th decade of life (de Rijk et al., 1997), suggesting that Lewy body disorders will become more frequent as humans live longer. Current therapies only manage the symptoms of Lewy body disorders, and there is no treatment available to decrease the accumulation of Lewy aggregates in the central nervous system, as this process is still not well understood.

α-synucleinopathies

Alpha-synuclein is a small 140 amino acid protein that is located primarily at presynaptic terminals (Iwai et al., 1995), but can also be found in the nucleus, mitochondria, and endoplasmic reticulum (Maroteaux et al., 1988). It has been detected extracellularly in cerebrospinal fluid and plasma, suggesting that α-synuclein is not exclusively an intracellular protein (Mollenhauer et al., 2008; Tokuda et al., 2006). While the role of α-synuclein is still not known, it is likely involved in synaptic vesicle dynamics, intracellular trafficking, and mitochondrial homeostasis (Vekrellis et al., 2011; Wales et al., 2013). In aqueous solutions, α-synuclein is an unfolded monomer that does not adopt a distinct and well-defined structure (Stefanis, 2012). When associated with lipid micelles, α-synuclein can adopt an alpha-helical conformation (Burre et al., 2014; Dev et al., 2003) that may coalesce into tetramers, which could be the more prevalent form within neurons (Bartels et al., 2011; Dettmer et al., 2013). Regardless of the exact conformation, the form of α-synuclein associated with vesicles is more prone to aggregation than the cytosolic form (Galvagnion et al., 2015).

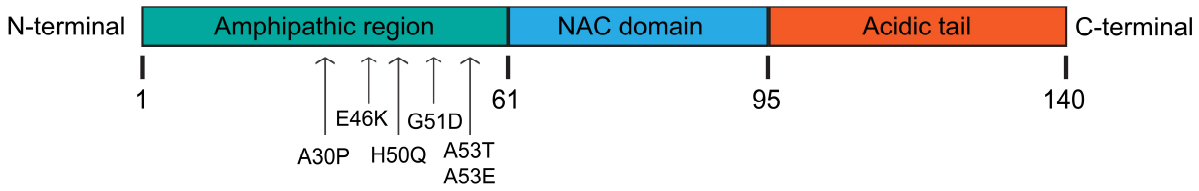

Figure 1. The structural domains of α-synuclein. The protein sequence of α-synuclein can be divided into three structurally unique domains: the N-terminus amphipathic region, the non-amyloid-β component (NAC) domain, and the c-terminus acidic tail. The six missense mutations known to cause familial PD are in the N-terminus amphipathic region.

Alpha-synuclein has three distinct structural domains; the N-terminus (amino acids 1-60), the hydrophobic non-amyloid component (amino acids 61-95), and the C-terminus (amino acids 96-140) (Stefanis, 2012). The N-terminus region is responsible for binding membranes and is predicted to adopt an α-helical structure upon binding (**Figure 1**). This portion of α-synuclein can be glycated, which reduces membrane binding and promotes the accumulation of α-synuclein oligomers (Vicente Miranda et al., 2017). The central region is the amyloidogenic component (Rodriguez et al., 2015). It is highly hydrophobic and when exposed, will readily bind to other hydrophobic domains (Ueda et al., 1993). The C-terminus domain is negatively charged and able to bind calcium, which helps localize α-synuclein to the synapse (Lautenschlager et al., 2018). Misfolding of α-synuclein exposes the hydrophobic core and encourages the formation of β-sheets that are prone to interact with other proteins and form detergent insoluble protein aggregates (Saxena & Caroni, 2011).

As it relates to Lewy body disorders, α-synuclein is the primary component of Lewy bodies and Lewy neurites (Baba et al., 1998; Duda et al., 2000; Spillantini et al., 1997), but cortical Lewy aggregates can contain approximately 300 different proteins (Leverenz et al., 2007). Other proteins found in Lewy bodies include vimentin, γ-tubulin, synphilin-1, proteasome subunits, as well as chaperone proteins (Junn et al., 2002). Most but not all Lewy aggregates also contain ubiquitin (Kuzuhara et al., 1988; Spillantini et al., 1998), a modification that directs proteins to the cell's degradation machinery. Lewy bodies are found within neuronal perikarya and Lewy neurites are found within dendrites and axons (Pollanen et al., 1993). For these insoluble inclusions to form, the native α-synuclein monomers must aggregate into oligomers, which range in size from 4 to 24 nm (S.W. Chen et al., 2015), then transient protofibrils (Lashuel et al., 2002), and eventually

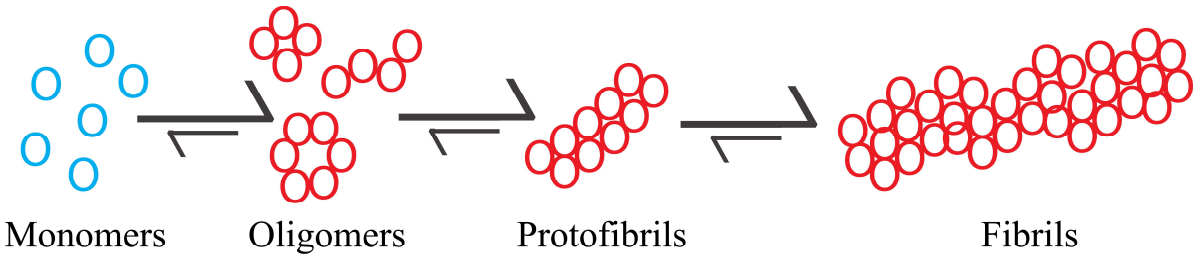

Figure 2. Pathway for insoluble α-synuclein fibril formation. Toxic forms of α-synuclein (red) are formed as α-synuclein monomers (blue) aggregate into oligomers, protofibrils, and finally insoluble fibrils.

coalesce into large insoluble protein aggregates with a dense amyloid core (Gallea & Celej, 2014)(**Figure 2**). Large somatic inclusions appear to undergo different stages of maturation ultimately forming a dense and compact phenotype coinciding with a reduction of soluble α-synuclein (Osterberg et al., 2015). It has also been posited that there may be different forms or strains of aggregated α-synuclein that may have unique characteristics including potentially different seeding and aggregation properties (Bousset et al., 2013; Peelaerts et al., 2015; Pieri et al., 2016; Yonetani et al., 2009). Similarly, different forms of α-synuclein oligomers have been detected in the brains of patients with Lewy pathology (Ingelsson, 2016). Oligomers are

heterogeneous in structure and may from spheres, chains, or annular structures (Cremades et al., 2017).

It is still not resolved whether Lewy bodies and Lewy neurites are toxic themselves, but it has been shown that α-synuclein oligomers can cause toxicity by disrupting synaptic membrane dynamics and seeding the misfolding and aggregation of endogenous α-synuclein (Danzer et al., 2007; Danzer et al., 2009; Winner et al., 2011). In neuroblastoma cells, oligomer-induced membrane disruption resulted in nanopore formation that altered neuronal ion homeostasis and activated the nitric oxide synthase machinery leading to S-nitrosylation of many cytoplasmic proteins including Hsp70 and Parkin (Kumar et al., 2018). The oligomers are particularly likely to disrupt lipid bilayer integrity as they are comprised of a highly lipophilic region that readily attaches to membranes as well as a rigid structural component that can insert into and disrupt the lipid bilayer (Fusco et al., 2017). Oligomers can also interact with metal ions and increase the generation of hydrogen peroxide and superoxide (Deas et al., 2016). It has also been reported that α-synuclein oligomers impair both the ubiquitin proteasome system and autophagy-lysosomal pathway (Xilouri et al., 2013). For these reasons, oligomers are suggested to be the most toxic species of α-synuclein (el-Agnaf et al., 1997; El-Agnaf et al., 2003; Goldberg & Lansbury, 2000). Indeed, soluble α-synuclein oligomers are elevated in brain homogenates of patients with DLB and PD compared to healthy controls (Paleologou et al., 2009; Sharon et al., 2003).

Patterns of neurodegeneration

The symptoms of Lewy body disorders can be divided into three categories: physical symptoms, cognitive impairment, and psychiatric/behavioral issues (Donaghy & McKeith, 2014). The physical symptoms can be further subdivided into motor and nonmotor symptoms. The prototypical motor symptoms associated with PD include rigidity, bradykinesia, resting tremor, and postural instability, which are attributable to the loss of dopaminergic neurons within the substantia nigra (SN) pars compacta and subsequent decrease of dopamine (DA) levels within the striatum (Alexander, 2004; Jankovic, 2008). According to one stereological assessment, PD patients have 82% nigra neuron loss, and ILBD patients have 40% loss compared to controls (Iacono et al., 2015). Neuron loss in the SN has also been observed in DLB (Seidel et al., 2015).

Dopaminergic neurons may be particularly vulnerable to Lewy pathology for several reasons. DA neurons are autonomous oscillators, neurons that rhythmically generate action potentials even in the absence of external post-synaptic depolarization (Grace & Bunney, 1983). Nigral DA neurons also have long, unmyelinated axons with approximately 1-2.4 million synapses each (Bolam & Pissadaki, 2012; Pissadaki & Bolam, 2013). This high level of neuronal activity requires increased levels of mitochondrial activity, and mitochondria generate reactive oxygen species (ROS) like superoxide as a by-product of metabolism. Nigral DA neurons also lack myelination, a fatty axon sheath that decreases the energy requirements of signal transmission. With constant stimulation and relatively inefficient transmission, DA neurons rely heavily on detoxification of ROS. A loss of homeostatic balance in these mechanisms can rapidly cause oxidative stress leading to apoptosis.

DOPAL (3,4-dihydroxyphenylacetaldehyde) is a toxic intermediary formed through dopamine metabolism (Kristal et al., 2001). As Lewy aggregates can interfere with vesicular dynamics and impair synaptic function (Volpicelli-Daley et al., 2011), DA can accumulate which leads to the generation of more DOPAL (Goldstein et al., 2012) within the cell. This can function as a negative feedback loop as DOPAL can induce the oligomerization of α-synuclein (Burke et al., 2003; Werner-Allen et al., 2017). Alpha-synuclein may also be involved with regulating dopamine biosynthesis as it shares sequence homology with the chaperone molecule 14-3-3, which is reported to activate tyrosine hydroxylase, the rate-limiting enzyme in the DA synthesis pathway (Perez et al., 2002)

Neuron loss in the SN is particularly damaging because loss of these neurons reduces DA within the striatum. The striatum is a hub that regulates goal-oriented actions, and loss of DA reduces the ability of this region to respond to cortical and thalamic signals (Zhai et al., 2018). DA is an inhibitory neurotransmitter and without it, the cortostriatal glutamatergic excitatory input from the indirect pathway is no longer inhibited (Braak & Del Tredici, 2008), leading to loss of control of motor functions. Glutamate excitotoxicity is also particularly toxic to dopaminergic neurons (Sawada et al., 1996), which may further increase the vulnerability of the striatum. PD patients are typically prescribed L-DOPA, a DA precursor that can increase DA levels within the brain and reduce some of the symptoms associated with the striatal DA deficit. L-DOPA is not stored or buffered well within the brain, and as more DA terminals are lost over the course of the disease, the stimulation of DA receptors becomes increasingly inconsistent (Vijayakumar & Jankovic, 2016a, 2016b).

The nonmotor symptoms of Parkinson's disease can be manifested long before the motor symptoms begin and may represent a prodromal stage. By the time the telltale motor symptoms emerge, as many as 50-70% of dopaminergic neurons in the SN are already lost (Damier et al., 1999; Kordower et al., 2013; Marsden, 1990), and, therefore, diagnosing PD early is crucial to maintaining a patient's quality of life. This prodromal phase is estimated to be 20 years for patients who present with PD in the sixth decade of life (Hawkes et al., 2010). Nonmotor symptoms include olfactory impairments, rapid eye movement sleep behavior disorder (RBD), gastrointestinal dysfunction, dysphagia, and orthostatic hypotension (Adler & Beach, 2016; Postuma et al., 2012; Siderowf et al., 2012). Olfactory impairment is a well-established premotor symptom of Parkinson's disease (Doty et al., 1988; Hawkes et al., 1997). The presence of Lewy aggregates in the olfactory bulb (OB) is correlated with olfactory dysfunction in PD (Driver-Dunckley et al., 2014; Wilson et al., 2011), and olfactory dysfunction is associated with ILBD (Ross et al., 2006).

Gastrointestinal symptoms in PD include dysphagia, gastroparesis, prolonged GI transit time, and constipation (Natale et al., 2008). One study of 245 autopsied men found that those with less than one bowel movement per day were 4.3-fold more likely to have ILBD compared to those with more than one bowel movement per day (Abbott et al., 2007), but the SN and locus coeruleus were the only brain regions analyzed. Other studies have found that only 25% of ILBD subjects have Lewy aggregates in the colon (Annerino et al., 2012), and that constipation may be more associated with Lewy pathology in the spinal cord than the G.I. tract (Beach et al., 2010; Tamura et al., 2012; VanderHorst et al., 2015). Loss of neurons in the dorsal motor nucleus of the vagus nerve, which occurs early in PD, could also be the cause of constipation (Del Tredici et al., 2002).

Immunoreactive α-synuclein aggregations have also been reported in neurons of the submucosal tissue of the intestines and stomach (Braak, de Vos, et al., 2006).

Rapid eye movement sleep behavior disorder is a common prodromal symptom of Lewy body disorders and is characterized by the loss of paralysis that normally occurs during sleep. Degeneration of the locus coeruleus could result in less noradrenergic (excitatory) signaling to the magnocellular reticular formation, which is involved with inhibitory signaling to spinal motor neurons during sleep (Boeve, 2010). One study found that 79% of autopsied cases with RBD had pathologically defined DLB or PD (Boeve et al., 2013). This symptom is reported in up to 65% of PD patients (Adler et al., 2011; Boeve et al., 2001; Postuma et al., 2006; Schenck et al., 1996). RBD also increases the likelihood of developing PD, and patients with RBD often present with additional nonmotor symptoms of PD such as olfactory dysfunction (Postuma et al., 2006). Patients with both RBD and olfactory dysfunction may also progress to clinically diagnosed Lewy body disorders at a faster rate (Mahlknecht et al., 2015; Postuma, Gagnon, et al., 2015; Postuma, Iranzo, et al., 2015). Cases of concurrent PD and RBD were also found to have increased α-synuclein deposition in 9 out of 10 brain regions analyzed (Postuma, Adler, et al., 2015).

Dysphagia and orthostatic hypotension are less common nonmotor early symptoms and their pathological underpinnings are not as well understood. It has been reported that there is a higher density of Lewy aggregates in the pharyngeal nerves in PD cases, which may be responsible for dysphagia (Mu et al., 2013). Orthostatic hypotension can occur early in PD but is more often present in advanced stages of the disease and may be related to Lewy aggregates in cardiac tissue or the sympathetic ganglia (Beach et al., 2010; Fumimura et al., 2007; Gelpi et al., 2014).

The most common cognitive and behavioral/psychiatric symptoms are cognitive impairment, anxiety, and depression. Cognitive impairment is indeed a premotor symptom of PD, as approximately 15% of PD patients present with mild cognitive impairments before the onset of motor symptoms (Aarsland, 2016). Cognitive impairment differs from dementia, as the latter is diagnosed when cognitive impairments are so severe that one can no longer function independently and perform activities of daily living. When dementia symptoms emerge within a year prior to or simultaneously with parkinsonism, patients are diagnosed with DLB (McKeith et al., 2005). When the motor symptoms of PD are well established before dementia symptoms emerge, patients are diagnosed with PDD (Goetz et al., 2008; McKeith et al., 2005). PD patients have a much greater risk of developing dementia than healthy elderly controls (Aarsland et al., 2017), and 75-90% of PD patients will eventually develop dementia (Aarsland et al., 2003; Aarsland & Kurz, 2010a; Gratwicke et al., 2015).

While there are some conflicting reports, most studies agree that the primary cause of cognitive decline in Lewy body disorders is limbic and cortical Lewy pathology (Aarsland, 2016; Aarsland et al., 2017; Kalaitzakis & Pearce, 2009). Neocortical Lewy bodies are associated with cognitive impairment (Aarsland et al., 2005) and dementia (Hurtig et al., 2000). Some have found that cortical Lewy bodies do not always predict dementia (Colosimo et al., 2003), but one study reported a 10-fold increase in neocortical and limbic Lewy aggregates in the brains of PDD patients compared to PD patients without dementia (Apaydin et al., 2002) suggesting the density of Lewy pathology in these regions is key to cognitive impairment. Atrophy of the hippocampus has also been associated with cognitive decline (Nagano-Saito et al., 2005), and DLB patients with

hippocampal atrophy are at greater risk of mortality (Graff-Radford et al., 2016; Lemstra et al., 2017).

The link between Lewy pathology and the symptoms of anxiety and depression is less well understood. Anxiety may be linked to pathology in the amygdala, which often presents with the most Lewy aggregates of any brain region (Beach, Adler, et al., 2009). The amygdala is also known to atrophy significantly in both DLB and PD (Cordato et al., 2000). Pathology is the coeruleus-subcoeruleus complex may be responsible for symptoms of depression. This region has strong serotonergic inputs from the caudal raphe nuclei and a reduction in norepinephrine activity at the synapse in this region has been linked to depression (Klimek et al., 1997). PD patients can also experience significant neuron loss in this area (Kalaitzakis & Pearce, 2009).

PD and DLB staging

It is important to understand the progression of PD because there is never a case where Lewy pathology is only present in the SN (Adler & Beach, 2016), suggesting that this area is not where Lewy aggregates first develop. In 2003, Heiko Braak and colleagues proposed a six-stage pattern of Lewy body development in Parkinson's disease (Braak et al., 2003) that was based on autopsies of 168 brains (69 incidental cases, 41 clinically diagnosed PD patients, and 58 age and gender matched controls) (Braak, Bohl, et al., 2006). The first three stages are the presymptomatic stages, in which Lewy aggregates appear within the brain but do not cause overt motor symptoms. In the first stage, Lewy aggregates are found in the OB, anterior olfactory nucleus (AON), dorsal IX/X motor nucleus, and enteric nervous system (Braak et al., 2003; Hawkes et al., 2010). In Stage 2, aggregates are found in the magnocellular portions of the reticular formation, the caudal raphe

nuclei, and the coeruleus-subcoerulus complex. In Stage 3, the midbrain begins to develop Lewy aggregates. At this stage, degeneration in the SN pars compacta begins. In Stage 4, the Lewy aggregates can be identified in the cortex, but it is typically constrained to the temporal mesocortex and allocortex. The accessory cortical and basolateral nuclei of the amygdala and interstitial nucleus of the stria terminalis are also affected at this stage (Hawkes et al., 2010). In Braak Stages 3 and 4, Lewy pathology appears in the entorhinal cortex and hippocampus, which may lead to cognitive decline. In Stage 5, the pathology progresses to higher order sensory association areas of the neocortex and prefrontal cortex. Stage 6, the final stage, is reached when the entire neocortex succumbs to Lewy pathology. Stages 5 and 6 typically have extensive cortical damage.

One of the limitations of Braak's work is that he did not analyze the brain tissue of patients diagnosed with DLB or investigate pathology in the spinal cord or peripheral nervous system, where α-synuclein pathology also presents in Lewy body disorders (Gelpi et al., 2014). After autopsying 417 brains of patients with PD, DLB, ILBD, and Alzheimer's disease with Lewy Bodies (ADLB), Beach and colleagues found that 42% with Lewy pathology could not be classified by the Braak staging system, and 50% could not be classified by the DLB consortium system (Beach, Adler, et al., 2009). According to both staging systems, approximately one-third of the unclassifiable patients had pathology only in the OB, and two-thirds had pathology in the limbic system in the absence of pathology in the brainstem (Beach, Adler, et al., 2009). Beach and colleagues also found that there was not a single case of pathology in the periphery when it was absent from the central nervous system (CNS), suggesting the enteric nervous system is not the site of induction (Adler & Beach, 2016). Indeed, others have found that the dorsal motor nucleus

of the vagus nerve, a connection to the enteric nervous system, does not always present with Lewy pathology when pathology is present within the SN (Kalaitzakis et al., 2008).

Given these caveats of prior staging systems, Beach and colleagues proposed a new staging system that could include all cases of Lewy pathology they observed. In this system, Stage I is when the OB alone develops Lewy pathology, but as the OB is occasionally unaffected, it may be skipped and subjects can be classified to higher stages. From the OB, Stage II is divided into 2 substages as pathology may progress through two different pathways. Stage IIa has brainstem-predominant Lewy pathology and Stage IIb has limbic-predominant Lewy pathology. In Stage III, both the brainstem and limbic system are affected, and in Stage IV, the pathology emerges in the neocortex. Most ILBD subjects are classified as Stage IIa and most ADLB subjects are Stage I or Stage IIb. Most PD and DLB patients are Stage III or IV. This staging system is based on probability of where pathology develops and not deterministic factors. There were not any cases of DLB or PD where only a single brain region was affected, but in ADLB and ILBD cases, some had only a single brain region affected, and it was most often the OB (Beach, Adler, et al., 2009). There are several limitations in attempting identify and stage pathology including differences between researchers in tissue processing, immunohistochemical methods, tissue sample collection, and inter-observer assessment of the pathology (Alafuzoff et al., 2008; Croisier et al., 2006; Muller et al., 2005).

Alzheimer's disease and Lewy body disorders are not mutually exclusive. Patients often present with the hallmark inclusions of both pathologies and some have observed that the occurrence of neocortical Lewy pathology often coincides with β-amyloid deposits and neurofibrillary tangles

(Apaydin et al., 2002). Indeed, diffuse β-amyloid plaques have been observed in PDD and DLB patients (Aarsland, 2016), and Lewy pathology has been frequently observed in Alzheimer's patients, most often confined to the limbic system (Beach, Adler, et al., 2009; Toledo et al., 2016). The reasons for these overlaps are unclear, but it has been observed that phosphorylated α-synuclein can promote the phosphorylation of tau and disrupt its normal functioning (Guo et al., 2013). Mice over expressing both α-synuclein and β-amyloid have been reported to exhibit more robust Lewy-like pathology than mice overexpressing α-synuclein alone (Irwin et al., 2013), suggesting that there may be cumulative effects.

Transmission of α-synucleinopathy

The first evidence of Lewy pathology transmission in humans was observed after embryonic mesencephalic neurons were transplanted into the striatum of patients with PD. Years later, the transplanted neurons exhibited Lewy bodies, which indicated a host-to-graft transmission of pathology (Kordower et al., 2008; Li et al., 2008). A host-to-graft transmission of α-synuclein from host cells to grafted dopaminergic neurons was then confirmed in an *in vivo* mouse model (Hansen et al., 2011). Since then, much has been learned about the cell-to-cell spread of misfolded α-synuclein. In animal models, transmission of pathology has been observed after injections of recombinant α-synuclein fibrils (Luk, Kehm, Carroll, et al., 2012) and brain homogenates from both transgenic α-synuclein mice (Luk, Kehm, Zhang, et al., 2012; Mougenot et al., 2011) and patients with Lewy body disorders (Prusiner et al., 2015; Recasens et al., 2014). These observations support the theory that misfolded α-synuclein can be transmitted between neurons

across anatomically connected brain regions (Jucker & Walker, 2013; Luk, Kehm, Zhang, et al., 2012).

It is not known for certain how misfolded α-synuclein enters a neuron, but it has been demonstrated that α-synuclein can enter the central nervous system by crossing the blood brain barrier after intravenous injection of α-synuclein assemblies (Peelaerts et al., 2015). Exogenous α-synuclein fibrils are capable of interacting with 178 neuron and 108 astrocyte membrane proteins, 58 of which are common to both (Shrivastava et al., 2015). The lymphocyte-activation gene 3 (LAG3) receptor is a likely candidate involved with misfolded α-synuclein internalization as it had the high binding affinity for biotin-tagged preformed α-synuclein fibrils in a streptavidin-alkaline phosphatase assay and did not bind biotin-tagged α-synuclein monomers, tau or β-amyloid (Mao et al., 2016). Free intercellular oligomeric α-synuclein is not internalized as efficiently as oligomers associated with exosomes (Danzer et al., 2012), and neuronal uptake of α-synuclein aggregates can be reduced by pretreatment with endocytosis inhibitors monodansylcadaverine and dynasore (Hansen et al., 2011), suggesting endocytosis rather than passive diffusion is the primary means of entry.

Once inside the cell, α-synuclein aggregates can escape into the cytoplasm from endosome/lysosome compartments and evade degradation (Flavin et al., 2017). The misfolded α-synuclein can then act as a template and induce the misfolding and aggregation of endogenous α-synuclein (Luk et al., 2009; Volpicelli-Daley et al., 2011). While α-synuclein aggregates have been observed to move in neurons in both anterograde and retrograde directions *in vitro* (Freundt et al., 2012), the spread of α-synuclein aggregates is primarily in a retrograde direction *in vivo* (Luna &

Luk, 2015; Uchihara et al., 2016). This agrees with the reports that Lewy bodies are enriched with dynein, a protein associated with retrograde transport (Volpicelli-Daley, 2017).

For the pathology to transmit to neighboring cells the aggregates must exit the neuron. Failure to degrade aggregated α-synuclein can result in exocytosis that is not mediated by the endoplasmic reticulum and Golgi apparatus (Alvarez-Erviti et al., 2011). The release is related to neuronal activity (Yamada & Iwatsubo, 2018) and can be increased by proteotoxic and mitochondrial stress (Jang et al., 2010; H. J. Lee et al., 2005). As astrocytes can engulf and degrade misfolded α-synuclein assemblies (Loria et al., 2017), exocytosis by neurons may be an attempt to share the proteotoxic stress burden with support cells.

Risk Factors

There are many risk factors than can increase the likelihood of developing Lewy body disorders. In PD, 5-10% of cases are linked to a genetic mutation (Poewe et al., 2017). The most significant mutations related to familial PD are the genes for α-synuclein, PINK1, parkin, DJ-1, GBA, and LRRK2 (Bonifati et al., 2003; L. N. Clark et al., 2009; Kitada et al., 1998; Paisan-Ruiz et al., 2004; Polymeropoulos et al., 1997; Sidransky et al., 2009; Valente et al., 2004). With regard to α-synuclein, A53T, H50Q, E43K, and A30K mutations all have been reported to increase the aggregation of α-synuclein *in vitro* (Conway et al., 2000; Ghosh et al., 2013; Greenbaum et al., 2005). Changes in charged amino acid residues can influence the conformation of α-synuclein and increase its likelihood to form into an insoluble aggregate. Duplication of triplication of the gene encoding for α-synuclein also increases the likelihood of developing PD (Singleton et al., 2003).

The environmental risk factors of Lewy body disorders are less well understood, but in a case-control study in China, exposure to industrial chemicals increased the likelihood of developing PD (Tanner et al., 1989). Indeed, chronic exposure to certain herbicides and pesticides, particularly paraquat and rotenone can increase the risk of developing PD (Gorell et al., 1998; Gorell et al., 2004; Hertzman et al., 1990; Liou et al., 1996; Semchuk et al., 1993; Tanner et al., 2011). Exposure to heavy metals including lead, copper, iron, and mercury also increase the risk of developing PD (Gorell et al., 2004; Ngim & Devathasan, 1989). PD patients often have elevated levels of these metals in the SN (Dexter et al., 1989; Gerlach et al., 2008; Sofic et al., 1988).

The reason for a PD-specific phenotype after exposure to these agents is only partially understood. It has been reported that paraquat kills neurons within the SN (Liou et al., 1996), and that iron and paraquat can synergistically increase the age-related loss of dopaminergic neurons within the SN (Peng et al., 2007). Paraquat inhibits complex 1 of the mitochondria, which increases ROS within the cell (Castello et al., 2007; Jenner, 2003). It has also been reported that heavy metals and pesticides promote the aggregation of α-synuclein (Uversky et al., 2001). Treatment with charged metal ions are reported to increase the rate of α-synuclein fibril formation (Uversky et al., 2001), possibly by inducing a conformation change in the protein that favors aggregation. Heavy metals like mercury and lead inhibit glutamine synthetase, which is responsible for converting glutamate into less toxic glutamine (Sierra & Tiffany-Castiglioni, 1991).

Lifestyle risk factors favoring PD include a history of head trauma (Semchuk et al., 1993) and circadian disruption (Lauretti et al., 2017). Additionally, a high fat and high calorie diet

(Logroscino et al., 1996), diabetes (Hu et al., 2007), and obesity (Abbott et al., 2002; Hu et al., 2006) may also be risk factors for developing Lewy body disorders. These risk factors may be related to increased glycation of Lewy bodies with chronic high blood sugar levels (Vicente Miranda et al., 2016). Glycation of α-synuclein is reported to increase its propensity to aggregate (Vicente Miranda et al., 2017), and advanced glycation end products are reportedly increased in the SN, amygdala, and frontal cortex of ILBD patients compared to age-matched controls (Dalfo et al., 2005), or the observations that cholesterol metabolites can increase α-synuclein fibrilization (Eriksson et al., 2017), and that obese patients typically have lower levels of the dopamine D2 receptor in the striatum (H. Chen et al., 2004).

Gender and aging

Two often reported and particularly important risk factors in the context of this dissertation are age and male gender. Age is the strongest risk factor for developing PD (Bennett et al., 1996; Morens et al., 1996; Tanner & Goldman, 1996). Rapid Eye Movement (REM) sleep disorders, a common prodromal symptom of Lewy body disorders and risk factor discussed earlier, is more prevalent with age (Sixel-Doring et al., 2011). The increased risk of PD with age is likely related to increased susceptibility to α-synucleinopathy, as normal aging does not result in significant loss of dopaminergic neurons within the SN (Alladi et al., 2009). This effect was confirmed in non-human primates as aging failed to cause a significant loss DA neurons, but did lower phenotypic expression of tyrosine hydroxylase (McCormack et al., 2004). Normal aging does lead to a progressive accumulation of α-synuclein within dopaminergic neurons of the SN in rhesus monkeys, but it is the soluble, non-pathogenic form (Chu & Kordower, 2007). In addition to the

patient's age, the age of onset of PD is also associated with a greater risk of developing dementia (Aarsland & Kurz, 2010b), suggesting the effects of age are not limited to the nigrostriatal pathway. In PD patients, age, severity of motor symptoms, cognitive impairment, but also male gender are associated with an increased risk of death (Forsaa et al., 2010).

While the reasons are not well understood, many studies have reported that females develop Lewy body disorders less often than males (Beach, Adler, et al., 2009; Savica et al., 2017; Savica et al., 2013; K. M. Smith & Dahodwala, 2014; Twelves et al., 2003). Females are also diagnosed with PD on average two years later than men (Haaxma et al., 2007) suggesting that clinical symptoms manifest later in women. Only in men but not women was plasma α-synuclein concentration associated with sleep disorders, hallucinations, and cognitive impairment (Caranci et al., 2013). Neocortical Lewy pathology appears in the advanced stages of PD, is related to cognitive decline, and is more prevalent in men (Nelson et al., 2010), suggesting that gender can affect the development and spread of α-synuclein pathology.

The symptoms and risk factors of Lewy body disorders can also differ amongst the genders. In PD, males are more likely to experience hyposmia, urinary symptoms, sexual dysfunction, gait disturbances, and rigidity, while females are more likely to experience depression, dyskinesia, anxiety, postural instability, more pain symptoms, and a tremor-dominant phenotype (Farhadi et al., 2017; Georgiev et al., 2017). Risk factors more associated with male gender are head trauma and exposure to pesticides while anemia is more associated with females (Georgiev et al., 2017). In terms of treatment, male PD patients are more likely to be prescribed antipsychotics while

female PD patients are more likely to be prescribed antidepressants (Fernandez et al., 2000), possibly as a consequence of the differing symptoms between genders.

The differences in PD etiology may be a result of natural underlying differences between males and females. Female brains also have a greater percentage composition of gray matter (Geevarghese et al., 2015), and females below 60 years of age have 8.4% higher DAT binding compared to men (Wong et al., 2012). It has been reported that males typically have a higher baseline oxidative stress level than women (Ide et al., 2002), which may contribute to their greater vulnerability. From a genetic standpoint, the MAO-A gene, involved with neurotransmitter metabolism is on the X chromosome and so with only one copy, males might express lower levels. To compensate for this insufficiency, the SRY gene on the Y chromosome can become activated. The SRY gene produces the SRY protein, and the expression of this protein is associated with increased levels of tyrosine hydroxylase (TH), dopamine β-hydroxylase, DOPA decarboxylase, the D2 receptor, and monoamine oxidases (Tao et al., 2012; Wu et al., 2009). The MAO-A gene has a SRY binding site on the core promoter. The SRY gene is expressed in the SN and the SRY protein specifically localizes with TH positive neurons (Dewing et al., 2006). The SRY gene may therefore have evolved on the Y chromosome to compensate for the increased oxidative stress and reduced estrogen levels in the male brain.

Estrogens are neuroprotective and in a cross-sectional study of female PD patients, increased duration of estrogen exposure was associated with a later age of diagnosis and less severe motor impairment (Cereda et al., 2013; Haaxma et al., 2007). Females who develop PD also experience menopause earlier than age-matched controls (Benedetti et al., 2001; Nitkowska et al., 2014).

Estrogen replacement therapy at the onset of menopause reduces the risk of developing dementia in female patients (Marder et al., 1998), which suggests that estrogens may reduce the spread of α-synucleinopathy to regions where Lewy pathology is associated with cognitive decline. This agrees with reports men are more than twice as likely to develop both the limbic predominant and diffuse neocortical subsets of DLB as women (Nelson et al., 2010), and is consistent with observations that estrogens can disaggregate aggregated forms of α-synuclein (Hirohata et al., 2009).

Olfactory dysfunction

As discussed previously, olfactory dysfunction is a well-established premotor symptom of Parkinson's disease (Doty et al., 1988; Hawkes et al., 1997), but it is somewhat nonspecific, as other neurodegenerative diseases can also reduce olfactory capability. Olfactory impairment is also age-related, as approximately 75% of people report a reduction in their sense of smell after the seventh decade of life (Doty, 2009). This age-related loss of olfaction is more severe for men than women (Godoy et al., 2015), possibly because females have significantly more neuronal and non-neuronal cells in their OBs (Oliveira-Pinto et al., 2014) or have a larger orbitofrontal cortex, a part of the olfactory system (Gur et al., 1999). Females typically perform better on olfactory exams (Doty et al., 1984), and female PD patients also often perform better than male PD patients on smell tests (Stern et al., 1994).

Loss of olfaction is associated with ILBD (Ross et al., 2006), and is often reported years before the motor symptoms of PD emerge (Hawkes et al., 1997). The presence of Lewy aggregates in the OB is correlated with olfactory dysfunction in PD (Driver-Dunckley et al., 2014; Wilson et al.,

2011). In the OB, Lewy pathology is most often observed in the mitral and tufted cells, but also in the granule and periglomular cells (Sengoku et al., 2008). PD patients often show reduced volume and sulcus depth (Palatini et al., 1992), and loss of mitral and substance P containing cells in the OB (Ferrer et al., 2012).

Mechanisms of neurodegeneration

Lewy aggregates can be toxic to neurons through several related mechanisms. As mentioned earlier, misfolded α-synuclein molecules can bind to many different proteins on the cell surface. In doing so, they can cause a deleterious protein clustering effect, in which many membrane proteins bind to an aggregate of misfolded α-synuclein, leaving some areas with reduced density of vital cell-surface receptors such as ion channels (Shrivastava et al., 2017; Shrivastava et al., 2015). If the misfolded α-synuclein is endocytosed, the aggregates can sequester synaptic proteins such as VAMP2 and SNAP25 (Choi et al., 2018), which can inhibit synaptic vesicle recycling and reduce neurotransmitter release (Nemani et al., 2010; Volpicelli-Daley et al., 2011). Inside the cell, the aggregates can induce vesicle rupture (Danzer et al., 2007; Samuel et al., 2016) and impair intracellular transport (Volpicelli-Daley, Gamble, et al., 2014).

Under normal conditions, misfolded proteins can be degraded by the ubiquitin-proteasome system (UPS) or the lysosome autophagy system (LAS). Aggregated α-synuclein is difficult to degrade by these systems and can inhibit the proteasome (Lindersson et al., 2004; Rideout et al., 2001; W. W. Smith et al., 2005; Y. Tanaka et al., 2001) as well as the lysosome (Cuervo et al., 2004). Oligomeric α-synuclein has also been detected in mitochondria (Nakamura et al., 2008) where it

can inhibit complex 1 (Luth et al., 2014; Reeve et al., 2015), and lead to the generation of ROS and induce apoptosis (Eschbach et al., 2015; W. W. Smith et al., 2005). Aggregated α-synuclein can also form pores in the cell membrane that cause loss of calcium ion homeostasis and lead to apoptosis (Danzer et al., 2007). Neurons that express calcium binding proteins and are able to buffer calcium ion levels are reported to be resistant to developing Lewy aggregates (Gomez-Tortosa et al., 2001). While there are many downstream negative effects of misfolded α-synuclein, the toxicity of the α-synucleinopathy is ultimately a function of the accumulation of misfolded or deleteriously modified proteins and the generation of oxidative stress.

Accumulation of misfolded proteins

The accumulation of misfolded proteins into large insoluble aggregates causes proteotoxic stress within neurons and is a key feature of neurodegenerative diseases (Morimoto, 2008). The primary mechanisms used by cells to mitigate proteotoxic stress are the UPS and LAS. Depending on the conformation, misfolded α-synuclein can be targeted to either the UPS or LAS (Shin et al., 2005) and cleared by both systems (Cuervo et al., 2004; Emmanouilidou et al., 2010; Rideout et al., 2004). In order to target large misfolded proteins to the proteosome, they must first be tagged with ubiquitin proteins, which requires multiple enzymes. Phosphorylation of serine 129 may direct misfolded α-synuclein to the UPS when the LAS in not adequately preventing α-synuclein accumulation (Arawaka et al., 2017).

In the first step of ubiquitination, E1, an ubiquitin-activating enzyme hydrolyzes ATP and prepares the C terminus of ubiquitin for nucleophilic attack (Pickart, 2001). E2, an ubiquitin-conjugating

enzyme binds to the activated ubiquitin and carries it to E3, an ubiquitin-ligase. E3 binds both E2 and ubiquitin and can then transfer the ubiquitin to a lysine residue on the protein targeted for degradation (Richly et al., 2005). The Parkin protein, commonly mutated in familial early onset PD, is an E3 ubiquitin ligase involved with protein degradation (Baptista et al., 2004), and proteasome dysfunction has been reported in the SN of PD patients (McNaught et al., 2003; McNaught & Jenner, 2001), confirming the crucial role of the UPS. Oligomeric α-synuclein can also induce the S-nitrosylation of Parkin, enhancing its degradation and reducing the functionality of the UPS (Wilkaniec et al., 2018). Activity of the UPS also decreases normally as a consequence of aging in nearly every tissue (Martinez-Vicente et al., 2005), but this natural process may be exacerbated by misfolded α-synuclein, as it can bind the proteasome and reduce its activity (Cuervo et al., 2004; Lindersson et al., 2004).

While both the UPS and LAS can degrade misfolded α-synuclein, the LAS has been reported to be more important for degrading oligomeric α-synuclein (Xilouri et al., 2013). Autophagy can be subdivided into at least three distinct forms: microautophagy, macroautophagy, and chaperone-mediated autophagy. Microautophagy involves the lysosome directly engulfing cytosolic material. Macroautophagy involves the engulfment of substrates by a double membrane and the formation of an intermediate structure called the autophagosome, which then fuses with the lysosome (Lopez Meza et al., 2010). Chaperone-mediated autophagy involves the delivery of targeted proteins to the lysosome by chaperones, followed by transport across the membrane by the LAMP2A receptor (Kaushik & Cuervo, 2012; Yang & Klionsky, 2010).

The large misfolded α-synuclein aggregates that are the hallmarks of Lewy body disorders are most likely degraded through the macroautophagy and chaperone-mediated autophagy systems. Overexpression of α-synuclein is reported to impair autophagosome formation both *in vitro* and *in vivo* (Winslow et al., 2010). The A53T and A30P mutant forms of α-synuclein may also inhibit the LAMP2A receptor and block the translocation of materials into the lysosome (Cuervo et al., 2004; Martinez-Vicente et al., 2008). Furthermore, chloroquine, a lysosome inhibitor, increases the formation of α-synuclein aggregates (Sacino et al., 2017). Impairment of the LAS can also increase secretion of aggregated α-synuclein by exosomes into the extracellular space (Alvarez-Erviti et al., 2011).

There is growing evidence to support the theory that Lewy bodies may be a form of failed aggresome. An aggresome is a protein-filled insoluble inclusion that forms at the centrosome in response to proteotoxic stress (Bence et al., 2001; Kopito, 2000). Centrosomes can serve as a scaffold to direct the degradation of misfolded proteins (Kopito, 2000), and misfolded proteins are actively transported to the centrosome (Johnston et al., 2002; Johnston et al., 1998; Kawaguchi et al., 2003; Wigley et al., 1999; Wojcik, 1997; Wojcik et al., 1996). Many of the same proteins trafficked to the centrosome (chaperone proteins, components of the UPS, substrates for proteolysis) are also found in Lewy bodies, suggesting that Lewy bodies are not formed though a chaotic process of protein accretion, but rather through a regulated attempt to degrade misfolded proteins (McNaught et al., 2002; Olanow et al., 2004). In cells that are stressed with proteasome inhibitors, inhibiting microtubule transport impedes the development of the aggresome and increases toxicity (Bence et al., 2001; Johnston et al., 1998; Junn et al., 2002; H. J. Lee & Lee,

2002). Furthermore, Lewy neurites may be protein aggregates en route to the centrosome (Olanow et al., 2004).

After formation, the aggresome can recede or persist as an insoluble mass (Bence et al., 2001), quite similar to the prototypical Lewy body. Aggresomes are believed to be neuroprotective, as aggresomes appear in 60% of non-apoptotic cells but only 10% of apoptotic cells (M. Tanaka et al., 2004). Similarly, some authors report that Lewy bodies do not deleteriously affect neuron structure or function (Gertz et al., 1994). Furthermore, it has been reported that neurons with Lewy bodies in the SN appear more resistant to apoptosis than neurons without Lewy bodies (Tompkins & Hill, 1997).

Oxidative stress

Oxidative stress is defined as the imbalance between the cellular mechanisms responsible for mitigating ROS and those responsible for their generation (Sies, 2015). Neurons are particularly susceptible to oxidative stress as they contain a relatively large amount of unsaturated lipids that can be deleteriously modified by oxidative stress (Uttara et al., 2009). The components of the UPS are also particularly vulnerable to damage from ROS (Bulteau et al., 2001; Sitte et al., 2000). Oxidative stress in neurons can be caused by dysregulation of the UPS as well as mitochondrial dysfunction (Double et al., 2010). Defective mitochondria are typically removed from the cell by the LAS (Brunk & Terman, 2002a, 2002b), but as discussed earlier, this system can be inhibited by α-synuclein aggregates. The increased oxidative stress levels caused by dysfunctional

mitochondria can also reduce the effectiveness of the LAS (Dehay et al., 2010), further reducing the ability of the cell to mitigate oxidative stress.

Oligomeric forms of α-synuclein can interact with metal ions to induce the generation of superoxide and hydrogen peroxide (Deas et al., 2016), and oxidative stress has been reported to increase the accumulation of α-synuclein aggregates *in vitro* (Hashimoto et al., 1999; Souza et al., 2000). Dopaminergic neurons contain relatively high levels of iron (Halliwell, 1992), and iron can generate ROS through the Fenton reaction (Rhodes & Ritz, 2008). DA can also be metabolized into cytotoxic free radicals, including hydrogen peroxide and dopamine quinones (Greenamyre & Hastings, 2004; Halliwell, 1992), and dopaminergic neurons are also particularly susceptible to damage from oxidative stress (Fahn & Cohen, 1992; Olanow, 1990). The enhanced vulnerability of dopaminergic cells to ROS may contribute to the neurodegeneration of the nigrostriatal pathway in PD. Indeed, there is an upregulation in ROS production (Dias et al., 2013) and high levels of oxidatively damaged proteins within the SN of PD patients (Alam et al., 1997; Good et al., 1998; Yoritaka et al., 1996). In addition, DA neurons exposed to α-synuclein fibrils exhibit an increase in mitochondrial and cytoplasmic oxidative stress markers (Dryanovski et al., 2013).

Importance of glutathione/N-acetyl cysteine

Glutathione (GSH) is the most abundant antioxidant in the central nervous system and is found in millimolar concentrations in most cell types (Pocernich & Butterfield, 2012). GSH is produced by both neurons and glia (Dickinson & Forman, 2002) and efficiently detoxifies ROS (Dringen, 2000; Griffith, 1999). The GSH concentration is neurons (~2.5 mM) is lower than that of astrocytes (~3.8 mM) (Bolanos et al., 1995; Rice & Russo-Menna, 1998), but astrocytes can release GSH

into the extracellular space to supply it to nearby neurons (Rice & Russo-Menna, 1998). GSH can be conjugated to compounds to target them for efflux though multidrug resistance efflux transporters (Marchan et al., 2008), and thereby help rid the cell of potentially toxic substances. GSH is particularly important in the brain as the brain consumes 20% of the oxygen but only weighs 2% of total bodyweight. Of the 20% of oxygen consumed by the brain, approximately 90% is used by the mitochondria to produce ATP to fuel the energy intensive process of neurotransmission (Ballatori et al., 2009).

The rate of synthesis of GSH is determined by the activity of the enzyme gamma-glutamylcysteine ligase and by the availability of the amino acid cysteine (Dickinson et al., 2004; Stringer et al., 2004). N-Acetyl cysteine (NAC) is metabolized into cysteine, which provides the rate-limiting substrate necessary to increase the production of GSH (Aldini et al., 2018). While NAC is indeed neuroprotective by enhancing GSH production (Unnithan et al., 2014), it has also been reported to have beneficial GSH-independent effects (Jiang et al., 2013; Unnithan et al., 2014), which are less well understood.

NAC supplementation has proven beneficial in a variety of neurological disorders. NAC is reported improve symptoms of akathisia in schizophrenia patients (Berk, Copolov, Dean, Lu, Jeavons, Schapkaitz, Anderson-Hunt, Judd, et al., 2008), some cognitive impairments in Alzheimer's patients (Adair et al., 2001), and the depressive symptoms in bipolar patients (Berk, Copolov, Dean, Lu, Jeavons, Schapkaitz, Anderson-Hunt, & Bush, 2008). In patients with traumatic brain injury, NAC supplementation doubled the chance of symptom resolution (Hoffer et al., 2013).

A decrease in GSH levels is one of the earliest reported pathologies in PD (Martin & Teismann, 2009). GSH depletion occurs before neurodegeneration of the SN (Chinta & Andersen, 2006) and there are reports of a 40-90% loss of GSH in this brain region (Dexter et al., 1994; Perry et al., 1982; Sian, Dexter, Lees, Daniel, Agid, et al., 1994; Sian, Dexter, Lees, Daniel, Jenner, et al., 1994). The severity of PD symptoms has been correlated to the degree of GSH loss (Jenner, 1998; Riederer et al., 1989). DA injection into the striatum of rats causes a significant depletion of GSH (Rabinovic & Hastings, 1998), suggesting that GSH may mitigate the toxicity associated with DA metabolism. Baseline GSH levels decrease with age, and male mice experience a greater age-associated decline in GSH (Liu et al., 2004), possibly contributing the increased risks of PD in males and with aging discussed earlier.

There is mounting evidence that NAC therapy could be beneficial to PD patients. In cell lines, NAC is reported to decrease DOPAL-quinone formation and reduce the formation of α-synuclein oligomers (D. G. Anderson et al., 2016; Goldstein et al., 2017; Jinsmaa et al., 2018). In α-synuclein overexpressing mice, oral NAC administration reduced α-synuclein aggregate formation and preserved striatal dopaminergic terminals (J. Clark et al., 2010). NAC has also shown to mitigate the toxicity of the dopaminergic neurotoxins MPTP and 6-OHDA (Aluf et al., 2010; K. W. Lee et al., 2004; Perry et al., 1985; Sharma et al., 2007). In PD patients, NAC administration increases GSH levels in the CNS (Holmay et al., 2013; Katz et al., 2015) and increases dopamine transporter binding in the striatum by 4.4 to 7.8% (Monti et al., 2016).

Preformed fibril model

The development of exogenous recombinant α-synuclein fibrils was an important innovation for modeling Lewy body disorders. In 2012, *Luk et al.* demonstrated that striatal injections of these fibrils could seed Lewy-like pathology that spreads to neuroanatomically connected brain regions and causes nigral cell loss and motor impairments in non-transgenic animals (Luk, Kehm, Carroll, et al., 2012; Luk, Kehm, Zhang, et al., 2012). A few years earlier, the prevailing theory had been that transgenic animals are essential to study α-synucleinopathy (Dawson et al., 2010). Upon injection, the preformed fibrils induce the accumulation of the endogenous mouse α-synuclein into an aggregated and pathogenic form that decreases synaptic proteins, impairs neuronal excitability, reduces neuronal connectivity, and eventually leads to apoptosis (Volpicelli-Daley et al., 2011). The endogenous α-synuclein misfolds into an insoluble, hyperphosphorylated and ubiquitinated form (Luk, Kehm, Carroll, et al., 2012; Luk, Kehm, Zhang, et al., 2012). As little as 0.1 μg of preformed fibrils is enough to induce Lewy-like pathology in wild-type mice (Tarutani et al., 2018), and fibrils 50 nm or less in length are the most efficient at inducing pathology (Tarutani et al., 2016). While uptake of the preformed fibrils can occur at either the soma or dendrites (Bieri et al., 2018), the aggregates are typically first detected in axons and then travel to the cell soma where Lewy body-like aggregates form (Volpicelli-Daley et al., 2011). It has also been reported that there are different strains of α-synuclein fibrils that can induce distinct α-synucleinopathies *in vivo* (Bousset et al., 2013; Pieri et al., 2016; Yonetani et al., 2009). *Bousset et al.* demonstrated that α-synuclein could assemble into structurally distinct aggregates he differentiated as "fibrils" or "ribbons," which induce endogenous α-synuclein to form aggregates of the same architecture. The fibril form was found to be more toxic to cells and the A30P α-synuclein mutation made α-synuclein incapable of forming ribbons, possibly contributing to increased toxicity (Bousset et al.,

2013). The PFF model is the first reproducible and progressive model to recapitulate many key features of human Lewy body disorders, such as nigrostriatal pathway degeneration.

Materials and Methods

Animals and surgeries

All treatments and procedures were approved by the Duquesne University Institutional Animal Care and Use Committee (protocol nos. 1403-04 and 1604-05), and performed in accordance with NIH regulations. Male and female CD-1 mice were purchased from Charles River (Horsham, PA) and housed and bred in the Duquesne University animal care facility. All animals were housed in a 12:12 photoperiod with *ad libitum* access to UV-disinfected water and food. Sprague Dawley rats were purchased from Hilltop Lab Animals (Scottsdale, Pennsylvania). Female Sprague Dawley rats were singly housed and part of an in-house breeding colony maintained to generate rat pup tissue for postnatal cultures.

Every effort was made to reduce pain and suffering related to experimental procedures. Prior to surgeries, the animals were anesthetized with 3% isoflurane. A stereotaxic frame was used to stabilize the animals for surgeries. Paxinos and Franklin's "*The Mouse Brain in Stereotaxic Coordinates*" (Franklin and Paxinos, 2013), was used to determine coordinates for injection. The stereotaxic coordinates were confirmed with injections of blue food dye into the target structure. Unilateral injections were made to the right OB/AON region of mice defined stereotaxically as AP +4.0, ML -1.0, DV -2.5 mm from Bregma at the top of the skull. The AP coordinate was increased to +4.1 in the 11-month-old mice to account for the slightly larger skull size. Injections into the

hippocampus were defined as AP -2.5, ML -2.8, DV -3.6 mm from Bregma. The infusion occurred at a rate of 0.25 µL/min followed by a 4-minute rest period before the needle was withdrawn. Following the surgery, the animals received 0.015 mg/kg buprenorphine subcutaneously and were placed on a heating pad. Lidocaine and antibiotic ointment were applied to the wound for three days after the surgery. At the end of the experiment, the animals were anesthetized with isoflurane and perfused through the left ventricle with 50 mL of saline followed by 100 mL of 4% paraformaldehyde in 0.1 M phosphate buffer.

Alpha-synuclein

Kelvin Luk (University of Pennsylvania Perelman School of Medicine) generously provided the α-synuclein fibrils. The stock solution of the fibrils was kept frozen at -80 °C until thawed prior to sonication. Approximately 10 µL of fibrils were sonicated either with a probe sonicator (Misonix XL2020, Misonix incorporated, Farmingdale NY) for 60 pulses of approximately 0.2 seconds or with a waterbath sonicator (Bransonic series model M1800, Branson Ultrasonics Corporation, Danbury CT) for either 1 or 24 hours. After sonication, the fibrils were kept at room temperature. The fibrils were infused at a maximum of four hours post-sonication. Excess fibrils were discarded and no solutions were reused.

Male mice (2, 3, 5, 11, and 17 months old) or female mice (3 months old) were infused with sonicated preformed full-length wild-type mouse α-synuclein. The mice were infused with 5 µg in 1 µL of the preformed fibrils or 1 µL of phosphate buffered saline (PBS).

Chemicals and antibodies

The primary and secondary antibodies used in these experiments are listed **Tables 2** & **3**. A no-primary control was always performed to confirm specificity of the secondary antibody. MG132 (UBPBio Aurora CO, Cat. No. F1101) was stored at -80 º C as 10 mM stock solution in dimethyl sulfoxide (DMSO). VER155008 (R&D systems, Minneapolis, MN) was used to inhibit Hsp70/Hsc70 activity as previously reported (Chatterjee et al., 2013; Saykally et al., 2012; Schlecht et al., 2013). It was stored at -80 º C as a 10 mM stock solution in DMSO. MAL3-101, an Hsp70/Hsc70 inhibitor (Braunstein et al., 2011; Huryn et al., 2011; Kilpatrick et al., 2013), was stored as a 10 mM stock in DMSO at -80 º C until use. Lactacystin (AdipoGen Corporation, San Diego, CA) was stored at -20 º C as 10 mM stock solution in DMSO. Paraquat (Sigma-Aldrich, St. Louis, MO) was dissolved in PBS (100 mM) and stored at -80 º C until use. DRAQ5 (1:10000 or 0.5 μM, Biostatus, Leicestershire, UK) was stored at 4 º C until use. NAC (Acros Organics, 160280250 Lot A0333137) for *in vitro* studies was prepared by dissolution in PBS, sterile filtering, and stored at a concentration of 1000 mM at -80 º C. A 0.15% NAC diet for *in vivo* studies was prepared by mixing 1.5 g of NAC per kg of 5001 PMI Laboratory Diet (Envigo Teklad Diets, Madison WI). FluoroGold (Fluorochrom LLC, Denver, CO) was stored at 4 º C as a concentration of 1.5% in PBS until use. In the *in vivo* experiment, 300 nL of a 1.5% Fluorogold solution or an equal volume of PBS was injected into the same region (OB/AON) in male CD-1 mice (2 months old). For this experiment, the mice were sacrificed one week following injection of FluoroGold.

Behavioral testing

All testing was performed within an arena (45 cm x 60 cm x 60 cm) of black polyvinylchloride plastic walls with a green polyvinylchloride floor. Two lamps were used to create a dim diffuse

light that minimized shadows in the arena. The arena was sprayed with 70% isopropyl alcohol between trials to remove olfactory cues.

Buried pellet test

To measure olfactory function, the buried pellet test was employed as described previously (Lehmkuhl et al., 2014). On the first day of testing, the animals were placed in a cage with corncob bedding piled in one half for three minutes. On the second day of testing, the animal was placed in a fresh cage with the corncob bedding piled in one half of the cage and a peanut was placed on the top of the pile. The latency of each mouse to contact the exposed peanut was recorded. On the third day, the mice were placed in an empty cage with the corncob bedding piled in the opposite half and a peanut was buried 0.5 cm deep in a random location. The latency to find and contact the buried peanut was then recorded. An observer blinded to the treatment group of each animal performed the video analysis. To account for the preference of the treat between animals, the time the animal took to contact the exposed peanut was subtracted from the time the animal required to find the buried peanut.

Novel object (NOR) and novel place (NPR) tests

The object and place recognition tasks were performed to measure learning and memory. For these tests, three identical bases were used—a bare floor for the acclimation, and two other identical floors with brackets fastened to hold the objects in place. A video camera was positioned above the arena so that the entire arena was visible in the camera's field of view. The camera was used to record behavior during the later phases of the tests. The objects were made of glass or plastic

with varying shapes and textures, including light bulbs and plastic bottles. The objects were fastened so that the animals could not displace or hide beneath them. On the first day, the animals were acclimated to the arena by placing them on the bare floor an allowing them to explore the arena for 10 minutes. On the next day, the floor of the arena was changed so that the arena contained two identical objects in fixed positions in opposite corners of the arena approximately 10 cm from the walls of the arena. The animals were allowed to explore the arena and interact with the objects for five minutes. On the next day, a novel object was substituted for one of the familiar objects in the arena and the animal was allowed to explore for a five-minute period. The time spent exploring the familiar and novel objects was recorded. The animal was considered to be interacting with the object if the head was within 4 cm and oriented within a 45-degree angle of the object. On the final day of testing, the animals were returned to the arena with the same two identical objects from the first familiarization phase but with one object moved to a novel location. The exploration time was scored the same as the novel object test and the exploration ratio for both tests was defined as the time the animal spent exploring the novel object/place divided by the time the animal spent exploring both the novel and familiar objects. The mice that spent less than 10 seconds exploring the objects during the testing phase were classified as "non-responders" and excluded from the data analysis (Cai et al., 2012).

Cylinder test

To measure spontaneous motor activity, the mice were placed in a clear, Plexiglass cylinder (8.9 cm diameter, 15.2 cm high) for 10 minutes. The Plexiglass cylinder placed on top of a clear base with a mirror underneath so that the camera had an upward view of the mouse and could see turning in all directions.

Challenge beam test

The challenge beam test was used to measure motor coordination. On the first two days, the mice were placed on the wide end of a trapezoid beam and trained to traverse the beam as described previously (Fleming et al., 2004). On the third day, a mesh grid was placed over the beam and the time to traverse the beam and the number of slips while crossing the beam was recorded. On the test day, the mice traversed the beam three times.

Histology

After perfusion, the brains were immersed in 30% sucrose in 10 mM PBS for 48 hours and cut into sections 40 or 50 μM thick on a freezing microtome in the sagittal place. The free-floating sections were stored in a cryoprotectant solution at -20 ° C. To immunostain the tissue, cryoprotectant was rinsed off with three washes of PBS and then heated to 80 ° C in a 10 mM sodium citrate tribasic dehydrate solution (pH 8.5) for 30 minutes to expose antigen binding sites (Jiao et al., 1999). The sections were then incubated at room temperature in a 1:1 solution of Odyssey block (LI-COR Bioscience, Lincoln, NE) in PBS for 1 hour on a shaker. Both primary and secondary antibodies were added to a 1:1 Odyssey Block in PBS with 0.3% Triton X-100. The primary antibodies listed in **Table 2** were then applied to the sections and incubated at 4 ° C for 24 hours on a shaker. The tissue sections were then washed three times and the secondary antibodies listed in **Table 3** were applied to the tissue for one hour at room temperature. Hoechst 33258 (bisBenzimide) and/or the infrared marker DRAQ5 were added at a concentration of 0.005 μM or 0.5 μM, respectively, during the secondary antibody incubation. The tissue was then washed three times with PBS and mounted onto glass slides (Superfrost Plus, Fisher Scientific, Pittsburgh, PA)

and coverslipped with either FluoroMount G (Southern Biotech, Birmingham AL) or Krystalon (EMD Chemicals, Gibbstown, NJ). Sections were then scanned on an infrared Odyssey imager or analyzed on an epifluorescent microscope (Olympus IX73, B&B Microscopes, Pittsburgh PA) with magnification objectives ranging from 4× to 100×. Sections from control and experimental groups were processed and analyzed in parallel. Primary antibodies were omitted from the immunohistochemical protocol in some sections to control for secondary antibody specificity. Loss of epifluorescent signal confirmed label of primary antibody.

Thioflavin staining

Thioflavin S staining was performed as published by Paumier and colleagues and our previous work (Paumier et al, 2015, Mason et al., 2016, Nouraei et al., 2016), as an additional measure of the aggregated and insoluble from of α-synuclein. The tissue was washed 3× in filtered PBS and mounted onto Superfrost Plus glass slides and dried. The slides were dipped into several solutions: 10 mM PBS for 5 minutes, 0.05% $KMnO_4$ in PBS for 20 minutes, 2 rinses of PBS for 2 minutes, 0.2% $K_2S_20_5$ and O.2% oxalic acid in PBS for 1 minute, 5 rinses of PBS for 2 minutes, freshly filtered 0.0125% Thioflavin S in 40% EtOH and 60% PBS for 3 minutes in darkness, 50% EtOH and 50% PBS for 10 minutes, 4 rinses of PBS for 5 minutes, 0.003 mM Hoechst 33258 bisBenzimide in 0.3% Triton X-100, a final rinse of sterile water for 5 minutes. After the immersions, the slides were allowed to dry and then coverslipped. Thioflavin S signal was measured in the 488 (green) channel of the Olympus IX73 microscope. Sections from control and experimental groups were prepared and analyzed in parallel.

Image analysis

In order to measure tyrosine hydroxylase (TH) and dopamine transporter (DAT) on the Licor Odyssey scanner, a blinded observer traced the boundaries of the regions of interest using TH and DAT signal as a guide. The background signal for each animal was subtracted by determining the signal per area in a brain region (occipital cortex) that has low endogenous DA levels (Brown et al., 1979). For counting TH^+ and $Hoechst^+$ cells, images taken with the 20× objective were stitched on the Olympus IX83 microscope, and a blinded observer used the multichannel images to define the TH^+ cells. In cellSens software, the observer drew a shape around the various areas containing TH^+ cells. Images were captured in grayscale (12-bit depth) and pseudocolored. The images were then saved with the shape in the Hoechst channel, so that the number of $Hoechst^+$ cells in that region could be counted automatically with ImageJ (NIH, Bethesda MD) software. Grayscale TIFF images were opened and a blinded observer used the "analyze particles" function to count inclusions after setting a binary threshold for each image. All photos were captured at the same exposure. High-resolution (100× oil objective) images were captured on the Olympus microscope with a 12-bit grayscale camera (CS-S-CCD High End Flash 4.0 Camera). For the VTA and SN counts in Aim 2, the TIFF images included a shape drawn around a region of interest. The threshold value was kept the same for all the images in each experiment. Particles with areas <50 pixels (background staining, not nuclear) or >1000 pixels (clusters of more than one cell) were excluded *a priori.* For the counts in Aim 3, the region of interest was cropped out of a 40× magnified image and counted in ImageJ using the methods described above.

Confocal microscopy

Confocal images in Aim 1 were captured with an Olympus Fluoview 1200 confocal system on an IX83 inverted frame with a 40× silicone oil objective (NA 1.25), using a gain of 1.0. Confocal

images in Aim 2 were captured on a Nikon A1R LU-NV confocal imaging system with a Nikon Ti2 microscope (Nikon Instruments Inc., Melville, NY). The gain was set to 1.0 and images captured with a 20× and 60× oil objective (NA 1.40). The Z-stacks were captured at 0.31 μm per pixel at 1.391 μm per section in the Z plane.

Electron microscopy

Unsonicated, probe-sonicated, 1-hour waterbath sonicated, and 24-hour waterbath sonicated fibrils were visualized with transmission electron microscopy using a JEOL JEM1210 at 60 kV (Jeol USA Inc., Peabody MA) using whole-mount preparations. The samples were first diluted 50% in PBS. They were then suspended on Formvar-coated 200 mesh copper grids (Electron Microscopy Sciences, Hatfield PA), and visualized by staining with 1% uranyl acetate. The images were captured with an ORCA-HR digital camera (Hamamatsu, Middlesex NJ). The fibrils were negatively stained as well as positively stained with the uranyl acetate, but more fibrils stained positively in all sonicated groups.

Blocking peptide experiments

A preadsorption control was used to confirm the specificity of the primary antibodies used to label aggregated α-synuclein in our experiments. Specifically, the preadsorption control was employed on polyclonal pSer129 antibodies; this type of control is not useful with monoclonal antibodies because there is only one binding site and thus incubating with the antigen will block all binding and not reveal unintended binding in the tissue. In our study, the rabbit polyclonal pSer129 (Abcam Ab59264) was incubated with 10-fold excess blocking peptide (Abcam Cat no. 188826) overnight prior to applying it to the tissue. Adjacent sections from the same animal were used to eliminate

any confounding variations in levels of background staining between animals. The tissue was exposed to the free polyclonal antibody or the blocked primary antibody for 24 hours at 4 ^{o}C and then rinsed prior to application of the secondary antibodies.

Primary neuron cultures

Animal use was approved by the Duquesne University IACUC (protocol no. 1505-04), and all experiments were performed in accordance with the guidelines described in the *NIH Guide*. Every effort was made to reduce the number of animals used and to minimize animal suffering. Tissue from the OB and hippocampus were dissected with microforceps from the brains of postnatal day 1 or 2 Sprague Dawley rat pups (Charles River, Wilmington, MA) and incubated in 10 units/mL of papain (Sigma-Aldrich, Cat. No. P3125) for 30 minutes. The tissue was homogenized and incubated in 10% type II-O trypsin inhibitor (Sigma-Aldrich, Cat. No. T9253). The cells were then triturated in Basal Medium Eagle (Sigma-Aldrich, Cat. No. B1522) containing 10% bovine calf serum (BME/BCS, HyClone Thermo Scientific, Logan, UT. Cat. No. 2151) and supplemented with 35 mM glucose (Sigma-Aldrich, Cat. No. G8769), and 1 mM L-glutamine (Gibco, Life Technologies, Cat. No. 25030-081). The dissociated cells were plated in Opti-MEM (Gibco, Life Technologies, Cat. No. 51985-034) with 20 mM glucose at a plating density of 80,000-100,000 cells/well in a 96-well plate (Corning, Inc 353072). The plates were precoated with laminin (1.88 ug/mL, BD Biosciences), and lysine (1 ug/mL) washed and dried prior to plating. After two hours in the Opti-MEM solution, a full media change was performed replacing the Opti-MEM for Neurobasal-A media (Gibco, Life Technologies) supplemented with 2% v/v serum-free B27 (Gibco, Life Technologies) and 2 mM L-glutamine.

Treatments

Treatments began on day-in-vitro 5 (DIV5), approximately 120 hours after plating. The cells were treated with a 10× stock of MG132 added to Neurobasal-A media supplemented with 2% v/v serum-free B27 and 2 mM L-glutamine. Cultures were treated with toxicants and NAC in a 2× media exchange on DIV5. On DIV7 viability assays were performed as described below. For α-synuclein fibril treatments, cultures were treated with α-synuclein fibrils and NAC in a full media exchange on DIV2 and then fixed on DIV9.

Viability assays

ATP levels were assessed using the luciferase-based Cell Titer Glo assay (Promega Inc, Madison, WI). Briefly, 25 µL of reagent was added to 50 µL of media. Within 15 minutes, 60 µL of solution was transferred to a white 96 well plate and analyzed on a microplate reader (VICTOR 1420 multilabel counter; PerkinElmer, Waltham, MA). To determine neuronal viability, cultures were stained for the neuronal marker microtubule associated protein 2 (MAP2) using an infrared In-Cell Western assay (Posimo et al., 2013; Posimo et al., 2014a). GSH levels were measured in the same manner. Nuclei were stained with the infrared marker DRAQ5 (1:10,000, 700 nm; Biostatus, Shepshed, Leicestershire, UK). MAP2, GSH, and DRAQ5 levels were then quantified on Odyssey imager with Odyssey software (Version 3.0, LI-COR, Lincoln, NE).

α-synuclein^{+} protein inclusions were visualized by immunostaining for the aggregated form of α-synuclein (phosphorylated at serine 129 or pSer129) (J. P. Anderson et al., 2006; Fujiwara et al., 2002; Hasegawa et al., 2002; Saito et al., 2003). For this experiment, nuclei were stained with Hoechst (10 µg/ml Hoechst 33258, bisBenzimide) in phosphate-buffered saline with 0.3% Triton-

X (ACROS, Cat. no. 21568-0010, Geel, Belgium) for one hour. Phospho-Ser129 and Hoechst staining was visualized on an epifluorescent microscope (EVOS, Life Technologies) at 200× magnification (0.213 mm^2 field of view, three fields per well). ImageJ software was used to quantify Hoechst-stained nuclear counts and α-synuclein$^+$ inclusions. The software displayed the following measurements: particle count, average particle size, and area fraction. The area fraction signifies the percentage of pixels in the image that have been segmented over background. "Background" was expressed at the same level for all microphotographs.

Statistical analyses

For In-Cell Westerns, wells with fluorescent lint or air bubbles were excluded from analysis. Statistical significance for the concentration-response curves was determined by one-way ANOVA followed by the Bonferonni *post-hoc* correction (IBM SPSS Statistics, Version 20, Armonk, NY). The data from the treatments were analyzed by two or three-way ANOVA followed by the Bonferroni *post hoc* correction. All *in vitro* experiments were performed in triplicate wells, and the data from the three wells was averaged to generate an "n" of 1. Each *in vitro* experiment was repeated on at least three independent occasions. The Grubb's outlier test was performed once on all the data.

For *in vivo* experiments, the data were analyzed by the appropriate ANOVA given the number of independent variables and followed by the Bonferroni *post hoc* correction (SPSS Version 20, Armonk, NY). The log-rank survival analysis was performed with GraphPad Prism software (Version 6.0h). In cases where there were only two groups, the two-tailed, unpaired Student's *t* test was performed. The threshold of $p \leq 0.05$ was used to define significance between groups.

Chapter 1

Rationale

Some of the first brain regions to develop Lewy aggregates in Lewy body disorders are the OB and AON (Beach, Adler, et al., 2009; Beach, White, et al., 2009; Braak et al., 2003). Lewy pathology in these regions contributes to the early olfactory dysfunction experienced by approximately 90% of PD patients (Doty, 2012; Wilson et al., 2011). At autopsy, Lewy pathology is observed in 97.1% of DLB cases, 94.8% of PD cases, 66.6% of ILBD cases, but only 7.2% of healthy controls (Beach, White, et al., 2009). In a separate autopsy study, every patient exhibiting a loss of pigmented neurons in the SN also displayed Lewy bodies in the OB (Sengoku et al., 2008). Despite these findings, α-synucleinopathy has been theorized to spread from neuron to neuron across interconnected brain regions with the brainstem as the primary starting point for α-synuclein pathology, with minimal transmission of pathology from olfactory structures (Braak et al., 2003; Dehay et al., 2016; Jones et al., 2015). As OB sensory neurons project into the nasal mucosa, the "olfactory vector hypothesis" proposes that an environmental insult such as bacteria, viruses or toxins may initiate α-synucleinopathy in the olfactory structures and then spread to additional brain regions (Dando et al., 2014; Doty, 2008). The primary goal of this Aim was to resolve whether α-synucleinopathy could indeed spread from the OB and AON into distant brain regions in wild-type mice that do not overexpress α-synuclein.

Before we commenced our experiments, Rey and colleagues published that human α-synuclein monomers and oligomers, but not preformed fibrils could be transmitted to some brain regions

including the piriform cortex within hours after injection into the OB (Rey et al., 2013). Nevertheless, Luk and colleagues had shown that PFFs elicit the spread of Lewy-like pathology in the dopaminergic system within three months following infusions in the striatum (Luk, Kehm, Carroll, et al., 2012). Longer time points may have led to transneuronal transmission of pathology in their model, but this was not confirmed with tract-tracing studies. Therefore, we decided to infuse PFFs into the OB/AON rather than monomers or oligomers and to sacrifice the mice at three months post-infusion to attempt to limit the spread to first-order circuitry, and to use a well-established tract-tracer to verify the afferent connections of the injection site.

Subsequent to our collection of the histological data, Rey published a review article with pilot data demonstrating long-term transmission from the OB into the entorhinal cortex, amygdala and hippocampus (Rey, George, et al., 2016). While these data were encouraging and consistent with our findings, the pathology appeared sparse, perhaps because their injections were in the rostral OB and they had not optimized fibril sonication parameters as we had (Rey, George, et al., 2016; Rey et al., 2013). As the AON develops more Lewy pathology than the OB in PD (Beach, White, et al., 2009; Braak et al., 2003; Ubeda-Banon et al., 2010), we had decided to inject the caudal OB, closer to the AON, before we commenced the study.

Fibril sonication parameters are of paramount importance for the generation of robust pathology as differences among sonicators and sonication protocols can affect PFF activity *in vitro* (Volpicelli-Daley, Luk, et al., 2014). Therefore, we tested various protocols for sonication of the preformed α-synuclein fibrils *in vivo,* as, to our knowledge, this has not been accomplished before. In two month-old mice, we infused vehicle, 1-minute probe-sonicated, or 1-hour waterbath-

sonicated α-synuclein fibrils into the OB/AON and sacrificed the mice three months later. To visualize the epicenter of the injection site, we performed injections at the same stereotaxic coordinates in a separate cohort of mice and sacrificed them after 90 minutes. This time point was chosen because Rey and colleagues had reported the greatest spread of human α-synuclein 90 minutes post-infusion (Rey et al., 2013). We employed the retrograde tract-tracer FluoroGold to determine if the brain regions that develop Lewy pathology are neuroanatomically connected to the site of infusion.

After the first study revealed that waterbath sonication was far more effective at eliciting robust Lewy-like pathology, we repeated the study comparing 1-hour waterbath sonicated fibrils to 24-hour waterbath sonicated fibrils. In that study, we injected the sonicated fibrils into the CA2/CA3 fields of the hippocampus—the primary hippocampal fields to develop pathology in Lewy body disorders (Braak et al., 2003; Dickson et al., 1994; Flores-Cuadrado et al., 2016). As age-related changes in the expression α-synuclein may alter the development of Lewy pathology (Chu & Kordower, 2007; Mak et al., 2009), we repeated the OB/AON infusions on 1-hour waterbath sonicated fibrils in older animals (17 months old) to determine if the transmission of pathology would be more extensive with aging.

Misfolded α-synuclein is typically phosphorylated at serine 129 and this post-translational modification is implicated in α-synucleinopathies (Fujiwara et al., 2002). Greater than 90% of α-synuclein that comprises Lewy bodies and Lewy neurites is phosphorylated at serine 129 (Sato et al., 2013) and only 4% of the soluble monomeric form has this modification (Fujiwara et al., 2002). Phosphorylation of serine 129 is the most frequent post-translational modification of α-synuclein

in Lewy bodies (J. P. Anderson et al., 2006; Fujiwara et al., 2002; Waxman et al., 2008). For these reasons, we employed antibodies against phosphorylated α-synuclein at Ser129 in our studies.

Specific Aim 1: To test whether α-synucleinopathy induced in rostral olfactory structures can be transmitted caudally into brain regions involved in Lewy body disorders. We hypothesize that some of the limbic α-synucleinopathy that develops in LBD patients may be attributable to spread from olfactory structures. Therefore we expect that fibril infusion in the OB/AON will result in the appearance of misfolded α-synuclein aggregations in deeper brain regions that harbor connections with the OB/AON, such as the amygdala and hippocampus.

Results

All images in Aim 1 are adapted from a paper published in *Molecular Neurodegeneration* (Mason et al. *Molecular Neurodegeneration* (2016) 11(1):49; doi: 10.1186/s13024-016-0113-4), and we made the raw images downloadable at Gumberg library's website: https://dsc.duq.edu/pharmacology/

Waterbath sonication increases the density of pSer129$^+$ inclusions in vivo

Mice infused in the right OB/AON region with fibrils sonicated for 1 hour in a waterbath exhibited more robust pSer129$^+$ pathology than mice infused with fibrils sonicated for 1 minute with a probe sonicator (**Figure 3, Table 1**). Longer sonication of the preformed α-synuclein fibrils reduced their size (**Figure 4**). Probe sonication is inherently less consistent than waterbath sonication, as the duration of each pulse is not easily controlled. Furthermore, probe sonication involves pausing to

prevent overheating the solution and may aerosolize toxic fibrils. Waterbath sonication is feasible even with smaller solution volumes, and the sonication occurs under water, which prevents the solution from overheating as rapidly as with a probe. The ability to sonicate closed containers also reduces the risk of human exposure.

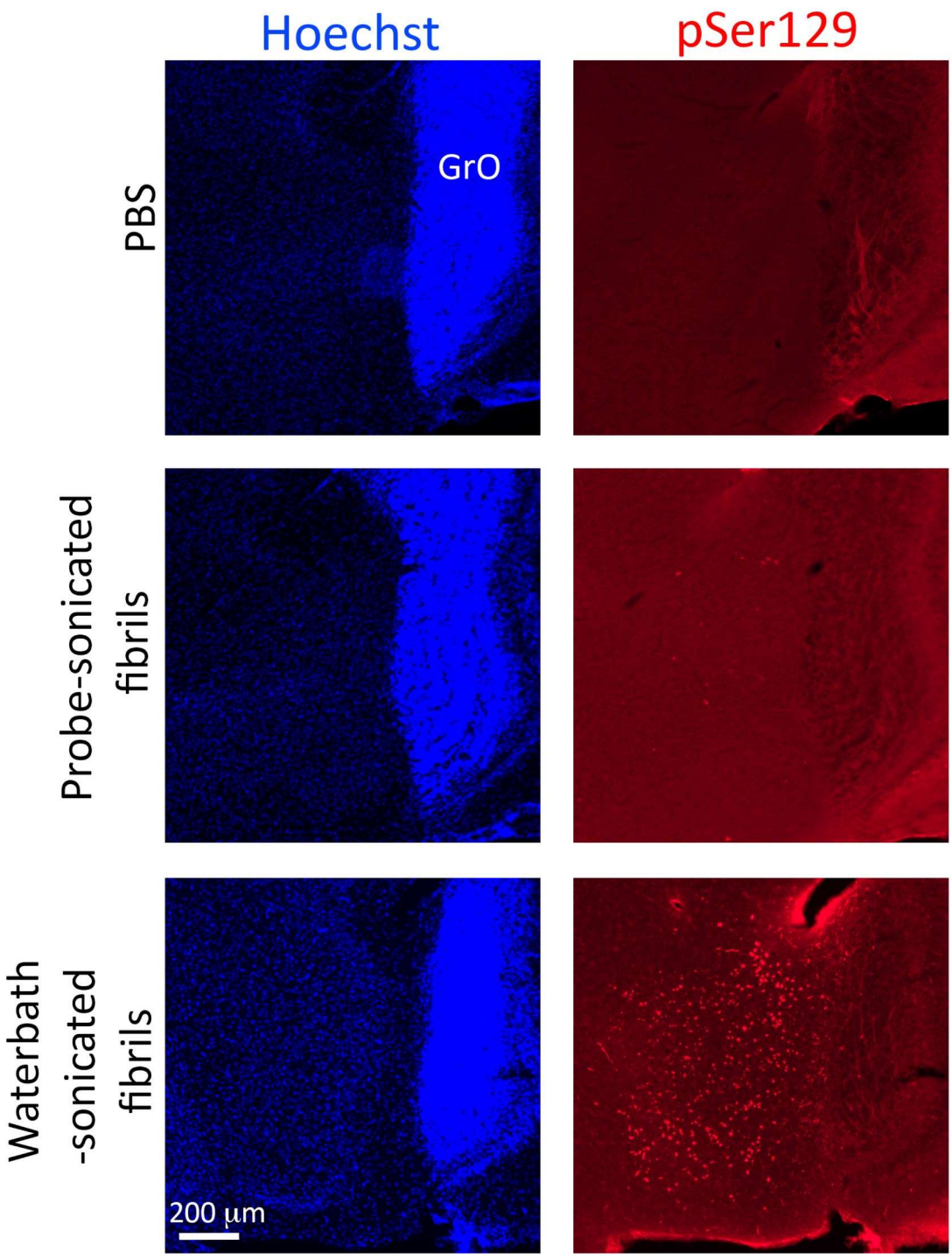

Figure 3. Waterbath sonication dramatically increases the amount of pSer129^{+} inclusions in olfactory structures 3 months after infusion of preformed fibrils. Mice were infused in the OB/AON with either PBS or 5 µg of preformed α-synuclein fibrils (1-minute probe sonicated of 1-hour waterbath sonicated). Sagittal brain sections were collected 3 months later and labeled with pSer129 (red) and Hoechst (blue). Shown is the tenia tecta, an olfactory structure caudal to the OB. Few inclusions were present in the main olfactory bulb.

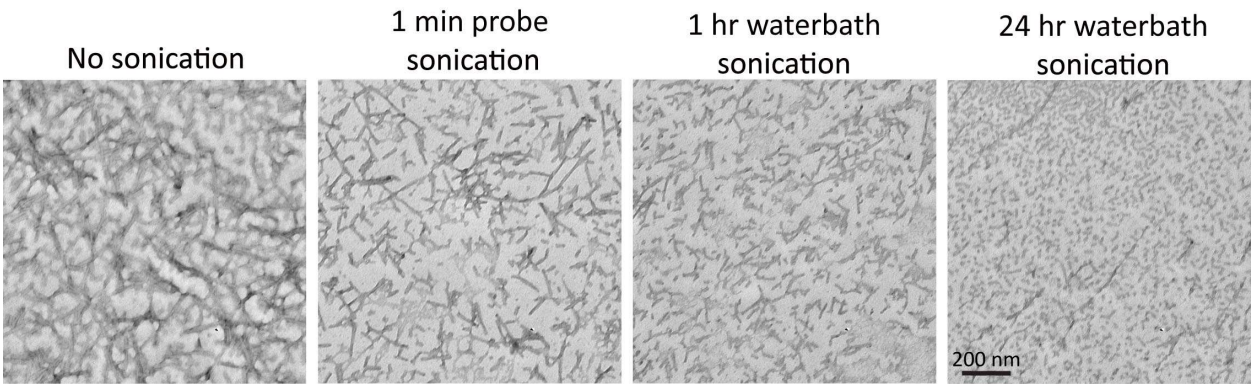

Figure 4. Preformed α-synuclein fibrils become smaller with waterbath sonication. Electron micrographs of α-synuclein fibrils before and after sonication (1 min probe sonication and 1 h or 24 h waterbath sonication). Most sonicated fibrils were positively, not negatively stained with uranyl acetate.

Unilateral injections of α-synuclein fibrils in the OB/AON lead to formation of pSer129$^+$ inclusions in neuroanatomically connected brain regions within three months post-infusion

Three months after fibril infusion into the OB/AON, the pSer129$^+$ inclusions formed most often in anatomically connected structures, such as the piriform cortex, the amygdala, the nucleus of the lateral olfactory tract, the subiculum, hippocampal CA1, and the entorhinal cortex. These structures are all key components of the limbic temporal lobe. A blinded analysis of the density of pSer129$^+$ protein aggregates revealed dramatically more pSer129 immunoreactivity in fibril-infused animals than PBS-infused animals in the olfactory peduncle (defined as the tenia tecta and AON complex), the piriform and entorhinal cortices, the amygdala, and hippocampal formation (CA1 and subiculum) (**Figure 5**). Additional pathology was also observed in some cases in hippocampal CA2/CA3, the dentate gyrus, and the ectorhinal cortex, consistent with the possibility of transynaptic spread, but pathology in these regions was sparse and not consistently observed (**Table 1**).

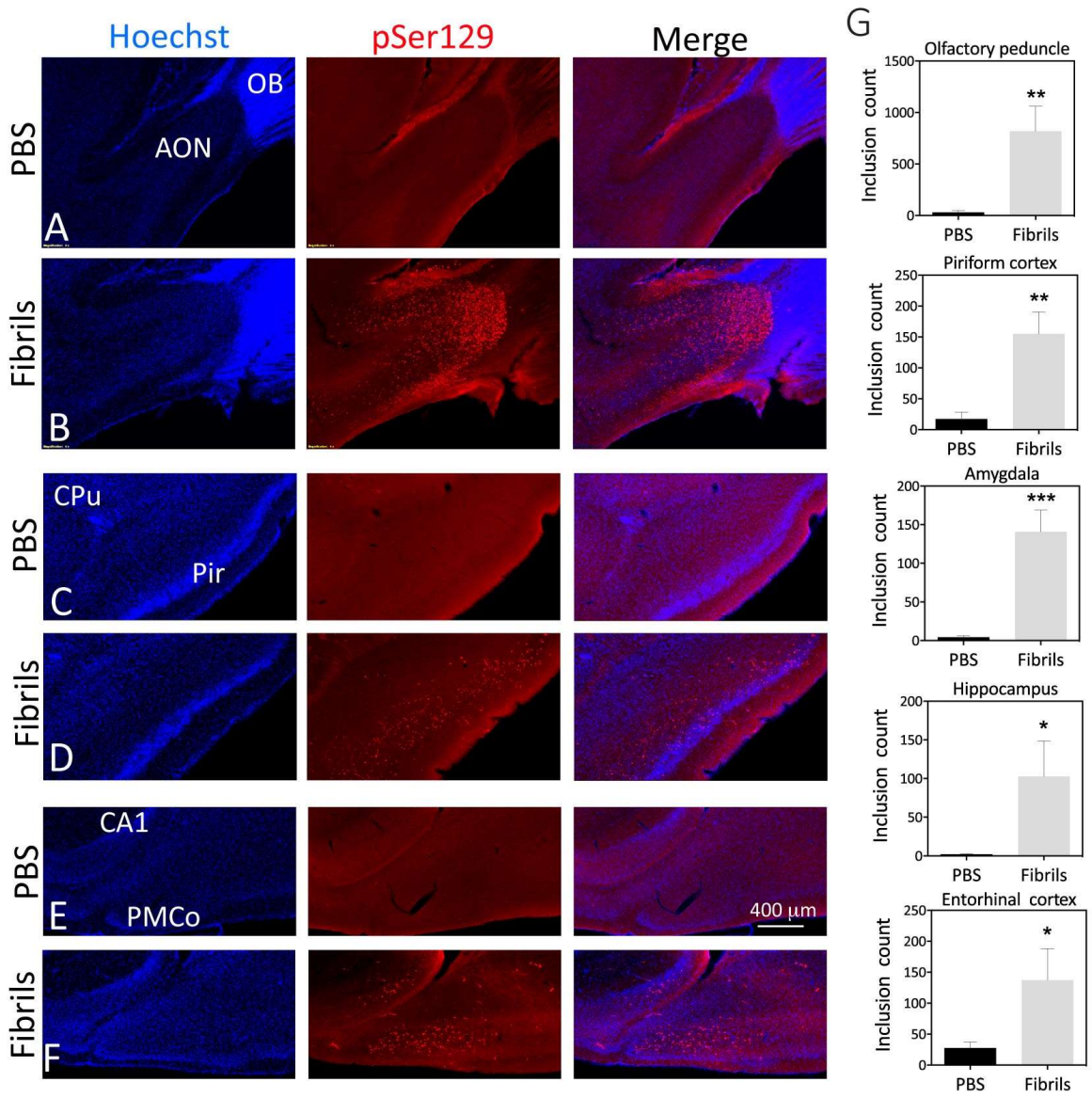

Figure 5: α-synucleinopathy is transmissible from the OB/AON to deeper brain regions. Two month-old CD1 mice were infused in the right OB/AON with α-synuclein fibrils (5 µg) or an equivalent volume of phosphate-buffered saline (1 µL). The α-synuclein fibrils were sonicated for 1 hour in a waterbath prior to infusion. After three months, sagittal brain sections were collected and immunostained for a marker of aggregated α-synuclein (pSer129; red). The Hoechst reagent (blue) was also applied to visualize nuclei. Shown are 40× images of the olfactory peduncle (**A-B**), the piriform cortex (**C-D**) and the hippocampus and amygdala (**E-F**) in PBS and fibril infused animals. pSer129^{+} inclusions were counted in ImageJ software by a blinded observer and the same threshold values were applied across all images. *$p \leq 0.05$, **$p \leq 0.01$, ***$p \leq 0.001$ vs PBS, Student's t test (n = 4–5 mice/group). All abbreviations are listed in **Table 4**.

Preadsorption of polyclonal anti-pSer129 antibody with pSer129 blocking peptide leads to a loss of immunoreactivity

To examine the specificity of pSer129 antibodies, we pre-incubated the polyclonal pSer129 antibody with pSer129 antigen and applied the "blocked" solution to the tissue. As expected, when the antigen site was already bound to a peptide, the primary antibody was unable to bind to the antigens in the tissue, leading to a loss of signal (**Figure 6**). We did not perform this test with the monoclonal mouse antibody, because preadsorption controls with monoclonal antibodies will

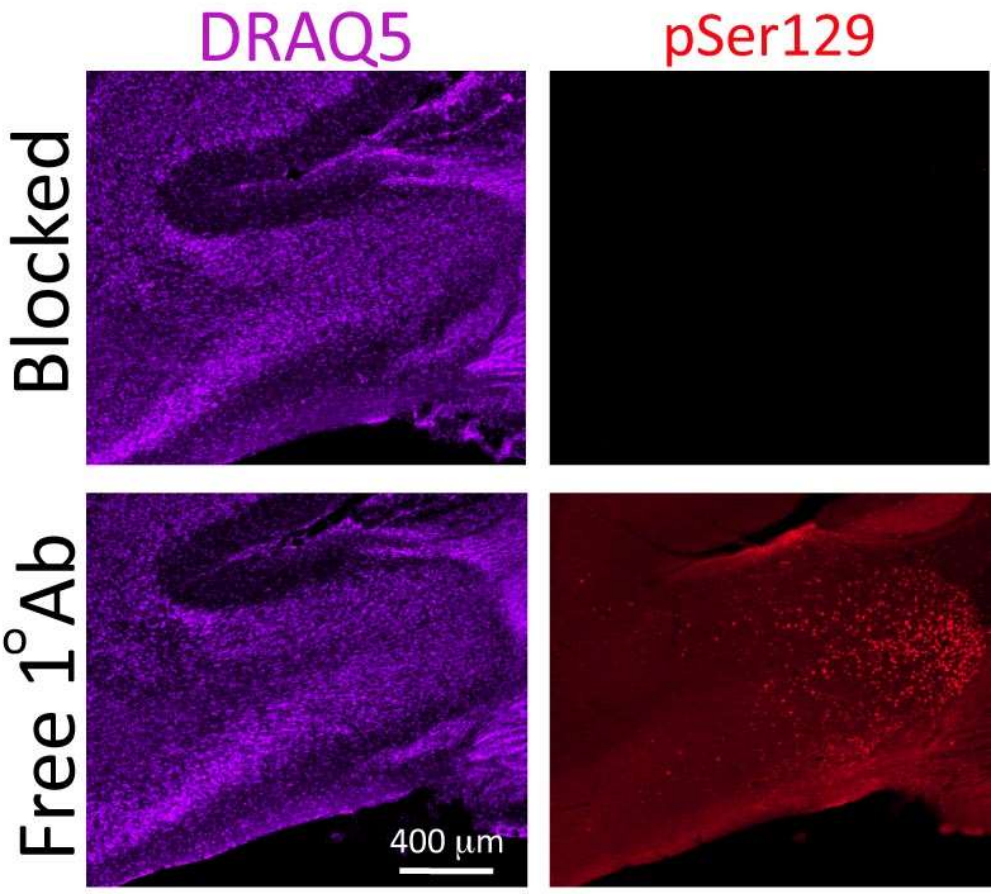

Figure 6: Polyclonal pSer129 antibody is specific for aggregated α-synuclein inclusions as demonstrated by preadsorption control. Phosphoserine129 blocking peptide was incubated with a rabbit polyclonal pSer129 antibody (Ab59264; see **Table 2**) for 24 hours prior to applying the antibody to the tissue. Shown are adjacent sagittal sections of the AON from the same animal infused with 1-hour waterbath sonicated preformed α-synuclein fibrils.

always result in a loss of labeling regardless of the presence of proteins they may bind nonspecifically in tissue (Saper, 2005). We also observed a loss of signal when primary antibodies were omitted, supporting the specificity of the fluorescent secondary antibodies used in our studies.

Immunostaining with monoclonal and polyclonal anti-pSer129 antibodies shows colocalization

We sought to test whether the monoclonal mouse and polyclonal rabbit anti-pSer129 antibodies

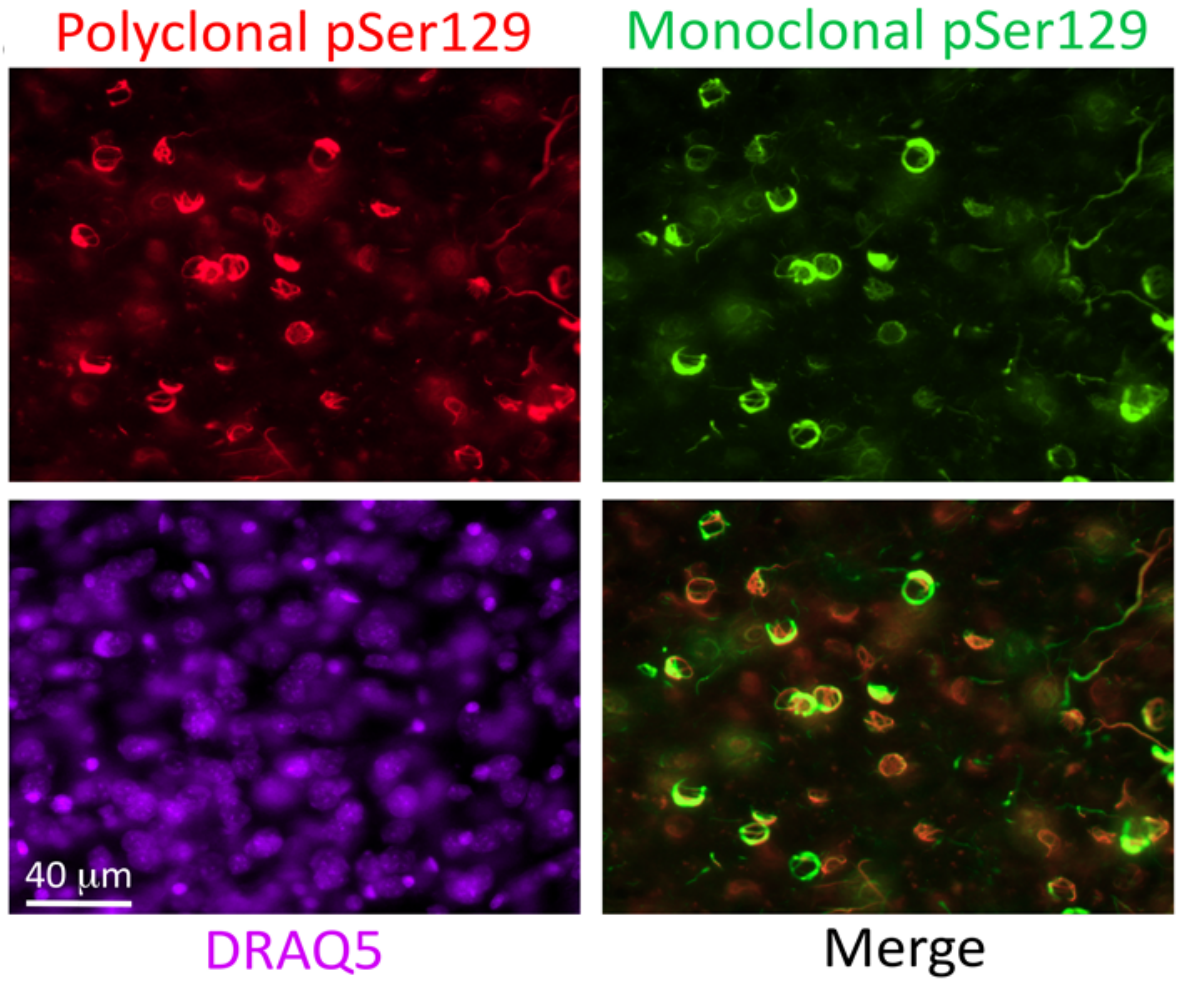

Figure 7: Monoclonal and Polyclonal antibodies show a high degree of overlap. Monoclonal pSer129 antibody (green) and polycloncal pSer129 antibody (red) (see **Table 2**) were applied simultaneously and visualized with distinct secondary antibodies. DRAQ5, an infrared nuclear stain (purple) was applied to reveal cytoarchitectonic boundaries. A few immunoreactive structures showed more staining with one antibody or the other.

are equally effective at labeling Lewy-like aggregates. In this study, we applied both antibodies simultaneously and employed different fluorescent secondary antibodies so that we could visualize

both antibodies in the same tissue. Here, we saw that both antibodies are indeed effective at labeling the aggregates and that there was considerable but imperfect colocalization of both antibodies (**Figure 7**), likely due to competition between clones with varying binding affinities (Saper, 2009).

Perinuclear pSer129^{+} aggregations form in neurons

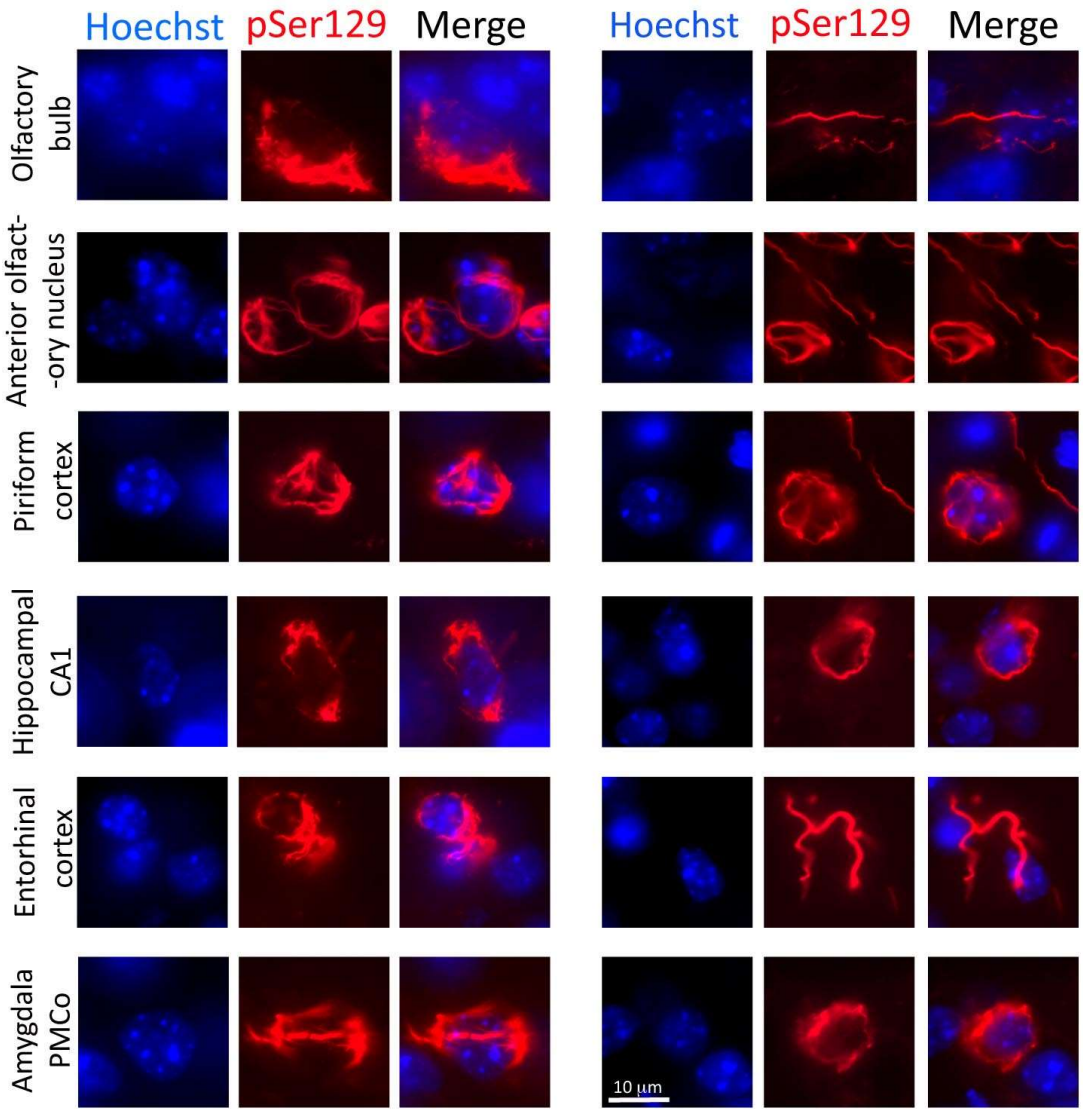

Figure 8: High resolutions images of pSer129^{+} protein aggregates display perinuclear and neuritic forms. Images of pSer129^{+} inclusions (red) (monoclonal 81A pSer129 antibody; see **Table 2**) and Hoechst-stained nuclei (blue) were captured using a 100× oil objective. The pSer129^{+} inclusions were perinuclear or found in processes. The pSer129^{+} cell in the OB (uppermost row) was in the mitral cell layer, which is known to house large somata.

In each of the primary regions of pSer129$^+$ inclusion formation (OB, AON, piriform cortex, amygdala, hippocampal CA1, and entorhinal cortex), both perinuclear inclusions and neuritic, perhaps axonal inclusions were observed (**Figure 8**). Perinuclear α-synuclein inclusions were most frequently observed within cells expressing the neuronal nuclear marker NeuN, as confirmed with a 100× oil objective (**Figure 9**). This is in agreement with human Lewy body disorders, in which Lewy aggregates are most often found within neurons, likely because α-synuclein is expressed predominantly at synaptic terminals in neurons (Iwai et al., 1995). Confocal analyses revealed that the perinuclear inclusions wrap themselves around the nuclei of NeuN$^+$ neurons (**Figure 9, right**). This dense perinuclear conformation is similar to the aggregates seen in the work of Osterberg and colleagues, who argued that these structures are the most mature form of aggregate and display

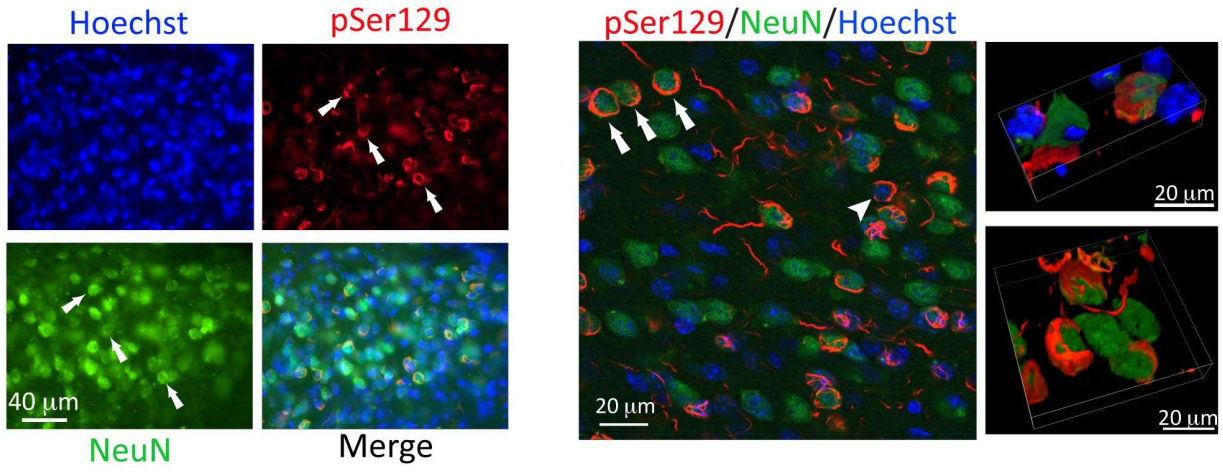

Figure 9: pSer129$^+$ protein aggregates are largely found within NeuN$^+$ cells. Two-month old mice were unilaterally infused with α-synuclein fibrils (5 µg) or an equal volume of phosphate-buffered saline (PBS) into the OB/AON. Fibrils were sonicated for 1 hour in a waterbath prior to infusion. Three months post-infusion, sagittal brain sections stained with antibodies against pSer129 (red) (monoclonal 81A pSer129 antibody; see **Table 2**) and the neuronal nuclear marker NeuN (green). Hoechst-labeled nuclei are shown in blue. (**Left**) epifluorescent microscopy. (**Right**) Confocal microscopy. Arrows point to some examples of the many triple-labeled cells in the AON. Arrowhead: Hoechst$^+$/NeuN$^-$/pSer129$^+$ profile.

post-translational hallmarks of human Lewy aggregates (Osterberg et al., 2015).

Some but not all pSer129^{+} inclusions harbor the proteasomeal degradation tag ubiquitin

To further examine the pSer129^{+} inclusions, we also stained the tissue for ubiquitin, an established marker of protein aggregations and Lewy pathology. Here, we observed that some, but not all of the perinuclear inclusions were also labeled by ubiquitin (**Figure 10**). The ubiquitin staining in the PBS group was diffuse and low in intensity, while the ubiquitin staining in the fibril-infused animals was compact and intense. The Thioflavin S stain for amyloid protein aggregates was also

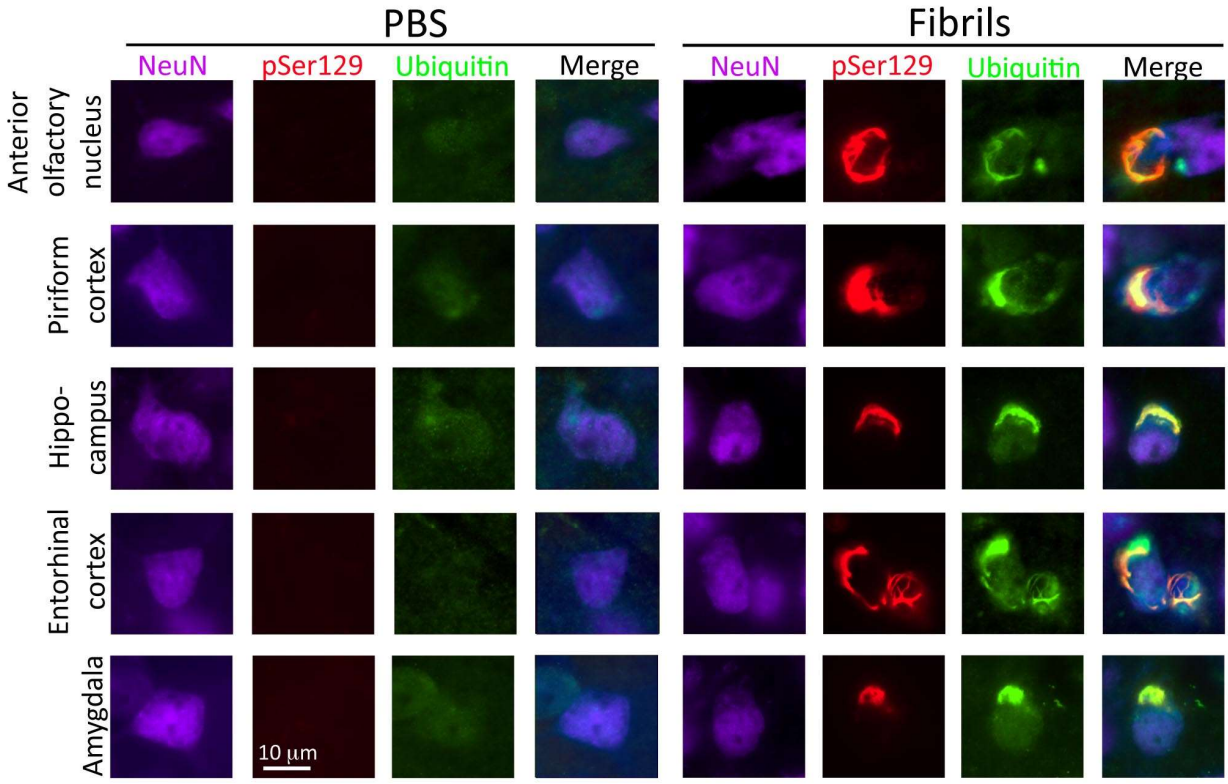

Figure 10: α-synucleinopathy is found within neuronal somata and some of it colocalizes with the ubiquitin marker of protein aggregates. Mice were infused in the OB/AON with 5 µg of 1-hour waterbath sonicated preformed α-synuclein fibrils and sacrificed three months later. Some but not all of the pSer129^{+} (red) protein aggregates colocalized with ubiquitin (green) in NeuN^{+} (purple) neurons. Antibodies are listed in **Table 2**. Photos from fibril and PBS treated animals were captured at the same exposure and intensity scaling.

applied to the tissue. With this stain, densely labeled structures were visible at the site of infusion and some diffuse labeling was present in the rostral OB (**Figure 11**). Few to no Thioflavin S^+ structures were visible in brain regions distant from the site of injection.

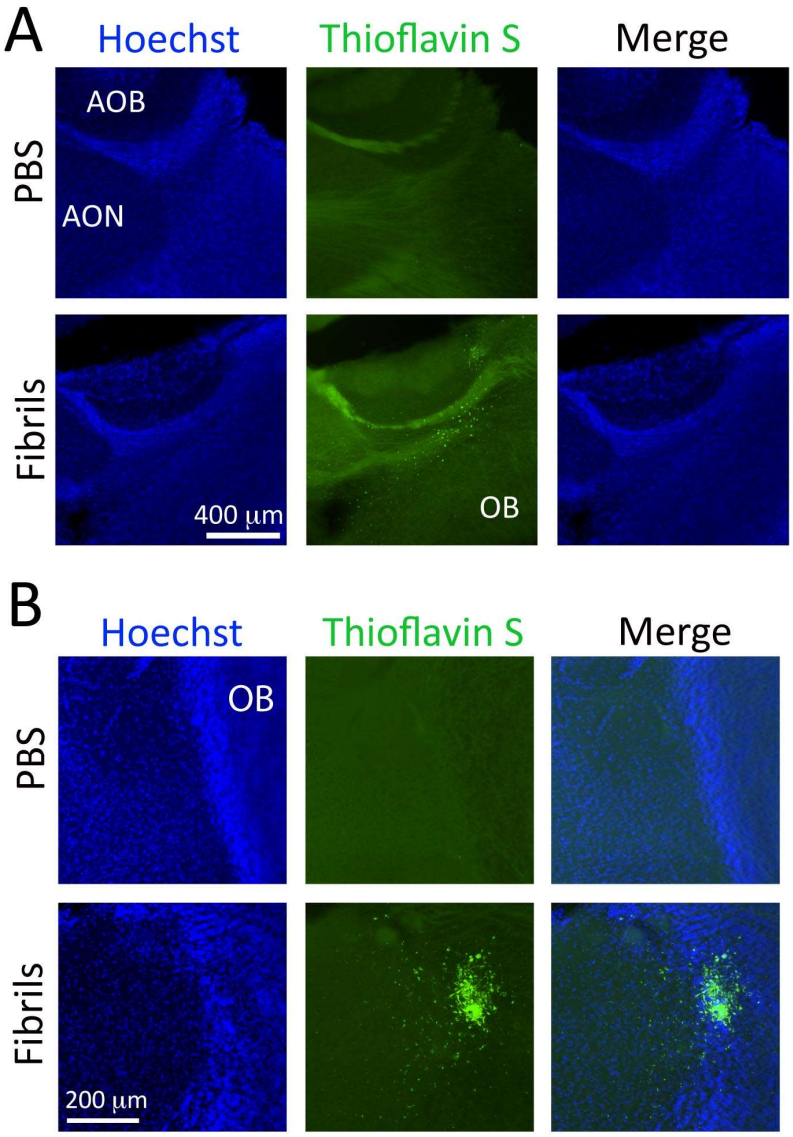

Figure 11: Amyloid stain Thioflavin S is only apparent at or very near the site of fibril injection. Mice were infused in the OB/AON with α-synuclein fibrils that were sonicated for 1 hour or PBS. Sagittal brain sections were labeled with Thioflavin S stain for amyloid (green) and Hoechst (blue). (**A**) Faint Thioflavin S stain is visible in the olfactory bulb rostral to the site of injection. (**B**) Dense Thioflavin S stain is visible at the site of injection in the dorsal OB. All abbreviations are listed in **Table 4**.

pSer129^{+} aggregations are likely formed from endogenous and not exogenous α-synuclein molecules

In order to define the site of injection, we injected 1-hour waterbath sonicated preformed α-synuclein fibrils into the OB/AON and sacrificed the mice 90 minutes later. This tissue was immunostained for pSer129 and total α-synuclein. Previous work has demonstrated that the preformed α-synuclein fibrils are not phosphorylated (Luk et al., 2009). In agreement with these findings, we did not observe any pSer129 immunoreaction 90 minutes after injection of the fibrils

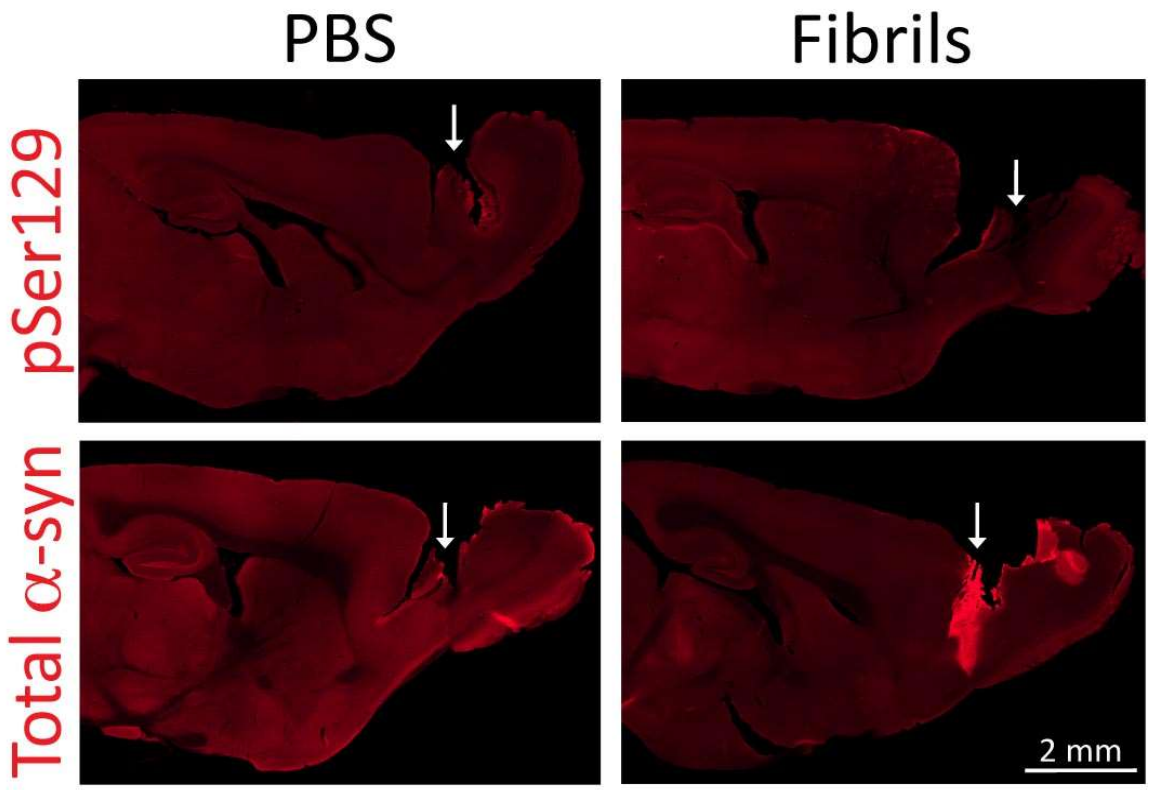

Figure 12: pSer129^{+} aggregates are absent from tissue 90 minutes after infusion. Mice were infused in the OB/AON with 5 µg α-synuclein fibrils (1 h waterbath-sonicated) or PBS and perfused 90 minutes later. Brain sections were stained with rabbit antibodies against phosphorylated or total α-synuclein (red) (see **Table 2**). The needle track is still apparent in the caudal OB at this early time point (white arrows. Images from PBS and fibril groups were captured at the same intensity scaling and exposure times. Differences in background staining are not the result of differential image processing.

into the OB/AON (**Figure 12**). Instead, these animals exhibited dense signal for total α-synuclein protein (non-phosphorylated) at the site of injection, in the caudal OB, which suggests that the preformed α-synuclein fibrils may encourage endogenous mouse α-synuclein molecules to misfold and adopt a pathogenic conformation.

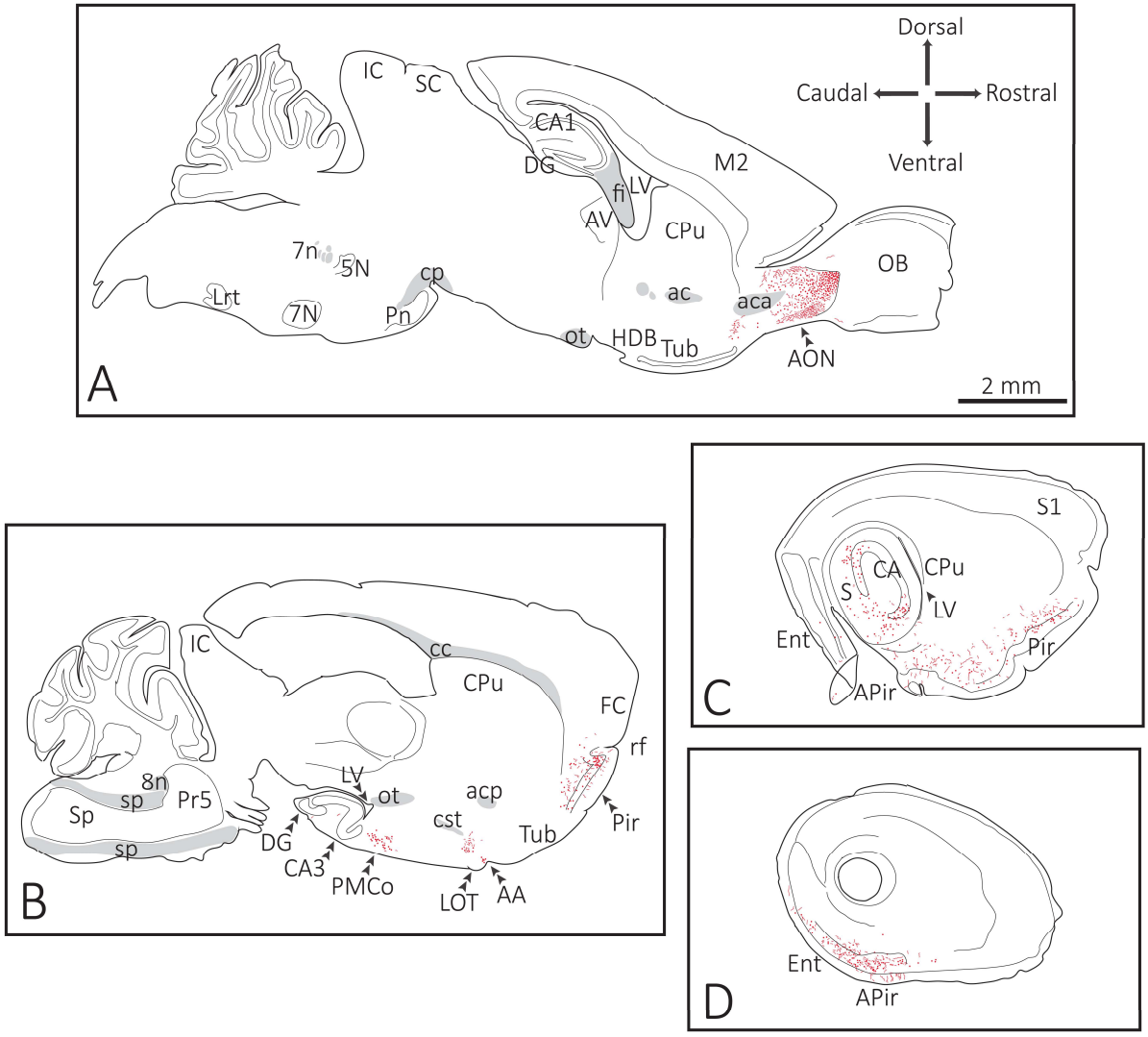

Figure 13: α-synucleinopathy is transmitted from the OB/AON to deeper limbic structures. Two-month old CD1 mice were infused unilaterally on the right side in the OB/AON with α-synuclein fibrils (5 µg) or an equivalent volume of phosphate buffered saline (PBS). Sagittal schematics of clearly visible brain cytoarchitectonics (solid lines), myelinated fiber bundles (gray shading), and pSer129^{+} neurites (red flourishes), and pSer129^{+} somal inclusions (red dots) are provided. The sections go from medial to lateral (**A-D**). All abbreviations are listed in **Table 4.**

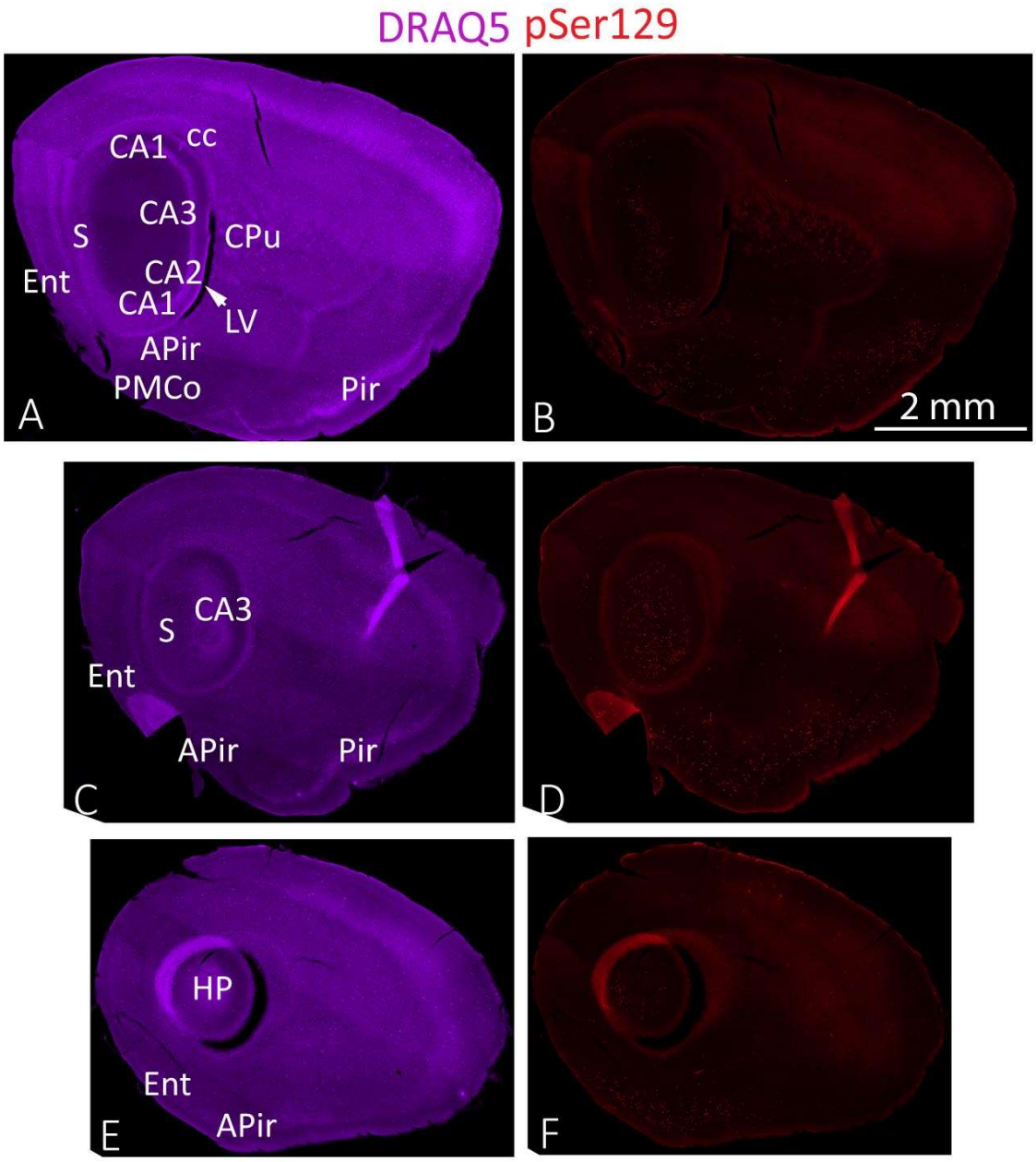

Figure 14: α-synucleinopathy is transmitted to limbic structures three months post-infusion. Two-month old mice were infused unilaterally in the OB/AON with α-synuclein fibrils that had been sonicated for 1 hour. After three months, sections were collected and stained for DRAQ5 (**A**,**C**,**E**) and pSer129 (**B**,**D**,**F**) (monoclonal 81A pSer129 antibody; see **Table 2**). The sections go from medial to lateral. Abbreviations are available in **Table 4**.

Sagittal schematics were generated to display the typical pattern of pSer129^{+} α-synucleinopathy in the ipsilateral hemisphere three months after infusion of 1-hour waterbath sonicated preformed α-synuclein fibrils (**Figure 13**). The most densely labeled region at this time point is the AON (**Figure 13A**). In more lateral sections, the rostral piriform cortex, nucleus of the lateral olfactory tract, posteromedial cortical amygdala, and ventral hippocampus exhibit pSer129^{+} pathology (**Figure 13B**). In lateral sections, pathology is also apparent throughout the piriform cortex and most of the amygdala. At this mediolateral level, the hippocampal CA1 and subiculum are the most densely affected regions of the hippocampus (**Figure 13C**). More laterally, the entorhinal cortex also exhibits dense pathology (**Figure 13D**). Overall, the pathology remains centered in the limbic system.

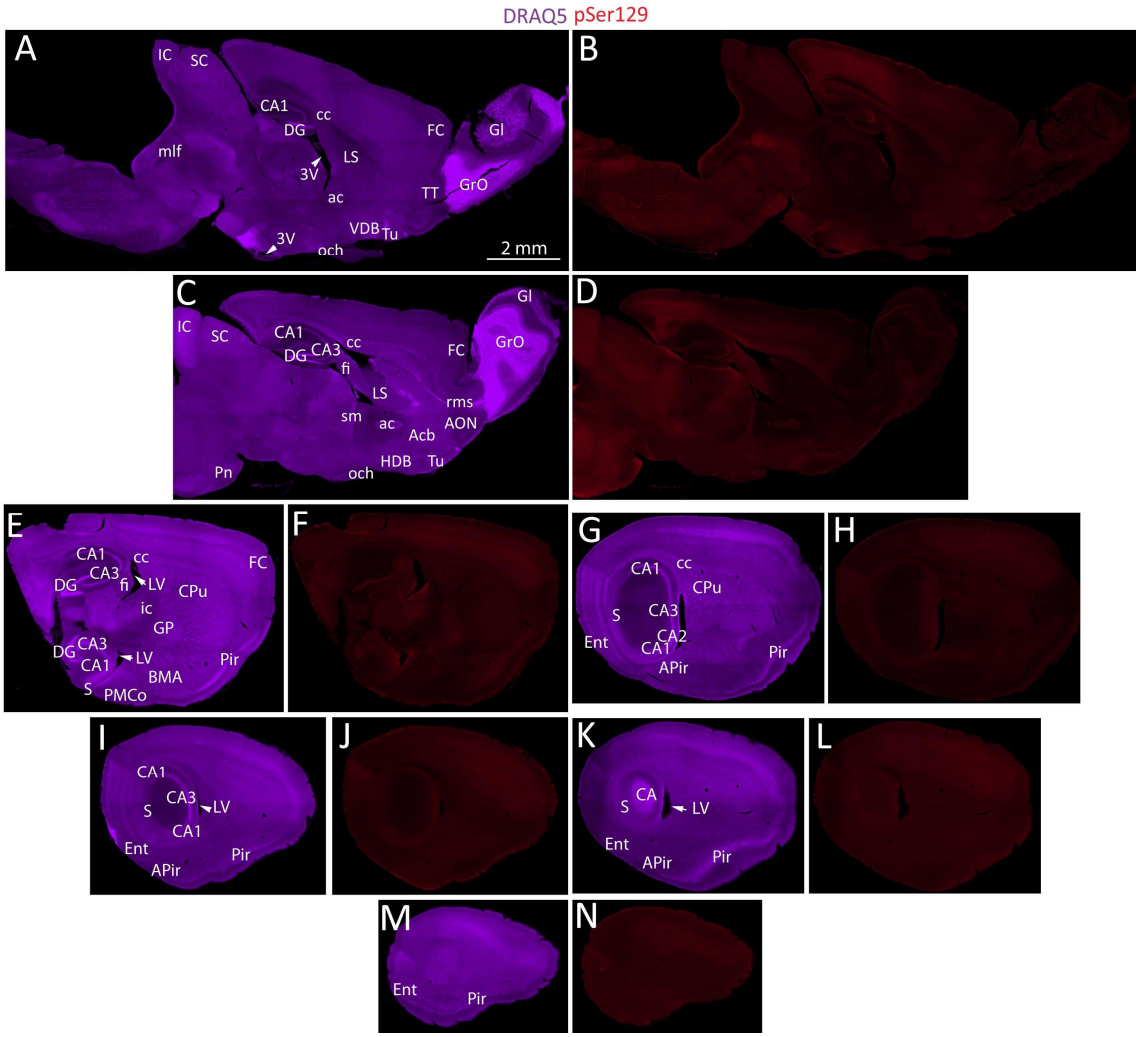

Figure 15: No pSer129^{+} structures are visible in PBS infused animals. Mice were infused with phosphate buffered saline (PBS) in the OB/AON. Three months post-infusion, sagittal brain sections were stained for pSer129 (**B,D,F,H,J,L,N**) (monoclonal 81A pSer129 antibody; see **Table 2**) and Draq5 (**A,C,E,G,I,K,N**). All abbreviations are listed in **Table 4.**

The sagittal schematics were generated based on the pSer129^{+} pathology visible in stitched images of the entire brain section. Examples of the stitched images used to generate these schematics are provided in **Figure 14**. PBS-infused sections are also provided to display the lack of pSer129^{+} inclusions in animals that were not infused with the preformed α-synuclein fibrils and to show the degree of background staining (**Figure 15**).

Examining first-order connections between brain regions with the tract-tracer FluoroGold

In order to label first-order afferent neurons that project directly to the injection site, the retrograde tracer FluoroGold was employed. Robust FluoroGold labeling of neurons was evident at all sites where inclusions were present, with the exception of occasional, sparse pSer129 inclusions in the nucleus accumbens, caudoputamen, CA2/CA3, dentate gyrus, and ectorhinal cortex (**Figure 16, Table 1**). Fluorogold^{+} neurons were also present at the horizontal limb of the diagonal band of Broca, which is known to project to the AON, but did not exhibit any pSer129^{+} inclusions. The olfactory tubercle, which does not project to the OB/AON, remained free of FluoroGold label as

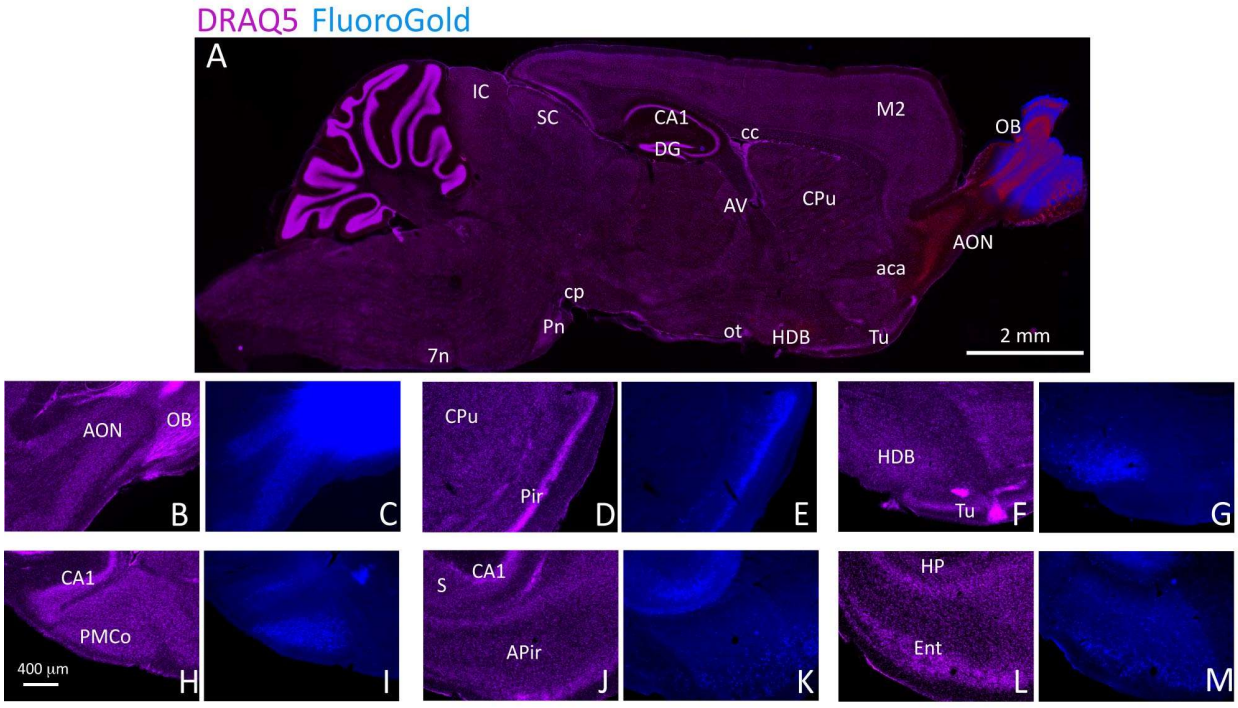

Figure 16: Areas that develop α-synuclein aggregates send first-order projections to the site of infusion in the OB/AON. The animals were infused at the same coordinates as the α-synuclein fibrils with the retrograde tract-tracer FluoroGold and perfused after seven days. The nuclear marker DRAQ5 (purple) was used to visualize cytoarchitecture and FluoroGold (blue) was visualized in the UV channel. The dual stained brain regions in (**A**) appear red. Dense FluoroGold label at multiple afferent sites is displayed at higher magnification in panels **C, E, G, I, K,** and **M**. Nuclear DRAQ5 label on the same sections is shown in panels **B, D, F, H, J**, and **L**. Abbreviations are available in **Table 4**.

well as pSer129^{+} inclusions, suggesting perhaps that the pathology travels most frequently in a retrograde direction.

α-synucleinopathy is primarily confined to first-order neuroanatomic connections in the limbic system three months after infusion of α-synuclein fibrils into the OB/AON

To display the variability of the pSer129 and FluoroGold staining among all animals in the study, a blinded observer semi-quantitatively rated the pathology after observing all of the tissue. The observer rated the pathology on a scale of 1-5 (1 = very sparse, 5 = very dense) (**Figure 17**), so that the pathology could accurately be displayed in tabular format (**Table 1**). It was evident that waterbath sonication led to a much more robust pattern of inclusion formation than probe sonication. In the waterbath sonicated fibril-infused animals, the pattern of aggregation

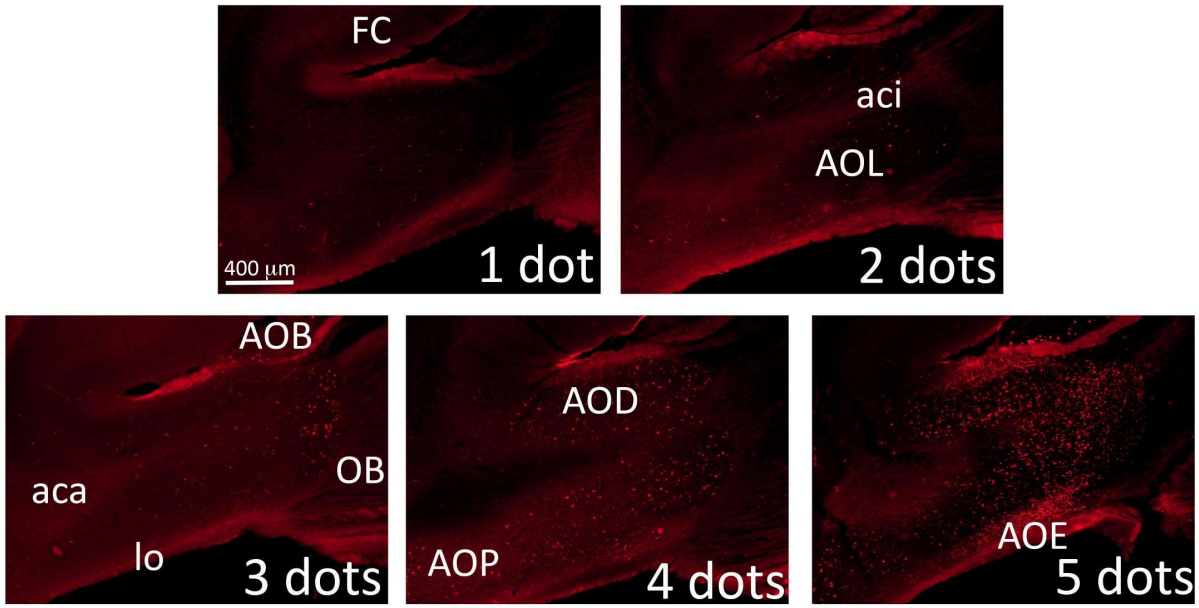

Figure 17: A blinded observer scored the inclusion density semi-quantitatively. Phospho-serine129 and FluoroGold labeling was semi-quantitatively described in both the ipsilateral and contralateral hemispheres. Shown is the range of inclusion density from "1 dot" (low density) to "5 dots" high density in the anterior olfactory nucleus three months after fibril infusion. All abbreviations are listed in **Table 4**.

development was similar among the different age groups, except that more inclusions developed in the nucleus accumbens of the 17-month-old animals (**Table 1**).

Generalizability of the model: Waterbath-sonicated α-synuclein fibrils also generate robust pathology upon injection into the hippocampus

		α-synuclein fibrils														FluoroGold				
		Probe-sonicated			Waterbath-sonicated															
		2 mo	2 mo	2 mo	2 mo	2 mo	2 mo	2 mo	2 mo	5 mo	5 mo	5 mo	17 mo	17 mo	17 mo	17 mo	2 mo	2 mo	2 mo	2 mo	2 mo
Region	**Hemisp**	15-327	15-329	15-330	15-332	15-333	15-334	15-340	15-341	15-439	15-441	15-443	15-445	15-447	15-449	15-451	15-452	15-453	15-454	15-455	15-456
Olfactory bulb	Ipsi (R)	•	•	•	•	•	••	•	•	•	•	•	••	••	••	•	•••••	•••••	•••••	•••••	•••••
	Contra	•	-	•	-	-	-	•	-	-	-	-	-	••	••	-	-	-	-	-	-
Anterior olfactory nucleus	Ipsi (R)	••	•	•	••••	••••	•••••	••	•••	•••	•••••	•	•••••	••••	•••••	•••••	•••••	•••••	•••••	•••••	•••••
	Contra	•	-	•	•••	••••	•••••	••	•	••	•••	•	•••••	••	••••	•••	•••••	•••••	•••••	•••••	•••••
Frontal cortex	Ipsi (R)	-	-	-	•	••	•	-	-	-	•••	-	•	-	•	•	-	••••	•••••	••	•••••
	Contra	-	-	-	-	-	•	•	-	-	•	-	•	-	-	-	-	••	•••	-	-
Accumbens	Ipsi (R)	-	-	-	-	-	-	-	-	-	•	-	•••	•	•••	•	-	-	-	-	-
	Contra	-	-	-	-	-	-	-	-	-	-	-	•	-	•	-	-	-	-	-	-
Caudoputamen	Ipsi (R)	-	-	-	-	•	•	-	-	-	-	-	•	-	-	•	-	-	-	-	-
	Contra	-	-	-	-	-	-	-	-	-	-	-	-	-	-	-	-	-	-	-	-
Horizontal limb of the diagonal band	Ipsi (R)	-	-	-	-	-	-	-	-	-	-	-	-	-	-	-	••	•••	•••	•••	•••
	Contra	-	-	-	-	-	-	-	-	-	-	-	-	-	-	-	-	-	-	-	-
Olfactory tubercle	Ipsi (R)	-	-	-	-	-	-	-	-	-	-	-	-	-	-	-	-	-	-	-	-
	Contra	-	-	-	-		-	-	-	-	-	-	-	-	-	-	-	-	-	-	-
Piriform cortex	Ipsi (R)	•	•	•	•••	•••••	•••••	••••	••	•••	••••	••	•••••	•••	•••••	•••••	••••	••••	••••	••••	•••••
	Contra	-	-	•	•	••	•••	•	•	•	•••	-	•••	•	••	•	••	••	•••	••	•••
Nucleus of the lateral olfactory tract	Ipsi (R)	-	-	–	•	•••	••••	••	••	•	•••	•	•••	••	••••	••	••••	•••	•••	••	•••
	Contra	-	-	-	•	•	•••	•	-	-	•	-	•	-	•	•••	•••	••	••	-	••
Cortical amygdaloid nuclei	Ipsi (R)	-	-	–	••	••••	••••	•••	••	•	•••••	-	••••	•••	••••	••••	••••	•••	••••	•••	••••
	Contra	-	-	-	-	••	•	-	-	-	•	-	••	-	-	••	••	•	••	•	••
Amygdalo-piriform transition area	Ipsi (R)	•	-	-	••••	••••	•••	••••	••	•	••	-	••••	•••	•••	••••	•••	••	•••	•	•••
	Contra	-	-	-	•	••	•	•	-	-	•	•	••	-	•	•	•	-	-	-	-
Hippocampus (CA1)	Ipsi (R)	-	-	-	••	••••	•••	••	•	•	••••	-	•••	•	••	•••	••	••	•••	••	•••
	Contra	-	-	-	-	•	-	-	-	-	•	-	•	-	-	•	-	-	-	-	-
Hippocampus (CA2/CA3)	Ipsi (R)	-	-	-	•	•••	••••	•	-	•	•••	-	••	-	•	•	-	-	-	-	-
	Contra	-	-	-	•	•	-	•	-	-	-	-	•	-	•	-	-	-	-	-	-
Hippocampus (dentate gyrus)	Ipsi (R)	-	-	-	•	•	•	•	•	-	•	-	••	-	••	•	-	-	-	-	-
	Contra	-	-	-	•	•	•	-	-	-	-	-	•	-	-	-	-	-	-	-	-
Subiculum	Ipsi (R)	-	-	-	•	••••	•••	••	•	•	••••	-	•••	•	••	••	•	•	••	-	••
	Contra	-	-	-	•	•	-	-	-	-	•	-	••	-	-	•	-	-	-	-	-
Entorhinal cortex	Ipsi (R)	•	-	-	•••••	•••••	•••	•••	••	•	••••	-	•••••	•••	••••	••••	•	•	•••	••	••
	Contra	-	-	-	••	••	-	•	-	•	••	-	•••	-	•	•	-	-	•	-	•

Table 1: Schematic of pSer129$^+$ inclusions from probe and waterbath sonicated fibrils three months after infusion and FluoroGold seven days after infusion. CD-1 mice were infused in the OB/AON with α-synuclein fibrils and sacrificed three months later. Separate mice were infused in the same region with FluoroGold and sacrificed seven days later. Animal IDs, are shown in the 4th row. Semi-quantitative density of label in the ipsilateral (red) and contralateral (black) hemispheres from * to ***** (sparsest to densest) of pSer129 (monoclonal 81A pSer129 antibody; see **Table 2**) or Fluorogold label is shown for individual mice. The animal age at the time of infusion is also provided.

To ensure that our fibril sonication protocol was reproducible in a separate set of neuroanatomical circuits, we prepared the fibrils in the exact same manner and injected them into the CA2/CA3 region of the hippocampus. To see if additional sonication in the waterbath would change the pathogenic characteristics of the fibrils, we also included a cohort of mice that were infused with fibrils sonicated for 24 hours. For this study, the perfused brains were cut coronally so that we could view the bilateral hippocampal formation. In the PBS-infused animals, little pSer129^{+} pathology was observed in the hippocampus (**Figure 18A**). Fibril-infused animals exhibited dense pSer129^{+} inclusions throughout the hippocampus and in the entorhinal cortex, which is suggestive of transmission of α-synuclein pathology through the perforant path (**Figure 18B**). The hippocampal pathology was more robust in the 1-hour sonicated fibril group than the 24-hour sonicated fibril group, perhaps because the fibrils became so small that there were easily degraded and could not serve as a template for seeding pathology.

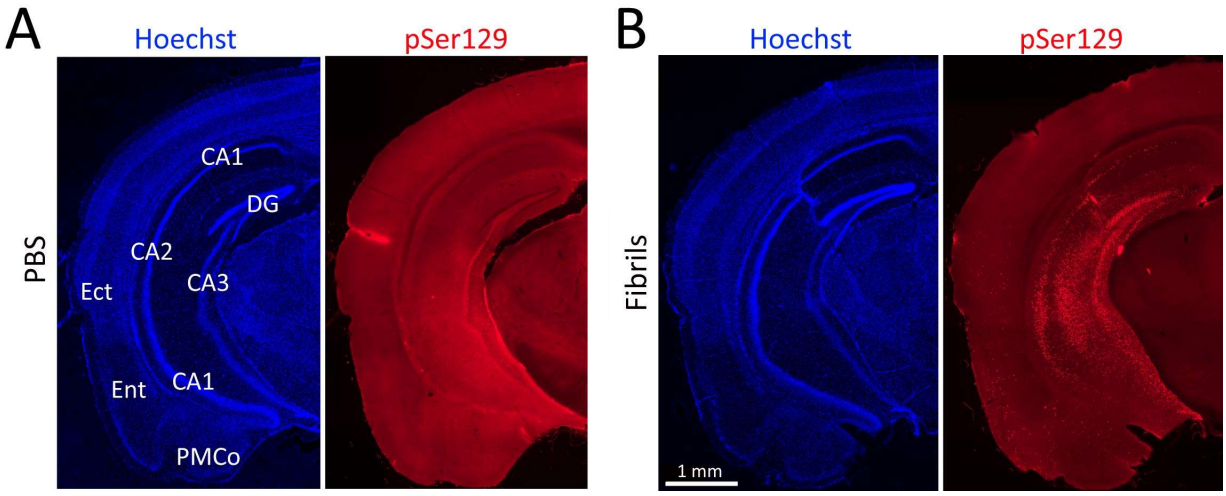

Figure 18: Waterbath sonicated α-synuclein fibrils also elicit robust pathology after infusion into the hippocampus. Two month-old mice were unilaterally infused with PBS (**A**) or α-synuclein fibrils (5 µg) (**B**) into CA2/CA3 of the hippocampus. Fibrils were sonicated for one hour in a waterbath prior to infusion. Three months later, coronal brain sections were collected. Shown are stitched montages of pSer129 (monoclonal 81A pSer129 antibody; see **Table 2**) and Hoechst staining in the hippocampus and entorhinal cortex in PBS and fibril-infused animals—both groups were stained in parallel and captured at the same exposure and intensity scaling. The fibril injection in this animal extended from CA2/CA3 into CA1. All abbreviations are listed in **Table 4**.

Discussion

We have demonstrated that α-synucleinopathy initiated in the OB/AON region can be transmitted to regions as distant as the hippocampus and entorhinal cortex within three months. Many of these regions are most often affected at the mid to end stages of PD, and pathology in these regions is commonly associated with cognitive dysfunction (Gomperts, 2016; Russell et al., 2014). This suggests that some of the pathology at the later stages of PD may be attributable to spread from olfactory structures. While the pattern of transmission outlined in this aim is not completely representative of PD, it concurs with Beach's Stage IIB limbic-predominant subset of Lewy body disorders (Beach, Adler, et al., 2009). There are indeed cases of DLB where pathology is primarily present in the limbic system (Nelson et al., 2010), and Lewy pathology in Alzheimer's disease is also largely confined to the limbic system (Beach, Adler, et al., 2009; Toledo et al., 2016). As discussed in the Introduction, according to Braak staging and the DLB consortium staging, approximately two-thirds of unclassifiable patients had pathology in the limbic system in the absence of pathology in the brainstem (Beach, Adler, et al., 2009). Therefore, our model may mimic the neuroanatomical features of a distinct subset of Lewy body disorders.

The limbic system is most commonly associated with maintaining emotional equilibrium, but it is also critical to learning and memory functions (Hyman et al., 1990; Zola-Morgan & Squire, 1993), and is involved with regulating endocrine and autonomic functions (Braak et al., 1994). Among other regions, the limbic system includes the amygdala, hippocampal formation, and entorhinal allocortex. These three regions are highly interconnected and project to the nucleus accumbens and some subdivisions of the caudoputamen (Del Tredici K, 2000-2013). While the

histopathological pattern of α-synucleinopathy in our model is not typically observed in PD, regions of the limbic system are often the most affected by Lewy-related lesions (Braak & Braak, 2000; Braak et al., 1994). Damage to higher order centers of the limbic system may contribute to affect-related dysfunction of emotional and voluntary motor systems, which are commonplace in the end stages of PD (Del Tredici K, 2000-2013). Our model most closely resembles the prototypical spread of α-synucleinopathy observed in what used to be defined as the Lewy body variant of Alzheimer's disease and is now known as ADLB. These observations suggest that some of the cognitive impairments of ADLB may be related to limbic α-synucleinopathy.

Within the hippocampus, FluoroGold$^+$ cells as well as the majority of pSer129$^+$ inclusions were present in the CA1 and subiculum regions. In PD and DLB, the CA2 field of the hippocampus develops the densest Lewy pathology (Adamowicz et al., 2017; Del Tredici K, 2000-2013), which suggests that pathology in CA2 is not transmitted from olfactory structures. In Alzheimer's disease, tau pathology is frequently highest in CA1 and the subiculum (Lace et al., 2009; Masurkar, 2018), suggesting that tau pathology may transmit along the olfactory/limbic route in humans.

The results of the FluoroGold tract-tracer experiments are consistent with the view that the spread of pathology in our model might be largely in a retrograde direction. Almost every brain region with FluoroGold$^+$ signal also developed Lewy-like inclusions, suggesting that the majority of the pSer129$^+$ inclusions may develop in the axon and travel to the cell body. One exception was the horizontal diagonal band of Broca, which appears to be resistant to the development of pSer129$^+$ protein aggregates despite sending dense projections to the OB/AON. The horizontal limb of the diagonal band of Broca is the primary source of cholinergic projections to the OB (Godfrey et al.,

1980), and perhaps cholinergic neurons are more resistant to developing pSer129^{+} inclusions. High-resolution microscopy demonstrated that the perinuclear inclusions are often wrapped around the nucleus in the cell body, and it may not be energetically favorable for a large aggregation to disengage from the nucleus and travel through an axon in an anterograde direction. This view is also supported by the observation that no inclusions developed in the olfactory tubercle at three months post infusion. The AON, which exhibited robust pSer129^{+} pathology, has many synapses at the olfactory tubercle, but the olfactory tubercle does not project back to the AON. Therefore, the lack of inclusions in the olfactory tubercle supports the speculation that α-synucleinopathy in this model may travel from the synapse to the cell body.

We have demonstrated that this model generates a consistent pattern of pathology in cohorts of various ages and that 1-hour waterbath sonicated PFFs can generate robust pathology after injection into a separate set of neuroanatomical circuits (i.e., the CA2/CA3 fields of the hippocampus). This is important because Lewy body disorders are heterogeneous diseases and Lewy pathology is rarely confined to a single brain region in patients. The ability to induce robust pathology in a variety of brain regions is important to further our understanding of the implications of regional Lewy pathology on symptom development and transmissibility. Robust Lewy-like pathology is also essential to adequately assess the efficacy of therapies against the development and spread of Lewy pathology.

The experiments in this aim clearly demonstrate that it is possible to generate robust α-synuclein pathology in wild-type mice. It was worth optimizing our sonication parameters *in vivo* as we demonstrated that an inexpensive waterbath sonicator (~300$) was more effective at generating

robust pathology than is evident in the literature, even when powerful probe sonicators costing thousands of dollars are employed. The pathology generated from waterbath-sonicated preformed α-synuclein fibrils is so dense that it is visible even at low magnification. Other groups in the field typically present pathology in images that are highly magnified and without the context of the entire brain section. Here, we have pioneered publishing large, high-resolution images of entire brain sections so that readers may zoom in and out as with a street map to determine the location and scale of the Lewy-like pathology. As computational power and image data storage methodologies improve, it is likely that scientific journals will transition to requiring such images for the independent verification of the topographical distribution of pathology.

It is unlikely that we misidentified α-synuclein pathology, as we confirmed the efficacy of our methodology in several ways. The preadsorption control, the co-application of both antibodies to the same tissue, and the overlap with ubiquitin support the conclusion that the immunolabeled structures are genuine inclusions. However, there are several limitations that must be acknowledged. First, there are obvious differences between rodent olfactory structures and human olfactory structures. Rodents rely heavily on olfaction and, consequently, the olfactory structures make up a relatively large portion of the rodent brain. It is therefore possible that the development of Lewy-like pathology in rodent olfactory structures is more aggressive than it would be in humans. Furthermore, the preformed α-synuclein fibrils are made from wild-type mouse α-synuclein, which harbors the A53T mutation that is reported to increase susceptibility of humans to developing Lewy body disorders. The endogenous α-synuclein in CD-1 mice also has this mutation, which suggests that the development and spread of aggregates in this model may be more aggressive than it is in the majority of human Lewy body disorders. As mice have a typical

lifespan of approximately two years, a more aggressive form of α-synucleinopathy is likely necessary to generate significant pathology within their lifespan. While we are confident in our identification and characterization of pSer129^{+} inclusions, a recent study indicated that even the most sensitive and specific commercially available anti-pSer129 antibodies also display non-specific bands in Western blots (Delic et al., 2018), which is discussed further in Aim 2.

Chapter 2

Rationale

In Aim 1, we developed a novel model of early stage Lewy body disorders. After infusion into the OB/AON, dense α-synucleinopathy emerges in olfactory/limbic structures within three months. This pattern of olfactory-initiated limbic pathology is similar to the Stage IIb pathology described by Beach and colleagues. This unified staging system proposes that after appearance in the pathology in the olfactory structures (Stage I), pathology then emerges in either brainstem predominant (Stage IIa) or limbic predominant (Stage IIb) patterns (Beach, Adler, et al., 2009). The Stage IIb pattern is observed in cases of ILBD and DLB, but most often in ADLB. Indeed, Toledo and colleagues observed that coincident α-synucleinopathy in demented subjects with AD most frequently begins in the OB and progresses through the limbic system while sparing the brainstem (Toledo et al., 2016).

As the pathological distribution of α-synucleinopathy in our model corresponds to a distinct subset of human patients (Beach's Stage IIb), the goal of this Aim is to examine this model in the context of two major risk factors for developing Lewy body disorders, age and gender. As discussed in the

introduction, age is the strongest risk factor for developing PD (Bennett et al., 1996; Morens et al., 1996; Tanner & Goldman, 1996), the most commonly clinically diagnosed Lewy body disorder. In Aim 1, aged mice did not exhibit greater α-synucleinopathy than young males at three months post-surgery. Therefore, we sought to examine the impact of aging at longer survival periods by performing the same OB/AON infusions in mice that were 11 months old at the time of fibril infusion and sacrificing half of the mice at six months and half at 12 months post-surgery.

Gender is another prominent risk factor in Lewy body disorders, as men are approximately twice as likely to develop Lewy body disorders are women (Baldereschi et al., 2000; Savica et al., 2013). When developing the unified staging theory, Beach *et al.* observed that ~61-69% of all subjects with ILBD, PD, or DLB were men (Beach, Adler, et al., 2009). DLB cases can be subdivided based on the distribution of α-synuclein pathology, and men are more than twice as likely to develop the limbic-predominant subtype of DLB (Nelson et al., 2010). In addition to prevalence, gender may affect the rate of progression of α-synucleinopathy as it was recently reported that greatest risk factor for cognitive decline in PD is the male gender (Cholerton et al., 2018). The relatively lower rates of Lewy body disorders in females may be related to the neuroprotective effects of estrogen. Estrogen replacement therapy started early in menopause reduces the risk of developing dementia in female PD patients (Marder et al., 1998), and bilateral oophorectomy increases the risk of females developing PD (Benedetti et al., 2001; Rocca et al., 2008). These observations may be related to the finding that estrogens can destabilize α-synuclein fibrils, leading to their disaggregation (Hirohata et al., 2009).

Gender differences have also been reported in older models of Parkinson's disease. In dopaminergic neurotoxicant models, several groups have reported that female rodents are more resistant than males to the loss of nigrostratal cells and subsequent motor deficits (Dluzen et al., 1996; Miller et al., 1998; Murray et al., 2003). Indeed, estrogen, estrogen receptor-α agonist propyl-pyrazome-triol, and some selective estrogen receptor modifiers are reported to protect dopaminergic neurons against MPTP toxicity *in vivo* (Litim et al., 2016). In α-synuclein transgenic mouse models, females often outperform males on sensorimotor tests (Dirr et al., 2018; Gerstenberger et al., 2016), and display more changes in gene expression than transgenic males (Yacoubian et al., 2008). However, little is known about how gender may affect the development and spread of α-synuclein aggregations throughout the brain. Therefore, the second goal of this Aim was to examine the impact of gender on the regional distribution and density of pSer129^{+} aggregations as well as any accompanying cell loss. To this end, we infused either pre-formed α-synuclein fibrils or PBS into the OB/AON of three-month-old male and female mice and sacrificed them six months after surgery.

Specific Aim 2: To examine the effects of age, gender, and disease duration in our model of early stage Lewy body disorders. We hypothesize that α-synuclein aggregation, neuron loss, and the spread of Lewy-like pathology through limbic circuitry is higher in male mice than females and exacerbated with aging in male mice.

Results

Aged animals exhibit greater mortality from OB/AON infusions of preformed α-synuclein fibrils and mortality is not related to changes in weight

At the beginning of this study, 64 CD-1 mice were infused with either preformed α-synuclein fibrils (n = 32) or an equivalent volume of PBS (n = 32). Of those 64 mice, half were 11 months old and half were three months old. To assess the effects of gender, age at infusion, and post-infusion interval, 8 three-month old male, 8 three-month-old female, and sixteen 11-month-old males received preformed α-synuclein fibril infusions into the OB/AON. An equal number of age and gender matched mice received PBS infusions. At six months post-infusion, there was no significant mortality observed when comparing all treatment groups (**Figure 19A**). When comparing only the 11-month-old mice, a trend towards increased mortality was observed at six months post-infusion (**Figure 19B**). As five of the fibril-infused animals had died compared to only one of the PBS-infused animals, we modified our experimental design by sacrificing five of the fibril infused animals and six of the PBS infused animals, instead of the originally planned design of sacrificing eight per group. Therefore, 10 PBS-infused and 11-fibril-infused mice were left to continue to the 12-month time point. However, by 10.5 months post-infusion, significant differences in mortality were observed between the PBS and fibril infused groups (**Figure 19C**), and only 3 of the 11 fibril-infused mice remained alive, compared to 8 of 10 age-matched PBS controls. We therefore ended the study at 10.5 months post-infusion and perfused the mice at 21.5 months of age.

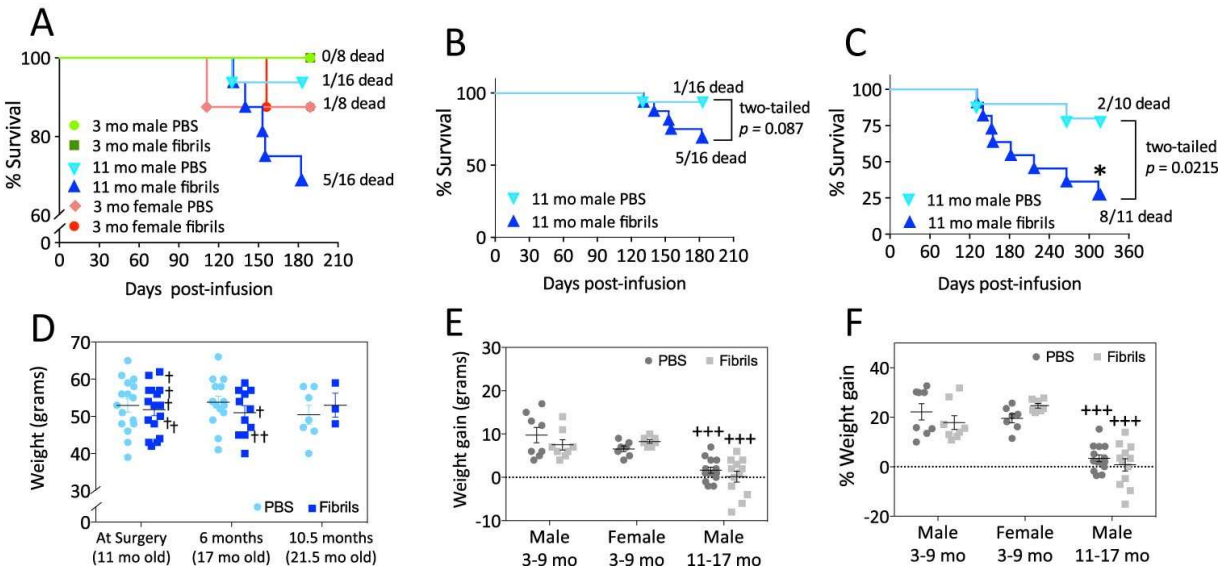

Figure 19: Preformed α-synuclein fibril injections in the mouse olfactory peduncle accelerate mortality in older mice without eliciting significant changes in body weight. Sixty-four mice were infused in the right rear olfactory bulb with either preformed α-synuclein fibrils (5 µg/1 µL) or an equivalent volume of PBS (1 µL) at the indicated ages. Logrank survival analyses were performed for all animals at 6 months post-infusion (**A**) and for the older males at 6 months (**B**) or 10.5 months (**C**) post-infusion. Note the broken Y axis in panel **A.** The two-tailed *p* values of the logrank survival analyses are shown. (**D**) The body weights of the older males at surgery (11 months old), 6 months post-surgery (17 months old), and 10.5 months post-surgery (21.5 months old) are displayed as scatter dot plots with mean and SEM bars. In panel **D**, crosses are placed next to mice that died before the planned time of assay. (**E-F**) Weight gained in both raw numbers (**E**) and percentage weight gain (**F**) six months after surgery in all experimental groups. For panels **D-F**, two-way ANOVAs were followed by the Bonferroni *post hoc* correction for multiple comparisons. In panels **E-F**, +++ $p \leq 0.001$ versus males that were infused at 3 months of age and perfused at 9 months of age (3-9 mo males).

Given the significant mortality observed in the older mice, we examined if the cause of death was related to any loss in body weight (**Figure 19D**). Crosses are placed next to the body weights of the 8 fibril-infused older males that died before the planned date of sacrifice. Graphs of the bodyweight gained and percent weight gained for all animals over the first 6 months of the experiment are shown in **Figures 19E-F**. While the older animals gained significantly less weight in the first six months than the younger animals, fibril infusions did not exert any significant effects in any group (**Figure 19E-F**). These results suggest that the increased mortality was not related to a loss of weight or a lack of food intake.

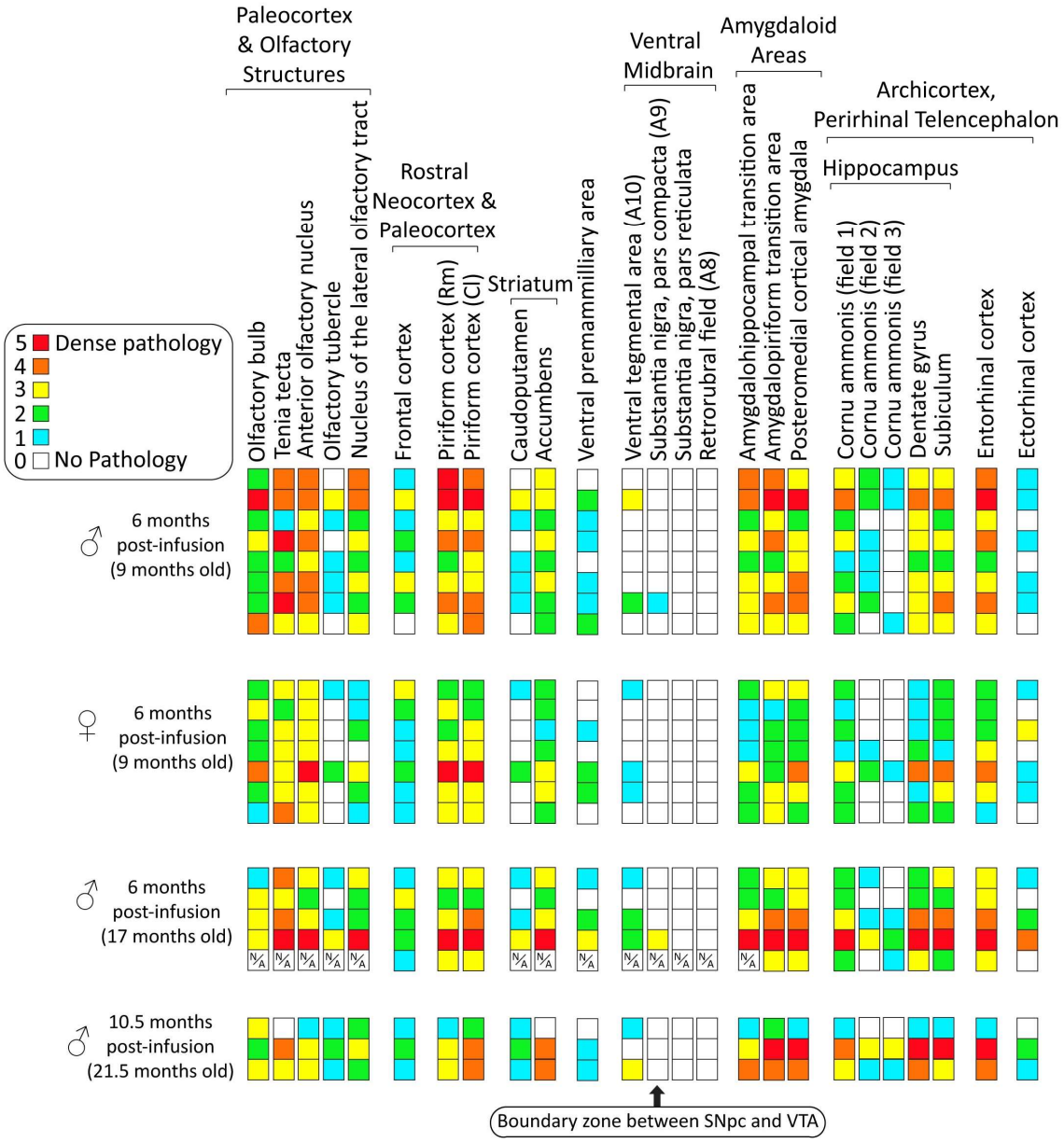

Figure 20: Heat map of α-synucleinopathy following preformed α-synuclein fibril injections in the mouse olfactory peduncle. Qualitative assessments of the density of pSer129^{+} inclusions in the indicated brain regions of all fibril-infused animals that survived until the planned assay time. Each row represents one animal. A blinded investigator systematically examined the entire 1-in-5 series of sagittal brain sections of the ipsilateral, right hemisphere following immunostaining of pathologically phosphorylated α-synuclein with the rabbit monoclonal EP1536Y pSer129 antibody (**Table 2**) as well as staining of nuclei with the Hoechst marker to visualize cytoarchitectonic boundaries. Brain regions with pSer129^{+} immunolabeling are arranged rostrocaudally and/or by anatomical/functional groupings. Most of the midbrain pathology was confined to the ventral tegmental area and only two male animals exhibited pSer129^{+} inclusions at the boundary zone between the substantia nigra, pars compacta, and the ventral tegmental area at 6 months post-infusion.

Fibril infusions in the OB/AON elicit α-synucleinopathy centered in the limbic connectome

The brains collected at 6 and 10.5 months post-infusion were sectioned sagittally and the ipsilateral hemisphere was immunostained. The density of α-synucleinopathy was scored from 0 to 5, with 5 being the densest (**Figure 20**). As observed in Aim 1, the site of injection in the OB exhibited minimal pSer129^{+} pathology compared to other olfactory structures including the AON and tenia tecta (**Table 1)**. The olfactory tubercle developed pathology at 6 months post-infusion in this experiment while in Aim 1 we noted that at three months post-infusion, the olfactory tubercle failed to develop any pSer129^{+} inclusions (**Table 1**), suggesting that additional time (3 months) facilitates the emergence of pathology in this structure. At six months post-infusion, we also observed pathology in the midbrain, specifically the ventral tegmental area and the most medial sections of the SN. No pSer129^{+} inclusions were observed in the lateral segments of the SN pars compacta, which is the most vulnerable nigral subregion in PD patients (Braak et al., 2003; Damier et al., 1999; Fearnley & Lees, 1991; Jellinger, 2012). Additionally, more pSer129^{+} inclusions were observed in the caudoputamen and the nucleus accumbens at 6 months post infusion than at 3 months post infusion.

Some nonspecific immunolabeling is visible in the SN, pars reticulata, and the brainstem

With both the rabbit and mouse anti-pSer129 antibodies used in this Aim (see **Table 2**), single or clusters of immunopositive structures were frequently visible in the brainstem, and in some cases the SN, pars reticulata (**Figure 21A-B**). A recent study found that multiple commercially available

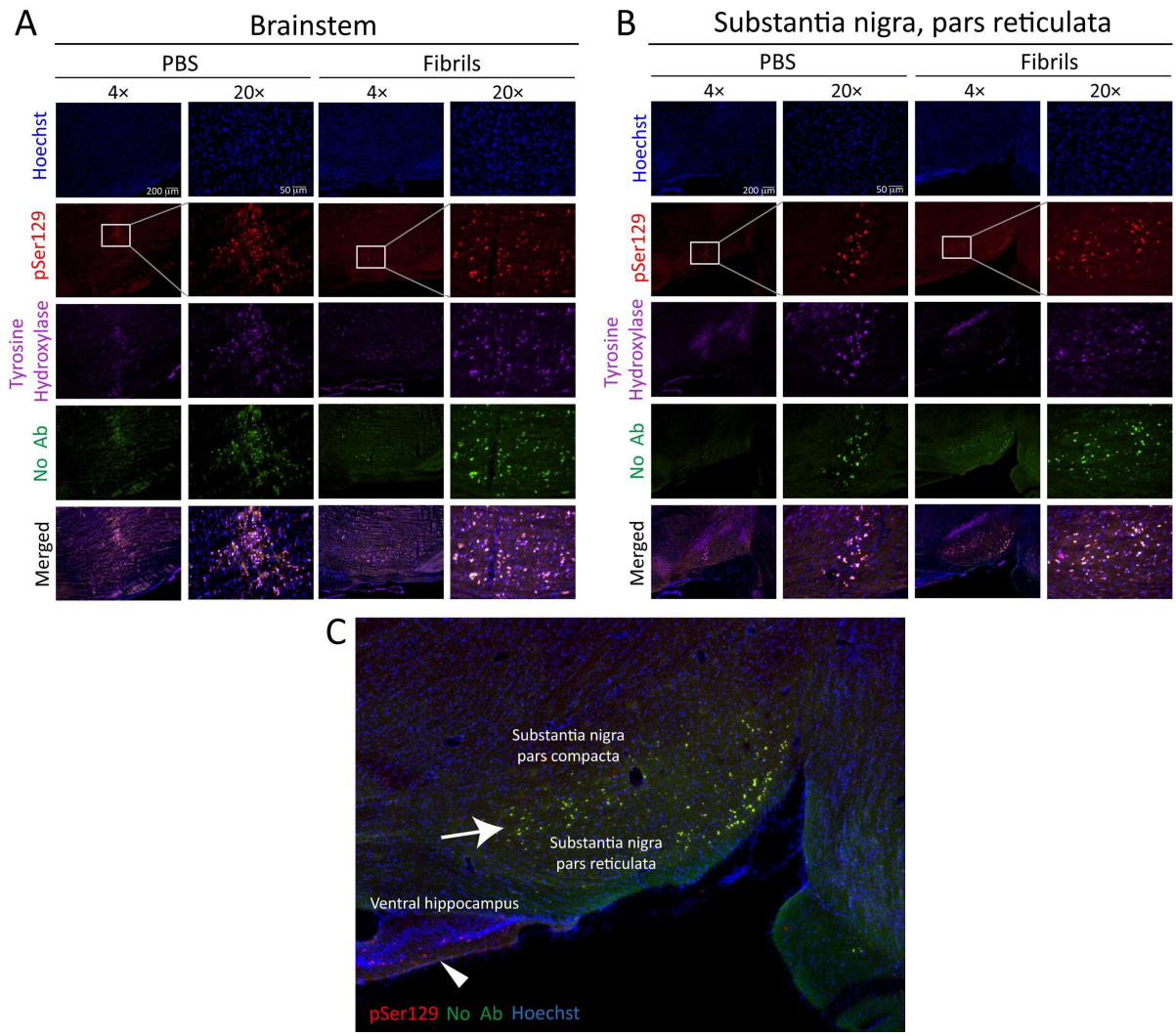

Figure 21: **Nonspecific fluorescence in the substantia nigra, pars reticulata, and brainstem.** Fluorescent structures in the substantia nigra, pars reticulata (**A**) and brainstem (**B**) were observed in three fluorescent channels, and examples of the latter are displayed in images captured with 4× and 20× objectives. This fluorescence is not attributable to specific pSer129 immunostaining, as it is present in vehicle-infused groups and even in the GFP (green) channel, in which neither primary nor secondary antibodies were applied, and was therefore not included in any of our analyses in other figures. (**C**) Nonspecific fluorescence (yellow) in the substantia nigra, pars reticulata. Arrowhead points to specific pSer129 immunofluorescence only present in the appropriate channel in the ventral hippocampus (immunostaining with the EP1536Y pSer129 rabbit monoclonal antibody is pseudocolored in red; see **Table 2**). Panel C is an enlargement of the images of the fibril-infused animal from panel B.

anti-pSer129 antibodies can label non-specific structures, even in α-synuclein knockout animals, but also shows that the rabbit monoclonal pSer129 antibody employed in this Aim is the best one on the market (Delic et al., 2018). Currently, there is no method better than pSer129

immunostaining to label Lewy-like pathology (J. P. Anderson et al., 2006). The non-specific labeled structures that we observed did not have the appearance of genuine pSer129^{+} aggregations, fluoresced in the GFP channel even when no primary or secondary antibodies were applied, and were present in PBS-infused animals. This nonspecific pathology was easily distinguishable for genuine inclusions by the morphology (perinuclear tendrils and threadlike neurites) and the fact that the nonspecific label fluoresced in the RFP, GFP, and Cy5 channels while genuine inclusions only had a fluorescent signal in the RFP channel, corresponding to the appropriate secondary antibody. This is evident in **Figure 21C** in a merged image of the DAPI, RFP and GFP channels. In the ventral hippocampus, genuine inclusions only appear in red and have the typical perinuclear and neuritic appearance, whereas the nonspecific label in the SN pars reticulata fluoresces in both the RFP and GFP channel and appears yellow in the merged image.

Fibril-induced α-synucleinopathy causes cell loss in some brain regions

Female mice displayed fewer pSer129^{+} inclusions than males of the same age in the OB and AON (**Figure 22A-B**). Older males exhibited fewer inclusions in the OB and olfactory tubercle compared to the younger males at six months post-infusion (**Figure 22A, C**). The additional 4.5 month post-infusion interval in the older male group did not influence the overall inclusion density in these structures. Only three fibril-infused mice survived to 10.5 months post-infusion, which suggests that those mice displayed the mildest pathology. Our findings in aim 1 suggest that 17-month-old animals did not exhibit significant increases in the extent or densities of pSer129^{+} inclusions compared to 2 and 5 month-old animals at three months post-infusion, with the exception of some additional pathology in the caudoputamen and nucleus accumbens (**Table 1**).

The pathology in mice sacrificed at six months post-infusion is comparable to those that survived to 10.5-months post infusion, which suggests that the mice that survived to this time point are "super-agers" likely exhibiting milder pathology than those that died.

Figure 22: Impact of α-synuclein fibril infusions in the mouse olfactory peduncle on pSer129$^+$ inclusion counts, NeuN$^+$ neuron counts, and Hoechst$^+$ cell numbers in the rostral rhinencephalon. Three and eleven month old mice were infused in the right rear olfactory bulb with either preformed α-synuclein fibrils (5 μg/1 μL) or an equivalent volume of PBS (1 μL). A blinded observer manually counted the number of pSer129$^+$ structures (monoclonal 81A pSer129 Ab; see **Table 2**) per field of view (200× magnification) and used cellSens software to count the number of NeuN$^+$ and Hoechst$^+$ nuclei in the olfactory bulb (OB; **A**), the anterior olfactory nucleus (AON; **B, E**), the olfactory tubercle (Tub; **C**), and the nucleus of the lateral olfactory tract (LOT; **D**) in the same field of view. Shown are the mean and SEM of raw, unnormalized data. N = 4-8 mice per group, with the exception of the oldest males, in which only 3 out of 8 fibril-infused mice survived to 21.5 months of age (see **Figure 19**). Two-way ANOVAs were followed by the Bonferroni correction for multiple comparisons. Comparisons were only made *a priori* across groups differing by a single independent variable (either gender, age at surgery, or the passage of time since surgery). * $p \leq 0.05$, ** $p \leq 0.01$, *** $p \leq 0.001$ PBS vs fibrils; + $p \leq 0.05$ ++ $p \leq 0.01$ vs 3-9 month males; ~ $p \leq 0.05$ vs 11-17 month males.

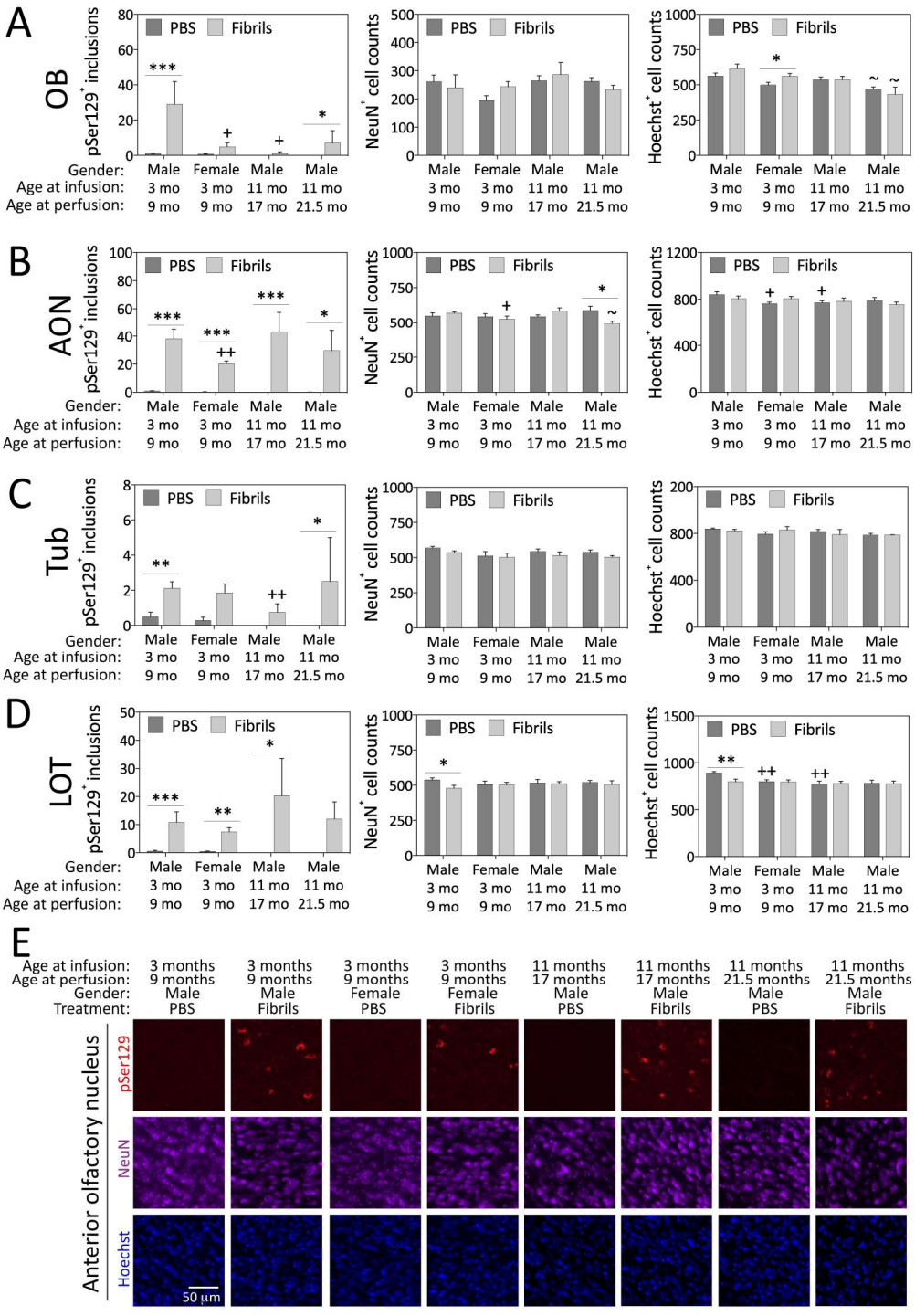

To determine if the pSer129^{+} inclusions cause neurotoxicity, we also counted NeuN^{+} neurons and Hoechst^{+} nuclei in the 17 brain regions most often exhibiting pathology. The major finding from counting NeuN^{+} neurons and Hoechst^{+} nuclei is that fibril infusions did not elicit significant

toxicity in any brain regions in females and induced a mild increase in Hoechst$^+$ cells in the OB in females at six months post-infusion (**Figure 22A**). In the young male group, there was a loss of NeuN$^+$ neurons the lateral olfactory tract, and in the oldest male group there was a loss of NeuN$^+$ neurons in the AON (**Figure 22B, D**). As the piriform cortex is a large brain region, we subdivided it into the rostral-medial and caudal lateral areas. In the caudolateral piriform cortex, the amygdalopiriform transition area, and the posteromedial cortical amygdala, female mice exhibited significantly fewer pSer129$^+$ inclusions than males (**Figure 23B-D**). Fibril-infusions resulted in a loss of Hoechst$^+$ cells in both subregions of the piriform cortex (**Figure 23A-B**), the posteromedial cortical amygdala (**Figure 23D**), and the nucleus accumbens (**Figure 23F**), but only in the young male group. This discrepancy could perhaps have arisen because the older males have lost more cells in these regions as a result of aging. In the caudoputamen, the only group displaying significant inclusions was the 17-month-old males that were sacrificed at 6 months post-infusion (**Figure 23E**), but the overall amount of inclusions to develop in this region was relatively low. Within the hippocampus, females developed similar

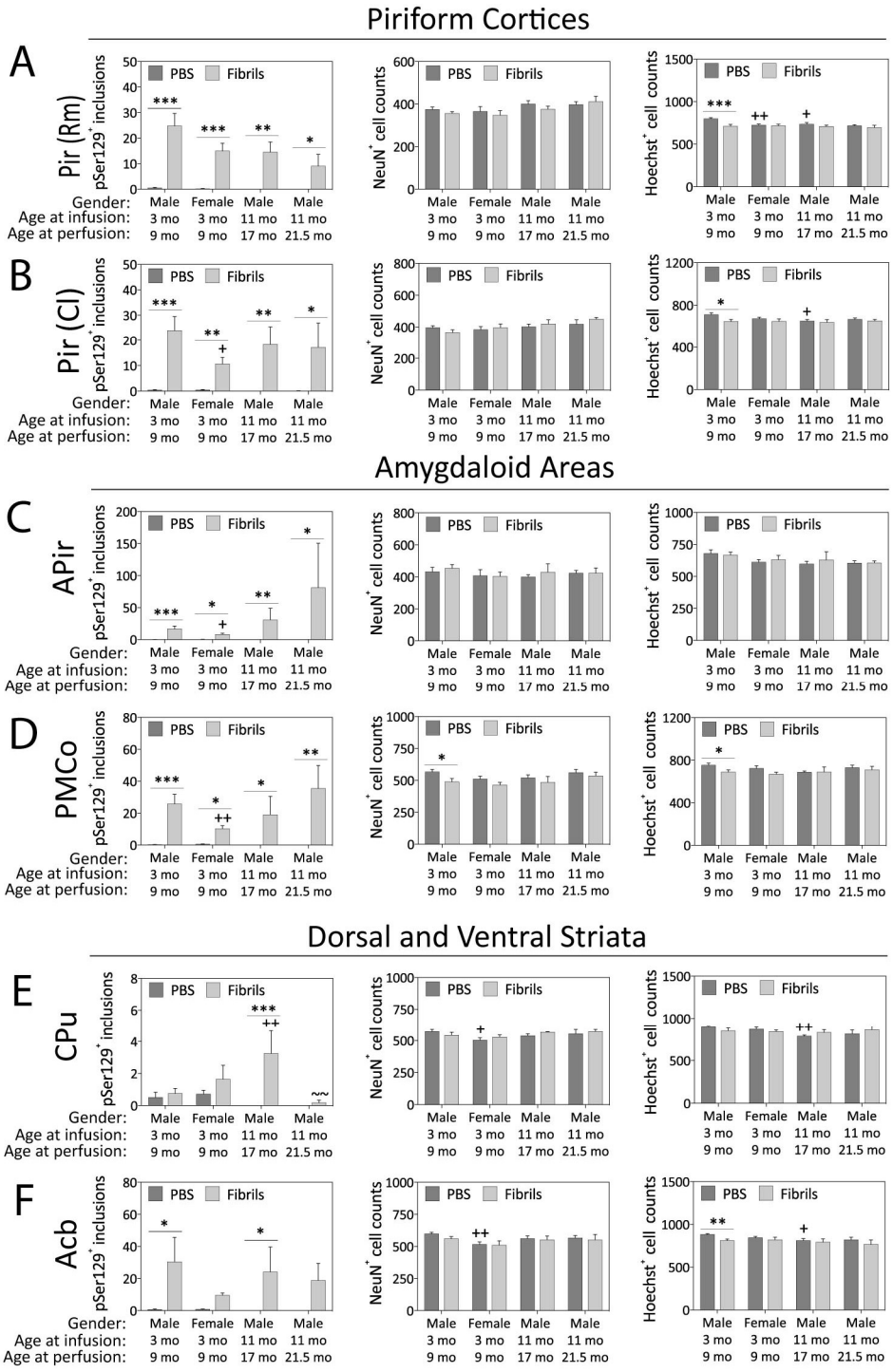
Piriform Cortices
A
Pir (Rm)
pSer129+ inclusions
NeuN+ cell counts
Hoechst+ cell counts
B
Pir (Cl)
Amygdaloid Areas
C
APir
D
PMCo
Dorsal and Ventral Striata
E
CPu
F
Acb
PBS
Fibrils
Gender: Male Female Male Male
Age at infusion: 3 mo 3 mo 11 mo 11 mo
Age at perfusion: 9 mo 9 mo 17 mo 21.5 mo

Figure 23: Impact of α-synuclein fibril infusions in the mouse olfactory peduncle on pSer129$^+$ inclusion counts, NeuN$^+$ neuron counts, and Hoechst$^+$ cell numbers in the piriform cortex (paleocortex), amygdala, and striata. Three and eleven month old mice were infused in the right rear olfactory bulb with either preformed α-synuclein fibrils (5 μg/1 μL) or an equivalent volume of PBS (1 μL). A blinded observer manually counted the number of pSer129$^+$ structures (monoclonal 81A pSer129 Ab; see **Table 2**) per field of view (200× magnification) and used cellSens software to count the number of NeuN$^+$ and Hoechst$^+$ nuclei in the rostromedial piriform cortex (Pir Rm; **A**), caudolateral piriform cortex (Pir Cl; **B**), amygdalopiriform transition area (APir; **C**), posteromedial cortical amygdala (PMCo; **D**), caudoputamen (CPu; **E**), and nucleus accumbens (Acb; **F**). Shown are the mean and SEM of raw, unnormalized data. N = 4-8 mice per group, with the exception of the oldest male group, in which only 3 out of 8 fibril-infused mice survived to 21.5 months of age (see **Figure 19**). Two-way ANOVAs were followed by the Bonferroni correction for multiple comparisons. Comparisons were only made *a priori* across groups differing by a single independent variable (either gender, age at surgery, or the passage of time since surgery). * $p \leq 0.05$, ** $p \leq 0.01$, *** $p \leq 0.001$ PBS vs fibrils; + $p \leq 0.05$, ++ $p \leq 0.01$ vs 3-9 month males; ~~ $p \leq 0.01$ vs 11-17 month males.

number of pSer129$^+$ inclusions as males in the CA1, CA2, and CA3 fields, but in the CA2, and CA3 field, few inclusions developed overall (**Figure 24A-C**). In the dentate gyrus, females were the only group that failed to develop a significant amount of pSer129$^+$ inclusions (**Figure 24D**), and in the subiculum, females developed significantly fewer inclusions than males of the same age (**Figure 24E**). The entorhinal cortex developed significant inclusions in all groups (**Figure 24F**), and in the older males, the ectorhinal cortex displayed significant inclusions at 6 but not 10.5 months post-infusion (**Figure 24G**). At 6 months post-infusion the older male group had decreased Hoechst$^+$ cell numbers in the ectorhinal cortex (**Figure 24G**), and at 10.5 months post-infusion, the oldest males exhibited a significant decrease in NeuN$^+$ cells in CA2 and the subiculum (**Figure 24B, E**).

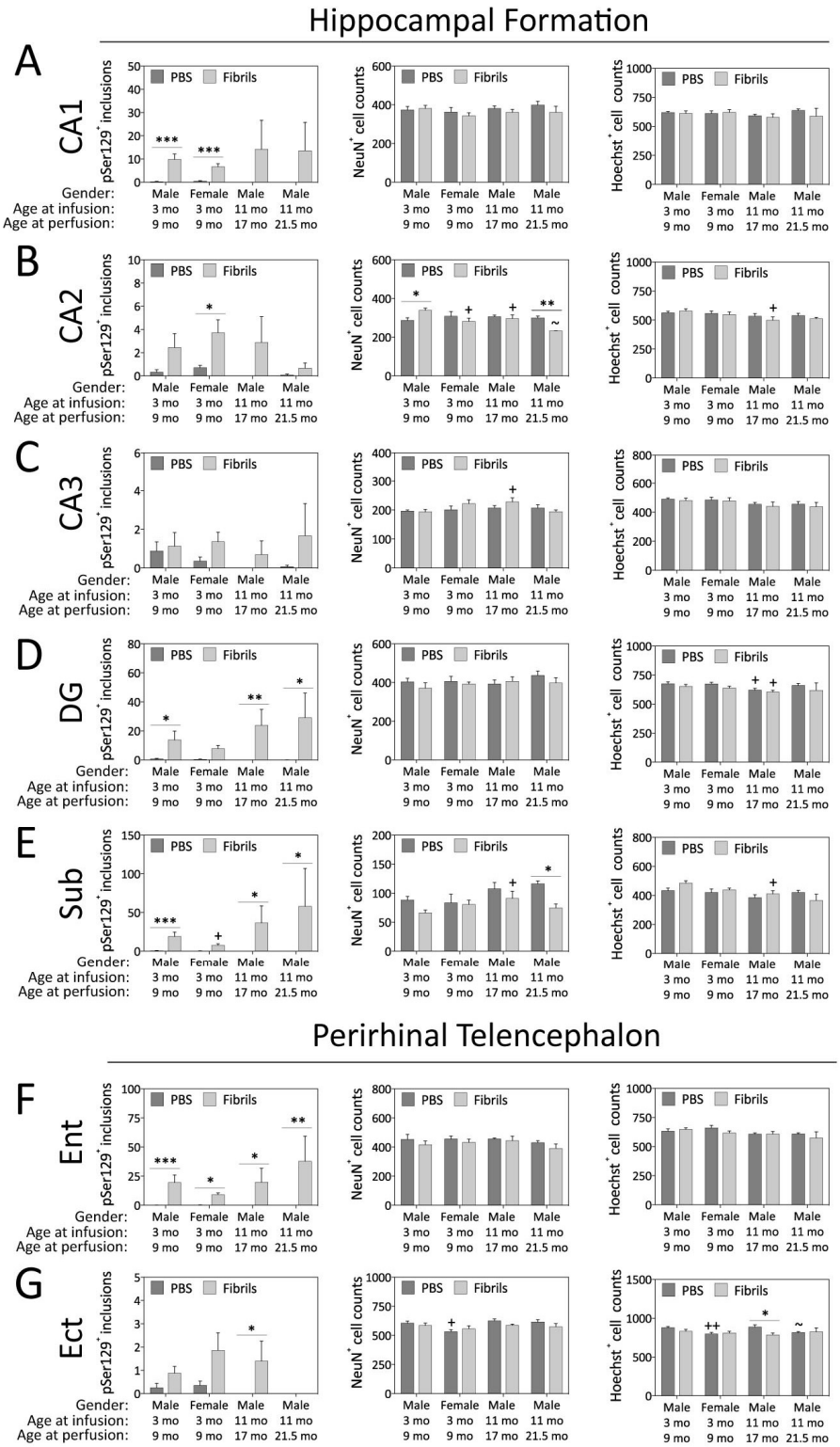
Hippocampal Formation
A
CA1
B
CA2
C
CA3
D
DG
E
Sub
Perirhinal Telencephalon
F
Ent
G
Ect
pSer129+ inclusions
NeuN+ cell counts
Hoechst+ cell counts
PBS
Fibrils
Gender:
Age at infusion:
Age at perfusion:
Male Female Male Male
3 mo 3 mo 11 mo 11 mo
9 mo 9 mo 17 mo 21.5 mo

Figure 24: Impact of α-synuclein fibril infusions in the mouse olfactory peduncle on pSer129$^+$ inclusion counts, NeuN$^+$ neuron counts, and Hoechst$^+$ cell numbers in the hippocampal formation and perirhinal telencephalon. Three and eleven month old mice were infused in the right rear olfactory bulb with either preformed α-synuclein fibrils (5 μg/1 μL) or an equivalent volume of PBS (1 μL). A blinded observer manually counted the number of pSer129$^+$ structures (monoclonal 81A pSer129 Ab; see **Table 2**) per field of view (200× magnification) and used cellSens software to count the number of NeuN$^+$ and Hoechst$^+$ nuclei in the pyramidal cell layers of hippocampal fields CA1 (**A**), CA2 (**B**) and CA3 (**C**), the stratum granulosum of the dentate gyrus (DG; **D**), the subiculum (Sub; **E**), and entorhinal cortex (Ent; **F**), and the ectorhinal cortex (Ect; **G**). Shown are the mean and SEM of raw, unnormalized data. N = 5-8 mice per group, with the exception of the oldest male group, in which only 3 out of 8 fibril-infused mice survived to 21.5 months of age (see **Figure 19**). Two-way ANOVAs were followed by the Bonferroni correction for multiple comparisons. Comparisons were only made *a priori* across groups differing by a single independent variable (either gender, age at surgery, or the passage of time since surgery). * $p \leq 0.05$, ** $p \leq 0.01$, *** $p \leq 0.001$ PBS vs fibrils, + $p \leq 0.05$ vs 3-9 month males, ~ $p \leq 0.05$ vs 11-17 month males.

Fibril infusions in the OB/AON induce atrophy in some cell layers

In DLB, hippocampal atrophy is associated with the degree of cognitive dysfunction (Elder et al., 2017). Therefore, in addition to counting Hoechst$^+$ nuclei we also examined regional changes in the width of pyramidal and granule cell layers clearly visible with the Hoechst reagent. To measure cell layer width, a blinded investigator used the "arbitrary line" tool in cellSens software to draw lines across the width of the pyramidal layer of both subregions of the piriform cortex (rostromedial and caudolateral), CA1, CA2, CA3, and the stratum granulosum of the ventral portion of the dentate gyrus (**Figure 25A-B**). This area of the dentate gyrus was chosen because it develops the most pSer129$^+$ inclusions in this model. Here we observed that in the youngest males, fibril infusions reduced the width of the rostromedial and caudolateral piriform cortex, CA1, and the dentate gyrus. Compared to this group, fibril-infused females had significantly thicker pyramidal cell layers of the rostromedial piriform cortex and CA1 as well as thicker granule cell layers of the dentate gyrus. Fibril infusions also reduced the width of CA2 and CA3 in females and the older males sacrificed at 6 months post-infusion. No fibril-induced changes in cell layer

widths were observed in the older males sacrificed 10.5 months post-infusion which may be a result of a low n, or the result of higher mortality in this group, as only the least affected "super-agers" remained. To determine if changes in regional size were related to changes in neuronal processes or nuclei shrinkage, we also examined the area of Hoechst$^+$ nuclei in each region. In the rostromedial and caudolateral piriform cortex as well as the dentate gyrus, the young male group exhibited an increase in Hoechst$^+$ nuclear area (**Figure 25C**). These same areas that exhibited hypertrophy in Hoechst$^+$ nuclei displayed shrinkage of the cell layers, which suggests that changes

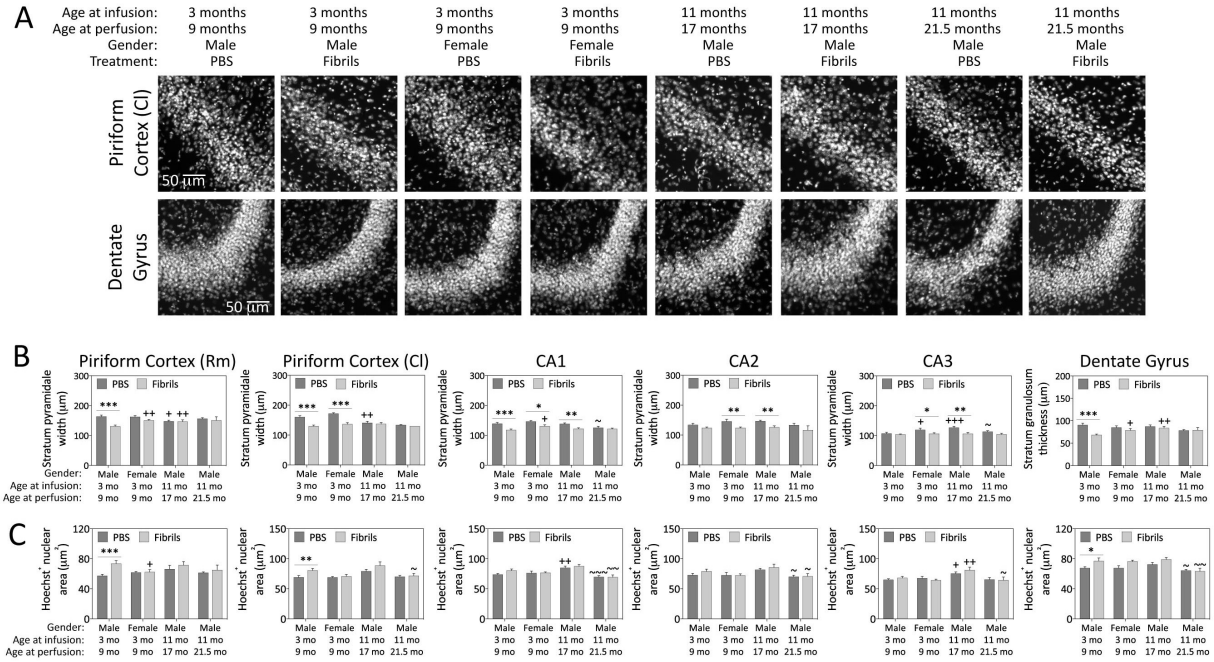

Figure 25: Preformed α-synuclein fibril injections in the olfactory peduncle induce atrophy of pyramidal and granule cell layers of the limbic allocortex in young male mice. Mice were infused in the right rear olfactory bulb with either preformed α-synuclein fibrils (5 µg/1 µL) or an equivalent volume of PBS (1 µL). A blinded observer employed the "arbitrary line" tool in CellSens software to measure the width of the compact Hoechst$^+$ pyramidal cell layer in the rostromedial piriform cortex, caudolateral piriform cortex, CA1, CA2, and CA3 of the hippocampus, or the stratum granulosum of the dentate gyrus. Representative grayscale micrographs for the caudolateral piriform cortex and dentate gyrus are displayed in panel **A** and the quantification of pyramidal and granule cell layers width (**B**) and Hoechst$^+$ nuclear size (**C**) is graphed below. Shown are the mean and SEM of raw, unnormalized data. N = 4-8 mice per group, with the exception of the oldest male group, in which only 3 fibril-infused mice survived to 21.5 months of age (see **Figure 19**). Two-way ANOVAs were followed by the Bonferroni correction for multiple comparisons. Comparisons were only made *a priori* across groups differing by a single independent variable (either gender, age at surgery, or the passage of time since surgery). * $p \leq 0.05$, ** $p \leq 0.01$, *** $p \leq 0.001$ PBS vs fibrils; + $p \leq 0.05$, ++ $p \leq 0.01$ +++ $p \leq 0.001$ versus vs 3-9 month males; ~ $p \leq 0.05$, ~~ $p \leq 0.01$, ~~~ $p \leq 0.001$ vs 11-17 month males.

to layer width are related to changes to cellular processes. An increase in nuclear volume could indicate an increase in gene transcription whereas changes in the entire tissue layer may represent a change in cell soma size possibly through osmotic shrinkage.

Perinuclear pSer129$^+$ aggregates colocalize with Proteostat aggresome dye

As discussed in the introduction, an aggresome is a cellular structure that emerges to mitigate proteotoxic stress when normal protein degradation mechanisms are insufficient. As Lewy bodies are theorized to be failed aggresomes (Olanow et al., 2004), we immunostained tissue from fibril-infused and PBS-infused animals with the anti-pSer129 antibody and applied the well-characterized Proteostat dye for aggresomes (Shen et al., 2011) and the Hoechst reagent. Here we observed that the majority of perinuclear pSer129$^+$ inclusions in the AON, piriform cortex, amygdala, hippocampus, and entorhinal cortex were also labeled with the Proteostat dye (**Figure 26A**), suggesting that perinuclear inclusions in the model may represent a form of aggresome. Neuritic inclusions were not labeled by the Proteostat dye, which agrees with the perinuclear location of aggresomes (**Figure 26B**). In some cells of PBS animals, the Proteostat dye, but not the anti-pSer129 antibody weakly labeled a structure near the nucleus, possibly the centrosome, which may represent a low level of aggregated proteins in cells under physiological conditions.

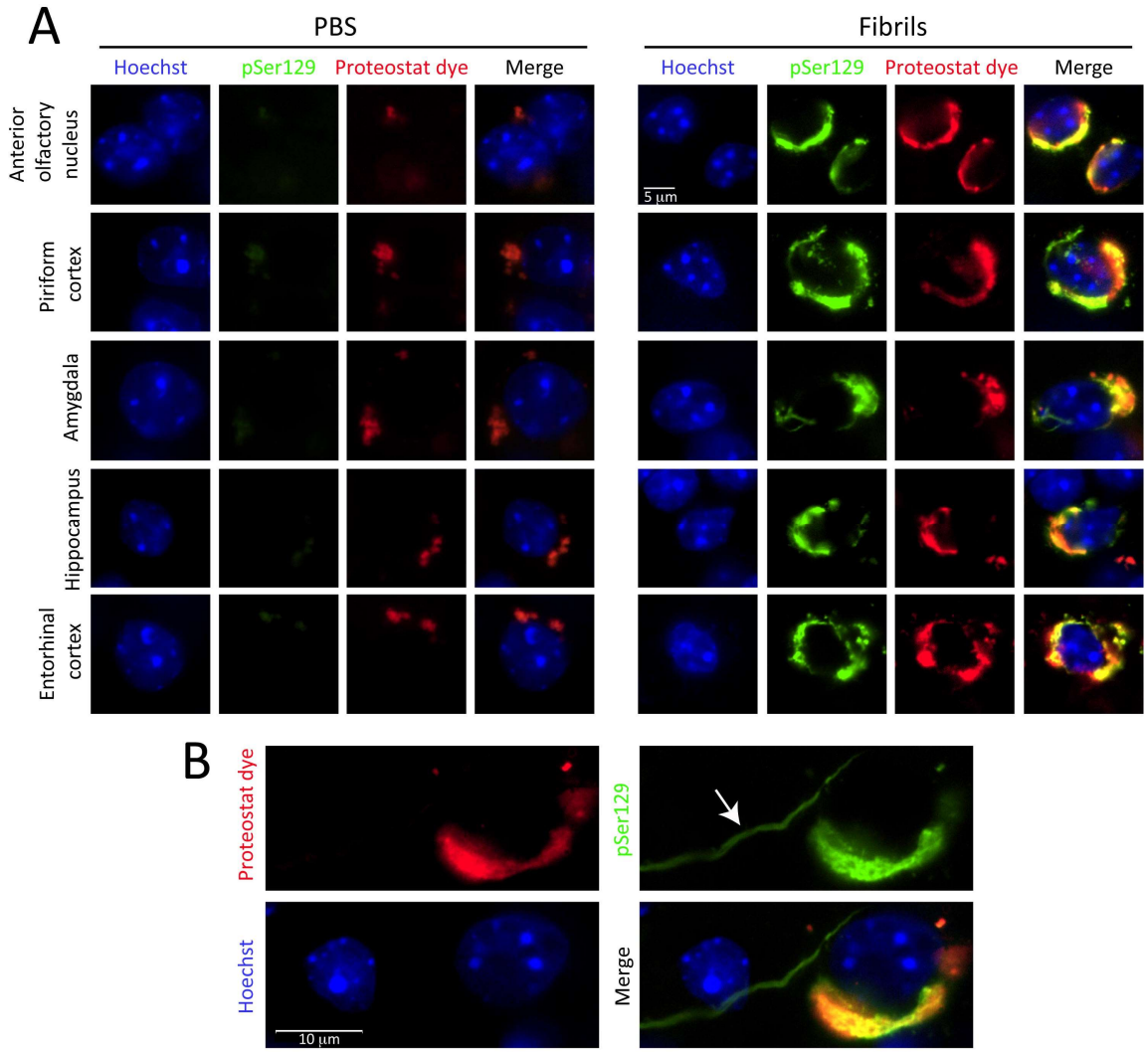

Figure 26: Preformed α-synuclein fibril injections in the mouse olfactory peduncle induce the formation of aggregations that colocalize with perinuclear but not neuritic pSer129^{+} inclusions. Mice were infused in the right rear olfactory bulb with either preformed α-synuclein fibrils (5 µg/1 µL) or an equivalent volume of PBS (1 µL). Sagittal brain sections from young male mice were immunostained for pathologically phosphorylated α-synuclein (monoclonal 81A pSer129 antibody; see **Table 2**). The Proteostat detection reagent was also applied to the tissue and the Hoechst reagent was used to stain nuclei. Images were captured with a 100× objective under oil immersion. (**A**) Perinuclear inclusions in the anterior olfactory nucleus, piriform cortex, posteromedial cortical nucleus of the amygdala, hippocampal CA1, and entorhinal cortex are displayed in young male mice infused with PBS or fibrils six months earlier. (**B**) Lack of colocalization of neuritic inclusions with the Proteostat dye.

Similar patterns of pSer129^{+} aggregations observed with two independent antibodies

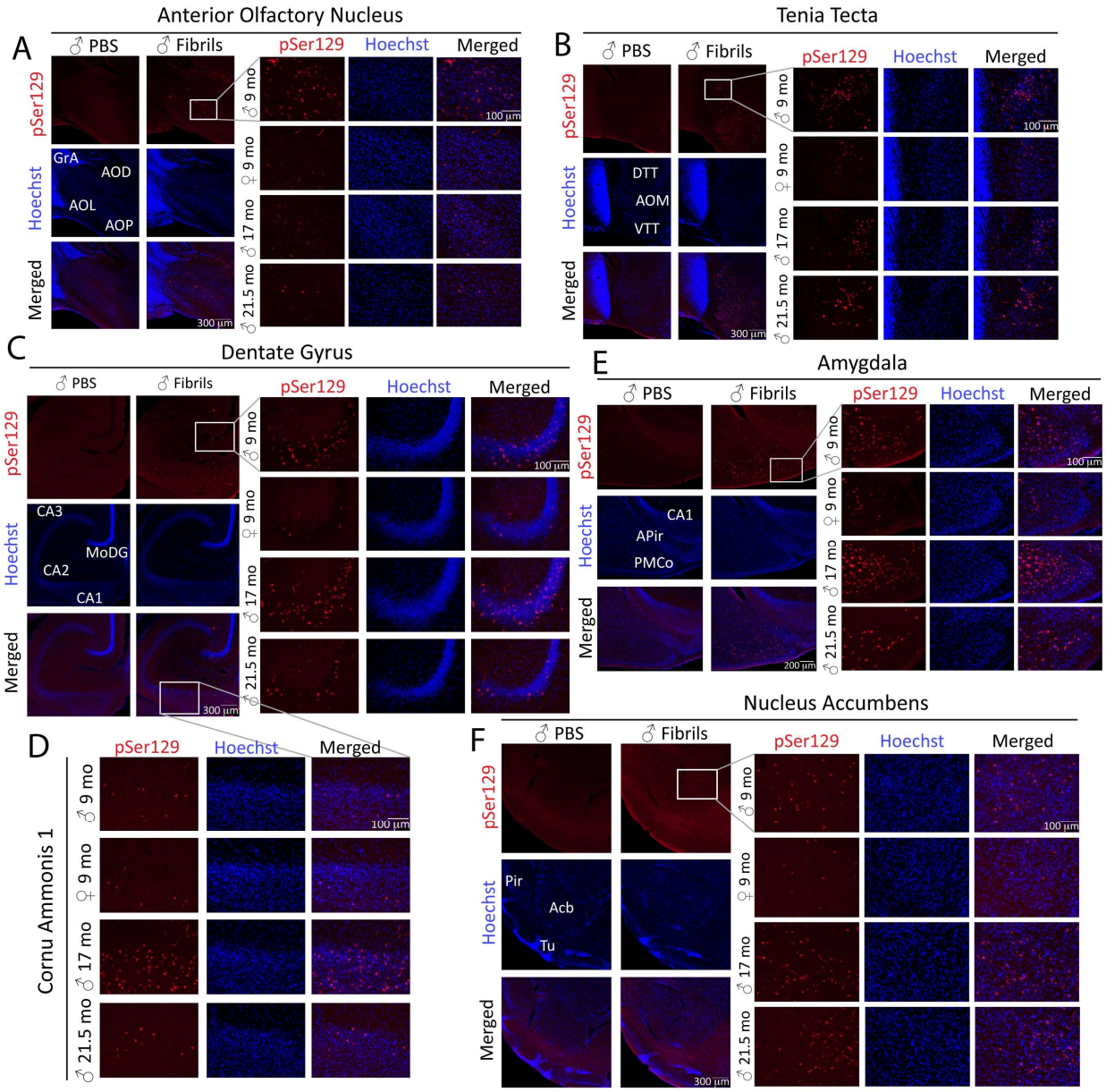

Figure 27: Preformed α-synuclein fibril injections in the mouse olfactory peduncle elicit α-synucleinopathy in olfactory/limbic regions of the temporal lobe. Mice were infused in the right rear olfactory bulb with either preformed α-synuclein fibrils (5 µg/1 µL) or an equivalent volume of PBS (1 µL). Sagittal brain sections were immunostained for pathologically phosphorylated α-synuclein (EP1536Y rabbit monoclonal pSer129 antibody; see **Table 2**). The Hoechst reagent was used to stain nuclei and identify anatomical boundaries. Images were captured at 40× and 200× (insets) magnification in the anterior olfactory nucleus (**A**), tenia tecta (**B**), dentate gyrus (**C**), and hippocampal CA1 (**C,D**), the posteromedial cortical amygdala (**E**), and the nucleus accumbens (**F**). All abbreviations are listed in **Table 4**.

The abovementioned pSer129 inclusion counts in this aim were performed with a mouse monoclonal anti-pSer129 antibody to the same epitope as used in Aim 1. The following experiments of this Aim were performed with a rabbit polyclonal anti-pSer129 antibody to the EP1536Y epitope, which has been used effectively by other labs (Rey et al., 2018), and has been shown to be the most sensitive and specific anti-pSer129 antibody of four commercially available antibodies tested (Delic et al., 2018). Indeed, with this antibody, we observed a greater signal-to-noise ratio and more visible pSer129^{+} aggregates (**Figure 27**). In the rostral olfactory structures (**Figure 27A-B**), the young male group typically exhibited the most pathology, while in more caudal structures such as the hippocampus and amygdala, the older males exhibited the most pathology (**Figure 27C-D**). Females overall developed fewer pSer129^{+} inclusions than males (**Figure 28**), but there is some variability within the treatment groups (**Figure 20**).

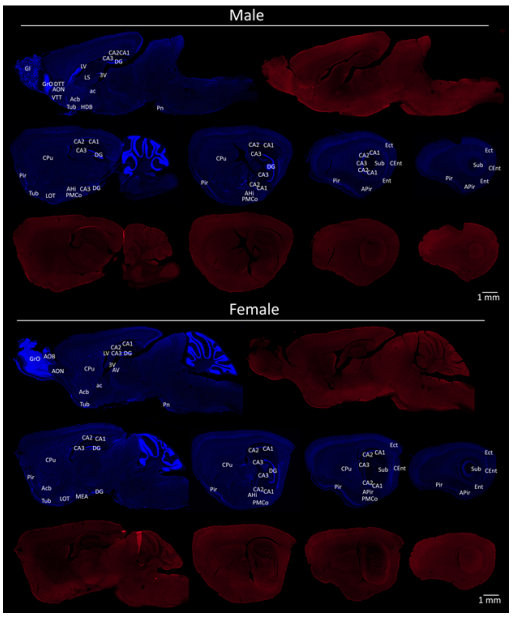

Figure 28: Preformed α-synuclein fibril injections in the olfactory peduncle induce a similar topographic extent of α-synucleinopathy in males and females. Mice were infused in the right rear olfactory bulb with either preformed α-synuclein fibrils (5 µg/1 µL) or an equivalent volume of PBS (1 µL). Sections were immunostained for pathologically phosphorylated α-synuclein (EP1536Y rabbit monoclonal pSer129 antibody; see **Table 2**). The nuclear marker Hoechst (pseudocolored blue) was used to denote cytoarchitectonic boundaries. Stitched images of sagittal brain sections from young male (top) and female (bottom) perfused 6 months post-infusion are displayed from medial to lateral. All sections were processed in parallel and images were captured at the same camera and exposure settings. All abbreviations are listed in **Table 4**.

17-month-old male sacrificed 6 months post-infusion developed most robust and widespread pSer129^{+} pathology

A 17-month-old animal sacrificed at 6 months post-infusion had developed the maximal extent of α-synucleinopathy following OB/AON infusions of preformed α-synuclein of all mice examined in this study (**Figure 29**). This series of stitched images includes sections from 3.00 to 3.72 mm from the midline of the brain. In the most medial section, dense pathology is visible in the amygdala, hippocampal CA1, and the ventral portions of dentate gyrus (**Figure 29A**). In the next section, pathology is concentrated in the amygdala, and in the hippocampus. CA1 is primarily occupied by perinuclear inclusions whereas the molecular layer of the dentate gyrus is filled with neuritic inclusions (**Figure 29B**). In this section as well as the following one, the inclusions appear in the entorhinal cortex as well as the ectorhinal cortex (**Figure 29B-C**). In all sections, pathology is visible throughout the piriform cortex and in the amygdalopiriform transition area and is primarily confined to brain regions within the limbic system (**Figure 29A-D**). The 21.5-month-old mice sacrificed 10.5 months post-infusion developed a similar pattern of α-synucleinopathy, but it was less robust than this animal sacrificed 6 months post-infusion (**Figure 30**). This observation agrees with other groups who have reported that at longer time points, the amount of pSer129^{+} aggregations may diminish in some structures (Rey et al., 2018), suggesting that there is some aggregated α-synuclein clearance over time possibly through an immune response.

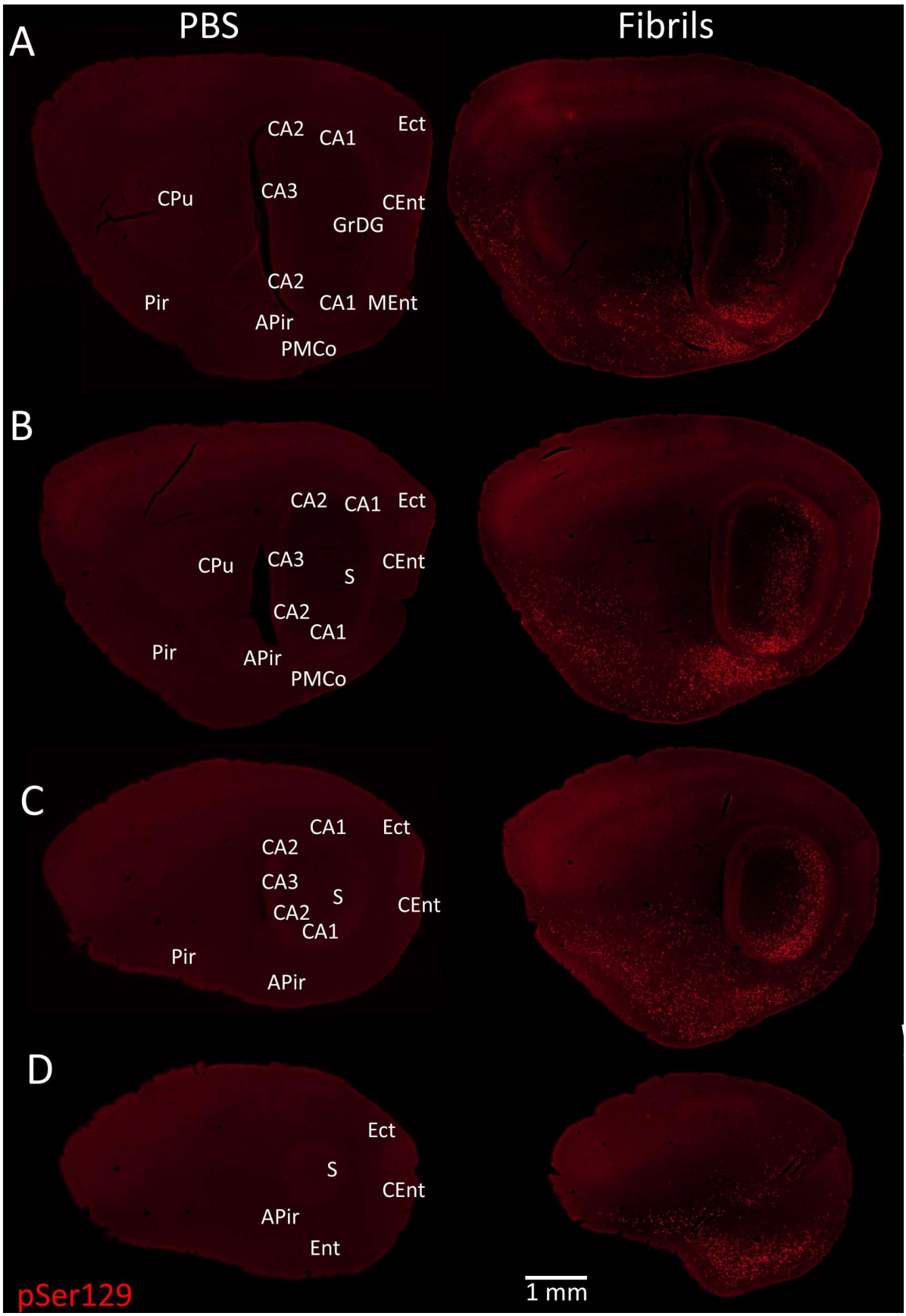
A
PBS
Fibrils
CA2
CA1
Ect
CPu
CA3
CEnt
GrDG
CA2
Pir
CA1
MEnt
APir
PMCo
B
CA2
CA1
Ect
CPu
CA3
CEnt
S
CA2
CA1
Pir
APir
PMCo
C
CA1
Ect
CA2
CA3
S
CEnt
CA2
CA1
Pir
APir
D
Ect
S
CEnt
APir
Ent
pSer129
1 mm

Figure 29: Specific α-synucleinopathy is centered in the limbic allocortex six months following infusions of preformed α-synuclein fibrils in the olfactory peduncle. A series of stitched images of sagittal brain sections from 11-month-old animals sacrificed six months after infusion of 1 µL PBS (left) or 5 µg/1 µL fibrils (right) into the olfactory peduncle. All sections were stained in parallel with the monoclonal EP1536Y pSer129 antibody for pathologically phosphorylated α-synuclein (see **Table 2**). Anatomical labels are based on cytoarchitectonic details provided by the Hoechst nuclear marker (not shown). All sections were and photographed at the same exposure and camera settings. All abbreviations are listed in **Table 4**.

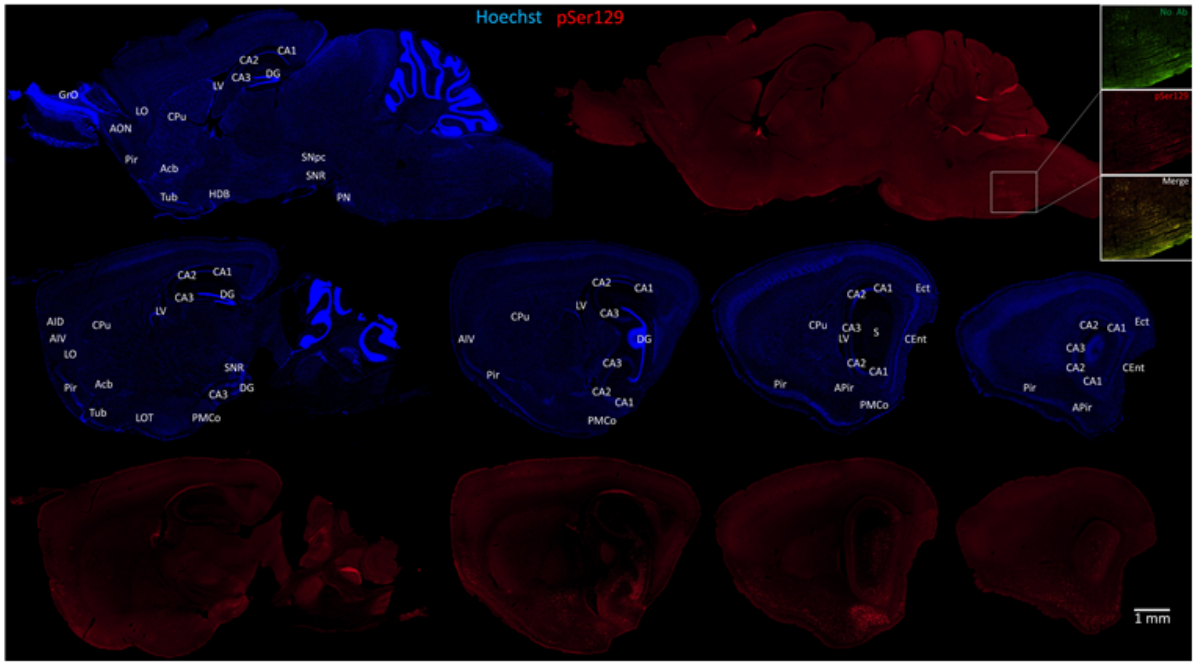

Figure 30: Preformed α-synuclein fibril injections in the olfactory peduncle induce α-synucleinopathy centered in the limbic system at 10.5 months post-infusion. Mice were infused in the right rear olfactory bulb with either preformed α-synuclein fibrils (5 µg/1 µL) or an equivalent volume of PBS (1 µL). Sections were immunostained for pathologically phosphorylated α-synuclein (EP1536Y rabbit monoclonal pSer129 antibody; see **Table 2**). The nuclear marker Hoechst (pseudocolored blue) was used to denote cytoarchitectonic boundaries. Stitched images of sagittal brain sections from 21.5 month-old mice perfused 10.5 months after fibril infusions are displayed. All abbreviations are listed in **Table 4**.

α-synucleinopathy can develop in the midbrain after 6 months following OB/AON infusions of preformed α-synuclein fibrils

In a medial section from the same animal in **Figure 29**, pSer129$^+$ aggregates are visible within the midbrain (**Figure 31A, D**). Dense pathology is visible in the AON and nucleus accumbens at this level (**Figure 31A-C**). Some pathology is also visible in the bed nucleus of stria terminalis and the premammillary area, which are also part of the limbic system. Pathology in these areas was rare and therefore was not included in the heatmap in **Figure 20**. Nonspecific label is visible in the brainstem (**Figure 31A**), but as discussed earlier, we did not define this material as genuine pSer129$^+$ inclusions because it was morphologically distinct and also visible in the GFP channel, which did not have any secondary antibodies (**Figures 21A, 30**). Within the ventral midbrain, this animal developed somal as well as neuritic pSer129$^+$ inclusions (**Figure 31D-L**). Tyrosine hydroxylase, the rate-limiting enzyme for dopamine biosynthesis (pseudocolored green) exhibited minimal colocalization with pSer129$^+$ inclusions (**Figure 31H, L**). The arrow in

Figure 31: α-synucleinopathy is centered medially in limbic-related parts of the midbrain following infusions of preformed α-synuclein fibrils in the OB/AON. A fibril-injected 17 month-old mouse with the most widespread Lewy-related pathology of all cases is displayed in this figure. (**A**) A stitched image containing the ventral midbrain is displayed. This type of specific α-synucleinopathy in the boundary zone between the ventral tegmental area and substantia nigra, pars compacta (as identified with antibodies against the dopaminergic marker tyrosine hydroxylase) was only observed in two out of 22 fibril-infused mice by six months post-infusion (see heatmap in **Figure 20**). Dense pSer129 inclusions were observed in the anterior olfactory nucleus (AON) and nucleus accumbens (Acb) in the animal featured in panel A, and sparse inclusions were observed in the olfactory bulb (OB), bed nucleus of stria terminalis (BST), frontal cortex, and ventral midbrain. Merged, higher-magnification images of Hoechst$^+$ cells (pseudocolored blue) and pSer129 immunostaining (pseudocolored red; EP1536Y rabbit monoclonal pSer129 antibody; see **Table 2**) in the AON (**B**) and accumbens (**C**), respectively. (**D**) Tyrosine hydroxylase (TH; pseudocolored green) and pSer129 (pseudocolored red) immunostaining in the ventral midbrain of the same animal. (**E-H**) Lack of convincing colocalization of pSer129 and tyrosine hydroxylase in confocal images of the same animal as shown in panels **A-D**. All abbreviations are listed in **Table 4**.

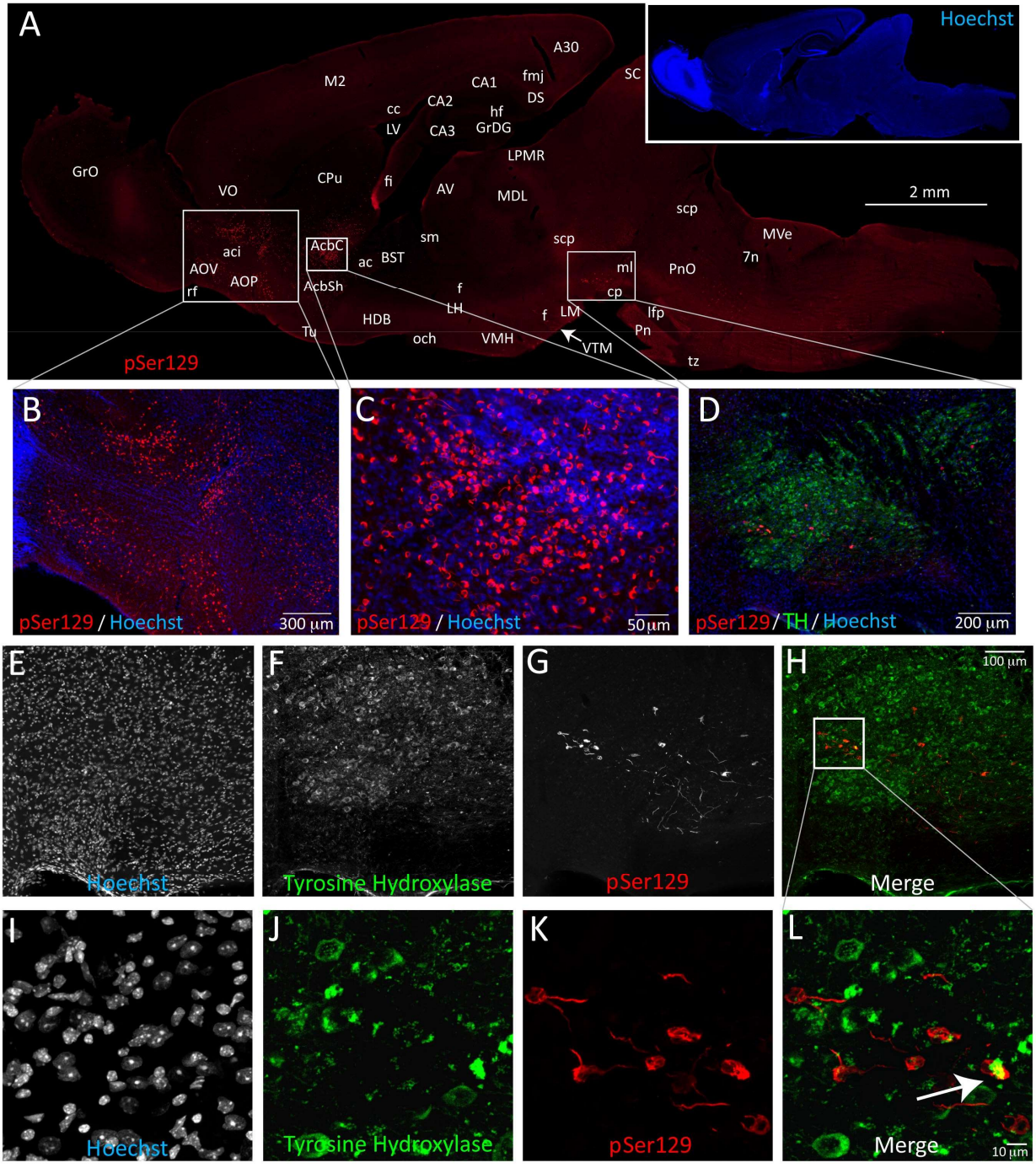
A
Hoechst
A30
M2
CA1
fmj
SC
DS
CA2
cc
hf
LV
CA3
GrDG
LPMR
GrO
CPu
fi
AV
VO
MDL
2 mm
scp
MVe
sm
scp
aci
AcbC
ac
BST
7n
AOV
ml
PnO
AOP
AcbSh
f
cp
rf
LH
f
LM
lfp
HDB
Pn
Tu
och
VMH
VTM
tz
pSer129
B
C
D
pSer129 / Hoechst
300 µm
pSer129 / Hoechst
50 µm
pSer129 / TH / Hoechst
200 µm
E
F
G
H
100 µm
Hoechst
Tyrosine Hydroxylase
pSer129
Merge
I
J
K
L
Hoechst
Tyrosine Hydroxylase
pSer129
Merge
10 µm

Figure 31L points to a single area of colocalization, but when examining this area via 3D video generated on a confocal microscope, it was clearly in another plane of focus. This section is at the boundary of the lateral ventral tegmental area and medial SN, whereas the ventrolateral posterior subregion of the SN is reported to be more vulnerable in PD (Damier et al., 1999; Fearnley & Lees, 1991)., The ventral tegmental area harbored pSer129^{+} inclusions more frequently that the SN (**Figure 20**), and this area also displayed minimal colocalization of tyrosine hydroxylase with aggregated α-synuclein (**Figure 32**).

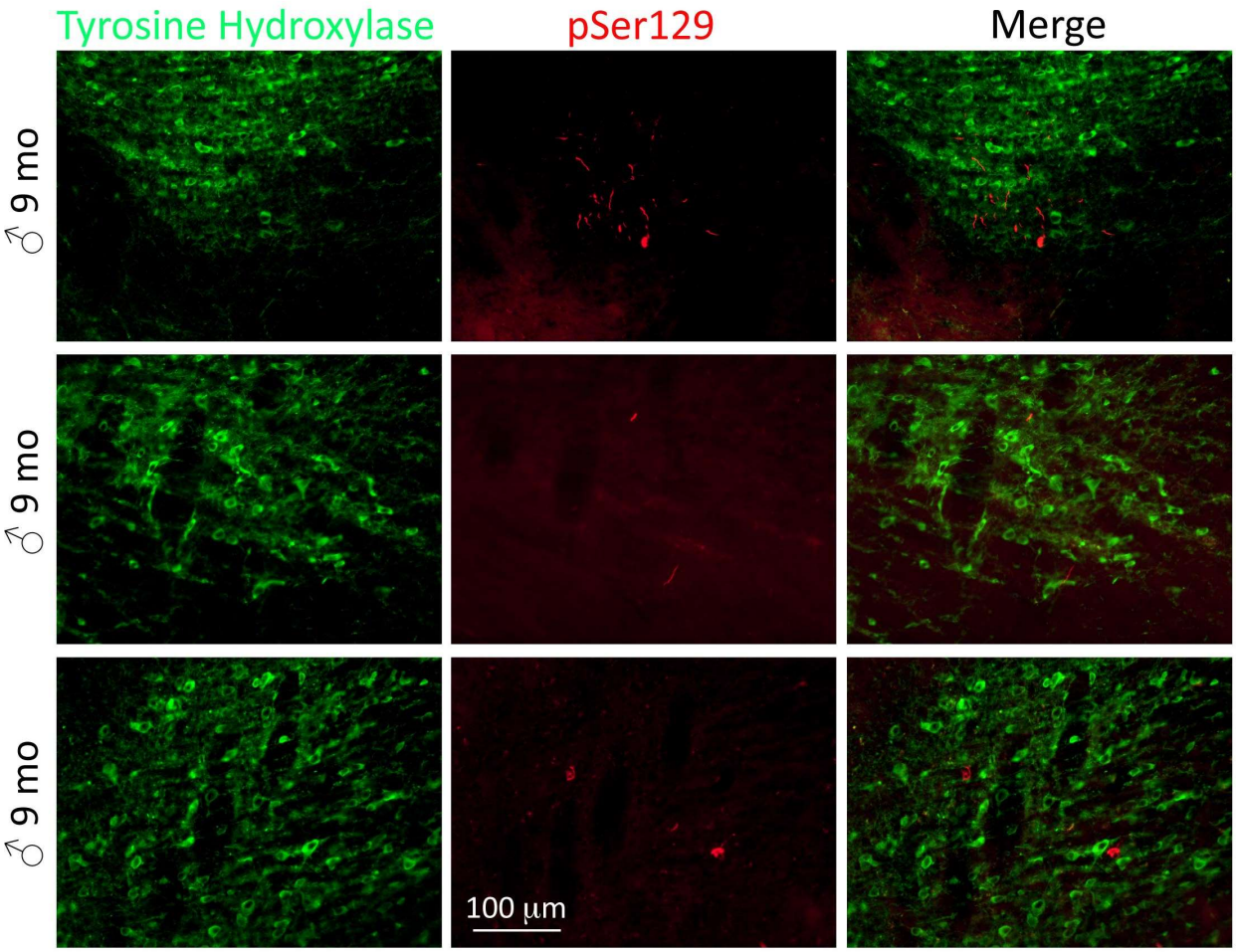

Figure 32: α-synucleinopathic inclusions in the ventral tegmental area are not found in tyrosine hydroxylase^{+} neurons. Three-month-old mice were infused in the right rear olfactory bulb with either preformed α-synuclein fibrils (5 µg/1 µL) or an equivalent volume of PBS (1 µL). After 6 months, sagittal brain sections were stained with the rabbit monoclonal EP1536Y pSer129 antibody (pseudocolored red) for pathologically phosphorylated α-synuclein (see **Table 2**) and tyrosine hydroxylase (pseudocolored green). No colocalization of the two markers was observed.

α-synucleinopathy in the limbic system affects dopaminergic markers in the nigrostriatal pathway

The same tissue used to generate the heatmap and stitched images in this Aim was also immunostained for Tyrosine Hydroxylase (TH) and the Dopamine Transporter (DAT), and analyzed on the Licor Odyssey scanner. A blinded observer traced the outlines of the nucleus accumbens, caudoputamen, ventral tegmental area, and SN (pars compact and reticulata), and determined the area of the traced shape (**Figure 33A**) and fluorescent signal for both dopaminergic markers (**Figure 33B, D**). Using these measurements, the signal per area for both TH and DAT was calculated (**Figure 33C, E**). In the older males that were sacrificed 10.5 post-infusion, fibril infusions elicited a robust increase in the TH signal per area in every region. This pattern was also seen in the older males sacrificed 6 months post infusion, except in the ventral tegmental area (**Figure 33C**). Females also exhibited a fibril-induced increase in TH signal per area in the caudoputamen and nucleus accumbens, whereas fibril infusions did not significantly increase TH signal per area in the young males. A similar pattern observed with the DAT signal/area (**Figure 33D-F)**, as males sacrificed 10.5 months post-infusion displayed a fibril-induced increase in DAT signal per area in every region. The older males sacrificed 6 months post-infusion also displayed increased DAT signal per area in the caudoputamen and SN and females only in the caudoputamen. The young male group did not show any significant changes in DAT in any brain region.

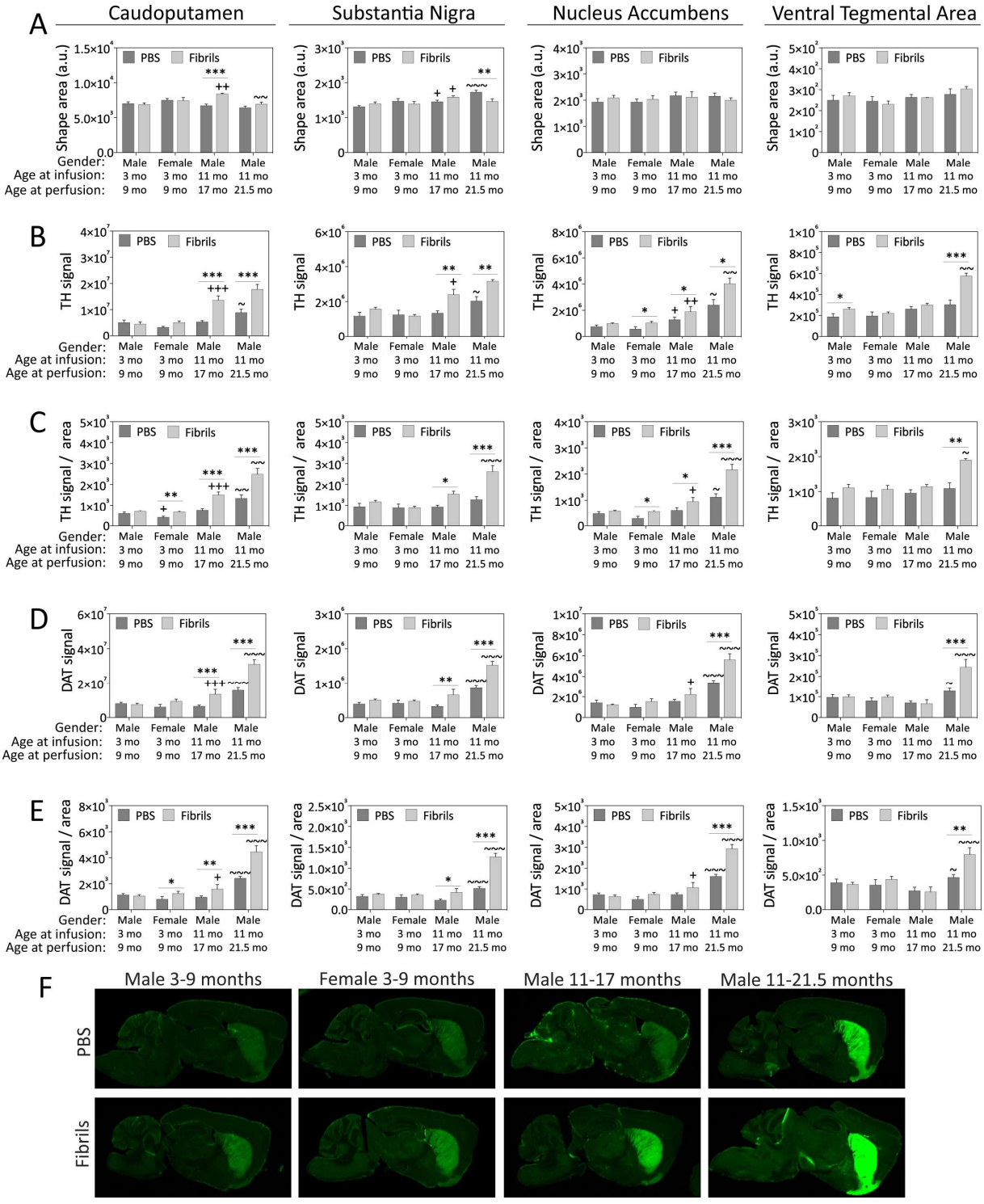
A
Caudoputamen
Substantia Nigra
Nucleus Accumbens
Ventral Tegmental Area
Shape area (a.u.)
PBS
Fibrils
B
TH signal
C
TH signal / area
D
DAT signal
E
DAT signal / area
Gender:
Age at infusion:
Age at perfusion:
Male
Female
3 mo
9 mo
11 mo
17 mo
21.5 mo
F
Male 3-9 months
Female 3-9 months
Male 11-17 months
Male 11-21.5 months
PBS
Fibrils

Figure 33: Preformed α-synuclein fibril injections in the olfactory peduncle increase dopaminergic markers in the nigrostriatal and mesolimbic pathways in older male mice. Mice were infused in the right rear olfactory bulb with either preformed α-synuclein fibrils (5 μg/1 μL) or an equivalent volume of PBS (1 μL). Sagittal brain sections were immunostained with antibodies against the dopaminergic markers tyrosine hydroxylase (TH) and the dopamine transporter (DAT) and scanned on an ultrasensitive infrared imager (LiCor). A blinded observer traced the anatomical boundaries of the dorsal striatum (caudoputamen), ventral striatum (nucleus accumbens), the substantia nigra, and the ventral tegmental area in LiCor ImageStudio software. (**A**) The shape areas drawn around the regions of interest are shown as raw data (unnormalized, arbitrary units). (**B**) The fluorescence reflecting raw TH^+ signal is also displayed in raw, unnormalized, and arbitrary units. (**C**) TH signal is also displayed after normalization to area, reflecting TH signal "density". (**D**) The fluorescence reflecting raw DAT^+ signal is displayed as raw data (unnormalized, arbitrary units). (**E**) DAT signal per unit area is also shown, reflecting DAT signal density. (**F**) Representative pseudocolored images of DAT immunostaining in all groups. Two-way ANOVAs were performed and followed by the Bonferroni correction for multiple comparisons. Shown are the mean and SEM. N = 4-8 mice per group, with the exception of the oldest male group, in which only 3 fibril-infused mice survived to 21.5 months of age (see **Figure 19**). Comparisons were only made *a priori* across groups differing by a single independent variable (either gender, age at surgery, or the passage of time since surgery). * $p \leq 0.05$, ** $p \leq 0.01$, *** $p \leq 0.001$ PBS vs fibrils; + $p \leq 0.05$ ++ $p \leq 0.01$ vs 3-9 month males; ~ $p \leq 0.05$, ~~ $p \leq 0.01$, ~~~ $p \leq 0.001$ vs 11-17 month males.

α-synucleinopathy in the limbic system increases TH expression in the ventral midbrain

To count the dopaminergic cells and $Hoechst^+$ nuclei in the ventral midbrain, we photographed every available midbrain in high-resolution (200×) stitched images. Stitched images were necessary because the entire brain region could not be photographed within the field of view with objectives powerful enough to provide the resolution necessary to distinguish individual cells. In 624 high-resolution images, the TH staining was used to identify the retrorubral field (A8), SN pars compacta (A9), and ventral tegmental area (A10). A blinded observer traced the boundaries of each region (**Figure 34A**), and every TH^+ cell and $Hoechst^+$ nuclei within each region were counted (**Figure 34B, D**). To ensure that differences in trace size were not confounding our results, we also calculated TH^+ cells and $Hoechst^+$ nuclei per area (**Figure 34C, E**). In sagittal sections, the ventral tegmental area presents as a single unit (**Figure 34F**), but at different levels the SN was subdivided into anterior, posterior, and lateral sections with clearly identifiable neuroanatomical

boundaries (**Figure 34G**). In both the TH^+ cell counts and $Hoechst^+$ nuclei counts, there were few significant or robust differences attributable to fibril infusions, and no effects that were the same across groups. To determine the TH signal per cell in the ventral tegmental area and SN pars compacta (**Figure 34H-I**), we divided the TH signal for each animal in **Figure 33B** by the number of TH^+ cells for each animal in **Figure 34B**. Here we observed that all male groups exhibited a significant fibril-induced

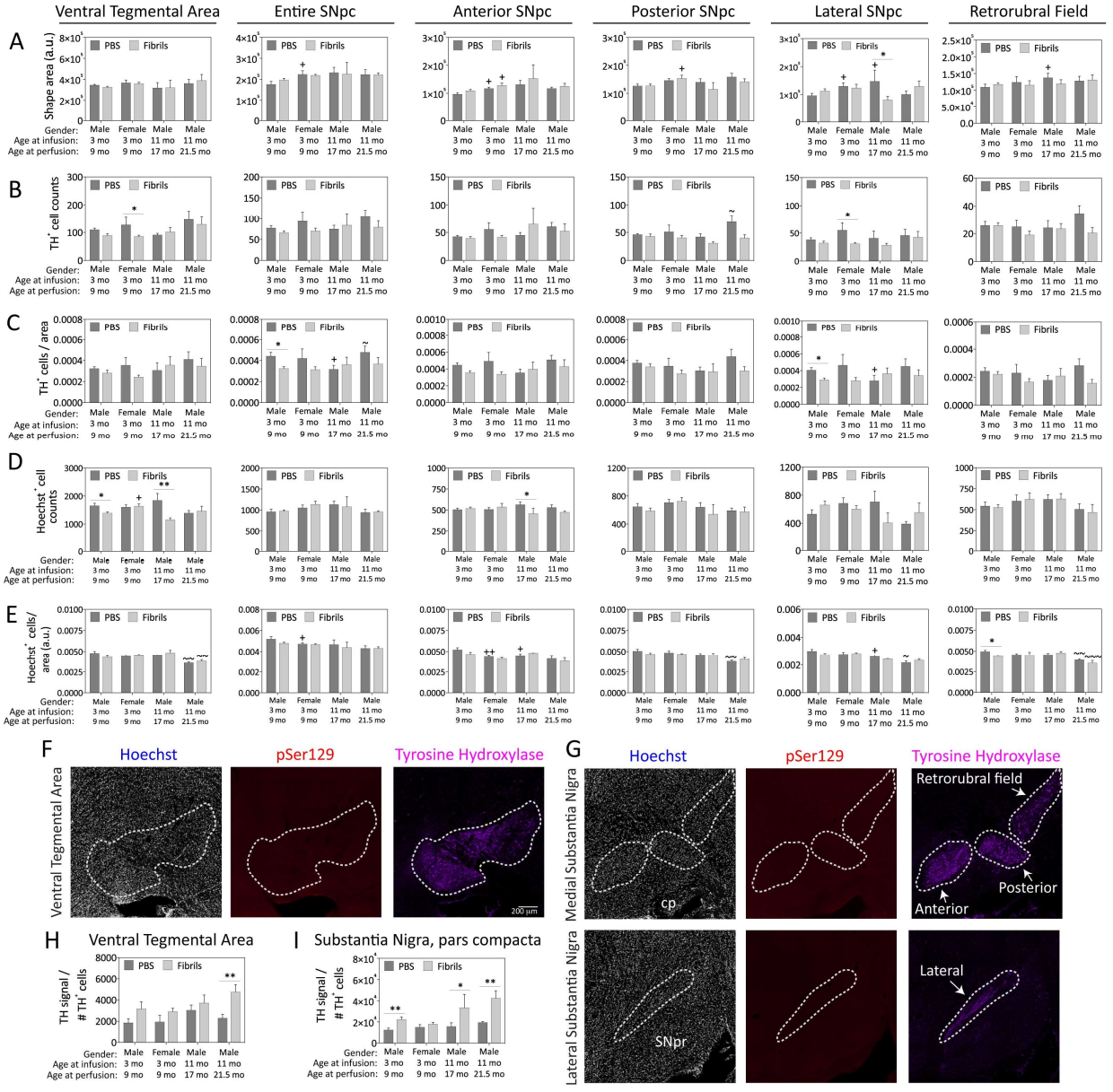

Figure 34: Impact of preformed α-synuclein fibril injections in the olfactory peduncle on dopaminergic cell numbers in the substantia nigra, pars compacta, of the ventral mesencephalon. Mice were infused in the right rear olfactory bulb with either preformed α-synuclein fibrils (5 μg/1 μL) or an equivalent volume of PBS (1 μL). Sagittal brain sections were stained with antibodies against the dopaminergic marker tyrosine hydroxylase (TH) (see **Table 2**) and the nuclear marker Hoechst and 200× images were stitched together to form large, high-resolution photomontages of the ventral mesencephalon from every section of a 1-in-5 sagittal series. A blinded observer traced the anatomical boundaries of the ventral tegmental area and the anterior, posterior, and lateral subregions of the substantia nigra in cellSens software. (**A**) The shape areas drawn around the regions of interest are shown as raw data (unnormalized, arbitrary units per stitched section) from cellSens software. (**B**) Every single visible TH^+ cell encompassing a $Hoechst^+$ nucleus in all the ventral midbrain-containing sections was manually counted by a blinded observer. In the medial substantia nigra, pars compacta, counts were made separately in the anterior and posterior nigra based on boundaries in the TH staining (see panel **G**). The lateral substantia nigra was counted separately, also based on boundaries in the TH staining. Data are presented as area of the region of interest in arbitrary units (**A**), TH^+ cell counts (**B**), and TH^+ cell counts per unit area (cell densities); (**C**). $Hoechst^+$ cell counts (**D**) and $Hoechst^+$ cell densities (**E**) within the boundaries of the area of interest, as traced with dotted lines in panels **F-G**. Note that two of these panels are from fibril-infused mice exhibiting no pSer129 pathology in the ventral midbrain. Raw TH^+ cell counts per animal were divided by the total TH signal generated on the LiCor imager in **Figure 33B** for the ventral tegmental area (**H**) and substantia nigra pars compacta (**I**) as a measure of TH expression per cell. Two-way ANOVAs were performed and followed by the Bonferroni correction for multiple comparisons. Comparisons were only made *a priori* across groups differing by a single independent variable (either gender, age at surgery, or the passage of time since surgery). Shown are the mean and SEM from an n of 4-8 mice per group. * $p \leq 0.05$, ** $p \leq 0.01$, *** $p \leq 0.001$ for PBS vs fibrils; + $p \leq 0.05$ vs 3-9 month male group; ~ $p \leq 0.05$, ~~ $p \leq 0.01$, ~~~ $p \leq 0.001$ vs 11-17 month male group. All abbreviations are listed in **Table 4**.

increase in TH expression per cell in the SN pars compacta (**Figure 34I**). The older males sacrificed 10.5 month post-infusion were the only group to also display increased TH expression per cell in the ventral tegmental area (**Figure 34H**).

Fibril infusions in the OB/AON induce more olfactory deficits in males and mild motor deficits in females

Several behavioral tests were also employed in this study to examine olfaction, motor coordination, and learning and memory function. At three months post-infusion the buried pellet test was performed (**Figure 35A-C**). No differences in the latency to contact the visible treat were observed

between groups (**Figure 35A**). The fibril-induced young male mice exhibited greater latencies to contact the buried treat than fibril-infused females (**Figure 35B**). When the exposed-treat latency

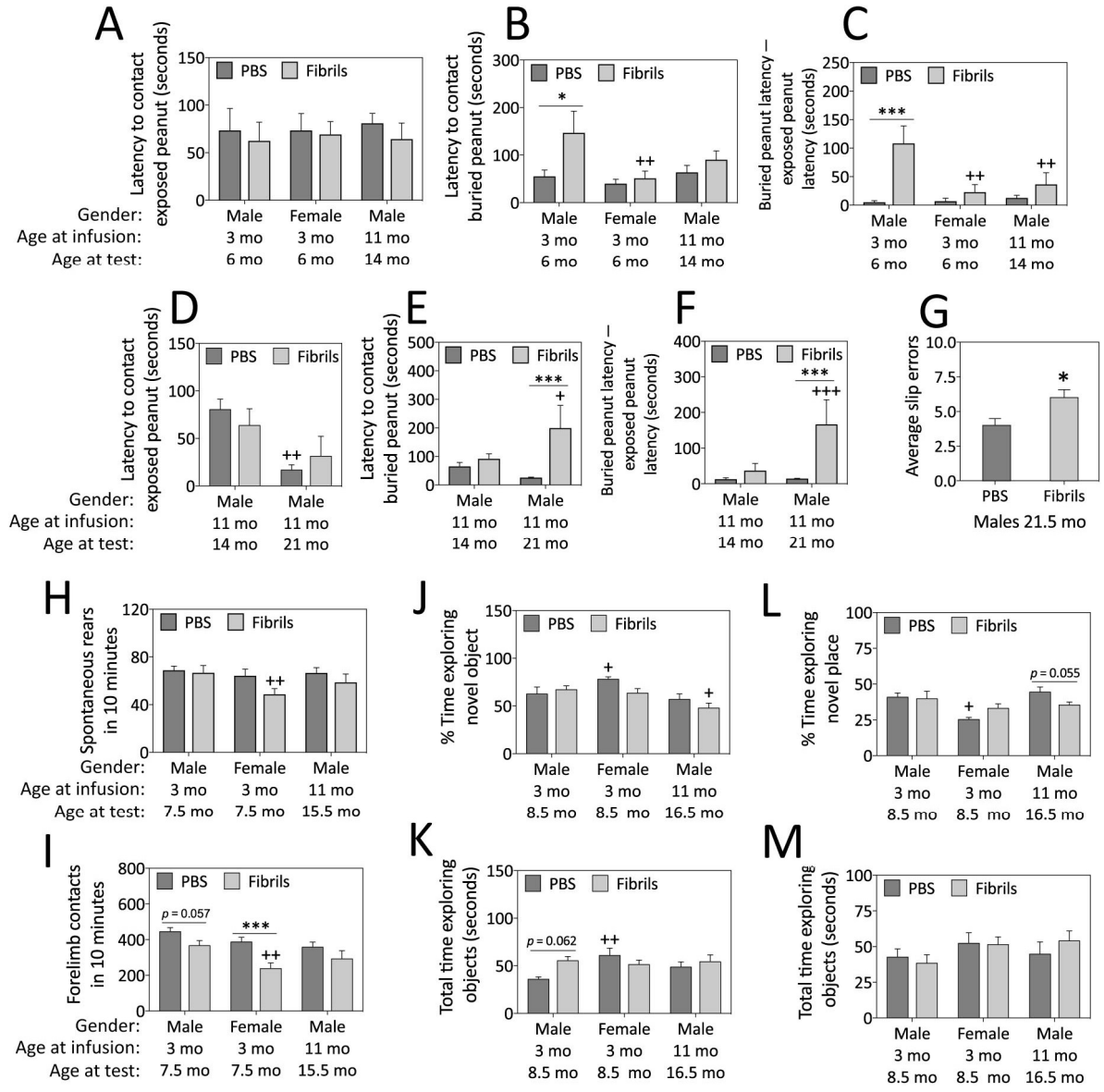

Figure 35: α-Synuclein fibril injections in the olfactory peduncle elicit behavioral deficits. Mice were infused in the right rear olfactory bulb with either preformed α-synuclein fibrils (5 µg/1 µL) or an equivalent volume of PBS (1 µL). The buried pellet test was conducted at 3 months post-infusion and measured the latency to approach an exposed peanut (**A**), the latency to approach a buried peanut (**B**), and the "exposed latency" subtracted from the "buried latency" (**C**). The buried pellet test was performed again at 10 months post-infusion in the older animals and the latter raw scores were contrasted with the raw scores at 3 months post-infusion (**D-F**). Two-weeks later, the challenge beam test was performed in the oldest animals (**G**). The cylinder test was performed at 4.5 months post-infusion (**H-I**). Shown are the number of rears (**H**) and forelimb contacts (**I**) with the walls of the cylinder in 10 minutes. The novel object/place test was performed at 5.5 months post-infusion (**J-M**). Shown are the mean and SEM from an n of 3-16 mice per group. * p≤0.05, ** p≤0.01, *** p≤0.001 PBS vs fibrils; + p≤0.05, ++ p≤0.01 + ++ p≤0.001 versus vs 3-9 month male group.

was subtracted from the buried-treat latency to account for individual preferences for the treat, the older fibril-infused animals were also significantly faster at uncovering the buried treat than the young males (**Figure 35C**). The buried pellet test was performed a second time in the older animals at 10 months post-infusion and their scores compared to the test at three months (**Figure 35D-G**). At 10 months post-infusion, the PBS-infused older males contacted the exposed treat faster than the fibril-infused males (**Figure 35D**), and the fibril-infused older males took longer to find the buried treat than they did at three months (**Figure 35E**). This effect was increased when accounting for each animal's preference for the treat (**Figure 35F**). Two weeks after the second buried pellet test was performed, the mice were subjected to the challenge beam test. Here we observed the fibril-infused males made significantly more slips when crossing the challenge beam (**Figure 35G**), but this effect was only observed in the second of three trials.

In the cylinder test for motor function, female fibril-infused mice reared onto their hind legs significantly less often the male fibril-infused animals of the same age (**Figure 35H**). Females were also the only group to exhibit a fibril-induced reduction in forelimb contacts within 10 minutes (**Figure 35I**), but this may be related to their decreased propensity to rear onto their hind legs.

To examine spatial memory and learning, the novel object and novel place tests were performed. The older fibril-infused males spent less time contacting the novel object than the younger fibril-infused males (**Figure 35J**). Female PBS-infused mice spent more time contacting the novel object as well as both objects compared to age-matched male mice (**Figure 35J-K**), and less time exploring the novel place (**Figure 35L**). In the novel place test, the older fibril-infused males spent

less time exploring the object in the novel place than PBS-infused males (**Figure 35L**) This effect was significant by a two-tailed *t* test, but was only a trend (p=0.055) when applying a two-way ANOVA with a Bonferroni *post-hoc* correction for multiple comparisons.

Discussion

The major findings of this aim are that the risk factors associated with Lewy body disorders are recapitulated in this model. Female mice developed fewer pSer129$^+$ protein aggregations than males in response fibril infusions in the OB/AON, and older mice experienced greater mortality, which is consistent with the increased risk of Lewy body disorders with age and male gender discussed in the introduction. The pattern of pSer129$^+$ inclusions following injection of PFFs into the OB/AON was similar across groups and not dramatically more extensive at 6 and 10.5 months post-infusion than we observed in Aim 1, at three months post-infusion. Even in the 11-month-old mice that survived until 10.5 months post-infusion, the α-synucleinopathy was primarily sequestered within the limbic system. Pathology in extralimbic sites was rare, sparse, and never consistently observed among animals. Unlike in Aim 1, pSer129$^+$ inclusions were observed in the olfactory tubercle and ventral midbrain at 6 and 10.5 months post-infusion, specifically in the ventral tegmental area, ventral premammillary area, and the most medial parts of the SN pars compacta. The medial SN is associated with the limbic system (Haber & Knutson, 2010), and therefore consistent with the "limbic-predominant" label. No pSer129$^+$ inclusions were observed in lateral sections of the SN, which are the most vulnerable to degeneration in PD (Damier et al., 1999; Fearnley & Lees, 1991; Jellinger, 2012).

An important finding of this aim is that female mice develop fewer inclusions than male mice in several brain regions following the induction of α-synucleinopathy in the OB/AON. Female mice did not develop significant inclusions in the olfactory tubercle or dorsal striatum, unlike their male counterparts. If one assumes that pathology travels primarily in a retrograde direction, these brain regions are more than one synapse away from the site of infusion, which suggests that females may be more resistant to the cell-to-cell spread of pathology in addition to pathology that develops from first-order circuitry from the site of infusion. Many of the inclusions that did develop in the olfactory tubercle were perinuclear, suggesting retrograde transport from another brain region rather than anterograde transmission from the OB/AON. Female mice did not exhibit significantly more inclusions than male mice in any brain region. This observation concurs with the greater risk of men to develop Lewy body disorders than women (Beach, Adler, et al., 2009; Savica et al., 2017; Savica et al., 2013; K. M. Smith & Dahodwala, 2014; Twelves et al., 2003), and suggests that this gender-dependent risk may be related to a reduced spread and development of α-synuclein pathology in addition to the general neuroprotective effects of estrogens (Engler-Chiurazzi et al., 2017).

Females also appeared resistant to fibril-induced neurodegeneration as fibril infusions failed to cause a significant loss of $Hoechst^+$ or $NeuN^+$ cells in any brain region. In male mice of the same age, a loss of $NeuN^+$ and $Hoechst^+$ cells was observed in the posteromedial cortical amygdala, a region that develops particularly dense $pSer129^+$ inclusions in this model. A loss of both markers was also observed in the nucleus of the lateral olfactory tract. A loss of $Hoechst^+$ cells but not $NeuN^+$ cells was observed in the both subregions of the piriform cortex as well as in the nucleus

accumbens, suggesting a reduction in non-neuronal cells. Females displayed an increased number of Hoechst^{+} cells in the OB, which could be related to gliosis.

Nelson and colleagues reported that males are more than twice as likely to develop the limbic-predominant subtype of DLB, but that there was not difference in risk to develop the brainstem-predominant subtype (Nelson et al., 2010). This suggests that the gender difference in propensity to develop α-synucleinopathy may be unique to the limbic system. Another group reported no difference between genders 6 months after PFF infusions into the striatum of nontransgenic mice (Kim et al., 2016), but they used human α-synuclein fibrils, which typically do not seed as well in mice as mouse α-synuclein fibrils (Luk et al., 2016; Rey et al., 2018). They also employed different sonication parameters, which can greatly impact the pathogenicity of the fibrils (Polinski et al., 2018). Nevertheless, this may suggest females are more protected from limbic than nigrostriatal α-synucleinopathy. Indeed, female PD patients are more likely to experience dyskinesia, postural instability, and a tremor-dominant phenotype, whereas male PD patients are more likely to experience symptoms of hyposmia and cognitive impairment, which are more dependent upon the limbic temporal lobe (Cholerton et al., 2018; Farhadi et al., 2017; Georgiev et al., 2017).

Olfactory dysfunction is more common in the limbic-predominant subtype of Lewy body disorders than in the brainstem predominant subtype (Beach, White, et al., 2009; Wilson et al., 2011), and as males are more likely to develop the limbic-predominant subtype, it is logical that they would be more likely to experience olfactory dysfunction. Male PD patients typically perform worse than female patients on olfactory exams (Stern et al., 1994). In the buried pellet test, male mice exhibited fibril-induced olfactory dysfunction and females did not (**Figure 35B-C)**, which

suggests that the increased propensity for males to experience hyposmia was recapitulated in this model. Likewise, female mice reared less often and made less forelimb contacts (**Figure 35H-I**), perhaps suggesting that they were experiencing more postural instability, a symptom more associated with women. As females exhibited only mild changes in TH and DAT expression in compared to other groups, it is unlikely that changes in the nigrostriatal pathway are responsible for these motor symptoms.

The older male animals performed the worst on the novel place recognition test, as PFFs reduced their ability to recognize a familiar object in a novel place ($p = 0.055$). Dementia in patients with Lewy body disorders is associated with pathology in the amygdala, cortex, hippocampus, and basal forebrain (Aarsland et al., 2017; Hall et al., 2014; Hurtig et al., 2000). As dense hippocampal Lewy-like pathology following infusions into the hippocampus failed to induce any overt memory deficits (Nouraei et al., 2018), it is unlikely that pathology in the hippocampus alone is sufficient to induce memory deficits. If memory impairment in this model is related to α-synuclein aggregates, it likely requires their presence in multiple interconnected regions to elicit substantial memory deficits. The mild memory deficit that we observed may also be related to the significant loss of $NeuN^+$ cells in the subiculum and CA2 field of the hippocampus in the oldest males. However, the mild memory loss in this model might be also be an advantage in terms of modeling early mild cognitive impairment (MCI) in ADLB.

The α-synucleinopathy was not dramatically more dense or widespread in the animals that were 11 months old at the time of fibril infusion, compared to those that were three months old, but the older animals did exhibit significantly greater mortality in response to fibril infusion. *Rey et al.* did

not report an increase in mortality following olfactory-seeded α-synucleinopathy (Rey et al., 2018; Rey, Steiner, et al., 2016), but their mice were all three months old at the time of infusion. We also did not observe any increased mortality in the mice that were three months old at the time of infusion, at least for the six months that we followed them.

Mice in every fibril-infused group developed some pSer129^{+} inclusions within the ventral midbrain, primarily within the ventral tegmental area. With both epifluorescent and confocal microscopy, minimal colocalization was observed of the TH and pSer129 signal. This may be related to α-synucleinopathy suppressing TH expression (Chu & Kordower, 2007; Chu et al., 2006), or non-dopaminergic neurons in these regions developing pathology. Both the SN pars compacta and ventral tegmental area have non-dopaminergic projections to the amygdala (Loughlin & Fallon, 1983). A tract-tracing study in rats reported a direct projection from the SN to the OB (Hoglinger et al., 2015), and following injection in the OB, the tracer appeared in the medial part of the SN, similar to where we observe pSer129^{+} inclusions. Regardless of the route of transmission, the medial SN pars compacta is less vulnerable to α-synucleinopathy and cell loss in PD (Damier et al., 1999; Fearnley & Lees, 1991), which suggests that this model is more akin to other Lewy body disorders.

Despite a relative dearth of inclusions in the nigrostriatal system compared to the limbic system, we observed a dramatic increase in nigrostriatal TH and DAT signal per area, particularly in older mice. An increase in striatal DAT binding has been reported in monkeys after MPTP injection but before motor deficits appeared (Vezoli et al., 2014). In Lewy body disorders, TH and DAT levels within the nigrostriatal pathway typically decrease as the disease progresses and cases of ILBD

can have as much as a 50% decrease in TH expression without any apparent symptoms (Beach, Adler, et al., 2009). Cases with the abovementioned Stage IIb pathology have the least nigrostriatal degeneration. It is unclear if OB/AON fibril infusions induced the increase in dopaminergic markers in the nigrostriatal pathway or if aged animals with the highest dopaminergic fiber densities were more likely to survive the α-synucleinopathy. The former seems more likely as fibril-induced increases in TH and DAT signal per area were observed in the younger mice without significant mortality. Female mice were least vulnerable to the α-synucleinopathy and were the only group that failed to demonstrate an increase in TH expression per TH^+ cell in the SN, suggesting that the presence of $pSer129^+$ aggregates and changes in dopaminergic markers in the nigrostriatal pathway may be related.

Many of the perinuclear $pSer129^+$ aggregates in the tissue colocalized with the Proteostat aggresome dye. Aggresomes are thought to be a transient protective structure that helps the cell survive conditions of high proteotoxic stress (M. Tanaka et al., 2004; Taylor et al., 2003), by sequestering misfolded and insoluble material at a single location within the cell and helping facilitate degradation. Human Lewy bodies tend to be spherical and not perinuclear, which suggests that somal aggregations in this model may be a less toxic form, more akin to an aggresome. LRRK2 mutations, which increase the likelihood of developing PD, are reported to reduce the formation of aggresomes (Bang et al., 2016), suggesting that the ability to form aggresomes may reduce the toxicity associated with α-synuclein accumulation. It is perhaps for this reason that we observe little to no cell loss in brain regions that are heavily occupied with perinuclear $pSer129^+$ aggregations.

Given the potential for cross-reaction of anti-pSer129 antibodies (Sacino et al., 2014), and that many such antibodies display nonspecific bands in Western blots (Delic et al., 2018), we were very conservative in our approach to identifying and counting inclusions. For the regional counts using the 81a antibody (See **Table 2**) in **Figures 22-24**, no pSer129^{+} structures were excluded from the blinded counts, even in PBS-infused animals, and when qualitatively scoring pathology with the EP15365 antibody used to generate the heatmap figure (**Figure 20**), the GFP channel was always checked for nonspecific label. It is important to note that pSer129^{+} structures that fluoresced in multiple channels were always excluded from the blinded analysis. Thus, the ability to observe nonspecific staining by checking multiple fluorescent channels is an advantage of our method of histological examination. Rey and colleagues reported a more extensive spread of pathology at 6 and 12 months post-infusion into the rostral OB (Rey et al., 2018; Rey, Steiner, et al., 2016), but we observed a greater of abundance of inclusions within our tissue. These differences in reported α-synucleinopathy may be attributable to difference in the injection site, strain of mouse, fibril sonication parameters, and immunohistochemical methodology.

We were somewhat limited in this aim by the high level of mortality in our oldest cohort. The histopathology in the animals sacrificed at 6 and 10.5 months post-infusion agrees with Aim 1, but we do not know if the animals that died prematurely exhibited a different pattern of staining or a concentration of pathology in any particular region. Therefore, while the pathology in the perfused animals corresponds with Beach's Stage IIb pathology, it is possible that the animals that died prematurely had pathology in additional regions, such as the brainstem. We can only speculate as to the cause of mortality in the aged animals. It may be related to the particularly dense pathology we observe in the amygdala as this region is involved with regulating endocrine and autonomic

functions (Braak et al., 1994). The caudoputamen was the only region to develop significantly more inclusions in 11-month-old fibril-infused mice than in the 3-month-old mice at 6 months post-infusion, and the ectorhinal cortex only developed significant pathology at this time in the 11-month-old animals. This could suggest that the development of pathology in these regions is related to mortality in this model, as the animals that survived for an additional 4.5 months had few inclusions in these regions.

Chapter 3

Rationale

N-Acetyl Cysteine (NAC) is an inexpensive and off-patent medication with an excellent safety profile and minimal side effects. In PD patients, NAC can reduce striatal dopamine transporter loss, provide a mild reduction in motor deficits (Monti et al., 2016), and boost GSH levels in the brain (Holmay et al., 2013). While NAC supplementation may be beneficial to PD patients, the mechanism of action is thought to be upregulation of GSH synthesis via the rate-limiting cysteine precursor. Although the Leak lab reported NAC-induced protection against proteotoxicity in multiple cell types (Heinemann et al., 2016; Jiang et al., 2013; Unnithan et al., 2014), we also found that inhibition of GSH synthesis does not necessarily abolish NAC-mediated protection (Gleixner et al., 2017). Furthermore, it is not known if NAC can reduce the development and spread of α-synucleinopathy in non-transgenic mice that do not overexpress α-synuclein. Thus, the goal of this Aim is to begin to address these gaps.

As detailed in the Introduction, Lewy body disorders are characterized by both proteotoxic and oxidative stress. Our lab published data reporting that NAC can protect neurons from proteotoxic and oxidative stress in GSH-dependent and GSH-independent manners. In N2a neuroblastoma cells, NAC was able to attenuate the loss of GSH after dual treatments of the oxidative stressor hydrogen peroxide (Unnithan et al., 2014). However, NAC also protected against a single treatment of the proteasome inhibitor MG132 without affecting GSH levels (Unnithan et al., 2012). When multiple treatments of MG132 were applied, NAC was still protective and GSH levels were only then upregulated. The collective data suggested that NAC can protect against the proteotoxic stress of one treatment of MG132 independent of any changes in GSH. Consistent with this hypothesis, *Jiang et al.* later showed that NAC facilitates the heat shock protein response to injury and increases Hsp70 expression (Jiang et al., 2013). NAC was able to reduce the accumulation of ubiquitin-conjugated proteins in response to MG132 treatment, and Hsp70 inhibition attenuated NAC mediated protection against the proteotoxicity.

Heat shock proteins are anti-apoptotic chaperones that can be upregulated in neurodegenerative diseases. Misfolded proteins will often expose a hydrophobic motif with multiple Hsp70 binding sites (Rudiger et al., 1997). Hsp70 binding promotes proteasomal degradation by coordinating the interaction between the misfolded proteins and the 20s proteasome (Shiber & Ravid, 2014). Hsc70 is the constitutively expressed form of Hsp70, and Hsc70 levels decline in the SN and amygdala in PD patients (Alvarez-Erviti et al., 2010). Hsp70 is the stress-inducible form, but it becomes less inducible with age (Fargnoli et al., 1990), possibly contributing to the higher risk of developing neurodegenerative diseases with advancing age. Hsp70 is reported to reduce α-synuclein toxicity

(Danzer et al., 2011; Klucken et al., 2004), inhibit the assembly of α-synuclein fibrils (Luk et al., 2008), and reduce α-synuclein aggregates *in vitro* (Kilpatrick et al., 2013).

In primary OB neurons, Crum *et al.* demonstrated that both proteotoxic and oxidative stressors increase Hsp70 levels. The proteasome inhibitors MG132 and lactacystin and the oxidative stressor paraquat increased levels of Hsp70, Hsp25, Hsp32 (Crum et al., 2015). The Hsp70 inhibitors MAL3-101 and VER155008 exacerbated the toxicity of the proteasome inhibitors but not of paraquat, suggesting that Hsp70 is better able to mitigate proteotoxic than oxidative stress. Similarly, in primary hippocampal neurons, NAC was reported to be protective against multiple hits of MG132 but not paraquat (Heinemann et al., 2016).

The abovementioned findings reveal that NAC may protect cells against proteotoxicity and oxidative stress. However, studies of the mechanism underlying the protective effects of NAC were only conducted in neuroblastoma cell lines, which are immortalized and display a number of pro-survival mutations, unlike post-mitotic neurons. Therefore, the first goal of this aim was to build on previous findings, examine the ability of NAC to protect postnatal primary OB and hippocampal neurons from proteasome inhibition and oxidative stress *in vitro*, and determine the underlying mechanism of action, using three independent measures of cell viability. The OB and hippocampus were chosen because the OB is affected in the early stages of Lewy body disorders, whereas the hippocampus is affected in the later stages, allowing us to study the two temporal extremes of these conditions. Pathology in the olfactory structures is associated with a declining sense of smell (Wilson et al., 2011), and starting a treatment when this symptom first emerges may help delay the more debilitating symptoms associated with Lewy body disorders. Dementia is a

common symptom at the end stages of Lewy body disorders and it is associated with Lewy pathology in the hippocampus (Hall et al., 2014). Preserving the functional integrity of this region may help delay this debilitating and costly outcome. Both regions develop pathology in the *in vivo* model of limbic α-synucleinopathy developed in Aim 1.

As Jiang and colleagues had demonstrated that the GSH-independent protective actions of NAC may be mediated by Hsp70 induction in N2a cells that are derived from a murine sympathetic nervous tissue (Schubert et al., 1969), we tested the hypothesis that NAC might protect primary OB and hippocampal neurons against proteasome inhibition by upregulating Hsp70. To this end, we used multiple Hsp70 inhibitors with different mechanisms of action. VER155008 is an adenosine-derived ATP-competitive inhibitor that binds to the nucleotide-binding domain of Hsp70 and inhibits its ATPase and chaperone activity (Schlecht et al., 2013). MAL-3101 is a pyrimidinone that blocks Hsp40-dependent ATP hydrolysis by Hsp70 (Fewell et al., 2004). MAL3-101 treatment was also reported to increase α-synuclein aggregation in neuroglioma cells, whereas the Hsp70 activator 115-7c reduced α-synuclein aggregation (Kilpatrick et al., 2013).

As α-synuclein fibril treatment is typically not lethal to cells, we employed multiple toxicants to recapitulate the cell loss that is frequently observed in Lewy body disorders. MG132 and lactacystin are proteasome inhibitors that block the proteolytic activity of the proteasome (D. H. Lee & Goldberg, 1998). MG132 can also inhibit cathepsins and calpains, which are also involved with protein degradation, but it is approximately 10-fold more selective for the proteasome (Kisselev & Goldberg, 2001). Lactacystin is a bacterial toxin that can also inhibit cathepsin A (Aikawa et al., 2006). Paraquat inhibits complex 1 of the mitochondria and increases the generation

of ROS (Castello et al., 2007; Jenner, 2003). Paraquat exposure increases the risk of developing PD (Tanner et al., 2011).

NAC was reported to decrease the levels of human α-synuclein and attenuate the loss of dopaminergic terminals in transgenic mice over-expressing human α-synuclein (J. Clark et al., 2010). In that study, the mice received approximately 1000 mg/kg/day for over 10 months while in clinical trials in Alzheimer's and PD patients, the typical oral dose is between 50 and 100 mg/kg/day (Adair et al., 2001) (NCT02212678; NCT01470027). Clark *et al.* also did not examine the effect of NAC on cell loss *in vivo,* because the animal models of α-synuclein overexpression typically do not recapitulate the dopaminergic cell loss that characterizes PD. Therefore, the second goal of this aim is to test the hypothesis that NAC can reduce the development and spread of α-synucleinopathy and protect against cell loss in a non-transgenic mouse model at a more translatable dosage. Thus, we fed a cohort of mice a specially formulated diet consisting of 0.15% NAC, beginning immediately after stereotaxic injection with preformed α-synuclein fibrils. Our final measurements suggested that the dose was ~200 mg/kg/day per mouse, which is comparable to human studies. After three months, the animals were sacrificed and Lewy-like inclusions were counted to examine if NAC can reduce the development and spread of α-synucleinopathy. The number of $NeuN^+$ neurons and $Hoechst^+$ cells were also counted to determine if NAC prevented proteotoxicity-induced cell loss *in vivo*. If successful at facilitating the Hsp70 response to proteotoxicity and reducing limbic α-synucleinopathy, NAC may be a potentially viable treatment strategy for other neurodegenerative diseases.

Specific Aim 3 – To test the hypothesis that NAC can decrease the development and spread of PD-related pathology *in vivo* and *in vitro.*

Results

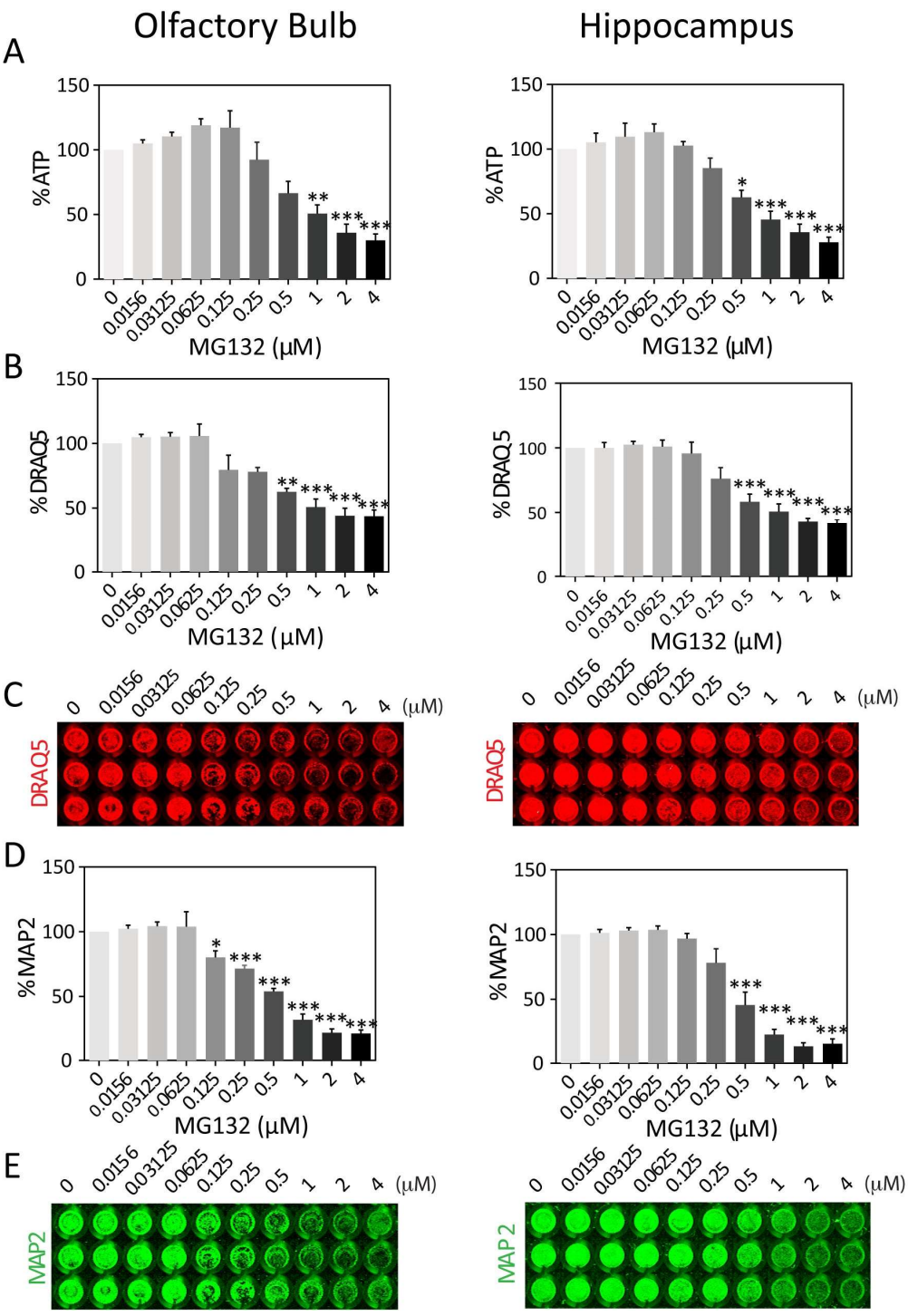

Figure 36: Concentration response curves for MG132 in olfactory bulb and hippocampal cultures. Cultures were treated with MG132 on DIV5 and assayed for viability on DIV7. (**A**) The Cell Titer Glo luminescent assay for ATP. (**B**) In-Cell Western assay for DRAQ5 levels with (**C**) representative image. (**D**) In-Cell Western assay for MAP2 levels with (**E**) representative image. Displayed are the mean and SEM of 3-4 independent experiments that were performed in triplicate. One-way ANOVA with Bonferroni *post hoc* correction. * $p \leq 0.05$, ** $p \leq 0.01$, *** $p \leq 0.001$ vs 0 µM MG132.

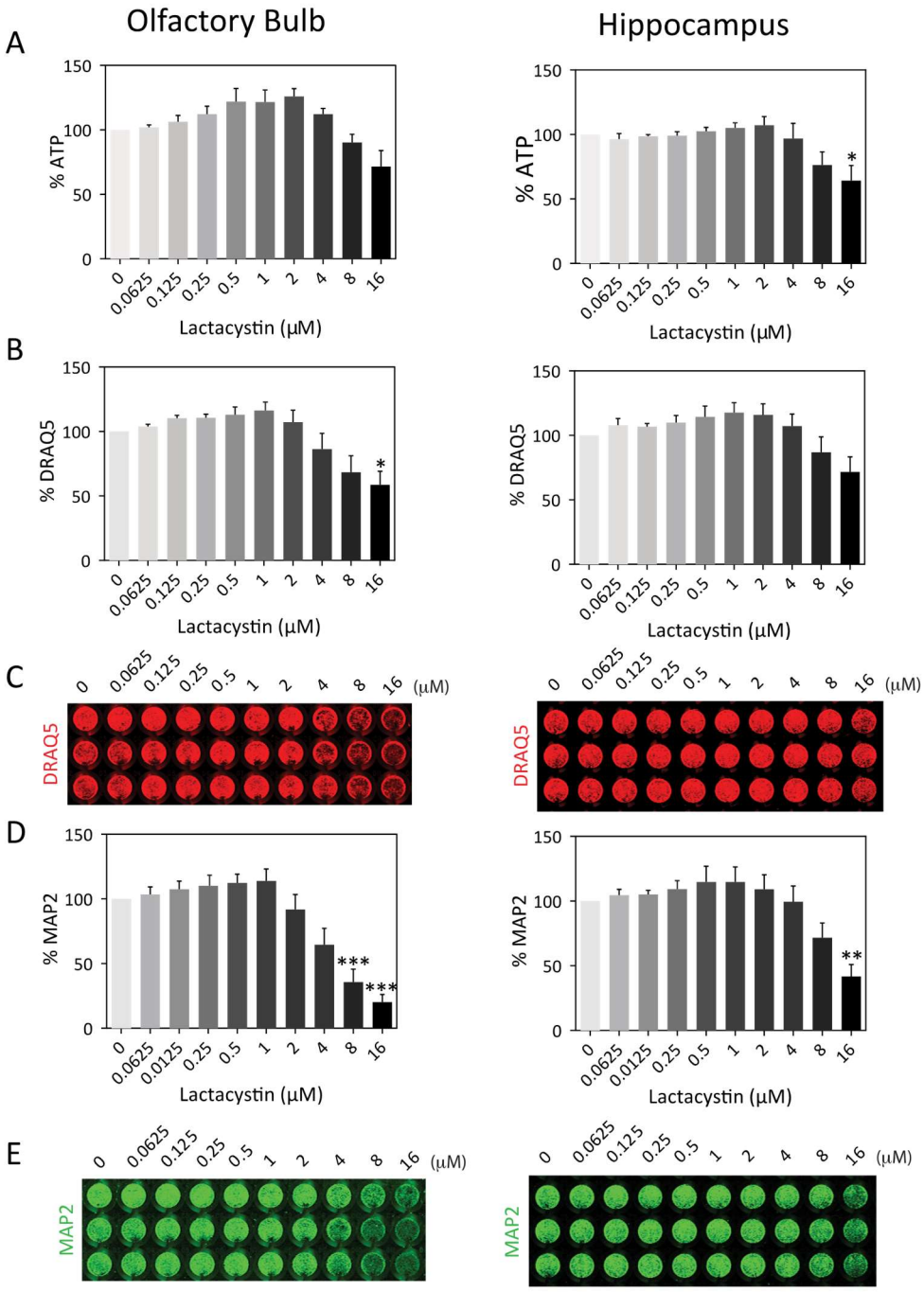

Figure 37: Concentration response curves for lactacystin in olfactory bulb and hippocampal cultures. Cultures were treated with lactacystin on DIV5 and assayed for viability on DIV7. (**A**) The Cell Titer Glo luminescent assay for ATP. (**B**) In-Cell Western assay for DRAQ5 levels with (**C**) representative image. (**D**) In-Cell Western assay for MAP2 levels with (**E**) representative image. Displayed are the mean and SEM of 3-4 independent experiments that were performed in triplicate. One-way ANOVA with Bonferroni *post hoc* correction. * $p \leq 0.05$, ** $p \leq 0.01$, *** $p \leq 0.001$ vs 0 μM lactacystin.

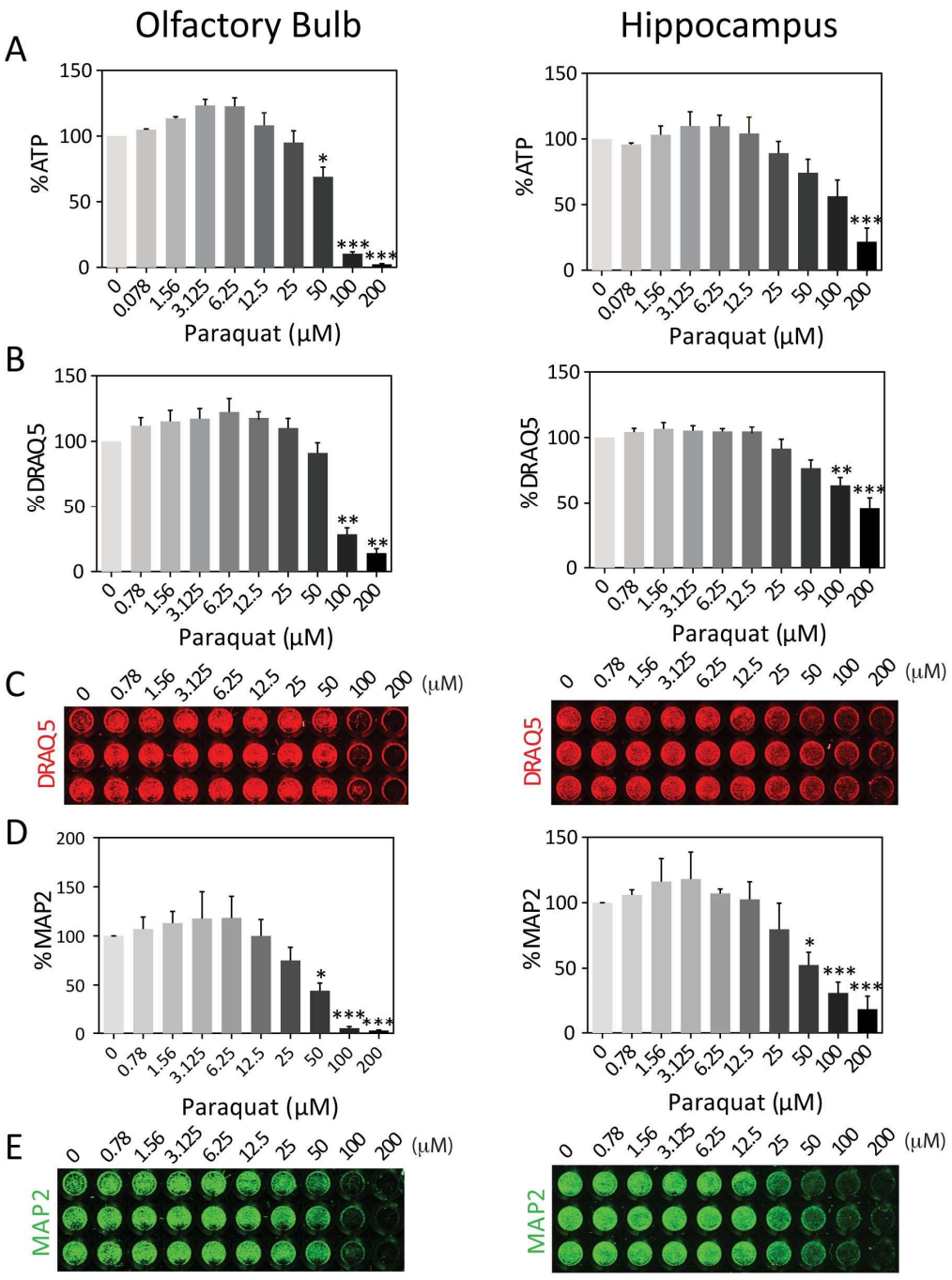

Figure 38: Concentration response curves for paraquat in olfactory bulb and hippocampal cultures. Cultures were treated with paraquat on DIV5 and assayed for viability on DIV7. (**A**) The Cell Titer Glo luminescent assay for ATP. (**B**) In-Cell Western assay for DRAQ5 levels with (**C**) representative image. (**D**) In-Cell Western assay for MAP2 levels with (**E**) representative image. Displayed are the mean and SEM of 3-4 independent experiments that were performed in triplicate. One-way ANOVA with Bonferroni *post hoc* correction. * $p \leq 0.05$, ** $p \leq 0.01$, *** $p \leq 0.001$ vs 0 μM paraquat.

MG132, lactacystin, and paraquat exhibit concentration-dependent toxicity in primary OB and hippocampus neurons

In both OB and hippocampus primary neuron cultures, MG132, lactacystin, and paraquat elicited significant concentration-dependent toxicity that was similar in neurons from both brain regions (**Figures 36-38**). As lactacystin was not consistently significantly toxic in all viability assays at concentrations as high as 16 μM (**Figure 37**), and Crum *et al.* demonstrated that Hsp70 inhibition potentiates the toxicity of MG132 more than lactacystin (Crum et al., 2015), we chose to use MG132 as our proteasome inhibitor in subsequent studies. Paraquat treatment did not result in a consistent IC_{50} across all assays (**Figure 38**), and Heinemann *et al* subsequently showed that NAC is not protective against paraquat toxicity (Heinemann et al., 2016). For these reasons, we did not pursue the effects of NAC on paraquat toxicity further.

NAC protects primary OB and hippocampal neurons from MG132-induced proteotoxicity independent of GSH

After deciding to use MG132 to model proteotoxic stress in primary neurons, we examined the effect of increasing concentrations of NAC in the presence of the IC_{50} value determined with the concentration-response curve in **Figure 34** (0.5 μM MG132). Here we observed a concentration-dependent increase in cell viability with the highest viability at 1000 μM NAC. Significant protection from MG132 toxicity was observed in both the OB and hippocampus cultures in the ATP and MAP2 assays at this concentration. DRAQ5 is less specific for neurons and did not reveal

any protection at this concentration of NAC. When the GSH signal was normalized to the DRAQ5 signal for cellular nuclei, we observed that MG132 significantly increased GSH levels per cell at lower concentrations of NAC but not at higher concentrations in cultures from both brain regions. This could suggest that as NAC can act as an antioxidant on its own, and that high levels of NAC may reduce the cellular demand for GSH production.

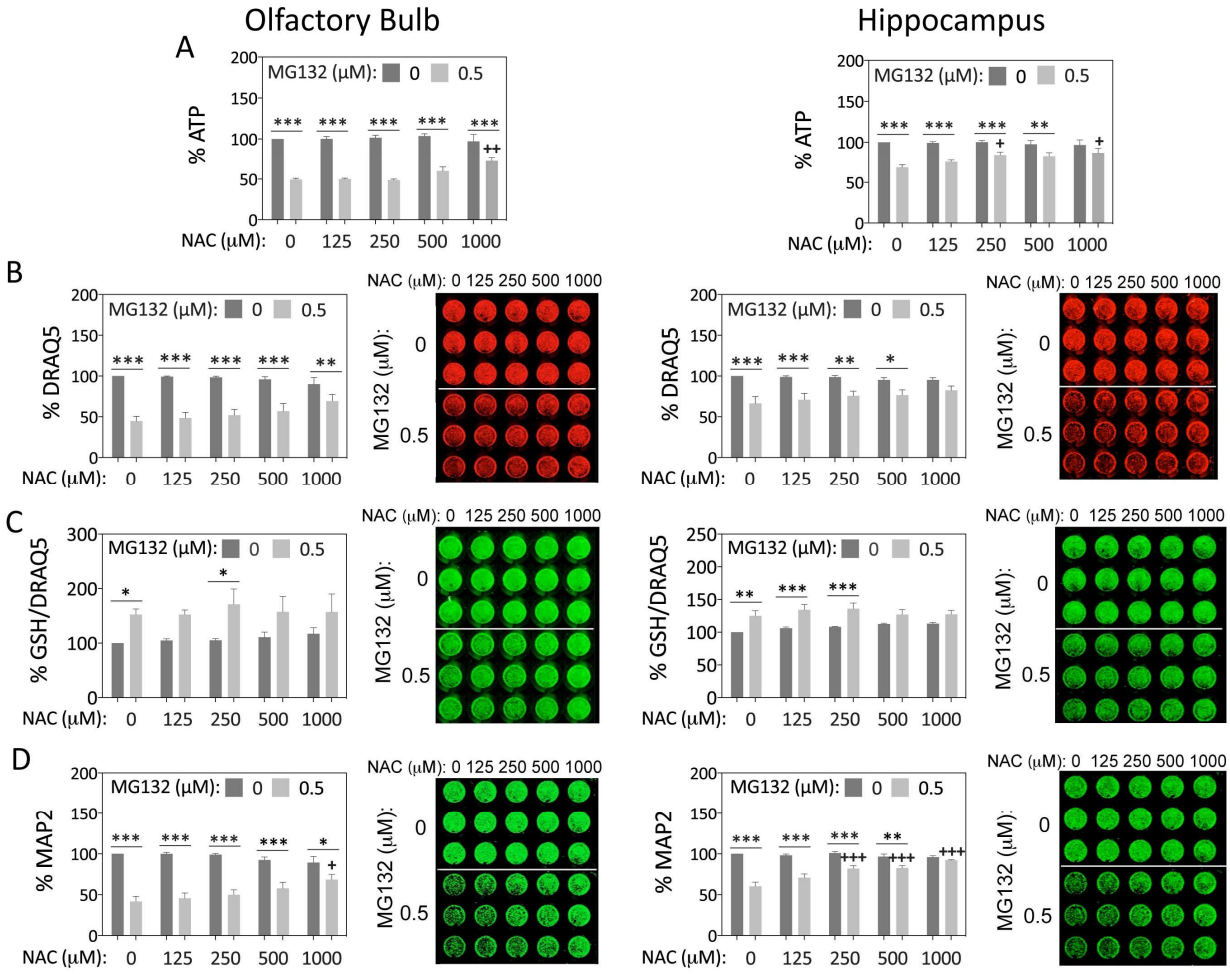

Figure 39: N-acetyl cysteine protects OB and hippocampal neurons against proteotoxicity without increasing glutathione levels. Primary OB and hippocampus cultures were treated with MG132 and increasing concentrations of NAC on DIV5 and assayed on DIV7. (**A**) The Cell Titer Glo luminescent assay for ATP. (**B**) In-Cell Western assay for DRAQ5 levels with representative image. (**C**) In-Cell Western for GSH expressed as a function of nuclear staining with DRAQ5 and representative GSH image. (**D**) In-Cell Western assay for MAP2 levels with representative image. Displayed are the mean and SEM of 3-4 independent experiments that were performed in triplicate. Two-way ANOVA with Bonferroni *post hoc* correction. * $p \leq 0.05$, ** $p \leq 0.01$, *** $p \leq 0.001$ vs 0 μM MG132. + $p \leq 0.05$, ++ $p \leq 0.01$, +++ $p \leq 0.001$ vs 0 μM NAC

Hsp70 inhibition reduces the protective effect of NAC

As 1000 µM was the most protective NAC concentration examined here, and hippocampal cultures were more responsive to NAC and survived the culturing process more readily, we performed the Hsp70 inhibitor studies at this concentration in primary hippocampal neurons. MAL-3101 blocks Hsp40-dependent ATP hydrolysis by Hsp70 (Fewell et al., 2004), and therefore inhibits its protein chaperone function. In the absence of MAL3-101, NAC was able to provide significant protection against MG132 toxicity in the Cell Titer Glo assay for ATP levels and MAP2 In-Cell Western

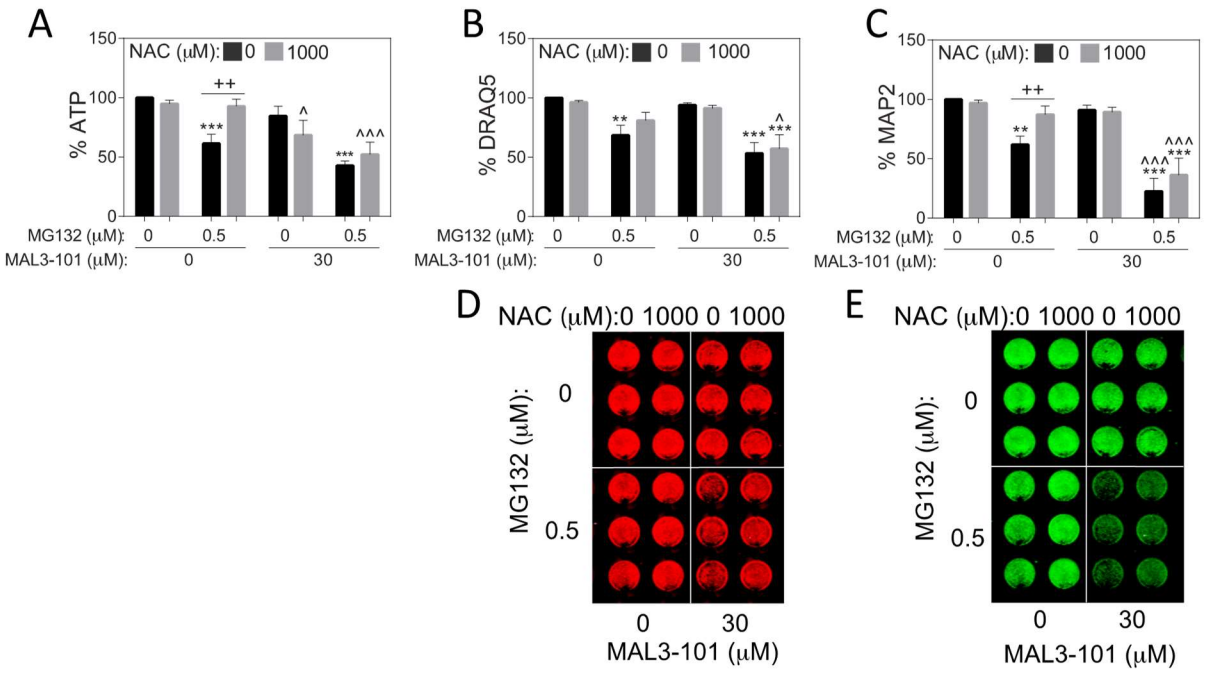

Figure 40: Heat shock protein 70 inhibition by MAL3-101 reduces NAC mediated protection against MG132. Primary hippocampus cultures were treated with MG132, NAC, and MAL3-101 on DIV5 and assayed on DIV7. (**A**) The Cell Titer Glo luminescent assay for ATP. (**B**) In-Cell Western assay for DRAQ5. (**C**) In-Cell Western assay for MAP2 levels. (D) Representative DRAQ5 image. (E) Representative MAP2 image. Displayed are the mean and SEM of 3-4 independent experiments that were performed in triplicate. Three-way ANOVA with Bonferroni *post hoc* correction.* $p \leq 0.05$, ** $p \leq 0.01$, *** $p \leq 0.001$ vs 0 µM MG132. + $p \leq 0.05$, ++ $p \leq 0.01$, +++ $p \leq 0.001$ vs 0 µM NAC, ^ $p \leq 0.05$, ^^ $p \leq 0.01$, ^^^ $p \leq 0.001$ vs 0 µM MAL3-101

(**Figure 40A, C, E**). In the presence of 30 μM of MAL3-101, NAC was no longer able to protect hippocampal neurons. A similar effect was observed when Hsp70 inhibitor VER155008 was used (**Figure 41**). However, in the VER155008 experiments, a reduction in NAC-mediated protection was only observed in the Cell-Titer Glo assay for ATP levels (**Figure 41A**). It is possible that the VER155008 compound had degraded to some degree, and both MAL-3101 and VER155088 display some basal toxicity in primary neuron cultures.

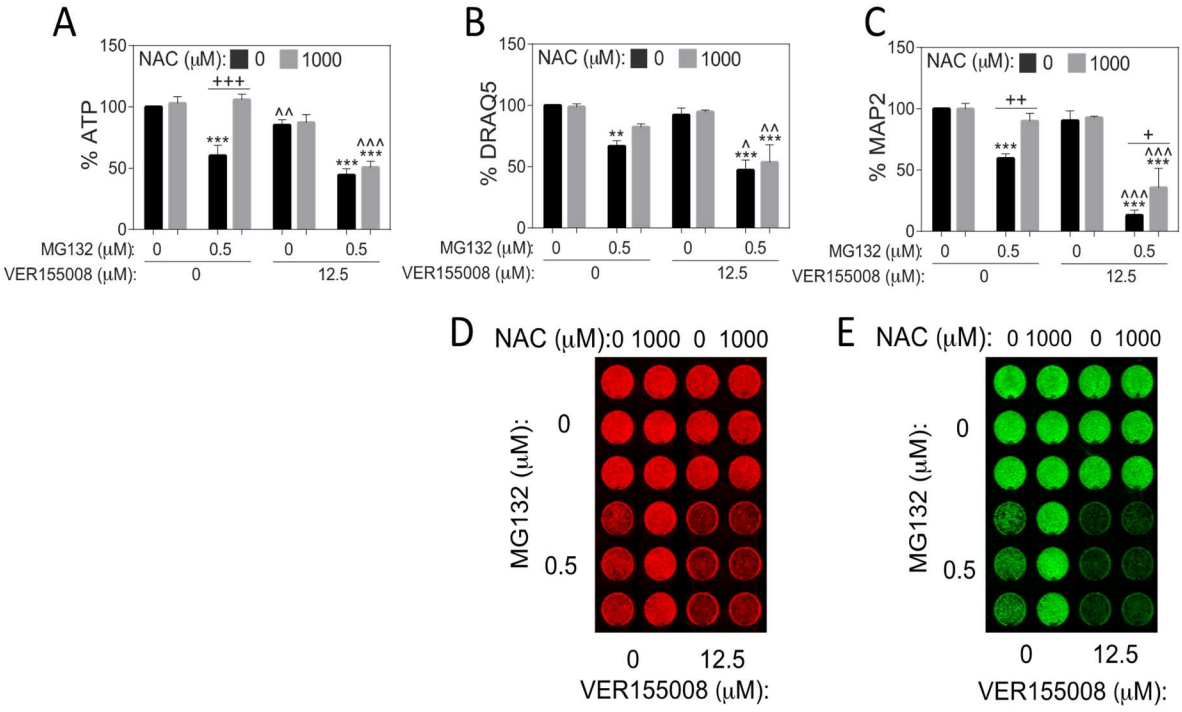

Figure 41: Heat shock protein 70 inhibition by VER155088 reduces NAC mediated protection against MG132. Primary hippocampus cultures were treated with MG132, NAC, and VER155088 on DIV5 and assayed on DIV7. (**A**) The Cell Titer Glo luminescent assay for ATP. (**B**) In-Cell Western assay for DRAQ5. (**C**) In-Cell Western assay for MAP2 levels. (**D**) Representative DRAQ5 image. (**E**) Representative MAP2 image. Displayed are the mean and SEM of 3-4 independent experiments that were performed in triplicate. Three-way ANOVA with Bonferroni *post hoc* correction.* $p \leq 0.05$, ** $p \leq 0.01$, *** $p \leq 0.001$ vs 0 μM MG132. + $p \leq 0.05$, ++ $p \leq 0.01$, +++ $p \leq 0.001$ vs 0 μM NAC, ^ $p \leq 0.05$, ^^ $p \leq 0.01$, ^^^ $p \leq 0.001$ vs 0 μM VER155088

NAC reduces the number of pSer129^{+} inclusions in response to α-synuclein fibril treatment in primary OB neurons

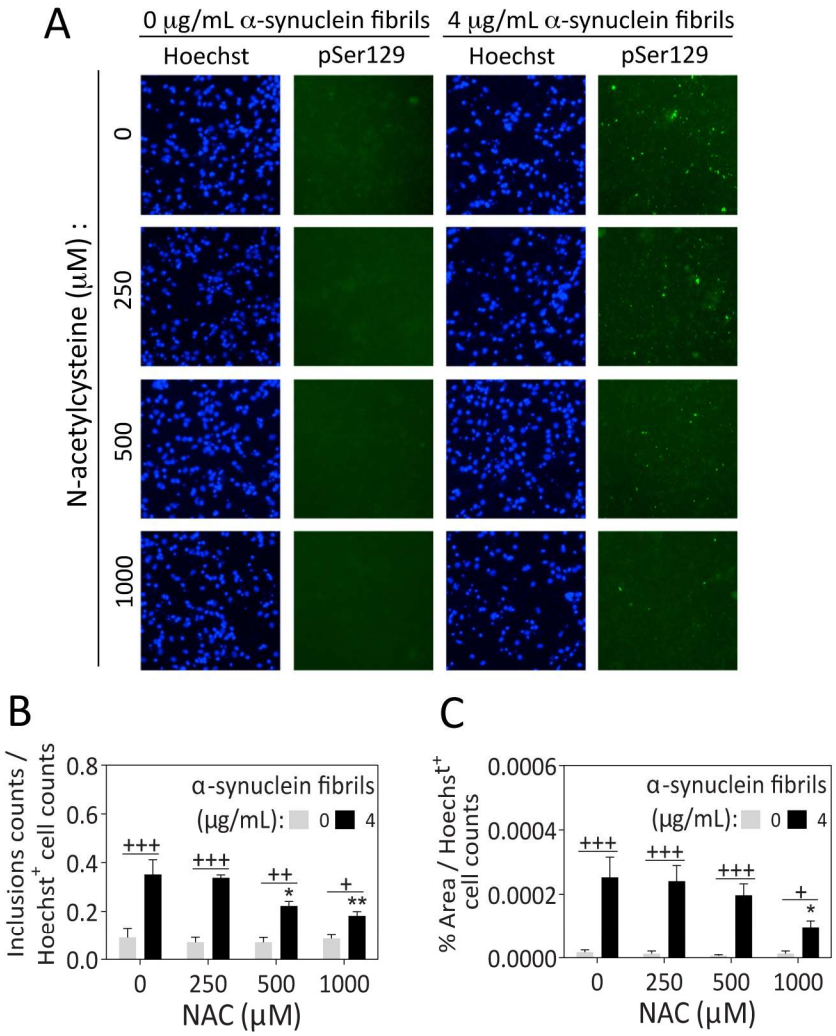

Figure 42: N-acetyl cysteine reduces the development of pSer129^{+} inclusions in primary OB neurons. Primary OB neuron cultures were treated 4 μg/mL α-synuclein fibrils and NAC on DIV2 and on DIV7, the plates were fixed and immunostained for anti-pSer129. Hoechst reagent was applied to visualize nuclei. Images were captured with the 20× objective on the EVOS microscope and analyzed with ImageJ software (**A**) Representative images of Hoechst^{+} cells and pSer129^{+} inclusions. (**B**) Pser129^{+} inclusion counts expressed as a fraction of Hoechst^{+} cells. (**C**) Percent area of pSer129^{+} inclusions (monoclonal 81A pSer129 antibody; see **Table 2**) expressed as a fraction of Hoechst^{+} cells. Displayed are the mean and SEM of 3-4 independent experiments that were performed in triplicate. Two-way ANOVA with Bonferroni *post hoc* correction. * $p \leq 0.05$, ** $p \leq 0.01$, *** $p \leq 0.001$ vs 0 μM NAC. + $p \leq 0.05$, ++ $p \leq 0.01$, +++ $p \leq 0.001$ vs 0 μg/mL α-synuclein fibrils

In OB neuron cultures, we then examined if NAC can reduce the amount of pSer129$^+$ inclusions that develop in response to treatment with preformed α-synuclein fibrils. Here we observed a concentration-dependent decrease in the amount of pSer129$^+$ inclusions with increasing NAC (**Figure 42A**). When normalized to the number of Hoechst$^+$ nuclei, both the amount and area fraction of the inclusions were significantly reduced (**Figure 42B-C**). These studies provided precedence for an extensive *in vivo* analysis of the therapeutic potential of NAC.

NAC supplemented diet does not affect food consumption or weight gain

The *in vivo* portion of this Aim involved stereotaxic infusions into the OB/AON of 40 CD-1 mice. The mice were three months old at the time of infusion and were sacrificed after three months of oral NAC treatment. Twenty mice were infused with 1 µL of 5 µg/µL of preformed α-synuclein fibrils and 20 mice were infused with an equivalent volume of PBS. Half of the mice in each treatment group received control rodent chow or a specially formulated diet containing 0.15%

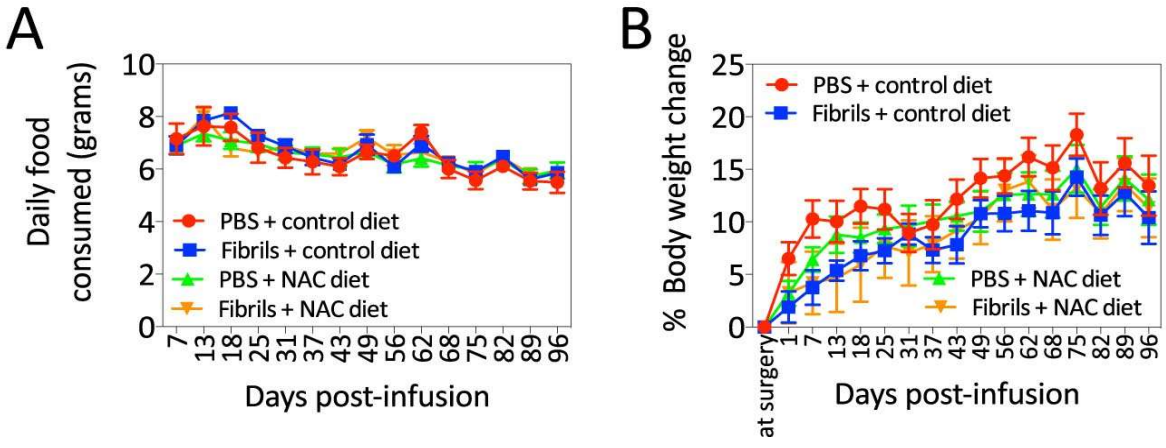

Figure 43: N-acetyl cysteine supplemented diet does not affect food consumption or bodyweight. CD-1 mice received either a specially formulated diet with 0.15% NAC (n = 20) or normal rodent chow (n = 20) for three months. Half of the mice on each diet were stereotaxically infused with either 1 µL of 5 µg/µL preformed α-synuclein fibrils or an equivalent volume of PBS for a total of 10 mice per group (**A**) Daily grams of food consumed over the course of the study. (**B**) Percent change in bodyweight over the course of the study

NAC. The amount of food consumed and the weight of each animal were measured every 5-7 days. Over the course of three months, no differences in the amount of food consumed or the weight gained were observed across treatment groups (**Figure 43**), suggesting that the NAC diet did not affect how much food the animals consumed. We did not collect plasma or CSF for measurements of NAC entry into the blood and brain to avoid disruption of the behavioral tests.

NAC only reduces the number of pSer129$^+$ inclusions that develop in the anterior olfactory nucleus after α-synuclein fibril infusions

At approximately three months post-infusion, the mice were sacrificed by perfusion under anesthesia and their brains were dissected. The brains were cut into sagittal sections in a 1-in-5 series and immunostained for pSer129 and NeuN. The Hoechst reagent was also applied to the tissue. This tissue was photographed on the Olympus microscope at 40× magnification and analyzed by a blinded observer using ImageJ software. In this experiment, the only region exhibiting a significant reduction in pSer129$^+$ inclusions with the NAC diet was the AON (**Figure 44A-B**), which is the site of the densest Lewy-like pathology in the brain. No loss of NeuN$^+$ of Hoechst$^+$ cells was observed in this region at three months post-fibril infusion. In all other regions examined, the NAC diet did not affect the amount of inclusions that developed, but the NAC diet did not significantly increase the amount of inclusions that developed in any brain region compared to the fibril-infused animals receiving the control diet. In the entorhinal cortex, the NAC diet appeared to significantly reduce both NeuN$^+$ and Hoechst$^+$ cell numbers (**Figure 44J**), although

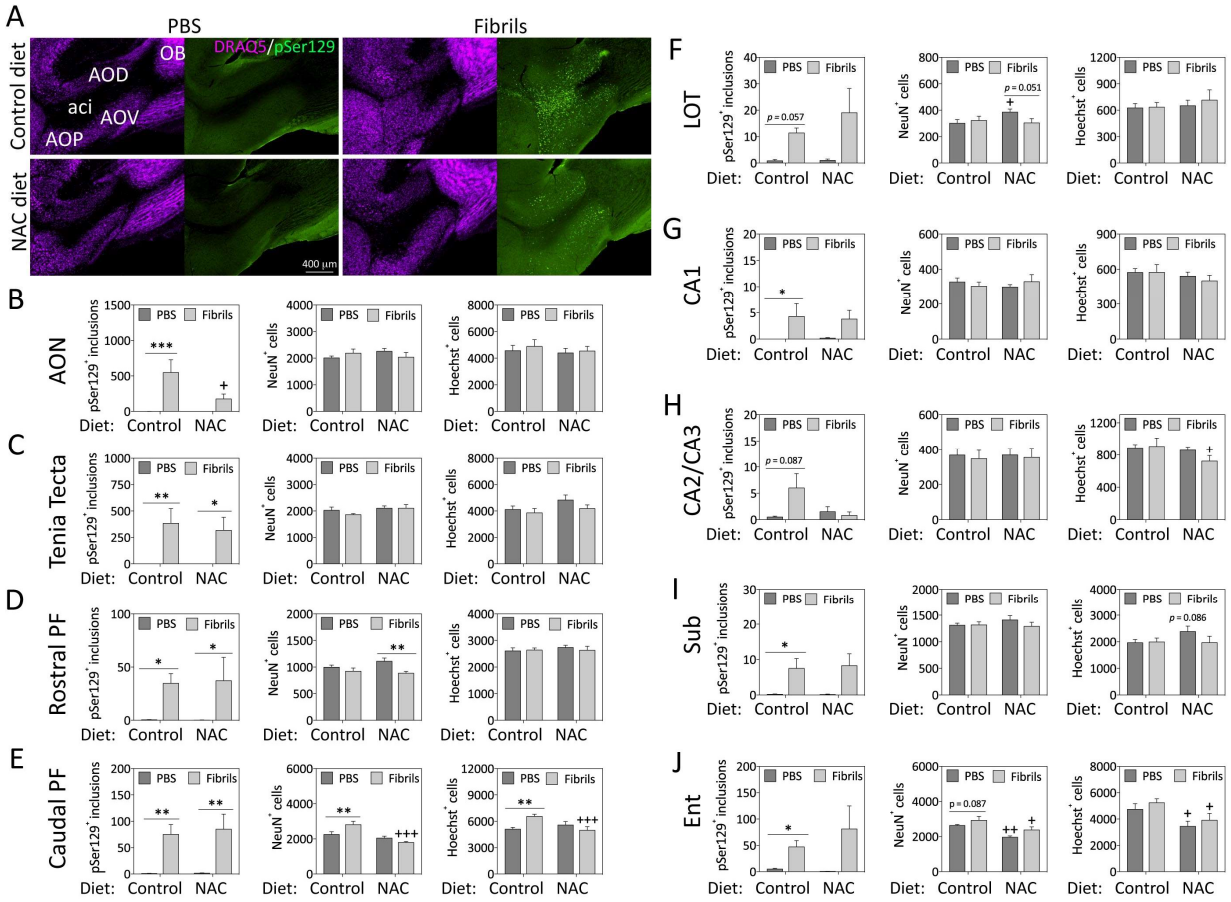

Figure 44: N-acetyl cysteine supplementation only reduces pSer129$^+$ inclusions in the AON after three months. Mice were infused in the right rear olfactory bulb with either preformed α-synuclein fibrils (5 µg/1 µL) or an equivalent volume of PBS (1 µL). A blinded observer counted the number of pSer129$^+$ structures (rb polyclonal antibody, see **Table 2**), NeuN$^+$ cells, and Hoechst$^+$ nuclei per field of view (40× magnification) using ImageJ software. The anterior olfactory nucleus (**A,B**) was the only region to exhibit a significant reduction in pSer129+ inclusions with NAC supplementation. Data for the tenia tecta (**C**), rostral and caudal portions of the piriform cortex (**D**,**E**), nucleus of the lateral olfactory tract, (LOT, F) CA1 (**G**), combined CA2/CA3 (**H**), subiculum (Sub, **I**) and entorhinal cortex (Ent, **J**) are also included. Shown are the mean and SEM of 10 mice per group, Two-way ANOVA was followed by the Bonferroni correction for multiple comparisons. * p≤0.05, ** p≤0.01, *** p≤0.001 PBS vs fibrils, + p≤0.05 control vs NAC diet. All abbreviations are listed in **Table 4**.

the dose was five-fold lower than that of the Clark *et al.* study (J. Clark et al., 2010). These largely negative findings may partly explain the lack of dramatically protective effects of NAC in PD patients (Monti et al., 2016) and reveal some degree of toxicity of dietary NAC, similar to intraperitoneally delivered NAC in our previous work (Nouraei et al., 2016).

Dietary NAC and α-synuclein fibril infusions had no effect on olfactory or learning and memory tests in the first three months post-infusion

In addition to histological analyses, behavioral analyses were also performed. The buried pellet test for olfactory function was performed at 1, 2, and 3 months post-infusion (**Figure 45A-C**) and

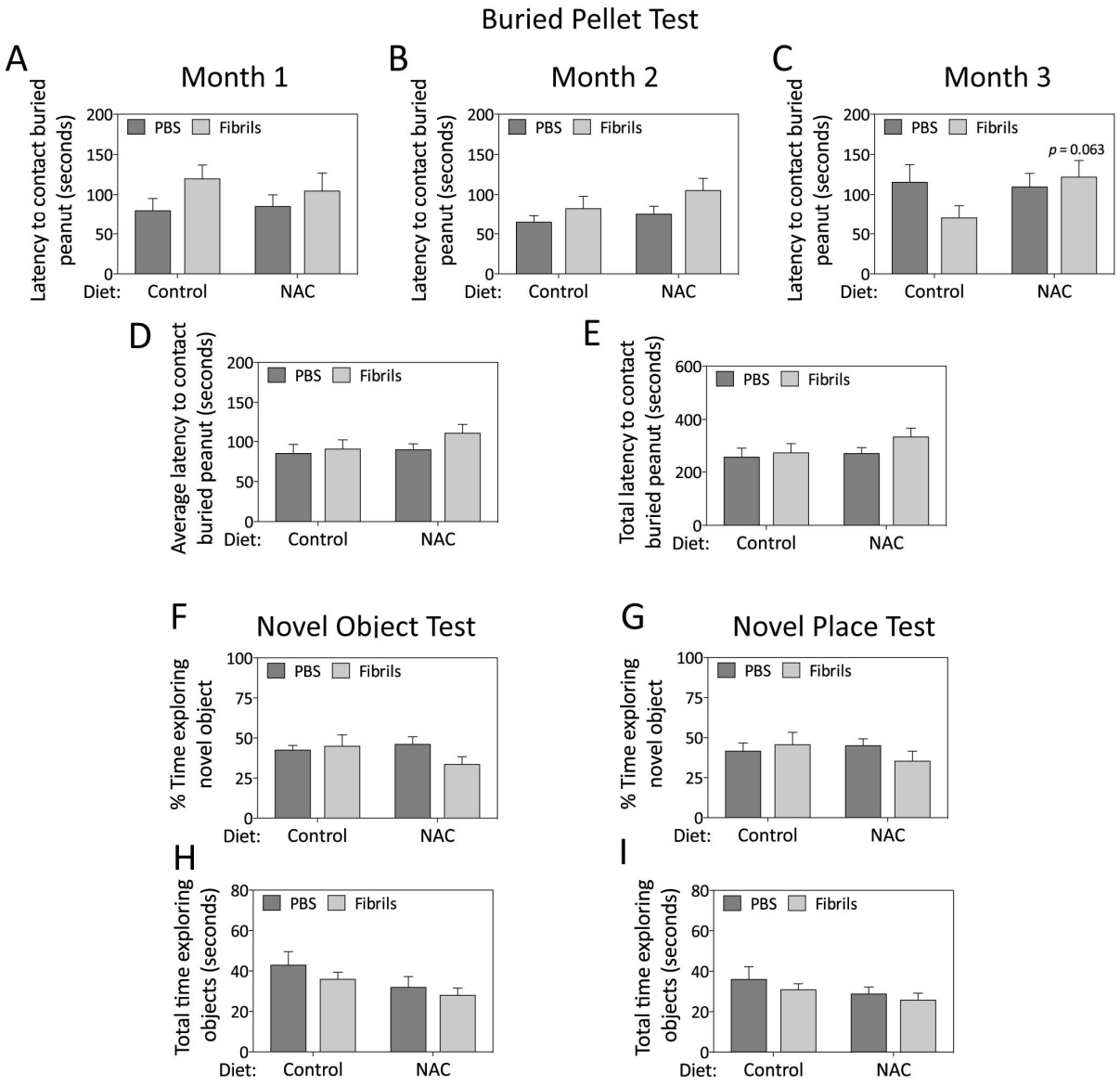

Figure 45: No significant changes in olfactory ability or learning and memory observed in any treatment group. Mice were infused in the right rear olfactory bulb with either preformed α-synuclein fibrils (5 μg/1 μL) or an equivalent volume of PBS (1 μL). The buried pellet test was performed at 1, 2, and 3 months post-infusion (**A,B,C**). The average latency to contact the buried peanut (**D**) and total latency (**E**) for all three trials are also included. The novel object/place test was performed at 2.5 months post-infusion (**F-I**). Shown are the mean and SEM from an n of 10 mice per group. Two-way ANOVA was followed by the Bonferroni correction for multiple comparisons.

the novel object/novel place tests for learning and memory were performed at 2.5 months post-infusion (**Figure 45F-I**). No significant differences in olfactory or learning and memory were observed between the groups. At three months post-infusion, there was a trend for fibril-infused animals in the NAC treated group to be slower in finding the buried peanut compared to fibril-infused animals on the normal diet (**Figure 45C**). This suggested that the NAC diet may have inhibited olfactory sensory processing. One might speculate that the strong odor of NAC may have masked any other odors. When the latency for all three trials was averaged (**Figure 45D**), or summed (**Figure 45E**), no differences in olfactory capability were observed between groups.

Discussion

As no one model adequately recapitulates all of the various pathologic aspects of Lewy body disorders, we examined multiple toxicants that model specific features of these disorders *in vitro.* The goal of our studies was to test the efficacy of the neuroprotective compound NAC against different forms of proteotoxic stress. Ensuring therapeutic efficacy in multiple models might facilitate the clinical translation of the compound. In the present study we tested the hypothesis that NAC could reduce the development of α-synucleinopathy by inducing the Hsp70 response and reducing proteotoxicity associated with proteasome inhibition. Here, were confirmed that NAC is able to protect neurons from proteasome inhibition partly through Hsp70. We also established that NAC is able to reduce pSer129^{+} inclusions *in vitro*. However, a significant reduction in inclusions was only observed at relatively high concentrations (500 and 1000 μM), which would be difficult to achieve in the CNS *in vivo* without toxicity*,* as discussed further below.

Oral NAC supplementation did not affect the amount of food the mice ate or the amount of weight gained over the course of three months. This suggests that there was minimal aversion to the unpleasant odor/taste of NAC when mixed into food at a relatively low concentration. We calculated the dose of NAC per animal to be approximately 200 mg/kg/day, but NAC only has an oral bioavailability of approximately 4-10% (Giustarini et al., 2012). Sixty minutes after a 10 mg/kg administration of NAC in a healthy human, the plasma concentration of NAC was 8.1 μM and the plasma concentration of its metabolite cysteine was 21.2 μM (Tsikas et al., 1998), approximately two fold higher than the basal levels. This suggests that, as NAC is rapidly metabolized *in vivo,* the beneficial effects of oral supplementation may be largely attributable to its thiol metabolite cysteine.

The pattern of pSer129$^+$ inclusions that developed in this study is consistent with the limbic-predominant pattern observed in Aims 1 and 2. A significant reduction in pSer129$^+$ inclusions *in vivo* was only observed in the AON, which is the region that develops the most inclusions in our model. This suggests that NAC was more effective at reducing the development of a high density of inclusions within this structure rather than the regional spread of α-synucleinopathy. The beneficial effect of NAC supplementation may have been limited to the AON due to the proximity of the AON to the site of infusion. The concentration of NAC may have been higher in the AON than in other brain regions due to the nearby disruption in the blood brain barrier. The lack of robust neuroprotective effects of NAC in the present study corresponds to the relatively mild benefits seen in clinical trials (Monti et al., 2016). Our study was conducted over a relatively short period (3 months), but the aggregation and spread of α-synucleinopathy in this model is more aggressive than in humans. Therefore, the mild effect of NAC at reducing pSer129$^+$ inclusions *in*

vivo may still be clinically relevant, as Lewy body disorders typically take years or even decades to develop. Oral NAC supplementation of 70 mg/kg for two days resulted in a CSF concentration of approximately 10 μM (Katz et al., 2015), but the NAC was consumed in a single dose each day and not over the course of 24 hours, as is the case with the mice in our study. As NAC is rapidly metabolized *in vivo*, it is unlikely that the concentration of NAC in the CNS of the mice in our study surpassed 10 μM, which is far less than the minimum concentration required to reduce α-synucleinopathy *in vitro.* In our *in vitro* treatments, there was a greater percentage of unmetabolized NAC, which we expect may upregulate Hsp70. *In vivo*, NAC goes through extensive first pass metabolism, and a greater percentage is present as the metabolite cysteine may not upregulate Hsp70.

It is also possible that NAC only induces Hsp70 transiently at the initial proteotoxic insult, which is not sustained in our chronic *in vivo* model. Hsp70 is indeed known to inhibit its own production through a negative feedback loop (Vjestica et al., 2013; Zorzi & Bonvini, 2011) and it may therefore be beneficial to supply exogenous Hsp70 to overcome the feedback loop. The development of many aggresome-like structures (perinuclear inclusions) may also reduce proteotoxic stress and therefore decrease Hsp70 production and activity.

In the behavioral tests in this aim, we did not observe any reduction in olfaction or learning and memory from fibril infusions or the NAC diet. We expected to observe olfactory deficits at three months post-infusion as we noted a significant increase in latency to find the buried treat in the three-month-old males in Aim 2. This discrepancy is likely due to performing the buried pellet test each month in this Aim, as multiple tests increase the likelihood that the mice will remember the

test and respond differently in subsequent trials (Hanell & Marklund, 2014). By the time olfactory deficits would have been apparent at three months post-fibril infusion, the mice had already been exposed to the test twice before. The novel object and novel place tests were performed three months earlier than in Aim 2, and there was no effect of fibril infusions at this earlier time point, perhaps consistent with the progressive nature of PFF-induced α-synucleinopathy.

The strength of our *in vitro* studies is that we performed three independent viability assays, which have been shown to correlate linearly with cell density in primary neuron cultures (Posimo et al., 2013; Posimo et al., 2014b). We also showed that NAC reduces MG132-induced proteotoxicity and reduces the amount of inclusions that develop in primary OB cultures from PFF treatment. PFFs led to no cell loss and, therefore, we could not examine any reduction in cell loss in this particular model of Lewy-like pathology. For partly these reasons, MG132 was employed to kill cells in vitro and test the neuroprotective capacity of NAC.

We employed two different Hsp70/Hsc70 inhibitors with different mechanisms of action to support our hypothesis that NAC promotes the activity of Hsp70 to inhibit proteotoxic stress and cell loss in neuronal cultures, as shown previously for astroglial and N2a cells (Gleixner et al., 2017; Jiang et al., 2013). Our studies identify a protective role for Hsp70 and a protective effect of NAC in OB and hippocampal neurons. NAC is theorized to provide protection through several mechanisms and, therefore, a total loss of protection through Hsp70 inhibition alone would not be expected. Although we measured Hsp70 levels in our in vitro model of NAC-mediated protection against proteotoxicity, there was no NAC-induced upregulation of Hsp70 protein by Western immunoblotting methods (data now shown), unlike the findings in N2a cells (Jiang et al., 2013).

Measurements of Hsp70 activity cannot be made in lysates of cells, but only with purified protein, as they are all dependent upon its ATPase activity and there are innumerable other ATPases present. Based upon the observation that Hsp70 activity loss reduced the protective effects of NAC, we then hypothesized that NAC directly influences the activation state of Hsp70 through acetylation and commissioned the production of an antibody against the acetylated form of Hsp70, but it was nonspecific. Given the lack of NAC-mediated protection in our model in the majority of brain regions examined, we abandoned this line of inquiry.

There are a number of caveats in the interpretation of the *in vitro* data. First, the *in vitro* cultures are primary neuronal. Astrocytes are the most abundant cell type in the brain (Sofroniew & Vinters, 2010), and therefore the primary neuron cultures are lacking physiological levels of this crucial support cell. Our primary neuron cultures are also inherently acutely injured from the culturing process and fundamentally different from neurons that have survived decades of proteotoxic and oxidative stress events. The three-dimensional network of different neuron types and interconnectedness of brain regions can also never be fully recapitulated *in vitro*. Nevertheless, our *in vitro* studies provided justification to examine NAC in an *in vivo* study. While NAC was not as protective against α-synucleinopathy as we expected, the *in vivo* study confirmed that our model can serve as an acceptable platform to examine therapies to treat Lewy body disorders.

Conclusions

In this dissertation, we have helped characterize the PFF model and reported a unique neuroanatomical pattern of α-synucleinopathy following infusions into the OB/AON. This pattern of limbic-predominant α-synucleinopathy is congruent with a subset of human Lewy body disorders (i.e. Beach's Stage IIb) and was reproduced in separate *in vivo* experiments in each aim

of this dissertation. PFF injections allow for the examination of the development and spread of α-synucleinopathy through interconnected brain regions, which cannot be accomplished with toxin-based or transgenic models. Our work has helped establish a model of early stage α-synucleinopathy that recapitulates many of the features seen in human Lewy body disorders and can potentially serve as a platform to investigate therapies.

Much of the work in this dissertation would not have been possible had we not optimized our PFF sonication parameters *in vivo.* By examining different sonication parameters, we were able to find a reproducible method for generating α-synucleinopathy in nontransgenic animals that is more robust than it typically reported in the literature. The pathology is so dense that it is even visible at relatively low magnification, which is conducive to generating stitched images of entire brain sections. Viewing the α-synucleinopathy in this manner is more useful to neuroanatomists than highly magnified images as it provides a snapshot of the spread through interconnected brain regions and the viewer can independently verify our interpretation of the boundaries anatomical subregions and the topography of the Lewy-like pathology.

By using the tract-tracer FluoroGold, we confirmed first-order efferent projections from the site of infusion to many of the brain regions that developed dense pSer129^{+} inclusions. For example, within the hippocampus, the CA1 field and subiculum frequently developed inclusions, and these were the regions also displaying FluoroGold signal. The CA2 and CA3 fields develop the most pathology in PD, and in our model did not display FluoroGold label and exhibited fewer, if any pSer129^{+} aggregations. The pathological distribution of pSer129^{+} aggregates suggests that our model is more comparable to Lewy body disorders other than PD.

The FluoroGold study supports the hypothesis that α-synucleinopathy travels primarily in a retrograde direction as the regions that develop the most pathology have first-order projections to the site of infusion and areas that receive projections from the OB but do not project back to it, such as the olfactory tubercle, do not develop pathology at early time points. At 6 and 10.5 months post-infusion, when pathology in the olfactory tubercle emerged, much of it was perinuclear, suggesting retrograde transport to the soma from another brain region rather than anterograde transport from the OB/AON to axon terminals. Our results also support the selective vulnerability hypothesis, as the horizontal diagonal band of Broca remained free of pSer129^{+} inclusions even at 10.5 months post-infusion, despite harboring intense FluoroGold label. Future studies to investigate the unique features of this brain region that make it resistant to the development of pSer129^{+} aggregations are warranted.

In addition to characterizing the pattern of α-synucleinopathy throughout the brain, we also characterized the inclusions with co-immunolabeling and high-resolution microscopy. Consistent with the literature, we observed that some but not all of the pSer129^{+} aggregates are labeled with ubiquitin and Thioflavin S labeled protein aggregates, primarily near the site of infusion. By using the Proteostat dye, we observed that many of the perinuclear inclusions overlap with the cytoprotective structure called the aggresome, which may help explain why only minor cell loss and behavioral deficits are observed in our model despite dense α-synucleinopathy. We are confident in our identification of Lewy-like inclusions, as we performed several control experiments on our anti-pSer129 antibodies and the specific anatomical morphology of the

inclusions (perinuclear and neuritic threads) are in agreement with the literature (Osterberg et al., 2015).

There were few significant behavioral outcomes that could be attributed to fibril infusions, which suggests that behavioral changes are more likely to be a function of neuronal cell loss rather than the presence of pSer129^{+} aggregates. The younger male mice exhibited fibril-induced olfactory deficits at three months post-infusion, and the older male mice also exhibited olfactory deficits at 10 months post-infusion that were significantly greater than at three-months post infusion, suggesting a progressive loss of olfactory capability. Fibril-infused females were not as impaired as males in the buried pellet test, but made fewer forelimb contacts and reared less often, perhaps indicating postural instability, a symptom more commonly associated with female patients with Lewy body disorders (Georgiev et al., 2017). A limitation to our behavioral testing is that the animals received unilateral infusions and the contralateral hemisphere may be able to compensate for dysfunction in the ipsilateral hemisphere. However, bilateral infusions in the CA2/CA3 region using 1-hour waterbath sonicated PFFs elicited dense pathology in both hemispheres with minimal behavioral deficits (Nouraei et al., 2018), supporting the theory that cell loss is required for changes in behavior.

Female mice tended to develop fewer pSer129^{+} inclusions in some brain regions and experienced less cell loss than male mice. There was a significant reduction in α-synucleinopathy in the OB, AON, caudolateral piriform cortex, amygdalopiriform transition area, posteromedial corticoamygdala, and subiculum in females compared to males. Females did not develop significantly more inclusions than males in any brain region and did not exhibit significant cell

loss in any brain region, strongly suggesting an important effect of gender. To our knowledge, this is the first example of a non-transgenic PFF mouse model of Lewy body disorders in which females are more resistant to histopathology than males.

At 6 and 10.5 months post-infusion, we observed pathology in the midbrain, most often in the ventral tegmental area, but also occasionally in the medial parts of the SN pars compacta. Degeneration of the SN pars compacta is responsible for the motor symptoms associated with Parkinson's disease (Alexander, 2004; Jankovic, 2008). In this model we do not observe pSer129^{+} aggregates in the lateral subregions of the SN pars compacta that are most vulnerable to degeneration in PD (Damier et al., 1999; Fearnley & Lees, 1991). This may be attributable to the ventrolateral SN projecting more to the dorsal striatum (Zhang et al., 2017), where fewer pSer129^{+} inclusions are observed in this model. It may also suggest that pathology in the lateral parts of the SN may arise in caudal brain structures, most likely the brainstem. This agrees with Beach's unified staging theory, as most cases of PD and DLB are classified as Stage III or Stage IV, with both limbic and brainstem pathology. In our model, the pathology is almost exclusively confined to the limbic system and absent from the brainstem. The nigrostriatal pathway may have been relatively spared from the development pSer129^{+} inclusions because of an absence of pathology emanating from the brainstem.

Despite an overall lack of α-synucleinopathy in the nigrostriatal pathway compared to brain regions of the limbic system, we observed dramatic changes to dopaminergic markers, particularly in the oldest mice. It is unclear if the "superager" mice that survived until 10.5 months post-infusion always exhibited high levels of these markers or survived because they were able to

upregulate the expression of TH and DAT. We observed a fibril-induced increase in TH expression per cell in all male groups in the SN pars compacta and an increase in this metric in the ventral tegmental area of the oldest mice. This suggests that there are changes in dopamine metabolism in the nigrostriatal pathway in response to fibril infusions that may or may not be associated with α-synucleinopathy.

We were limited by the substantial mortality that fibrils elicited in mice that were 11 months old at the time of infusion, although it was a key finding of Aim 2. To our knowledge, we are the first to report that higher mortality from olfactory/limbic synucleinopathy in older animals. While the α-synucleinopathy was not dramatically more dense or extensive than in the younger animals, the older animals were the only group with significant mortality following fibril infusions. This is important because age is associated with increased mortality in PD (Oosterveld et al., 2015). Therefore, our model also simulates the increased risk of mortality with age in human Lewy body disorders.

For our *in vitro* experiments, we applied multiple toxicants as well as PFFs to primary neurons from two different brain regions. The OB was chosen because the region is most often affected early in Lewy body disorders. The hippocampus also examined because this region is affected in the end stages of Lewy body disorders, and dysfunction in this region contributes to cognitive deficits (Hall et al., 2014). We investigated the response to multiple toxicants in neurons from multiple brain regions because no single model mimics the complex nature of Lewy body disorders. As discussed in the Introduction, α-synucleinopathy can be toxic through several mechanisms. Therefore, a potential treatment will likely be clinically relevant if it is protective

against multiple types of neurotoxicity. Our *in vitro* experiments established that NAC can protect primary neurons through GSH-independent means and that there is a beneficial interaction between NAC and Hsp70. These experiments provided justification for our *in vivo* study and confirmed the utility of our model in serving as a platform to test potential therapies.

In conclusion, we have developed an *in vivo* model of α-synucleinopathy that corresponds to a distinct subset of patients with Lewy body disorders. The strengths of this model are that it is reproducible and mimics two major risk factors associated with Lewy body disorders—age and gender. To our knowledge, no other wild-type mouse model as closely replicates the human condition. Further experiments with the PFF model may elucidate the mechanisms responsible for the induction of misfolding, aggregation, and neuronal toxicity caused by non-pathogenic endogenous α-synuclein. They may also reveal why some brain regions appear resistant to the development of pathology. Future therapies that are efficacious in this model may have greater potential for clinical translatability.

References

Aarsland, D. (2016). Cognitive impairment in Parkinson's disease and dementia with Lewy bodies. *Parkinsonism Relat Disord, 22 Suppl 1*, S144-148. doi: 10.1016/j.parkreldis.2015.09.034

Aarsland, D., Andersen, K., Larsen, J. P., Lolk, A., & Kragh-Sorensen, P. (2003). Prevalence and characteristics of dementia in Parkinson disease: an 8-year prospective study. *Arch Neurol, 60*(3), 387-392.

Aarsland, D., Ballard, C., McKeith, I., Perry, R. H., & Larsen, J. P. (2001). Comparison of extrapyramidal signs in dementia with Lewy bodies and Parkinson's disease. *J Neuropsychiatry Clin Neurosci, 13*(3), 374-379. doi: 10.1176/jnp.13.3.374

Aarsland, D., Creese, B., Politis, M., Chaudhuri, K. R., Ffytche, D. H., Weintraub, D., & Ballard, C. (2017). Cognitive decline in Parkinson disease. *Nat Rev Neurol, 13*(4), 217-231. doi: 10.1038/nrneurol.2017.27

Aarsland, D., & Kurz, M. W. (2010a). The epidemiology of dementia associated with Parkinson disease. *J Neurol Sci, 289*(1-2), 18-22. doi: 10.1016/j.jns.2009.08.034

Aarsland, D., & Kurz, M. W. (2010b). The epidemiology of dementia associated with Parkinson's disease. *Brain Pathol, 20*(3), 633-639. doi: 10.1111/j.1750-3639.2009.00369.x

Aarsland, D., Perry, R., Brown, A., Larsen, J. P., & Ballard, C. (2005). Neuropathology of dementia in Parkinson's disease: a prospective, community-based study. *Ann Neurol, 58*(5), 773-776. doi: 10.1002/ana.20635

Abbott, R. D., Ross, G. W., Petrovitch, H., Tanner, C. M., Davis, D. G., Masaki, K. H., . . . White, L. R. (2007). Bowel movement frequency in late-life and incidental Lewy bodies. *Mov Disord, 22*(11), 1581-1586. doi: 10.1002/mds.21560

Abbott, R. D., Ross, G. W., White, L. R., Nelson, J. S., Masaki, K. H., Tanner, C. M., . . . Petrovitch, H. (2002). Midlife adiposity and the future risk of Parkinson's disease. *Neurology, 59*(7), 1051-1057.

Adair, J. C., Knoefel, J. E., & Morgan, N. (2001). Controlled trial of N-acetylcysteine for patients with probable Alzheimer's disease. *Neurology, 57*(8), 1515-1517.

Adamowicz, D. H., Roy, S., Salmon, D. P., Galasko, D. R., Hansen, L. A., Masliah, E., & Gage, F. H. (2017). Hippocampal alpha-Synuclein in Dementia with Lewy Bodies Contributes to Memory Impairment and Is Consistent with Spread of Pathology. *J Neurosci, 37*(7), 1675-1684. doi: 10.1523/JNEUROSCI.3047-16.2016

Adler, C. H., & Beach, T. G. (2016). Neuropathological basis of nonmotor manifestations of Parkinson's disease. *Mov Disord, 31*(8), 1114-1119. doi: 10.1002/mds.26605

Adler, C. H., Hentz, J. G., Shill, H. A., Sabbagh, M. N., Driver-Dunckley, E., Evidente, V. G., . . . Caviness, J. N. (2011). Probable RBD is increased in Parkinson's disease but not in essential tremor or restless legs syndrome. *Parkinsonism Relat Disord, 17*(6), 456-458. doi: 10.1016/j.parkreldis.2011.03.007

Aikawa, S., Matsuzawa, F., Satoh, Y., Kadota, Y., Doi, H., & Itoh, K. (2006). Prediction of the mechanism of action of omuralide (clasto-lactacystin beta-lactone) on human cathepsin A based on a structural model of the yeast proteasome beta5/PRE2-subunit/omuralide complex. *Biochim Biophys Acta, 1764*(8), 1372-1380. doi: 10.1016/j.bbapap.2006.05.008

Alafuzoff, I., Parkkinen, L., Al-Sarraj, S., Arzberger, T., Bell, J., Bodi, I., . . . BrainNet Europe, C. (2008). Assessment of alpha-synuclein pathology: a study of the BrainNet Europe

Consortium. *J Neuropathol Exp Neurol, 67*(2), 125-143. doi: 10.1097/nen.0b013e3181633526

Alam, Z. I., Jenner, A., Daniel, S. E., Lees, A. J., Cairns, N., Marsden, C. D., . . . Halliwell, B. (1997). Oxidative DNA damage in the parkinsonian brain: an apparent selective increase in 8-hydroxyguanine levels in substantia nigra. *J Neurochem, 69*(3), 1196-1203.

Aldini, G., Altomare, A., Baron, G., Vistoli, G., Carini, M., Borsani, L., & Sergio, F. (2018). N-Acetylcysteine as an antioxidant and disulphide breaking agent: the reasons why. *Free Radic Res*, 1-12. doi: 10.1080/10715762.2018.1468564

Alexander, G. E. (2004). Biology of Parkinson's disease: pathogenesis and pathophysiology of a multisystem neurodegenerative disorder. *Dialogues Clin Neurosci, 6*(3), 259-280.

Alladi, P. A., Mahadevan, A., Yasha, T. C., Raju, T. R., Shankar, S. K., & Muthane, U. (2009). Absence of age-related changes in nigral dopaminergic neurons of Asian Indians: relevance to lower incidence of Parkinson's disease. *Neuroscience, 159*(1), 236-245. doi: 10.1016/j.neuroscience.2008.11.051

Aluf, Y., Vaya, J., Khatib, S., Loboda, Y., Kizhner, S., & Finberg, J. P. (2010). Specific oxidative stress profile associated with partial striatal dopaminergic depletion by 6-hydroxydopamine as assessed by a novel multifunctional marker molecule. *Free Radic Res, 44*(6), 635-644. doi: 10.3109/10715761003692529

Alvarez-Erviti, L., Rodriguez-Oroz, M. C., Cooper, J. M., Caballero, C., Ferrer, I., Obeso, J. A., & Schapira, A. H. (2010). Chaperone-mediated autophagy markers in Parkinson disease brains. *Arch Neurol, 67*(12), 1464-1472. doi: 10.1001/archneurol.2010.198

Alvarez-Erviti, L., Seow, Y., Schapira, A. H., Gardiner, C., Sargent, I. L., Wood, M. J., & Cooper, J. M. (2011). Lysosomal dysfunction increases exosome-mediated alpha-synuclein release and transmission. *Neurobiol Dis, 42*(3), 360-367. doi: 10.1016/j.nbd.2011.01.029

Anderson, D. G., Florang, V. R., Schamp, J. H., Buettner, G. R., & Doorn, J. A. (2016). Antioxidant-Mediated Modulation of Protein Reactivity for 3,4-Dihydroxyphenylacetaldehyde, a Toxic Dopamine Metabolite. *Chem Res Toxicol, 29*(7), 1098-1107. doi: 10.1021/acs.chemrestox.5b00528

Anderson, J. P., Walker, D. E., Goldstein, J. M., de Laat, R., Banducci, K., Caccavello, R. J., . . . Chilcote, T. J. (2006). Phosphorylation of Ser-129 is the dominant pathological modification of alpha-synuclein in familial and sporadic Lewy body disease. *J Biol Chem, 281*(40), 29739-29752. doi: 10.1074/jbc.M600933200

Annerino, D. M., Arshad, S., Taylor, G. M., Adler, C. H., Beach, T. G., & Greene, J. G. (2012). Parkinson's disease is not associated with gastrointestinal myenteric ganglion neuron loss. *Acta Neuropathol, 124*(5), 665-680. doi: 10.1007/s00401-012-1040-2

Apaydin, H., Ahlskog, J. E., Parisi, J. E., Boeve, B. F., & Dickson, D. W. (2002). Parkinson disease neuropathology: later-developing dementia and loss of the levodopa response. *Arch Neurol, 59*(1), 102-112.

Arawaka, S., Sato, H., Sasaki, A., Koyama, S., & Kato, T. (2017). Mechanisms underlying extensive Ser129-phosphorylation in alpha-synuclein aggregates. *Acta Neuropathol Commun, 5*(1), 48. doi: 10.1186/s40478-017-0452-6

Baba, M., Nakajo, S., Tu, P. H., Tomita, T., Nakaya, K., Lee, V. M., . . . Iwatsubo, T. (1998). Aggregation of alpha-synuclein in Lewy bodies of sporadic Parkinson's disease and dementia with Lewy bodies. *Am J Pathol, 152*(4), 879-884.

Baldereschi, M., Di Carlo, A., Rocca, W. A., Vanni, P., Maggi, S., Perissinotto, E., . . . Inzitari, D. (2000). Parkinson's disease and parkinsonism in a longitudinal study: two-fold higher incidence in men. ILSA Working Group. Italian Longitudinal Study on Aging. *Neurology, 55*(9), 1358-1363.

Ballatori, N., Krance, S. M., Notenboom, S., Shi, S., Tieu, K., & Hammond, C. L. (2009). Glutathione dysregulation and the etiology and progression of human diseases. *Biol Chem, 390*(3), 191-214. doi: 10.1515/BC.2009.033

Bang, Y., Kim, K. S., Seol, W., & Choi, H. J. (2016). LRRK2 interferes with aggresome formation for autophagic clearance. *Mol Cell Neurosci, 75*, 71-80. doi: 10.1016/j.mcn.2016.06.007

Baptista, M. J., Cookson, M. R., & Miller, D. W. (2004). Parkin and alpha-synuclein: opponent actions in the pathogenesis of Parkinson's disease. *Neuroscientist, 10*(1), 63-72. doi: 10.1177/1073858403260392

Bartels, T., Choi, J. G., & Selkoe, D. J. (2011). alpha-Synuclein occurs physiologically as a helically folded tetramer that resists aggregation. *Nature, 477*(7362), 107-110. doi: 10.1038/nature10324

Beach, T. G., Adler, C. H., Lue, L., Sue, L. I., Bachalakuri, J., Henry-Watson, J., . . . Arizona Parkinson's Disease, C. (2009). Unified staging system for Lewy body disorders: correlation with nigrostriatal degeneration, cognitive impairment and motor dysfunction. *Acta Neuropathol, 117*(6), 613-634. doi: 10.1007/s00401-009-0538-8

Beach, T. G., Adler, C. H., Sue, L. I., Vedders, L., Lue, L., White Iii, C. L., . . . Arizona Parkinson's Disease, C. (2010). Multi-organ distribution of phosphorylated alpha-synuclein histopathology in subjects with Lewy body disorders. *Acta Neuropathol, 119*(6), 689-702. doi: 10.1007/s00401-010-0664-3

Beach, T. G., White, C. L., 3rd, Hladik, C. L., Sabbagh, M. N., Connor, D. J., Shill, H. A., . . . Arizona Parkinson's Disease, C. (2009). Olfactory bulb alpha-synucleinopathy has high specificity and sensitivity for Lewy body disorders. *Acta Neuropathol, 117*(2), 169-174. doi: 10.1007/s00401-008-0450-7

Bence, N. F., Sampat, R. M., & Kopito, R. R. (2001). Impairment of the ubiquitin-proteasome system by protein aggregation. *Science, 292*(5521), 1552-1555. doi: 10.1126/science.292.5521.1552

Benedetti, M. D., Maraganore, D. M., Bower, J. H., McDonnell, S. K., Peterson, B. J., Ahlskog, J. E., . . . Rocca, W. A. (2001). Hysterectomy, menopause, and estrogen use preceding Parkinson's disease: an exploratory case-control study. *Mov Disord, 16*(5), 830-837.

Bennett, D. A., Beckett, L. A., Murray, A. M., Shannon, K. M., Goetz, C. G., Pilgrim, D. M., & Evans, D. A. (1996). Prevalence of parkinsonian signs and associated mortality in a community population of older people. *N Engl J Med, 334*(2), 71-76. doi: 10.1056/NEJM199601113340202

Berk, M., Copolov, D., Dean, O., Lu, K., Jeavons, S., Schapkaitz, I., . . . Bush, A. I. (2008). N-acetyl cysteine as a glutathione precursor for schizophrenia--a double-blind, randomized, placebo-controlled trial. *Biol Psychiatry, 64*(5), 361-368. doi: 10.1016/j.biopsych.2008.03.004

Berk, M., Copolov, D. L., Dean, O., Lu, K., Jeavons, S., Schapkaitz, I., . . . Bush, A. I. (2008). N-acetyl cysteine for depressive symptoms in bipolar disorder--a double-blind randomized placebo-controlled trial. *Biol Psychiatry, 64*(6), 468-475. doi: 10.1016/j.biopsych.2008.04.022

Bieri, G., Gitler, A. D., & Brahic, M. (2018). Internalization, axonal transport and release of fibrillar forms of alpha-synuclein. *Neurobiol Dis, 109*(Pt B), 219-225. doi: 10.1016/j.nbd.2017.03.007

Boeve, B. F. (2010). REM sleep behavior disorder: Updated review of the core features, the REM sleep behavior disorder-neurodegenerative disease association, evolving concepts, controversies, and future directions. *Ann N Y Acad Sci, 1184*, 15-54. doi: 10.1111/j.1749-6632.2009.05115.x

Boeve, B. F., Silber, M. H., Ferman, T. J., Lin, S. C., Benarroch, E. E., Schmeichel, A. M., . . . Dickson, D. W. (2013). Clinicopathologic correlations in 172 cases of rapid eye movement sleep behavior disorder with or without a coexisting neurologic disorder. *Sleep Med, 14*(8), 754-762. doi: 10.1016/j.sleep.2012.10.015

Boeve, B. F., Silber, M. H., Ferman, T. J., Lucas, J. A., & Parisi, J. E. (2001). Association of REM sleep behavior disorder and neurodegenerative disease may reflect an underlying synucleinopathy. *Mov Disord, 16*(4), 622-630.

Bolam, J. P., & Pissadaki, E. K. (2012). Living on the edge with too many mouths to feed: why dopamine neurons die. *Mov Disord, 27*(12), 1478-1483. doi: 10.1002/mds.25135

Bolanos, J. P., Heales, S. J., Land, J. M., & Clark, J. B. (1995). Effect of peroxynitrite on the mitochondrial respiratory chain: differential susceptibility of neurones and astrocytes in primary culture. *J Neurochem, 64*(5), 1965-1972.

Bonifati, V., Rizzu, P., van Baren, M. J., Schaap, O., Breedveld, G. J., Krieger, E., . . . Heutink, P. (2003). Mutations in the DJ-1 gene associated with autosomal recessive early-onset parkinsonism. *Science, 299*(5604), 256-259. doi: 10.1126/science.1077209

Bousset, L., Pieri, L., Ruiz-Arlandis, G., Gath, J., Jensen, P. H., Habenstein, B., . . . Melki, R. (2013). Structural and functional characterization of two alpha-synuclein strains. *Nat Commun, 4*, 2575. doi: 10.1038/ncomms3575

Braak, H., Bohl, J. R., Muller, C. M., Rub, U., de Vos, R. A., & Del Tredici, K. (2006). Stanley Fahn Lecture 2005: The staging procedure for the inclusion body pathology associated with sporadic Parkinson's disease reconsidered. *Mov Disord, 21*(12), 2042-2051. doi: 10.1002/mds.21065

Braak, H., & Braak, E. (2000). Pathoanatomy of Parkinson's disease. *J Neurol, 247 Suppl 2*, II3-10. doi: 10.1007/PL00007758

Braak, H., Braak, E., Yilmazer, D., de Vos, R. A., Jansen, E. N., Bohl, J., & Jellinger, K. (1994). Amygdala pathology in Parkinson's disease. *Acta Neuropathol, 88*(6), 493-500.

Braak, H., de Vos, R. A., Bohl, J., & Del Tredici, K. (2006). Gastric alpha-synuclein immunoreactive inclusions in Meissner's and Auerbach's plexuses in cases staged for Parkinson's disease-related brain pathology. *Neurosci Lett, 396*(1), 67-72. doi: 10.1016/j.neulet.2005.11.012

Braak, H., & Del Tredici, K. (2008). Cortico-basal ganglia-cortical circuitry in Parkinson's disease reconsidered. *Exp Neurol, 212*(1), 226-229. doi: 10.1016/j.expneurol.2008.04.001

Braak, H., Del Tredici, K., Rub, U., de Vos, R. A., Jansen Steur, E. N., & Braak, E. (2003). Staging of brain pathology related to sporadic Parkinson's disease. *Neurobiol Aging, 24*(2), 197-211.

Braunstein, M. J., Scott, S. S., Scott, C. M., Behrman, S., Walter, P., Wipf, P., . . . Batuman, O. (2011). Antimyeloma Effects of the Heat Shock Protein 70 Molecular Chaperone Inhibitor MAL3-101. *J Oncol, 2011*, 232037. doi: 10.1155/2011/232037

Brown, R. M., Crane, A. M., & Goldman, P. S. (1979). Regional distribution of monoamines in the cerebral cortex and subcortical structures of the rhesus monkey: concentrations and in vivo synthesis rates. *Brain Res, 168*(1), 133-150.

Brunk, U. T., & Terman, A. (2002a). Lipofuscin: mechanisms of age-related accumulation and influence on cell function. *Free Radic Biol Med, 33*(5), 611-619.

Brunk, U. T., & Terman, A. (2002b). The mitochondrial-lysosomal axis theory of aging: accumulation of damaged mitochondria as a result of imperfect autophagocytosis. *Eur J Biochem, 269*(8), 1996-2002.

Bulteau, A. L., Lundberg, K. C., Humphries, K. M., Sadek, H. A., Szweda, P. A., Friguet, B., & Szweda, L. I. (2001). Oxidative modification and inactivation of the proteasome during coronary occlusion/reperfusion. *J Biol Chem, 276*(32), 30057-30063. doi: 10.1074/jbc.M100142200

Burke, W. J., Li, S. W., Williams, E. A., Nonneman, R., & Zahm, D. S. (2003). 3,4-Dihydroxyphenylacetaldehyde is the toxic dopamine metabolite in vivo: implications for Parkinson's disease pathogenesis. *Brain Res, 989*(2), 205-213.

Burre, J., Sharma, M., & Sudhof, T. C. (2014). alpha-Synuclein assembles into higher-order multimers upon membrane binding to promote SNARE complex formation. *Proc Natl Acad Sci U S A, 111*(40), E4274-4283. doi: 10.1073/pnas.1416598111

Cai, L., Gibbs, R. B., & Johnson, D. A. (2012). Recognition of novel objects and their location in rats with selective cholinergic lesion of the medial septum. *Neurosci Lett, 506*(2), 261-265. doi: 10.1016/j.neulet.2011.11.019

Caranci, G., Piscopo, P., Rivabene, R., Traficante, A., Riozzi, B., Castellano, A. E., . . . Confaloni, A. (2013). Gender differences in Parkinson's disease: focus on plasma alpha-synuclein. *J Neural Transm (Vienna), 120*(8), 1209-1215. doi: 10.1007/s00702-013-0972-6

Castello, P. R., Drechsel, D. A., & Patel, M. (2007). Mitochondria are a major source of paraquat-induced reactive oxygen species production in the brain. *J Biol Chem, 282*(19), 14186-14193. doi: 10.1074/jbc.M700827200

Cereda, E., Barichella, M., Cassani, E., Caccialanza, R., & Pezzoli, G. (2013). Reproductive factors and clinical features of Parkinson's disease. *Parkinsonism Relat Disord, 19*(12), 1094-1099. doi: 10.1016/j.parkreldis.2013.07.020

Chatterjee, M., Andrulis, M., Stuhmer, T., Muller, E., Hofmann, C., Steinbrunn, T., . . . Bargou, R. C. (2013). The PI3K/Akt signaling pathway regulates the expression of Hsp70, which critically contributes to Hsp90-chaperone function and tumor cell survival in multiple myeloma. *Haematologica, 98*(7), 1132-1141. doi: 10.3324/haematol.2012.066175

Chen, H., Zhang, S. M., Schwarzschild, M. A., Hernan, M. A., Willett, W. C., & Ascherio, A. (2004). Obesity and the risk of Parkinson's disease. *Am J Epidemiol, 159*(6), 547-555.

Chen, S. W., Drakulic, S., Deas, E., Ouberai, M., Aprile, F. A., Arranz, R., . . . Cremades, N. (2015). Structural characterization of toxic oligomers that are kinetically trapped during alpha-synuclein fibril formation. *Proc Natl Acad Sci U S A, 112*(16), E1994-2003. doi: 10.1073/pnas.1421204112

Chinta, S. J., & Andersen, J. K. (2006). Reversible inhibition of mitochondrial complex I activity following chronic dopaminergic glutathione depletion in vitro: implications for Parkinson's disease. *Free Radic Biol Med, 41*(9), 1442-1448. doi: 10.1016/j.freeradbiomed.2006.08.002

Choi, M. G., Kim, M. J., Kim, D. G., Yu, R., Jang, Y. N., & Oh, W. J. (2018). Sequestration of synaptic proteins by alpha-synuclein aggregates leading to neurotoxicity is inhibited by small peptide. *PLoS One, 13*(4), e0195339. doi: 10.1371/journal.pone.0195339

Cholerton, B., Johnson, C. O., Fish, B., Quinn, J. F., Chung, K. A., Peterson-Hiller, A. L., . . . Edwards, K. L. (2018). Sex differences in progression to mild cognitive impairment and dementia in Parkinson's disease. *Parkinsonism Relat Disord, 50*, 29-36. doi: 10.1016/j.parkreldis.2018.02.007

Chu, Y., & Kordower, J. H. (2007). Age-associated increases of alpha-synuclein in monkeys and humans are associated with nigrostriatal dopamine depletion: Is this the target for Parkinson's disease? *Neurobiol Dis, 25*(1), 134-149. doi: 10.1016/j.nbd.2006.08.021

Chu, Y., Le, W., Kompoliti, K., Jankovic, J., Mufson, E. J., & Kordower, J. H. (2006). Nurr1 in Parkinson's disease and related disorders. *J Comp Neurol, 494*(3), 495-514. doi: 10.1002/cne.20828

Clark, J., Clore, E. L., Zheng, K., Adame, A., Masliah, E., & Simon, D. K. (2010). Oral N-acetyl-cysteine attenuates loss of dopaminergic terminals in alpha-synuclein overexpressing mice. *PLoS One, 5*(8), e12333. doi: 10.1371/journal.pone.0012333

Clark, L. N., Kartsaklis, L. A., Wolf Gilbert, R., Dorado, B., Ross, B. M., Kisselev, S., . . . Marder, K. (2009). Association of glucocerebrosidase mutations with dementia with lewy bodies. *Arch Neurol, 66*(5), 578-583. doi: 10.1001/archneurol.2009.54

Colosimo, C., Hughes, A. J., Kilford, L., & Lees, A. J. (2003). Lewy body cortical involvement may not always predict dementia in Parkinson's disease. *J Neurol Neurosurg Psychiatry, 74*(7), 852-856.

Conway, K. A., Lee, S. J., Rochet, J. C., Ding, T. T., Williamson, R. E., & Lansbury, P. T., Jr. (2000). Acceleration of oligomerization, not fibrillization, is a shared property of both alpha-synuclein mutations linked to early-onset Parkinson's disease: implications for pathogenesis and therapy. *Proc Natl Acad Sci U S A, 97*(2), 571-576.

Cordato, N. J., Halliday, G. M., Harding, A. J., Hely, M. A., & Morris, J. G. (2000). Regional brain atrophy in progressive supranuclear palsy and Lewy body disease. *Ann Neurol, 47*(6), 718-728.

Cremades, N., Chen, S. W., & Dobson, C. M. (2017). Structural Characteristics of alpha-Synuclein Oligomers. *Int Rev Cell Mol Biol, 329*, 79-143. doi: 10.1016/bs.ircmb.2016.08.010

Croisier, E., DE, M. R., Deprez, M., Goldring, K., Dexter, D. T., Pearce, R. K., . . . Roncaroli, F. (2006). Comparative study of commercially available anti-alpha-synuclein antibodies. *Neuropathol Appl Neurobiol, 32*(3), 351-356. doi: 10.1111/j.1365-2990.2006.00722.x

Crum, T. S., Gleixner, A. M., Posimo, J. M., Mason, D. M., Broeren, M. T., Heinemann, S. D., . . . Leak, R. K. (2015). Heat shock protein responses to aging and proteotoxicity in the olfactory bulb. *J Neurochem, 133*(6), 780-794. doi: 10.1111/jnc.13041

Cuervo, A. M., Stefanis, L., Fredenburg, R., Lansbury, P. T., & Sulzer, D. (2004). Impaired degradation of mutant alpha-synuclein by chaperone-mediated autophagy. *Science, 305*(5688), 1292-1295. doi: 10.1126/science.1101738

Dalfo, E., Portero-Otin, M., Ayala, V., Martinez, A., Pamplona, R., & Ferrer, I. (2005). Evidence of oxidative stress in the neocortex in incidental Lewy body disease. *J Neuropathol Exp Neurol, 64*(9), 816-830.

Damier, P., Hirsch, E. C., Agid, Y., & Graybiel, A. M. (1999). The substantia nigra of the human brain. II. Patterns of loss of dopamine-containing neurons in Parkinson's disease. *Brain, 122 (Pt 8)*, 1437-1448.

Dando, S. J., Mackay-Sim, A., Norton, R., Currie, B. J., St John, J. A., Ekberg, J. A., . . . Beacham, I. R. (2014). Pathogens penetrating the central nervous system: infection pathways and the cellular and molecular mechanisms of invasion. *Clin Microbiol Rev, 27*(4), 691-726. doi: 10.1128/CMR.00118-13

Danzer, K. M., Haasen, D., Karow, A. R., Moussaud, S., Habeck, M., Giese, A., . . . Kostka, M. (2007). Different species of alpha-synuclein oligomers induce calcium influx and seeding. *J Neurosci, 27*(34), 9220-9232. doi: 10.1523/JNEUROSCI.2617-07.2007

Danzer, K. M., Kranich, L. R., Ruf, W. P., Cagsal-Getkin, O., Winslow, A. R., Zhu, L., . . . McLean, P. J. (2012). Exosomal cell-to-cell transmission of alpha synuclein oligomers. *Mol Neurodegener, 7*, 42. doi: 10.1186/1750-1326-7-42

Danzer, K. M., Krebs, S. K., Wolff, M., Birk, G., & Hengerer, B. (2009). Seeding induced by alpha-synuclein oligomers provides evidence for spreading of alpha-synuclein pathology. *J Neurochem, 111*(1), 192-203. doi: 10.1111/j.1471-4159.2009.06324.x

Danzer, K. M., Ruf, W. P., Putcha, P., Joyner, D., Hashimoto, T., Glabe, C., . . . McLean, P. J. (2011). Heat-shock protein 70 modulates toxic extracellular alpha-synuclein oligomers and rescues trans-synaptic toxicity. *FASEB J, 25*(1), 326-336. doi: 10.1096/fj.10-164624

Dawson, T. M., Ko, H. S., & Dawson, V. L. (2010). Genetic animal models of Parkinson's disease. *Neuron, 66*(5), 646-661. doi: 10.1016/j.neuron.2010.04.034

de Rijk, M. C., Tzourio, C., Breteler, M. M., Dartigues, J. F., Amaducci, L., Lopez-Pousa, S., . . . Rocca, W. A. (1997). Prevalence of parkinsonism and Parkinson's disease in Europe: the EUROPARKINSON Collaborative Study. European Community Concerted Action on the Epidemiology of Parkinson's disease. *J Neurol Neurosurg Psychiatry, 62*(1), 10-15.

Deas, E., Cremades, N., Angelova, P. R., Ludtmann, M. H., Yao, Z., Chen, S., . . . Abramov, A. Y. (2016). Alpha-Synuclein Oligomers Interact with Metal Ions to Induce Oxidative Stress and Neuronal Death in Parkinson's Disease. *Antioxid Redox Signal, 24*(7), 376-391. doi: 10.1089/ars.2015.6343

Dehay, B., Bourdenx, M., Gorry, P., Przedborski, S., Vila, M., Hunot, S., . . . Meissner, W. G. (2015). Targeting alpha-synuclein for treatment of Parkinson's disease: mechanistic and therapeutic considerations. *Lancet Neurol, 14*(8), 855-866. doi: 10.1016/S1474-4422(15)00006-X

Dehay, B., Bove, J., Rodriguez-Muela, N., Perier, C., Recasens, A., Boya, P., & Vila, M. (2010). Pathogenic lysosomal depletion in Parkinson's disease. *J Neurosci, 30*(37), 12535-12544. doi: 10.1523/JNEUROSCI.1920-10.2010

Dehay, B., Vila, M., Bezard, E., Brundin, P., & Kordower, J. H. (2016). Alpha-synuclein propagation: New insights from animal models. *Mov Disord, 31*(2), 161-168. doi: 10.1002/mds.26370

Del Tredici K, B. H. (2000-2013). Idiopathic Parkinson's Disease: Staging an α-Synucleinopathy with a Predictable Pathoanatomy. from Landes Bioscience https://http://www.ncbi.nlm.nih.gov/books/NBK6077/

Del Tredici, K., Rub, U., De Vos, R. A., Bohl, J. R., & Braak, H. (2002). Where does parkinson disease pathology begin in the brain? *J Neuropathol Exp Neurol, 61*(5), 413-426.

Delic, V., Chandra, S., Abdelmotilib, H., Maltbie, T., Wang, S., Kem, D., . . . West, A. B. (2018). Sensitivity and Specificity of Phospho-Ser129 alpha-Synuclein Monoclonal Antibodies. *J Comp Neurol*. doi: 10.1002/cne.24468

Dettmer, U., Newman, A. J., Luth, E. S., Bartels, T., & Selkoe, D. (2013). In vivo cross-linking reveals principally oligomeric forms of alpha-synuclein and beta-synuclein in neurons and non-neural cells. *J Biol Chem, 288*(9), 6371-6385. doi: 10.1074/jbc.M112.403311

Dev, K. K., Hofele, K., Barbieri, S., Buchman, V. L., & van der Putten, H. (2003). Part II: alpha-synuclein and its molecular pathophysiological role in neurodegenerative disease. *Neuropharmacology, 45*(1), 14-44.

Dewing, P., Chiang, C. W., Sinchak, K., Sim, H., Fernagut, P. O., Kelly, S., . . . Vilain, E. (2006). Direct regulation of adult brain function by the male-specific factor SRY. *Curr Biol, 16*(4), 415-420. doi: 10.1016/j.cub.2006.01.017

Dexter, D. T., Sian, J., Rose, S., Hindmarsh, J. G., Mann, V. M., Cooper, J. M., . . . et al. (1994). Indices of oxidative stress and mitochondrial function in individuals with incidental Lewy body disease. *Ann Neurol, 35*(1), 38-44. doi: 10.1002/ana.410350107

Dexter, D. T., Wells, F. R., Lees, A. J., Agid, F., Agid, Y., Jenner, P., & Marsden, C. D. (1989). Increased nigral iron content and alterations in other metal ions occurring in brain in Parkinson's disease. *J Neurochem, 52*(6), 1830-1836.

Dias, V., Junn, E., & Mouradian, M. M. (2013). The role of oxidative stress in Parkinson's disease. *J Parkinsons Dis, 3*(4), 461-491. doi: 10.3233/JPD-130230

Dickinson, D. A., & Forman, H. J. (2002). Glutathione in defense and signaling: lessons from a small thiol. *Ann N Y Acad Sci, 973*, 488-504.

Dickinson, D. A., Levonen, A. L., Moellering, D. R., Arnold, E. K., Zhang, H., Darley-Usmar, V. M., & Forman, H. J. (2004). Human glutamate cysteine ligase gene regulation through the electrophile response element. *Free Radic Biol Med, 37*(8), 1152-1159. doi: 10.1016/j.freeradbiomed.2004.06.011

Dickson, D. W., Schmidt, M. L., Lee, V. M., Zhao, M. L., Yen, S. H., & Trojanowski, J. Q. (1994). Immunoreactivity profile of hippocampal CA2/3 neurites in diffuse Lewy body disease. *Acta Neuropathol, 87*(3), 269-276.

Dirr, E. R., Ekhator, O. R., Blackwood, R., Holden, J. G., Masliah, E., Schultheis, P. J., & Fleming, S. M. (2018). Exacerbation of sensorimotor dysfunction in mice deficient in Atp13a2 and overexpressing human wildtype alpha-synuclein. *Behav Brain Res, 343*, 41-49. doi: 10.1016/j.bbr.2018.01.029

Dluzen, D. E., McDermott, J. L., & Liu, B. (1996). Estrogen alters MPTP-induced neurotoxicity in female mice: effects on striatal dopamine concentrations and release. *J Neurochem, 66*(2), 658-666.

Donaghy, P. C., & McKeith, I. G. (2014). The clinical characteristics of dementia with Lewy bodies and a consideration of prodromal diagnosis. *Alzheimers Res Ther, 6*(4), 46. doi: 10.1186/alzrt274

Doty, R. L. (2008). The olfactory vector hypothesis of neurodegenerative disease: is it viable? *Ann Neurol, 63*(1), 7-15. doi: 10.1002/ana.21327

Doty, R. L. (2009). The olfactory system and its disorders. *Semin Neurol, 29*(1), 74-81. doi: 10.1055/s-0028-1124025

Doty, R. L. (2012). Olfactory dysfunction in Parkinson disease. *Nat Rev Neurol, 8*(6), 329-339. doi: 10.1038/nrneurol.2012.80

Doty, R. L., Deems, D. A., & Stellar, S. (1988). Olfactory dysfunction in parkinsonism: a general deficit unrelated to neurologic signs, disease stage, or disease duration. *Neurology, 38*(8), 1237-1244.

Doty, R. L., Shaman, P., Applebaum, S. L., Giberson, R., Siksorski, L., & Rosenberg, L. (1984). Smell identification ability: changes with age. *Science, 226*(4681), 1441-1443.

Double, K. L., Reyes, S., Werry, E. L., & Halliday, G. M. (2010). Selective cell death in neurodegeneration: why are some neurons spared in vulnerable regions? *Prog Neurobiol, 92*(3), 316-329. doi: 10.1016/j.pneurobio.2010.06.001

Dringen, R. (2000). Metabolism and functions of glutathione in brain. *Prog Neurobiol, 62*(6), 649-671.

Driver-Dunckley, E., Adler, C. H., Hentz, J. G., Dugger, B. N., Shill, H. A., Caviness, J. N., . . . Arizona Parkinson Disease, C. (2014). Olfactory dysfunction in incidental Lewy body disease and Parkinson's disease. *Parkinsonism Relat Disord, 20*(11), 1260-1262. doi: 10.1016/j.parkreldis.2014.08.006

Dryanovski, D. I., Guzman, J. N., Xie, Z., Galteri, D. J., Volpicelli-Daley, L. A., Lee, V. M., . . . Surmeier, D. J. (2013). Calcium entry and alpha-synuclein inclusions elevate dendritic mitochondrial oxidant stress in dopaminergic neurons. *J Neurosci, 33*(24), 10154-10164. doi: 10.1523/JNEUROSCI.5311-12.2013

Duda, J. E., Lee, V. M., & Trojanowski, J. Q. (2000). Neuropathology of synuclein aggregates. *J Neurosci Res, 61*(2), 121-127. doi: 10.1002/1097-4547(20000715)61:2<121::AID-JNR1>3.0.CO;2-4

el-Agnaf, O. M., Irvine, G. B., & Guthrie, D. J. (1997). Conformations of beta-amyloid in solution. *J Neurochem, 68*(1), 437-439.

El-Agnaf, O. M., Walsh, D. M., & Allsop, D. (2003). Soluble oligomers for the diagnosis of neurodegenerative diseases. *Lancet Neurol, 2*(8), 461-462.

Elder, G. J., Mactier, K., Colloby, S. J., Watson, R., Blamire, A. M., O'Brien, J. T., & Taylor, J. P. (2017). The influence of hippocampal atrophy on the cognitive phenotype of dementia with Lewy bodies. *Int J Geriatr Psychiatry, 32*(11), 1182-1189. doi: 10.1002/gps.4719

Emmanouilidou, E., Stefanis, L., & Vekrellis, K. (2010). Cell-produced alpha-synuclein oligomers are targeted to, and impair, the 26S proteasome. *Neurobiol Aging, 31*(6), 953-968. doi: 10.1016/j.neurobiolaging.2008.07.008

Engler-Chiurazzi, E. B., Covey, D. F., & Simpkins, J. W. (2017). A novel mechanism of non-feminizing estrogens in neuroprotection. *Exp Gerontol, 94*, 99-102. doi: 10.1016/j.exger.2016.10.013

Eriksson, I., Nath, S., Bornefall, P., Giraldo, A. M., & Ollinger, K. (2017). Impact of high cholesterol in a Parkinson's disease model: Prevention of lysosomal leakage versus stimulation of alpha-synuclein aggregation. *Eur J Cell Biol, 96*(2), 99-109. doi: 10.1016/j.ejcb.2017.01.002

Eschbach, J., von Einem, B., Muller, K., Bayer, H., Scheffold, A., Morrison, B. E., . . . Danzer, K. M. (2015). Mutual exacerbation of peroxisome proliferator-activated receptor gamma coactivator 1alpha deregulation and alpha-synuclein oligomerization. *Ann Neurol, 77*(1), 15-32. doi: 10.1002/ana.24294

Fahn, S., & Cohen, G. (1992). The oxidant stress hypothesis in Parkinson's disease: evidence supporting it. *Ann Neurol, 32*(6), 804-812. doi: 10.1002/ana.410320616

Fargnoli, J., Kunisada, T., Fornace, A. J., Jr., Schneider, E. L., & Holbrook, N. J. (1990). Decreased expression of heat shock protein 70 mRNA and protein after heat treatment in cells of aged rats. *Proc Natl Acad Sci U S A, 87*(2), 846-850.

Farhadi, F., Vosoughi, K., Shahidi, G. A., Delbari, A., Lokk, J., & Fereshtehnejad, S. M. (2017). Sexual dimorphism in Parkinson's disease: differences in clinical manifestations, quality of life and psychosocial functioning between males and females. *Neuropsychiatr Dis Treat, 13*, 329-338. doi: 10.2147/NDT.S124984

Fearnley, J. M., & Lees, A. J. (1991). Ageing and Parkinson's disease: substantia nigra regional selectivity. *Brain, 114 (Pt 5)*, 2283-2301.

Fernandez, H. H., Lapane, K. L., Ott, B. R., & Friedman, J. H. (2000). Gender differences in the frequency and treatment of behavior problems in Parkinson's disease. SAGE Study Group. Systematic Assessment and Geriatric drug use via Epidemiology. *Mov Disord, 15*(3), 490-496.

Ferrer, I., Lopez-Gonzalez, I., Carmona, M., Dalfo, E., Pujol, A., & Martinez, A. (2012). Neurochemistry and the non-motor aspects of PD. *Neurobiol Dis, 46*(3), 508-526.

Fewell, S. W., Smith, C. M., Lyon, M. A., Dumitrescu, T. P., Wipf, P., Day, B. W., & Brodsky, J. L. (2004). Small molecule modulators of endogenous and co-chaperone-stimulated Hsp70 ATPase activity. *J Biol Chem, 279*(49), 51131-51140. doi: 10.1074/jbc.M404857200

Flavin, W. P., Bousset, L., Green, Z. C., Chu, Y., Skarpathiotis, S., Chaney, M. J., . . . Campbell, E. M. (2017). Endocytic vesicle rupture is a conserved mechanism of cellular invasion by amyloid proteins. *Acta Neuropathol, 134*(4), 629-653. doi: 10.1007/s00401-017-1722-x

Fleming, S. M., Salcedo, J., Fernagut, P. O., Rockenstein, E., Masliah, E., Levine, M. S., & Chesselet, M. F. (2004). Early and progressive sensorimotor anomalies in mice overexpressing wild-type human alpha-synuclein. *J Neurosci, 24*(42), 9434-9440. doi: 10.1523/JNEUROSCI.3080-04.2004

Flores-Cuadrado, A., Ubeda-Banon, I., Saiz-Sanchez, D., de la Rosa-Prieto, C., & Martinez-Marcos, A. (2016). Hippocampal alpha-synuclein and interneurons in Parkinson's disease: Data from human and mouse models. *Mov Disord, 31*(7), 979-988. doi: 10.1002/mds.26586

Forsaa, E. B., Larsen, J. P., Wentzel-Larsen, T., & Alves, G. (2010). What predicts mortality in Parkinson disease?: a prospective population-based long-term study. *Neurology, 75*(14), 1270-1276. doi: 10.1212/WNL.0b013e3181f61311

Freundt, E. C., Maynard, N., Clancy, E. K., Roy, S., Bousset, L., Sourigues, Y., . . . Brahic, M. (2012). Neuron-to-neuron transmission of alpha-synuclein fibrils through axonal transport. *Ann Neurol, 72*(4), 517-524. doi: 10.1002/ana.23747

Fujiwara, H., Hasegawa, M., Dohmae, N., Kawashima, A., Masliah, E., Goldberg, M. S., . . . Iwatsubo, T. (2002). alpha-Synuclein is phosphorylated in synucleinopathy lesions. *Nat Cell Biol, 4*(2), 160-164. doi: 10.1038/ncb748

Fumimura, Y., Ikemura, M., Saito, Y., Sengoku, R., Kanemaru, K., Sawabe, M., . . . Murayama, S. (2007). Analysis of the adrenal gland is useful for evaluating pathology of the peripheral autonomic nervous system in lewy body disease. *J Neuropathol Exp Neurol, 66*(5), 354-362. doi: 10.1097/nen.0b013e3180517454

Fusco, G., Chen, S. W., Williamson, P. T. F., Cascella, R., Perni, M., Jarvis, J. A., . . . De Simone, A. (2017). Structural basis of membrane disruption and cellular toxicity by

alpha-synuclein oligomers. *Science, 358*(6369), 1440-1443. doi: 10.1126/science.aan6160

Gallea, J. I., & Celej, M. S. (2014). Structural insights into amyloid oligomers of the Parkinson disease-related protein alpha-synuclein. *J Biol Chem, 289*(39), 26733-26742. doi: 10.1074/jbc.M114.566695

Galvagnion, C., Buell, A. K., Meisl, G., Michaels, T. C., Vendruscolo, M., Knowles, T. P., & Dobson, C. M. (2015). Lipid vesicles trigger alpha-synuclein aggregation by stimulating primary nucleation. *Nat Chem Biol, 11*(3), 229-234. doi: 10.1038/nchembio.1750

Geevarghese, R., Lumsden, D. E., Hulse, N., Samuel, M., & Ashkan, K. (2015). Subcortical structure volumes and correlation to clinical variables in Parkinson's disease. *J Neuroimaging, 25*(2), 275-280. doi: 10.1111/jon.12095

Gelpi, E., Navarro-Otano, J., Tolosa, E., Gaig, C., Compta, Y., Rey, M. J., . . . Ribalta, T. (2014). Multiple organ involvement by alpha-synuclein pathology in Lewy body disorders. *Mov Disord, 29*(8), 1010-1018. doi: 10.1002/mds.25776

Georgiev, D., Hamberg, K., Hariz, M., Forsgren, L., & Hariz, G. M. (2017). Gender differences in Parkinson's disease: A clinical perspective. *Acta Neurol Scand, 136*(6), 570-584. doi: 10.1111/ane.12796

Gerlach, M., Riederer, P., & Double, K. L. (2008). Neuromelanin-bound ferric iron as an experimental model of dopaminergic neurodegeneration in Parkinson's disease. *Parkinsonism Relat Disord, 14 Suppl 2*, S185-188. doi: 10.1016/j.parkreldis.2008.04.028

Gerstenberger, J., Bauer, A., Helmschrodt, C., Richter, A., & Richter, F. (2016). The novel adaptive rotating beam test unmasks sensorimotor impairments in a transgenic mouse model of Parkinson's disease. *Behav Brain Res, 304*, 102-110. doi: 10.1016/j.bbr.2016.02.017

Gertz, H. J., Siegers, A., & Kuchinke, J. (1994). Stability of cell size and nucleolar size in Lewy body containing neurons of substantia nigra in Parkinson's disease. *Brain Res, 637*(1-2), 339-341.

Ghosh, D., Mondal, M., Mohite, G. M., Singh, P. K., Ranjan, P., Anoop, A., . . . Maji, S. K. (2013). The Parkinson's disease-associated H50Q mutation accelerates alpha-Synuclein aggregation in vitro. *Biochemistry, 52*(40), 6925-6927. doi: 10.1021/bi400999d

Giustarini, D., Milzani, A., Dalle-Donne, I., Tsikas, D., & Rossi, R. (2012). N-Acetylcysteine ethyl ester (NACET): a novel lipophilic cell-permeable cysteine derivative with an unusual pharmacokinetic feature and remarkable antioxidant potential. *Biochem Pharmacol, 84*(11), 1522-1533. doi: 10.1016/j.bcp.2012.09.010

Gleixner, A. M., Hutchison, D. F., Sannino, S., Bhatia, T. N., Leak, L. C., Flaherty, P. T., . . . Leak, R. K. (2017). N-Acetyl-l-Cysteine Protects Astrocytes against Proteotoxicity without Recourse to Glutathione. *Mol Pharmacol, 92*(5), 564-575. doi: 10.1124/mol.117.109926

Godfrey, D. A., Ross, C. D., Herrmann, A. D., & Matschinsky, F. M. (1980). Distribution and derivation of cholinergic elements in the rat olfactory bulb. *Neuroscience, 5*(2), 273-292.

Godoy, M. D., Voegels, R. L., Pinna Fde, R., Imamura, R., & Farfel, J. M. (2015). Olfaction in neurologic and neurodegenerative diseases: a literature review. *Int Arch Otorhinolaryngol, 19*(2), 176-179. doi: 10.1055/s-0034-1390136

Goetz, C. G., Emre, M., & Dubois, B. (2008). Parkinson's disease dementia: definitions, guidelines, and research perspectives in diagnosis. *Ann Neurol, 64 Suppl 2*, S81-92. doi: 10.1002/ana.21455

Goldberg, M. S., & Lansbury, P. T., Jr. (2000). Is there a cause-and-effect relationship between alpha-synuclein fibrillization and Parkinson's disease? *Nat Cell Biol, 2*(7), E115-119. doi: 10.1038/35017124

Goldstein, D. S., Jinsmaa, Y., Sullivan, P., & Sharabi, Y. (2017). N-Acetylcysteine Prevents the Increase in Spontaneous Oxidation of Dopamine During Monoamine Oxidase Inhibition in PC12 Cells. *Neurochem Res, 42*(11), 3289-3295. doi: 10.1007/s11064-017-2371-0

Goldstein, D. S., Sullivan, P., Cooney, A., Jinsmaa, Y., Sullivan, R., Gross, D. J., . . . Sharabi, Y. (2012). Vesicular uptake blockade generates the toxic dopamine metabolite 3,4-dihydroxyphenylacetaldehyde in PC12 cells: relevance to the pathogenesis of Parkinson's disease. *J Neurochem, 123*(6), 932-943. doi: 10.1111/j.1471-4159.2012.07924.x

Gomez-Tortosa, E., Sanders, J. L., Newell, K., & Hyman, B. T. (2001). Cortical neurons expressing calcium binding proteins are spared in dementia with Lewy bodies. *Acta Neuropathol, 101*(1), 36-42.

Gomperts, S. N. (2016). Lewy Body Dementias: Dementia With Lewy Bodies and Parkinson Disease Dementia. *Continuum (Minneap Minn), 22*(2 Dementia), 435-463. doi: 10.1212/CON.0000000000000309

Good, P. F., Hsu, A., Werner, P., Perl, D. P., & Olanow, C. W. (1998). Protein nitration in Parkinson's disease. *J Neuropathol Exp Neurol, 57*(4), 338-342.

Gorell, J. M., Johnson, C. C., Rybicki, B. A., Peterson, E. L., & Richardson, R. J. (1998). The risk of Parkinson's disease with exposure to pesticides, farming, well water, and rural living. *Neurology, 50*(5), 1346-1350.

Gorell, J. M., Peterson, E. L., Rybicki, B. A., & Johnson, C. C. (2004). Multiple risk factors for Parkinson's disease. *J Neurol Sci, 217*(2), 169-174.

Grace, A. A., & Bunney, B. S. (1983). Intracellular and extracellular electrophysiology of nigral dopaminergic neurons--3. Evidence for electrotonic coupling. *Neuroscience, 10*(2), 333-348.

Graff-Radford, J., Lesnick, T. G., Boeve, B. F., Przybelski, S. A., Jones, D. T., Senjem, M. L., . . . Kantarci, K. (2016). Predicting Survival in Dementia With Lewy Bodies With Hippocampal Volumetry. *Mov Disord, 31*(7), 989-994. doi: 10.1002/mds.26666

Gratwicke, J., Jahanshahi, M., & Foltynie, T. (2015). Parkinson's disease dementia: a neural networks perspective. *Brain, 138*(Pt 6), 1454-1476. doi: 10.1093/brain/awv104

Greenamyre, J. T., & Hastings, T. G. (2004). Biomedicine. Parkinson's--divergent causes, convergent mechanisms. *Science, 304*(5674), 1120-1122. doi: 10.1126/science.1098966

Greenbaum, E. A., Graves, C. L., Mishizen-Eberz, A. J., Lupoli, M. A., Lynch, D. R., Englander, S. W., . . . Giasson, B. I. (2005). The E46K mutation in alpha-synuclein increases amyloid fibril formation. *J Biol Chem, 280*(9), 7800-7807. doi: 10.1074/jbc.M411638200

Griffith, O. W. (1999). Biologic and pharmacologic regulation of mammalian glutathione synthesis. *Free Radic Biol Med, 27*(9-10), 922-935.

Guo, J. L., Covell, D. J., Daniels, J. P., Iba, M., Stieber, A., Zhang, B., . . . Lee, V. M. (2013). Distinct alpha-synuclein strains differentially promote tau inclusions in neurons. *Cell, 154*(1), 103-117. doi: 10.1016/j.cell.2013.05.057

Gur, R. C., Turetsky, B. I., Matsui, M., Yan, M., Bilker, W., Hughett, P., & Gur, R. E. (1999). Sex differences in brain gray and white matter in healthy young adults: correlations with cognitive performance. *J Neurosci, 19*(10), 4065-4072.

Haaxma, C. A., Bloem, B. R., Borm, G. F., Oyen, W. J., Leenders, K. L., Eshuis, S., . . . Horstink, M. W. (2007). Gender differences in Parkinson's disease. *J Neurol Neurosurg Psychiatry, 78*(8), 819-824. doi: 10.1136/jnnp.2006.103788

Haber, S. N., & Knutson, B. (2010). The reward circuit: linking primate anatomy and human imaging. *Neuropsychopharmacology, 35*(1), 4-26. doi: 10.1038/npp.2009.129

Hall, H., Reyes, S., Landeck, N., Bye, C., Leanza, G., Double, K., . . . Kirik, D. (2014). Hippocampal Lewy pathology and cholinergic dysfunction are associated with dementia in Parkinson's disease. *Brain, 137*(Pt 9), 2493-2508. doi: 10.1093/brain/awu193

Halliwell, B. (1992). Reactive oxygen species and the central nervous system. *J Neurochem, 59*(5), 1609-1623.

Hanell, A., & Marklund, N. (2014). Structured evaluation of rodent behavioral tests used in drug discovery research. *Front Behav Neurosci, 8*, 252. doi: 10.3389/fnbeh.2014.00252

Hansen, C., Angot, E., Bergstrom, A. L., Steiner, J. A., Pieri, L., Paul, G., . . . Brundin, P. (2011). alpha-Synuclein propagates from mouse brain to grafted dopaminergic neurons and seeds aggregation in cultured human cells. *J Clin Invest, 121*(2), 715-725. doi: 10.1172/JCI43366

Hasegawa, M., Fujiwara, H., Nonaka, T., Wakabayashi, K., Takahashi, H., Lee, V. M., . . . Iwatsubo, T. (2002). Phosphorylated alpha-synuclein is ubiquitinated in alpha-synucleinopathy lesions. *J Biol Chem, 277*(50), 49071-49076. doi: 10.1074/jbc.M208046200

Hashimoto, M., Hsu, L. J., Xia, Y., Takeda, A., Sisk, A., Sundsmo, M., & Masliah, E. (1999). Oxidative stress induces amyloid-like aggregate formation of NACP/alpha-synuclein in vitro. *Neuroreport, 10*(4), 717-721.

Hawkes, C. H., Del Tredici, K., & Braak, H. (2010). A timeline for Parkinson's disease. *Parkinsonism Relat Disord, 16*(2), 79-84. doi: 10.1016/j.parkreldis.2009.08.007

Hawkes, C. H., Shephard, B. C., & Daniel, S. E. (1997). Olfactory dysfunction in Parkinson's disease. *J Neurol Neurosurg Psychiatry, 62*(5), 436-446.

Heinemann, S. D., Posimo, J. M., Mason, D. M., Hutchison, D. F., & Leak, R. K. (2016). Synergistic stress exacerbation in hippocampal neurons: Evidence favoring the dual-hit hypothesis of neurodegeneration. *Hippocampus, 26*(8), 980-994. doi: 10.1002/hipo.22580

Hely, M. A., Reid, W. G., Adena, M. A., Halliday, G. M., & Morris, J. G. (2008). The Sydney multicenter study of Parkinson's disease: the inevitability of dementia at 20 years. *Mov Disord, 23*(6), 837-844. doi: 10.1002/mds.21956

Hertzman, C., Wiens, M., Bowering, D., Snow, B., & Calne, D. (1990). Parkinson's disease: a case-control study of occupational and environmental risk factors. *Am J Ind Med, 17*(3), 349-355.

Hirohata, M., Ono, K., Morinaga, A., Ikeda, T., & Yamada, M. (2009). Anti-aggregation and fibril-destabilizing effects of sex hormones on alpha-synuclein fibrils in vitro. *Exp Neurol, 217*(2), 434-439. doi: 10.1016/j.expneurol.2009.03.003

Hoffer, M. E., Balaban, C., Slade, M. D., Tsao, J. W., & Hoffer, B. (2013). Amelioration of acute sequelae of blast induced mild traumatic brain injury by N-acetyl cysteine: a double-blind, placebo controlled study. *PLoS One, 8*(1), e54163. doi: 10.1371/journal.pone.0054163

Hoglinger, G. U., Alvarez-Fischer, D., Arias-Carrion, O., Djufri, M., Windolph, A., Keber, U., . . . Oertel, W. H. (2015). A new dopaminergic nigro-olfactory projection. *Acta Neuropathol, 130*(3), 333-348. doi: 10.1007/s00401-015-1451-y

Holmay, M. J., Terpstra, M., Coles, L. D., Mishra, U., Ahlskog, M., Oz, G., . . . Tuite, P. J. (2013). N-Acetylcysteine boosts brain and blood glutathione in Gaucher and Parkinson diseases. *Clin Neuropharmacol, 36*(4), 103-106. doi: 10.1097/WNF.0b013e31829ae713

Hu, G., Jousilahti, P., Bidel, S., Antikainen, R., & Tuomilehto, J. (2007). Type 2 diabetes and the risk of Parkinson's disease. *Diabetes Care, 30*(4), 842-847. doi: 10.2337/dc06-2011

Hu, G., Jousilahti, P., Nissinen, A., Antikainen, R., Kivipelto, M., & Tuomilehto, J. (2006). Body mass index and the risk of Parkinson disease. *Neurology, 67*(11), 1955-1959. doi: 10.1212/01.wnl.0000247052.18422.e5

Hurtig, H. I., Trojanowski, J. Q., Galvin, J., Ewbank, D., Schmidt, M. L., Lee, V. M., . . . Arnold, S. E. (2000). Alpha-synuclein cortical Lewy bodies correlate with dementia in Parkinson's disease. *Neurology, 54*(10), 1916-1921.

Huryn, D. M., Brodsky, J. L., Brummond, K. M., Chambers, P. G., Eyer, B., Ireland, A. W., . . . Wipf, P. (2011). Chemical methodology as a source of small-molecule checkpoint inhibitors and heat shock protein 70 (Hsp70) modulators. *Proc Natl Acad Sci U S A, 108*(17), 6757-6762. doi: 10.1073/pnas.1015251108

Hyman, B. T., Van Hoesen, G. W., & Damasio, A. R. (1990). Memory-related neural systems in Alzheimer's disease: an anatomic study. *Neurology, 40*(11), 1721-1730.

Iacono, D., Geraci-Erck, M., Rabin, M. L., Adler, C. H., Serrano, G., Beach, T. G., & Kurlan, R. (2015). Parkinson disease and incidental Lewy body disease: Just a question of time? *Neurology, 85*(19), 1670-1679. doi: 10.1212/WNL.0000000000002102

Ide, T., Tsutsui, H., Ohashi, N., Hayashidani, S., Suematsu, N., Tsuchihashi, M., . . . Takeshita, A. (2002). Greater oxidative stress in healthy young men compared with premenopausal women. *Arterioscler Thromb Vasc Biol, 22*(3), 438-442.

Ingelsson, M. (2016). Alpha-Synuclein Oligomers-Neurotoxic Molecules in Parkinson's Disease and Other Lewy Body Disorders. *Front Neurosci, 10*, 408. doi: 10.3389/fnins.2016.00408

Irwin, D. J., Lee, V. M., & Trojanowski, J. Q. (2013). Parkinson's disease dementia: convergence of alpha-synuclein, tau and amyloid-beta pathologies. *Nat Rev Neurosci, 14*(9), 626-636. doi: 10.1038/nrn3549

Iwai, A., Masliah, E., Yoshimoto, M., Ge, N., Flanagan, L., de Silva, H. A., . . . Saitoh, T. (1995). The precursor protein of non-A beta component of Alzheimer's disease amyloid is a presynaptic protein of the central nervous system. *Neuron, 14*(2), 467-475.

Jang, A., Lee, H. J., Suk, J. E., Jung, J. W., Kim, K. P., & Lee, S. J. (2010). Non-classical exocytosis of alpha-synuclein is sensitive to folding states and promoted under stress conditions. *J Neurochem, 113*(5), 1263-1274. doi: 10.1111/j.1471-4159.2010.06695.x

Jankovic, J. (2008). Parkinson's disease: clinical features and diagnosis. *J Neurol Neurosurg Psychiatry, 79*(4), 368-376. doi: 10.1136/jnnp.2007.131045

Jellinger, K. A. (2012). Neuropathology of sporadic Parkinson's disease: evaluation and changes of concepts. *Mov Disord, 27*(1), 8-30. doi: 10.1002/mds.23795

Jenner, P. (1998). Oxidative mechanisms in nigral cell death in Parkinson's disease. *Mov Disord, 13 Suppl 1*, 24-34.

Jenner, P. (2003). Oxidative stress in Parkinson's disease. *Ann Neurol, 53 Suppl 3*, S26-36; discussion S36-28. doi: 10.1002/ana.10483

Jiang, Y., Rumble, J. L., Gleixner, A. M., Unnithan, A. S., Pulugulla, S. H., Posimo, J. M., . . . Leak, R. K. (2013). N-Acetyl cysteine blunts proteotoxicity in a heat shock protein-dependent manner. *Neuroscience, 255*, 19-32. doi: 10.1016/j.neuroscience.2013.09.049

Jinsmaa, Y., Sharabi, Y., Sullivan, P., Isonaka, R., & Goldstein, D. S. (2018). 3,4-Dihydroxyphenylacetaldehyde-Induced Protein Modifications and Their Mitigation by N-Acetylcysteine. *J Pharmacol Exp Ther, 366*(1), 113-124. doi: 10.1124/jpet.118.248492

Johnston, J. A., Illing, M. E., & Kopito, R. R. (2002). Cytoplasmic dynein/dynactin mediates the assembly of aggresomes. *Cell Motil Cytoskeleton, 53*(1), 26-38. doi: 10.1002/cm.10057

Johnston, J. A., Ward, C. L., & Kopito, R. R. (1998). Aggresomes: a cellular response to misfolded proteins. *J Cell Biol, 143*(7), 1883-1898.

Jones, D. R., Delenclos, M., Baine, A. T., DeTure, M., Murray, M. E., Dickson, D. W., & McLean, P. J. (2015). Transmission of Soluble and Insoluble alpha-Synuclein to Mice. *J Neuropathol Exp Neurol, 74*(12), 1158-1169. doi: 10.1097/NEN.0000000000000262

Jucker, M., & Walker, L. C. (2013). Self-propagation of pathogenic protein aggregates in neurodegenerative diseases. *Nature, 501*(7465), 45-51. doi: 10.1038/nature12481

Junn, E., Lee, S. S., Suhr, U. T., & Mouradian, M. M. (2002). Parkin accumulation in aggresomes due to proteasome impairment. *J Biol Chem, 277*(49), 47870-47877. doi: 10.1074/jbc.M203159200

Kalaitzakis, M. E., Graeber, M. B., Gentleman, S. M., & Pearce, R. K. (2008). The dorsal motor nucleus of the vagus is not an obligatory trigger site of Parkinson's disease: a critical analysis of alpha-synuclein staging. *Neuropathol Appl Neurobiol, 34*(3), 284-295. doi: 10.1111/j.1365-2990.2007.00923.x

Kalaitzakis, M. E., & Pearce, R. K. (2009). The morbid anatomy of dementia in Parkinson's disease. *Acta Neuropathol, 118*(5), 587-598. doi: 10.1007/s00401-009-0597-x

Katz, M., Won, S. J., Park, Y., Orr, A., Jones, D. P., Swanson, R. A., & Glass, G. A. (2015). Cerebrospinal fluid concentrations of N-acetylcysteine after oral administration in Parkinson's disease. *Parkinsonism Relat Disord, 21*(5), 500-503. doi: 10.1016/j.parkreldis.2015.02.020

Kaushik, S., & Cuervo, A. M. (2012). Chaperone-mediated autophagy: a unique way to enter the lysosome world. *Trends Cell Biol, 22*(8), 407-417. doi: 10.1016/j.tcb.2012.05.006

Kawaguchi, Y., Kovacs, J. J., McLaurin, A., Vance, J. M., Ito, A., & Yao, T. P. (2003). The deacetylase HDAC6 regulates aggresome formation and cell viability in response to misfolded protein stress. *Cell, 115*(6), 727-738.

Kilpatrick, K., Novoa, J. A., Hancock, T., Guerriero, C. J., Wipf, P., Brodsky, J. L., & Segatori, L. (2013). Chemical induction of Hsp70 reduces alpha-synuclein aggregation in neuroglioma cells. *ACS Chem Biol, 8*(7), 1460-1468. doi: 10.1021/cb400017h

Kim, C., Lv, G., Lee, J. S., Jung, B. C., Masuda-Suzukake, M., Hong, C. S., . . . Lee, S. J. (2016). Exposure to bacterial endotoxin generates a distinct strain of alpha-synuclein fibril. *Sci Rep, 6*, 30891. doi: 10.1038/srep30891

Kisselev, A. F., & Goldberg, A. L. (2001). Proteasome inhibitors: from research tools to drug candidates. *Chem Biol, 8*(8), 739-758.

Kitada, T., Asakawa, S., Hattori, N., Matsumine, H., Yamamura, Y., Minoshima, S., . . . Shimizu, N. (1998). Mutations in the parkin gene cause autosomal recessive juvenile parkinsonism. *Nature, 392*(6676), 605-608. doi: 10.1038/33416

Klimek, V., Stockmeier, C., Overholser, J., Meltzer, H. Y., Kalka, S., Dilley, G., & Ordway, G. A. (1997). Reduced levels of norepinephrine transporters in the locus coeruleus in major depression. *J Neurosci, 17*(21), 8451-8458.

Klucken, J., Shin, Y., Masliah, E., Hyman, B. T., & McLean, P. J. (2004). Hsp70 Reduces alpha-Synuclein Aggregation and Toxicity. *J Biol Chem, 279*(24), 25497-25502. doi: 10.1074/jbc.M400255200

Kopito, R. R. (2000). Aggresomes, inclusion bodies and protein aggregation. *Trends Cell Biol, 10*(12), 524-530.

Kordower, J. H., Chu, Y., Hauser, R. A., Freeman, T. B., & Olanow, C. W. (2008). Lewy body-like pathology in long-term embryonic nigral transplants in Parkinson's disease. *Nat Med, 14*(5), 504-506. doi: 10.1038/nm1747

Kordower, J. H., Olanow, C. W., Dodiya, H. B., Chu, Y., Beach, T. G., Adler, C. H., . . . Bartus, R. T. (2013). Disease duration and the integrity of the nigrostriatal system in Parkinson's disease. *Brain, 136*(Pt 8), 2419-2431. doi: 10.1093/brain/awt192

Kowal, S. L., Dall, T. M., Chakrabarti, R., Storm, M. V., & Jain, A. (2013). The current and projected economic burden of Parkinson's disease in the United States. *Mov Disord, 28*(3), 311-318. doi: 10.1002/mds.25292

Kristal, B. S., Conway, A. D., Brown, A. M., Jain, J. C., Ulluci, P. A., Li, S. W., & Burke, W. J. (2001). Selective dopaminergic vulnerability: 3,4-dihydroxyphenylacetaldehyde targets mitochondria. *Free Radic Biol Med, 30*(8), 924-931.

Kumar, R., Kumari, R., Kumar, S., Jangir, D. K., & Maiti, T. K. (2018). Extracellular alpha-Synuclein Disrupts Membrane Nanostructure and Promotes S-Nitrosylation-Induced Neuronal Cell Death. *Biomacromolecules, 19*(4), 1118-1129. doi: 10.1021/acs.biomac.7b01727

Kuzuhara, S., Mori, H., Izumiyama, N., Yoshimura, M., & Ihara, Y. (1988). Lewy bodies are ubiquitinated. A light and electron microscopic immunocytochemical study. *Acta Neuropathol, 75*(4), 345-353.

Lace, G., Savva, G. M., Forster, G., de Silva, R., Brayne, C., Matthews, F. E., . . . Mrc, C. (2009). Hippocampal tau pathology is related to neuroanatomical connections: an ageing population-based study. *Brain, 132*(Pt 5), 1324-1334. doi: 10.1093/brain/awp059

Lashuel, H. A., Petre, B. M., Wall, J., Simon, M., Nowak, R. J., Walz, T., & Lansbury, P. T., Jr. (2002). Alpha-synuclein, especially the Parkinson's disease-associated mutants, forms pore-like annular and tubular protofibrils. *J Mol Biol, 322*(5), 1089-1102.

Lauretti, E., Di Meco, A., Merali, S., & Pratico, D. (2017). Circadian rhythm dysfunction: a novel environmental risk factor for Parkinson's disease. *Mol Psychiatry, 22*(2), 280-286. doi: 10.1038/mp.2016.47

Lautenschlager, J., Stephens, A. D., Fusco, G., Strohl, F., Curry, N., Zacharopoulou, M., . . . Schierle, G. S. K. (2018). C-terminal calcium binding of alpha-synuclein modulates synaptic vesicle interaction. *Nat Commun, 9*(1), 712. doi: 10.1038/s41467-018-03111-4

Lee, D. H., & Goldberg, A. L. (1998). Proteasome inhibitors: valuable new tools for cell biologists. *Trends Cell Biol, 8*(10), 397-403.

Lee, H. J., & Lee, S. J. (2002). Characterization of cytoplasmic alpha-synuclein aggregates. Fibril formation is tightly linked to the inclusion-forming process in cells. *J Biol Chem, 277*(50), 48976-48983. doi: 10.1074/jbc.M208192200

Lee, H. J., Patel, S., & Lee, S. J. (2005). Intravesicular localization and exocytosis of alpha-synuclein and its aggregates. *J Neurosci, 25*(25), 6016-6024. doi: 10.1523/JNEUROSCI.0692-05.2005

Lee, K. W., Lee, S. H., Kim, H., Song, J. S., Yang, S. D., Paik, S. G., & Han, P. L. (2004). Progressive cognitive impairment and anxiety induction in the absence of plaque

deposition in C57BL/6 inbred mice expressing transgenic amyloid precursor protein. *J Neurosci Res, 76*(4), 572-580. doi: 10.1002/jnr.20127
Lemstra, A. W., de Beer, M. H., Teunissen, C. E., Schreuder, C., Scheltens, P., van der Flier, W. M., & Sikkes, S. A. (2017). Concomitant AD pathology affects clinical manifestation and survival in dementia with Lewy bodies. *J Neurol Neurosurg Psychiatry, 88*(2), 113-118. doi: 10.1136/jnnp-2016-313775
Leverenz, J. B., Umar, I., Wang, Q., Montine, T. J., McMillan, P. J., Tsuang, D. W., . . . Zhang, J. (2007). Proteomic identification of novel proteins in cortical lewy bodies. *Brain Pathol, 17*(2), 139-145. doi: 10.1111/j.1750-3639.2007.00048.x
Li, J. Y., Englund, E., Holton, J. L., Soulet, D., Hagell, P., Lees, A. J., . . . Brundin, P. (2008). Lewy bodies in grafted neurons in subjects with Parkinson's disease suggest host-to-graft disease propagation. *Nat Med, 14*(5), 501-503. doi: 10.1038/nm1746
Lindersson, E., Beedholm, R., Hojrup, P., Moos, T., Gai, W., Hendil, K. B., & Jensen, P. H. (2004). Proteasomal inhibition by alpha-synuclein filaments and oligomers. *J Biol Chem, 279*(13), 12924-12934. doi: 10.1074/jbc.M306390200
Liou, H. H., Chen, R. C., Tsai, Y. F., Chen, W. P., Chang, Y. C., & Tsai, M. C. (1996). Effects of paraquat on the substantia nigra of the wistar rats: neurochemical, histological, and behavioral studies. *Toxicol Appl Pharmacol, 137*(1), 34-41. doi: 10.1006/taap.1996.0054
Litim, N., Morissette, M., & Di Paolo, T. (2016). Neuroactive gonadal drugs for neuroprotection in male and female models of Parkinson's disease. *Neurosci Biobehav Rev, 67*, 79-88. doi: 10.1016/j.neubiorev.2015.09.024
Liu, H., Wang, H., Shenvi, S., Hagen, T. M., & Liu, R. M. (2004). Glutathione metabolism during aging and in Alzheimer disease. *Ann N Y Acad Sci, 1019*, 346-349. doi: 10.1196/annals.1297.059
Logroscino, G., Marder, K., Cote, L., Tang, M. X., Shea, S., & Mayeux, R. (1996). Dietary lipids and antioxidants in Parkinson's disease: a population-based, case-control study. *Ann Neurol, 39*(1), 89-94. doi: 10.1002/ana.410390113
Lopez Meza, S., Kalbe, U., Berger, W., & Simon, F. G. (2010). Effect of contact time on the release of contaminants from granular waste materials during column leaching experiments. *Waste Manag, 30*(4), 565-571. doi: 10.1016/j.wasman.2009.11.022
Loria, F., Vargas, J. Y., Bousset, L., Syan, S., Salles, A., Melki, R., & Zurzolo, C. (2017). alpha-Synuclein transfer between neurons and astrocytes indicates that astrocytes play a role in degradation rather than in spreading. *Acta Neuropathol, 134*(5), 789-808. doi: 10.1007/s00401-017-1746-2
Loughlin, S. E., & Fallon, J. H. (1983). Dopaminergic and non-dopaminergic projections to amygdala from substantia nigra and ventral tegmental area. *Brain Res, 262*(2), 334-338.
Luk, K. C., Covell, D. J., Kehm, V. M., Zhang, B., Song, I. Y., Byrne, M. D., . . . Lee, V. M. (2016). Molecular and Biological Compatibility with Host Alpha-Synuclein Influences Fibril Pathogenicity. *Cell Rep, 16*(12), 3373-3387. doi: 10.1016/j.celrep.2016.08.053
Luk, K. C., Kehm, V., Carroll, J., Zhang, B., O'Brien, P., Trojanowski, J. Q., & Lee, V. M. (2012). Pathological alpha-synuclein transmission initiates Parkinson-like neurodegeneration in nontransgenic mice. *Science, 338*(6109), 949-953. doi: 10.1126/science.1227157
Luk, K. C., Kehm, V. M., Zhang, B., O'Brien, P., Trojanowski, J. Q., & Lee, V. M. (2012). Intracerebral inoculation of pathological alpha-synuclein initiates a rapidly progressive

neurodegenerative alpha-synucleinopathy in mice. *J Exp Med, 209*(5), 975-986. doi: 10.1084/jem.20112457

Luk, K. C., Mills, I. P., Trojanowski, J. Q., & Lee, V. M. (2008). Interactions between Hsp70 and the hydrophobic core of alpha-synuclein inhibit fibril assembly. *Biochemistry, 47*(47), 12614-12625. doi: 10.1021/bi801475r

Luk, K. C., Song, C., O'Brien, P., Stieber, A., Branch, J. R., Brunden, K. R., . . . Lee, V. M. (2009). Exogenous alpha-synuclein fibrils seed the formation of Lewy body-like intracellular inclusions in cultured cells. *Proc Natl Acad Sci U S A, 106*(47), 20051-20056. doi: 10.1073/pnas.0908005106

Luna, E., & Luk, K. C. (2015). Bent out of shape: alpha-Synuclein misfolding and the convergence of pathogenic pathways in Parkinson's disease. *FEBS Lett, 589*(24 Pt A), 3749-3759. doi: 10.1016/j.febslet.2015.10.023

Luth, E. S., Stavrovskaya, I. G., Bartels, T., Kristal, B. S., & Selkoe, D. J. (2014). Soluble, prefibrillar alpha-synuclein oligomers promote complex I-dependent, Ca2+-induced mitochondrial dysfunction. *J Biol Chem, 289*(31), 21490-21507. doi: 10.1074/jbc.M113.545749

Mahlknecht, P., Iranzo, A., Hogl, B., Frauscher, B., Muller, C., Santamaria, J., . . . Sleep Innsbruck Barcelona, G. (2015). Olfactory dysfunction predicts early transition to a Lewy body disease in idiopathic RBD. *Neurology, 84*(7), 654-658. doi: 10.1212/WNL.0000000000001265

Mak, S. K., McCormack, A. L., Langston, J. W., Kordower, J. H., & Di Monte, D. A. (2009). Decreased alpha-synuclein expression in the aging mouse substantia nigra. *Exp Neurol, 220*(2), 359-365. doi: 10.1016/j.expneurol.2009.09.021

Mao, X., Ou, M. T., Karuppagounder, S. S., Kam, T. I., Yin, X., Xiong, Y., . . . Dawson, T. M. (2016). Pathological alpha-synuclein transmission initiated by binding lymphocyte-activation gene 3. *Science, 353*(6307). doi: 10.1126/science.aah3374

Marchan, R., Hammond, C. L., & Ballatori, N. (2008). Multidrug resistance-associated protein 1 as a major mediator of basal and apoptotic glutathione release. *Biochim Biophys Acta, 1778*(10), 2413-2420. doi: 10.1016/j.bbamem.2008.06.011

Marder, K., Tang, M. X., Alfaro, B., Mejia, H., Cote, L., Jacobs, D., . . . Mayeux, R. (1998). Postmenopausal estrogen use and Parkinson's disease with and without dementia. *Neurology, 50*(4), 1141-1143.

Maroteaux, L., Campanelli, J. T., & Scheller, R. H. (1988). Synuclein: a neuron-specific protein localized to the nucleus and presynaptic nerve terminal. *J Neurosci, 8*(8), 2804-2815.

Marsden, C. D. (1990). Parkinson's disease. *Lancet, 335*(8695), 948-952.

Martin, H. L., & Teismann, P. (2009). Glutathione--a review on its role and significance in Parkinson's disease. *FASEB J, 23*(10), 3263-3272. doi: 10.1096/fj.08-125443

Martinez-Vicente, M., Sovak, G., & Cuervo, A. M. (2005). Protein degradation and aging. *Exp Gerontol, 40*(8-9), 622-633. doi: 10.1016/j.exger.2005.07.005

Martinez-Vicente, M., Talloczy, Z., Kaushik, S., Massey, A. C., Mazzulli, J., Mosharov, E. V., . . . Cuervo, A. M. (2008). Dopamine-modified alpha-synuclein blocks chaperone-mediated autophagy. *J Clin Invest, 118*(2), 777-788. doi: 10.1172/JCI32806

Masurkar, A. V. (2018). Towards a circuit-level understanding of hippocampal CA1 dysfunction in Alzheimer's disease across anatomical axes. *J Alzheimers Dis Parkinsonism, 8*(1).

McCormack, A. L., Di Monte, D. A., Delfani, K., Irwin, I., DeLanney, L. E., Langston, W. J., & Janson, A. M. (2004). Aging of the nigrostriatal system in the squirrel monkey. *J Comp Neurol, 471*(4), 387-395. doi: 10.1002/cne.20036

McKeith, I. G., Dickson, D. W., Lowe, J., Emre, M., O'Brien, J. T., Feldman, H., . . . Consortium on, D. L. B. (2005). Diagnosis and management of dementia with Lewy bodies: third report of the DLB Consortium. *Neurology, 65*(12), 1863-1872. doi: 10.1212/01.wnl.0000187889.17253.b1

McNaught, K. S., Belizaire, R., Isacson, O., Jenner, P., & Olanow, C. W. (2003). Altered proteasomal function in sporadic Parkinson's disease. *Exp Neurol, 179*(1), 38-46.

McNaught, K. S., & Jenner, P. (2001). Proteasomal function is impaired in substantia nigra in Parkinson's disease. *Neurosci Lett, 297*(3), 191-194.

McNaught, K. S., Shashidharan, P., Perl, D. P., Jenner, P., & Olanow, C. W. (2002). Aggresome-related biogenesis of Lewy bodies. *Eur J Neurosci, 16*(11), 2136-2148.

Miller, D. B., Ali, S. F., O'Callaghan, J. P., & Laws, S. C. (1998). The impact of gender and estrogen on striatal dopaminergic neurotoxicity. *Ann N Y Acad Sci, 844*, 153-165.

Mollenhauer, B., Cullen, V., Kahn, I., Krastins, B., Outeiro, T. F., Pepivani, I., . . . Schlossmacher, M. G. (2008). Direct quantification of CSF alpha-synuclein by ELISA and first cross-sectional study in patients with neurodegeneration. *Exp Neurol, 213*(2), 315-325. doi: 10.1016/j.expneurol.2008.06.004

Monti, D. A., Zabrecky, G., Kremens, D., Liang, T. W., Wintering, N. A., Cai, J., . . . Newberg, A. B. (2016). N-Acetyl Cysteine May Support Dopamine Neurons in Parkinson's Disease: Preliminary Clinical and Cell Line Data. *PLoS One, 11*(6), e0157602. doi: 10.1371/journal.pone.0157602

Morens, D. M., White, L. R., & Davis, J. W. (1996). Re: "The frequency of idiopathic Parkinson's disease by age, ethnic group, and sex in northern Manhattan, 1988-1993". *Am J Epidemiol, 144*(2), 198-199.

Morimoto, R. I. (2008). Proteotoxic stress and inducible chaperone networks in neurodegenerative disease and aging. *Genes Dev, 22*(11), 1427-1438. doi: 10.1101/gad.1657108

Mougenot, A. L., Bencsik, A., Nicot, S., Vulin, J., Morignat, E., Verchere, J., . . . Baron, T. G. (2011). Transmission of prion strains in a transgenic mouse model overexpressing human A53T mutated alpha-synuclein. *J Neuropathol Exp Neurol, 70*(5), 377-385. doi: 10.1097/NEN.0b013e318217d95f

Mu, L., Sobotka, S., Chen, J., Su, H., Sanders, I., Adler, C. H., . . . Arizona Parkinson's Disease, C. (2013). Alpha-synuclein pathology and axonal degeneration of the peripheral motor nerves innervating pharyngeal muscles in Parkinson disease. *J Neuropathol Exp Neurol, 72*(2), 119-129. doi: 10.1097/NEN.0b013e3182801cde

Muller, C. M., de Vos, R. A., Maurage, C. A., Thal, D. R., Tolnay, M., & Braak, H. (2005). Staging of sporadic Parkinson disease-related alpha-synuclein pathology: inter- and intra-rater reliability. *J Neuropathol Exp Neurol, 64*(7), 623-628.

Murray, H. E., Pillai, A. V., McArthur, S. R., Razvi, N., Datla, K. P., Dexter, D. T., & Gillies, G. E. (2003). Dose- and sex-dependent effects of the neurotoxin 6-hydroxydopamine on the nigrostriatal dopaminergic pathway of adult rats: differential actions of estrogen in males and females. *Neuroscience, 116*(1), 213-222.

Nagano-Saito, A., Washimi, Y., Arahata, Y., Kachi, T., Lerch, J. P., Evans, A. C., . . . Ito, K. (2005). Cerebral atrophy and its relation to cognitive impairment in Parkinson disease. *Neurology, 64*(2), 224-229. doi: 10.1212/01.WNL.0000149510.41793.50

Nakamura, K., Nemani, V. M., Wallender, E. K., Kaehlcke, K., Ott, M., & Edwards, R. H. (2008). Optical reporters for the conformation of alpha-synuclein reveal a specific interaction with mitochondria. *J Neurosci, 28*(47), 12305-12317. doi: 10.1523/JNEUROSCI.3088-08.2008

Natale, G., Pasquali, L., Ruggieri, S., Paparelli, A., & Fornai, F. (2008). Parkinson's disease and the gut: a well known clinical association in need of an effective cure and explanation. *Neurogastroenterol Motil, 20*(7), 741-749. doi: 10.1111/j.1365-2982.2008.01162.x

Nelson, P. T., Schmitt, F. A., Jicha, G. A., Kryscio, R. J., Abner, E. L., Smith, C. D., . . . Markesbery, W. R. (2010). Association between male gender and cortical Lewy body pathology in large autopsy series. *J Neurol, 257*(11), 1875-1881. doi: 10.1007/s00415-010-5630-4

Nemani, V. M., Lu, W., Berge, V., Nakamura, K., Onoa, B., Lee, M. K., . . . Edwards, R. H. (2010). Increased expression of alpha-synuclein reduces neurotransmitter release by inhibiting synaptic vesicle reclustering after endocytosis. *Neuron, 65*(1), 66-79. doi: 10.1016/j.neuron.2009.12.023

Ngim, C. H., & Devathasan, G. (1989). Epidemiologic study on the association between body burden mercury level and idiopathic Parkinson's disease. *Neuroepidemiology, 8*(3), 128-141. doi: 10.1159/000110175

Nitkowska, M., Czyzyk, M., & Friedman, A. (2014). Reproductive life characteristics in females affected with Parkinson's disease and in healthy control subjects - a comparative study on Polish population. *Neurol Neurochir Pol, 48*(5), 322-327. doi: 10.1016/j.pjnns.2014.08.004

Nouraei, N., Mason, D. M., Miner, K. M., Carcella, M. A., Bhatia, T. N., Dumm, B. K., . . . Leak, R. K. (2018). Critical appraisal of pathology transmission in the alpha-synuclein fibril model of Lewy body disorders. *Exp Neurol, 299*(Pt A), 172-196. doi: 10.1016/j.expneurol.2017.10.017

Nouraei, N., Zarger, L., Weilnau, J. N., Han, J., Mason, D. M., & Leak, R. K. (2016). Investigation of the therapeutic potential of N-acetyl cysteine and the tools used to define nigrostriatal degeneration in vivo. *Toxicol Appl Pharmacol, 296*, 19-30. doi: 10.1016/j.taap.2016.02.010

Olanow, C. W. (1990). Oxidation reactions in Parkinson's disease. *Neurology, 40*(10 Suppl 3), suppl 32-37; discussion 37-39.

Olanow, C. W., Perl, D. P., DeMartino, G. N., & McNaught, K. S. (2004). Lewy-body formation is an aggresome-related process: a hypothesis. *Lancet Neurol, 3*(8), 496-503. doi: 10.1016/S1474-4422(04)00827-0

Oliveira-Pinto, A. V., Santos, R. M., Coutinho, R. A., Oliveira, L. M., Santos, G. B., Alho, A. T., . . . Lent, R. (2014). Sexual dimorphism in the human olfactory bulb: females have more neurons and glial cells than males. *PLoS One, 9*(11), e111733. doi: 10.1371/journal.pone.0111733

Oosterveld, L. P., Allen, J. C., Jr., Reinoso, G., Seah, S. H., Tay, K. Y., Au, W. L., & Tan, L. C. (2015). Prognostic factors for early mortality in Parkinson's disease. *Parkinsonism Relat Disord, 21*(3), 226-230. doi: 10.1016/j.parkreldis.2014.12.011

Osterberg, V. R., Spinelli, K. J., Weston, L. J., Luk, K. C., Woltjer, R. L., & Unni, V. K. (2015). Progressive aggregation of alpha-synuclein and selective degeneration of lewy inclusion-bearing neurons in a mouse model of parkinsonism. *Cell Rep, 10*(8), 1252-1260. doi: 10.1016/j.celrep.2015.01.060

Paisan-Ruiz, C., Jain, S., Evans, E. W., Gilks, W. P., Simon, J., van der Brug, M., . . . Singleton, A. B. (2004). Cloning of the gene containing mutations that cause PARK8-linked Parkinson's disease. *Neuron, 44*(4), 595-600. doi: 10.1016/j.neuron.2004.10.023

Palatini, P., Racioppa, A., Raule, G., Zaninotto, M., Penzo, M., & Pessina, A. C. (1992). Effect of timing of administration on the plasma ACE inhibitory activity and the antihypertensive effect of quinapril. *Clin Pharmacol Ther, 52*(4), 378-383.

Paleologou, K. E., Kragh, C. L., Mann, D. M., Salem, S. A., Al-Shami, R., Allsop, D., . . . El-Agnaf, O. M. (2009). Detection of elevated levels of soluble alpha-synuclein oligomers in post-mortem brain extracts from patients with dementia with Lewy bodies. *Brain, 132*(Pt 4), 1093-1101. doi: 10.1093/brain/awn349

Peelaerts, W., Bousset, L., Van der Perren, A., Moskalyuk, A., Pulizzi, R., Giugliano, M., . . . Baekelandt, V. (2015). alpha-Synuclein strains cause distinct synucleinopathies after local and systemic administration. *Nature, 522*(7556), 340-344. doi: 10.1038/nature14547

Peng, J., Peng, L., Stevenson, F. F., Doctrow, S. R., & Andersen, J. K. (2007). Iron and paraquat as synergistic environmental risk factors in sporadic Parkinson's disease accelerate age-related neurodegeneration. *J Neurosci, 27*(26), 6914-6922. doi: 10.1523/JNEUROSCI.1569-07.2007

Perez, R. G., Waymire, J. C., Lin, E., Liu, J. J., Guo, F., & Zigmond, M. J. (2002). A role for alpha-synuclein in the regulation of dopamine biosynthesis. *J Neurosci, 22*(8), 3090-3099. doi: 20026307

Perry, T. L., Godin, D. V., & Hansen, S. (1982). Parkinson's disease: a disorder due to nigral glutathione deficiency? *Neurosci Lett, 33*(3), 305-310.

Perry, T. L., Yong, V. W., Clavier, R. M., Jones, K., Wright, J. M., Foulks, J. G., & Wall, R. A. (1985). Partial protection from the dopaminergic neurotoxin N-methyl-4-phenyl-1,2,3,6-tetrahydropyridine by four different antioxidants in the mouse. *Neurosci Lett, 60*(2), 109-114.

Pickart, C. M. (2001). Mechanisms underlying ubiquitination. *Annu Rev Biochem, 70*, 503-533. doi: 10.1146/annurev.biochem.70.1.503

Pieri, L., Madiona, K., & Melki, R. (2016). Structural and functional properties of prefibrillar alpha-synuclein oligomers. *Sci Rep, 6*, 24526. doi: 10.1038/srep24526

Pissadaki, E. K., & Bolam, J. P. (2013). The energy cost of action potential propagation in dopamine neurons: clues to susceptibility in Parkinson's disease. *Front Comput Neurosci, 7*, 13. doi: 10.3389/fncom.2013.00013

Pocernich, C. B., & Butterfield, D. A. (2012). Elevation of glutathione as a therapeutic strategy in Alzheimer disease. *Biochim Biophys Acta, 1822*(5), 625-630. doi: 10.1016/j.bbadis.2011.10.003

Poewe, W., Seppi, K., Tanner, C. M., Halliday, G. M., Brundin, P., Volkmann, J., . . . Lang, A. E. (2017). Parkinson disease. *Nat Rev Dis Primers, 3*, 17013. doi: 10.1038/nrdp.2017.13

Polinski, N. K., Volpicelli-Daley, L. A., Sortwell, C. E., Luk, K. C., Cremades, N., Gottler, L. M., . . . Dave, K. D. (2018). Best Practices for Generating and Using Alpha-Synuclein

Pre-Formed Fibrils to Model Parkinson's Disease in Rodents. *J Parkinsons Dis, 8*(2), 303-322. doi: 10.3233/JPD-171248

Pollanen, M. S., Dickson, D. W., & Bergeron, C. (1993). Pathology and biology of the Lewy body. *J Neuropathol Exp Neurol, 52*(3), 183-191.

Polymeropoulos, M. H., Lavedan, C., Leroy, E., Ide, S. E., Dehejia, A., Dutra, A., . . . Nussbaum, R. L. (1997). Mutation in the alpha-synuclein gene identified in families with Parkinson's disease. *Science, 276*(5321), 2045-2047.

Posimo, J. M., Titler, A. M., Choi, H. J., Unnithan, A. S., & Leak, R. K. (2013). Neocortex and allocortex respond differentially to cellular stress in vitro and aging in vivo. *PLoS One, 8*(3), e58596. doi: 10.1371/journal.pone.0058596

Posimo, J. M., Unnithan, A. S., Gleixner, A. M., Choi, H. J., Jiang, Y., Pulugulla, S. H., & Leak, R. K. (2014a). Viability assays for cells in culture. *Journal of visualized experiments : JoVE*(83). doi: 10.3791/50645

Posimo, J. M., Unnithan, A. S., Gleixner, A. M., Choi, H. J., Jiang, Y., Pulugulla, S. H., & Leak, R. K. (2014b). Viability assays for cells in culture. *J Vis Exp*(83), e50645. doi: 10.3791/50645

Postuma, R. B., Aarsland, D., Barone, P., Burn, D. J., Hawkes, C. H., Oertel, W., & Ziemssen, T. (2012). Identifying prodromal Parkinson's disease: pre-motor disorders in Parkinson's disease. *Mov Disord, 27*(5), 617-626. doi: 10.1002/mds.24996

Postuma, R. B., Adler, C. H., Dugger, B. N., Hentz, J. G., Shill, H. A., Driver-Dunckley, E., . . . Beach, T. G. (2015). REM sleep behavior disorder and neuropathology in Parkinson's disease. *Mov Disord, 30*(10), 1413-1417. doi: 10.1002/mds.26347

Postuma, R. B., Gagnon, J. F., Bertrand, J. A., Genier Marchand, D., & Montplaisir, J. Y. (2015). Parkinson risk in idiopathic REM sleep behavior disorder: preparing for neuroprotective trials. *Neurology, 84*(11), 1104-1113. doi: 10.1212/WNL.0000000000001364

Postuma, R. B., Iranzo, A., Hogl, B., Arnulf, I., Ferini-Strambi, L., Manni, R., . . . Montplaisir, J. Y. (2015). Risk factors for neurodegeneration in idiopathic rapid eye movement sleep behavior disorder: a multicenter study. *Ann Neurol, 77*(5), 830-839. doi: 10.1002/ana.24385

Postuma, R. B., Lang, A. E., Massicotte-Marquez, J., & Montplaisir, J. (2006). Potential early markers of Parkinson disease in idiopathic REM sleep behavior disorder. *Neurology, 66*(6), 845-851. doi: 10.1212/01.wnl.0000203648.80727.5b

Prusiner, S. B., Woerman, A. L., Mordes, D. A., Watts, J. C., Rampersaud, R., Berry, D. B., . . . Giles, K. (2015). Evidence for alpha-synuclein prions causing multiple system atrophy in humans with parkinsonism. *Proc Natl Acad Sci U S A, 112*(38), E5308-5317. doi: 10.1073/pnas.1514475112

Rabinovic, A. D., & Hastings, T. G. (1998). Role of endogenous glutathione in the oxidation of dopamine. *J Neurochem, 71*(5), 2071-2078.

Rahkonen, T., Eloniemi-Sulkava, U., Rissanen, S., Vatanen, A., Viramo, P., & Sulkava, R. (2003). Dementia with Lewy bodies according to the consensus criteria in a general population aged 75 years or older. *J Neurol Neurosurg Psychiatry, 74*(6), 720-724.

Recasens, A., Dehay, B., Bove, J., Carballo-Carbajal, I., Dovero, S., Perez-Villalba, A., . . . Vila, M. (2014). Lewy body extracts from Parkinson disease brains trigger alpha-synuclein pathology and neurodegeneration in mice and monkeys. *Ann Neurol, 75*(3), 351-362. doi: 10.1002/ana.24066

Reeve, A. K., Ludtmann, M. H., Angelova, P. R., Simcox, E. M., Horrocks, M. H., Klenerman, D., . . . Abramov, A. Y. (2015). Aggregated alpha-synuclein and complex I deficiency: exploration of their relationship in differentiated neurons. *Cell Death Dis, 6*, e1820. doi: 10.1038/cddis.2015.166

Rey, N. L., George, S., & Brundin, P. (2016). Review: Spreading the word: precise animal models and validated methods are vital when evaluating prion-like behaviour of alpha-synuclein. *Neuropathol Appl Neurobiol, 42*(1), 51-76. doi: 10.1111/nan.12299

Rey, N. L., George, S., Steiner, J. A., Madaj, Z., Luk, K. C., Trojanowski, J. Q., . . . Brundin, P. (2018). Spread of aggregates after olfactory bulb injection of alpha-synuclein fibrils is associated with early neuronal loss and is reduced long term. *Acta Neuropathol, 135*(1), 65-83. doi: 10.1007/s00401-017-1792-9

Rey, N. L., Petit, G. H., Bousset, L., Melki, R., & Brundin, P. (2013). Transfer of human alpha-synuclein from the olfactory bulb to interconnected brain regions in mice. *Acta Neuropathol, 126*(4), 555-573. doi: 10.1007/s00401-013-1160-3

Rey, N. L., Steiner, J. A., Maroof, N., Luk, K. C., Madaj, Z., Trojanowski, J. Q., . . . Brundin, P. (2016). Widespread transneuronal propagation of alpha-synucleinopathy triggered in olfactory bulb mimics prodromal Parkinson's disease. *J Exp Med, 213*(9), 1759-1778. doi: 10.1084/jem.20160368

Rhodes, S. L., & Ritz, B. (2008). Genetics of iron regulation and the possible role of iron in Parkinson's disease. *Neurobiol Dis, 32*(2), 183-195. doi: 10.1016/j.nbd.2008.07.001

Rice, M. E., & Russo-Menna, I. (1998). Differential compartmentalization of brain ascorbate and glutathione between neurons and glia. *Neuroscience, 82*(4), 1213-1223.

Richly, H., Rape, M., Braun, S., Rumpf, S., Hoege, C., & Jentsch, S. (2005). A series of ubiquitin binding factors connects CDC48/p97 to substrate multiubiquitylation and proteasomal targeting. *Cell, 120*(1), 73-84. doi: 10.1016/j.cell.2004.11.013

Rideout, H. J., Lang-Rollin, I., & Stefanis, L. (2004). Involvement of macroautophagy in the dissolution of neuronal inclusions. *Int J Biochem Cell Biol, 36*(12), 2551-2562. doi: 10.1016/j.biocel.2004.05.008

Rideout, H. J., Larsen, K. E., Sulzer, D., & Stefanis, L. (2001). Proteasomal inhibition leads to formation of ubiquitin/alpha-synuclein-immunoreactive inclusions in PC12 cells. *J Neurochem, 78*(4), 899-908.

Riederer, P., Sofic, E., Rausch, W. D., Schmidt, B., Reynolds, G. P., Jellinger, K., & Youdim, M. B. (1989). Transition metals, ferritin, glutathione, and ascorbic acid in parkinsonian brains. *J Neurochem, 52*(2), 515-520.

Rocca, W. A., Bower, J. H., Maraganore, D. M., Ahlskog, J. E., Grossardt, B. R., de Andrade, M., & Melton, L. J., 3rd. (2008). Increased risk of parkinsonism in women who underwent oophorectomy before menopause. *Neurology, 70*(3), 200-209. doi: 10.1212/01.wnl.0000280573.30975.6a

Rodriguez, J. A., Ivanova, M. I., Sawaya, M. R., Cascio, D., Reyes, F. E., Shi, D., . . . Eisenberg, D. S. (2015). Structure of the toxic core of alpha-synuclein from invisible crystals. *Nature, 525*(7570), 486-490. doi: 10.1038/nature15368

Ross, G. W., Abbott, R. D., Petrovitch, H., Tanner, C. M., Davis, D. G., Nelson, J., . . . White, L. R. (2006). Association of olfactory dysfunction with incidental Lewy bodies. *Mov Disord, 21*(12), 2062-2067. doi: 10.1002/mds.21076

Rudiger, S., Buchberger, A., & Bukau, B. (1997). Interaction of Hsp70 chaperones with substrates. *Nat Struct Biol, 4*(5), 342-349.

Russell, A., Drozdova, A., Wang, W., & Thomas, M. (2014). The impact of dementia development concurrent with Parkinson's disease: a new perspective. *CNS Neurol Disord Drug Targets, 13*(7), 1160-1168.

Sacino, A. N., Brooks, M., Thomas, M. A., McKinney, A. B., McGarvey, N. H., Rutherford, N. J., . . . Giasson, B. I. (2014). Amyloidogenic alpha-synuclein seeds do not invariably induce rapid, widespread pathology in mice. *Acta Neuropathol, 127*(5), 645-665. doi: 10.1007/s00401-014-1268-0

Sacino, A. N., Brooks, M. M., Chakrabarty, P., Saha, K., Khoshbouei, H., Golde, T. E., & Giasson, B. I. (2017). Proteolysis of alpha-synuclein fibrils in the lysosomal pathway limits induction of inclusion pathology. *J Neurochem, 140*(4), 662-678. doi: 10.1111/jnc.13743

Saito, Y., Kawashima, A., Ruberu, N. N., Fujiwara, H., Koyama, S., Sawabe, M., . . . Murayama, S. (2003). Accumulation of phosphorylated alpha-synuclein in aging human brain. *J Neuropathol Exp Neurol, 62*(6), 644-654.

Samuel, F., Flavin, W. P., Iqbal, S., Pacelli, C., Sri Renganathan, S. D., Trudeau, L. E., . . . Tandon, A. (2016). Effects of Serine 129 Phosphorylation on alpha-Synuclein Aggregation, Membrane Association, and Internalization. *J Biol Chem, 291*(9), 4374-4385. doi: 10.1074/jbc.M115.705095

Saper, C. B. (2005). An open letter to our readers on the use of antibodies. *J Comp Neurol, 493*(4), 477-478. doi: 10.1002/cne.20839

Saper, C. B. (2009). A guide to the perplexed on the specificity of antibodies. *J Histochem Cytochem, 57*(1), 1-5. doi: 10.1369/jhc.2008.952770

Sato, H., Kato, T., & Arawaka, S. (2013). The role of Ser129 phosphorylation of alpha-synuclein in neurodegeneration of Parkinson's disease: a review of in vivo models. *Rev Neurosci, 24*(2), 115-123. doi: 10.1515/revneuro-2012-0071

Savica, R., Grossardt, B. R., Bower, J. H., Ahlskog, J. E., Boeve, B. F., Graff-Radford, J., . . . Mielke, M. M. (2017). Survival and Causes of Death Among People With Clinically Diagnosed Synucleinopathies With Parkinsonism: A Population-Based Study. *JAMA Neurol, 74*(7), 839-846. doi: 10.1001/jamaneurol.2017.0603

Savica, R., Grossardt, B. R., Bower, J. H., Boeve, B. F., Ahlskog, J. E., & Rocca, W. A. (2013). Incidence of dementia with Lewy bodies and Parkinson disease dementia. *JAMA Neurol, 70*(11), 1396-1402. doi: 10.1001/jamaneurol.2013.3579

Sawada, H., Kawamura, T., Shimohama, S., Akaike, A., & Kimura, J. (1996). Different mechanisms of glutamate-induced neuronal death between dopaminergic and non-dopaminergic neurons in rat mesencephalic culture. *J Neurosci Res, 43*(4), 503-510. doi: 10.1002/(SICI)1097-4547(19960215)43:4<503::AID-JNR12>3.0.CO;2-2

Saxena, S., & Caroni, P. (2011). Selective neuronal vulnerability in neurodegenerative diseases: from stressor thresholds to degeneration. *Neuron, 71*(1), 35-48. doi: 10.1016/j.neuron.2011.06.031

Saykally, J. N., Rachmany, L., Hatic, H., Shaer, A., Rubovitch, V., Pick, C. G., & Citron, B. A. (2012). The nuclear factor erythroid 2-like 2 activator, tert-butylhydroquinone, improves cognitive performance in mice after mild traumatic brain injury. *Neuroscience, 223*, 305-314. doi: 10.1016/j.neuroscience.2012.07.070

Schenck, C. H., Bundlie, S. R., & Mahowald, M. W. (1996). Delayed emergence of a parkinsonian disorder in 38% of 29 older men initially diagnosed with idiopathic rapid eye movement sleep behaviour disorder. *Neurology, 46*(2), 388-393.

Schlecht, R., Scholz, S. R., Dahmen, H., Wegener, A., Sirrenberg, C., Musil, D., . . . Bukau, B. (2013). Functional analysis of Hsp70 inhibitors. *PLoS One, 8*(11), e78443. doi: 10.1371/journal.pone.0078443

Schubert, D., Humphreys, S., Baroni, C., & Cohn, M. (1969). In vitro differentiation of a mouse neuroblastoma. *Proc Natl Acad Sci U S A, 64*(1), 316-323.

Seidel, K., Mahlke, J., Siswanto, S., Kruger, R., Heinsen, H., Auburger, G., . . . Rub, U. (2015). The brainstem pathologies of Parkinson's disease and dementia with Lewy bodies. *Brain Pathol, 25*(2), 121-135. doi: 10.1111/bpa.12168

Semchuk, K. M., Love, E. J., & Lee, R. G. (1993). Parkinson's disease: a test of the multifactorial etiologic hypothesis. *Neurology, 43*(6), 1173-1180.

Sengoku, R., Saito, Y., Ikemura, M., Hatsuta, H., Sakiyama, Y., Kanemaru, K., . . . Murayama, S. (2008). Incidence and extent of Lewy body-related alpha-synucleinopathy in aging human olfactory bulb. *J Neuropathol Exp Neurol, 67*(11), 1072-1083. doi: 10.1097/NEN.0b013e31818b4126

Sharma, A., Kaur, P., Kumar, V., & Gill, K. D. (2007). Attenuation of 1-methyl-4-phenyl-1, 2,3,6-tetrahydropyridine induced nigrostriatal toxicity in mice by N-acetyl cysteine. *Cell Mol Biol (Noisy-le-grand), 53*(1), 48-55.

Sharon, R., Bar-Joseph, I., Frosch, M. P., Walsh, D. M., Hamilton, J. A., & Selkoe, D. J. (2003). The formation of highly soluble oligomers of alpha-synuclein is regulated by fatty acids and enhanced in Parkinson's disease. *Neuron, 37*(4), 583-595.

Shen, D., Coleman, J., Chan, E., Nicholson, T. P., Dai, L., Sheppard, P. W., & Patton, W. F. (2011). Novel cell- and tissue-based assays for detecting misfolded and aggregated protein accumulation within aggresomes and inclusion bodies. *Cell Biochem Biophys, 60*(3), 173-185. doi: 10.1007/s12013-010-9138-4

Shiber, A., & Ravid, T. (2014). Chaperoning proteins for destruction: diverse roles of Hsp70 chaperones and their co-chaperones in targeting misfolded proteins to the proteasome. *Biomolecules, 4*(3), 704-724. doi: 10.3390/biom4030704

Shin, Y., Klucken, J., Patterson, C., Hyman, B. T., & McLean, P. J. (2005). The co-chaperone carboxyl terminus of Hsp70-interacting protein (CHIP) mediates alpha-synuclein degradation decisions between proteasomal and lysosomal pathways. *J Biol Chem, 280*(25), 23727-23734. doi: 10.1074/jbc.M503326200

Shrivastava, A. N., Aperia, A., Melki, R., & Triller, A. (2017). Physico-Pathologic Mechanisms Involved in Neurodegeneration: Misfolded Protein-Plasma Membrane Interactions. *Neuron, 95*(1), 33-50. doi: 10.1016/j.neuron.2017.05.026

Shrivastava, A. N., Redeker, V., Fritz, N., Pieri, L., Almeida, L. G., Spolidoro, M., . . . Triller, A. (2015). alpha-synuclein assemblies sequester neuronal alpha3-Na+/K+-ATPase and impair Na+ gradient. *EMBO J, 34*(19), 2408-2423. doi: 10.15252/embj.201591397

Sian, J., Dexter, D. T., Lees, A. J., Daniel, S., Agid, Y., Javoy-Agid, F., . . . Marsden, C. D. (1994). Alterations in glutathione levels in Parkinson's disease and other neurodegenerative disorders affecting basal ganglia. *Ann Neurol, 36*(3), 348-355. doi: 10.1002/ana.410360305

Sian, J., Dexter, D. T., Lees, A. J., Daniel, S., Jenner, P., & Marsden, C. D. (1994). Glutathione-related enzymes in brain in Parkinson's disease. *Ann Neurol, 36*(3), 356-361. doi: 10.1002/ana.410360306

Siderowf, A., Jennings, D., Eberly, S., Oakes, D., Hawkins, K. A., Ascherio, A., . . . Investigators, P. (2012). Impaired olfaction and other prodromal features in the Parkinson At-Risk Syndrome Study. *Mov Disord, 27*(3), 406-412. doi: 10.1002/mds.24892

Sidransky, E., Nalls, M. A., Aasly, J. O., Aharon-Peretz, J., Annesi, G., Barbosa, E. R., . . . Ziegler, S. G. (2009). Multicenter analysis of glucocerebrosidase mutations in Parkinson's disease. *N Engl J Med, 361*(17), 1651-1661. doi: 10.1056/NEJMoa0901281

Sierra, E. M., & Tiffany-Castiglioni, E. (1991). Reduction of glutamine synthetase activity in astroglia exposed in culture to low levels of inorganic lead. *Toxicology, 65*(3), 295-304.

Sies, H. (2015). Oxidative stress: a concept in redox biology and medicine. *Redox Biol, 4*, 180-183. doi: 10.1016/j.redox.2015.01.002

Singleton, A. B., Farrer, M., Johnson, J., Singleton, A., Hague, S., Kachergus, J., . . . Gwinn-Hardy, K. (2003). alpha-Synuclein locus triplication causes Parkinson's disease. *Science, 302*(5646), 841. doi: 10.1126/science.1090278

Sitte, N., Merker, K., von Zglinicki, T., & Grune, T. (2000). Protein oxidation and degradation during proliferative senescence of human MRC-5 fibroblasts. *Free Radic Biol Med, 28*(5), 701-708.

Sixel-Doring, F., Trautmann, E., Mollenhauer, B., & Trenkwalder, C. (2011). Associated factors for REM sleep behavior disorder in Parkinson disease. *Neurology, 77*(11), 1048-1054. doi: 10.1212/WNL.0b013e31822e560e

Smith, K. M., & Dahodwala, N. (2014). Sex differences in Parkinson's disease and other movement disorders. *Exp Neurol, 259*, 44-56. doi: 10.1016/j.expneurol.2014.03.010

Smith, W. W., Jiang, H., Pei, Z., Tanaka, Y., Morita, H., Sawa, A., . . . Ross, C. A. (2005). Endoplasmic reticulum stress and mitochondrial cell death pathways mediate A53T mutant alpha-synuclein-induced toxicity. *Hum Mol Genet, 14*(24), 3801-3811. doi: 10.1093/hmg/ddi396

Sofic, E., Riederer, P., Heinsen, H., Beckmann, H., Reynolds, G. P., Hebenstreit, G., & Youdim, M. B. (1988). Increased iron (III) and total iron content in post mortem substantia nigra of parkinsonian brain. *J Neural Transm, 74*(3), 199-205.

Sofroniew, M. V., & Vinters, H. V. (2010). Astrocytes: biology and pathology. *Acta Neuropathol, 119*(1), 7-35. doi: 10.1007/s00401-009-0619-8

Souza, J. M., Giasson, B. I., Chen, Q., Lee, V. M., & Ischiropoulos, H. (2000). Dityrosine cross-linking promotes formation of stable alpha -synuclein polymers. Implication of nitrative and oxidative stress in the pathogenesis of neurodegenerative synucleinopathies. *J Biol Chem, 275*(24), 18344-18349. doi: 10.1074/jbc.M000206200

Spillantini, M. G., Crowther, R. A., Jakes, R., Cairns, N. J., Lantos, P. L., & Goedert, M. (1998). Filamentous alpha-synuclein inclusions link multiple system atrophy with Parkinson's disease and dementia with Lewy bodies. *Neurosci Lett, 251*(3), 205-208.

Spillantini, M. G., Schmidt, M. L., Lee, V. M., Trojanowski, J. Q., Jakes, R., & Goedert, M. (1997). Alpha-synuclein in Lewy bodies. *Nature, 388*(6645), 839-840. doi: 10.1038/42166

Stefanis, L. (2012). alpha-Synuclein in Parkinson's disease. *Cold Spring Harb Perspect Med, 2*(2), a009399. doi: 10.1101/cshperspect.a009399

Stern, M. B., Doty, R. L., Dotti, M., Corcoran, P., Crawford, D., McKeown, D. A., . . . Hurtig, H. (1994). Olfactory function in Parkinson's disease subtypes. *Neurology, 44*(2), 266-268.

Stevens, T., Livingston, G., Kitchen, G., Manela, M., Walker, Z., & Katona, C. (2002). Islington study of dementia subtypes in the community. *Br J Psychiatry, 180*, 270-276.

Stringer, K. A., Freed, B. M., Dunn, J. S., Sayers, S., Gustafson, D. L., & Flores, S. C. (2004). Particulate phase cigarette smoke increases MnSOD, NQO1, and CINC-1 in rat lungs. *Free Radic Biol Med, 37*(10), 1527-1533. doi: 10.1016/j.freeradbiomed.2004.08.008

Tamura, T., Yoshida, M., Hashizume, Y., & Sobue, G. (2012). Lewy body-related alpha-synucleinopathy in the spinal cord of cases with incidental Lewy body disease. *Neuropathology, 32*(1), 13-22. doi: 10.1111/j.1440-1789.2011.01211.x

Tanaka, M., Kim, Y. M., Lee, G., Junn, E., Iwatsubo, T., & Mouradian, M. M. (2004). Aggresomes formed by alpha-synuclein and synphilin-1 are cytoprotective. *J Biol Chem, 279*(6), 4625-4631. doi: 10.1074/jbc.M310994200

Tanaka, Y., Engelender, S., Igarashi, S., Rao, R. K., Wanner, T., Tanzi, R. E., . . . Ross, C. A. (2001). Inducible expression of mutant alpha-synuclein decreases proteasome activity and increases sensitivity to mitochondria-dependent apoptosis. *Hum Mol Genet, 10*(9), 919-926.

Tanner, C. M., Chen, B., Wang, W., Peng, M., Liu, Z., Liang, X., . . . Schoenberg, B. S. (1989). Environmental factors and Parkinson's disease: a case-control study in China. *Neurology, 39*(5), 660-664.

Tanner, C. M., & Goldman, S. M. (1996). Epidemiology of Parkinson's disease. *Neurol Clin, 14*(2), 317-335.

Tanner, C. M., Kamel, F., Ross, G. W., Hoppin, J. A., Goldman, S. M., Korell, M., . . . Langston, J. W. (2011). Rotenone, paraquat, and Parkinson's disease. *Environ Health Perspect, 119*(6), 866-872. doi: 10.1289/ehp.1002839

Tao, Q., Fan, X., Li, T., Tang, Y., Yang, D., & Le, W. (2012). Gender segregation in gene expression and vulnerability to oxidative stress induced injury in ventral mesencephalic cultures of dopamine neurons. *J Neurosci Res, 90*(1), 167-178. doi: 10.1002/jnr.22729

Tarutani, A., Arai, T., Murayama, S., Hisanaga, S. I., & Hasegawa, M. (2018). Potent prion-like behaviors of pathogenic alpha-synuclein and evaluation of inactivation methods. *Acta Neuropathol Commun, 6*(1), 29. doi: 10.1186/s40478-018-0532-2

Tarutani, A., Suzuki, G., Shimozawa, A., Nonaka, T., Akiyama, H., Hisanaga, S., & Hasegawa, M. (2016). The Effect of Fragmented Pathogenic alpha-Synuclein Seeds on Prion-like Propagation. *J Biol Chem, 291*(36), 18675-18688. doi: 10.1074/jbc.M116.734707

Taylor, J. P., Tanaka, F., Robitschek, J., Sandoval, C. M., Taye, A., Markovic-Plese, S., & Fischbeck, K. H. (2003). Aggresomes protect cells by enhancing the degradation of toxic polyglutamine-containing protein. *Hum Mol Genet, 12*(7), 749-757.

Tokuda, T., Salem, S. A., Allsop, D., Mizuno, T., Nakagawa, M., Qureshi, M. M., . . . El-Agnaf, O. M. (2006). Decreased alpha-synuclein in cerebrospinal fluid of aged individuals and subjects with Parkinson's disease. *Biochem Biophys Res Commun, 349*(1), 162-166. doi: 10.1016/j.bbrc.2006.08.024

Toledo, J. B., Gopal, P., Raible, K., Irwin, D. J., Brettschneider, J., Sedor, S., . . . Trojanowski, J. Q. (2016). Pathological alpha-synuclein distribution in subjects with coincident Alzheimer's and Lewy body pathology. *Acta Neuropathol, 131*(3), 393-409. doi: 10.1007/s00401-015-1526-9

Tompkins, M. M., & Hill, W. D. (1997). Contribution of somal Lewy bodies to neuronal death. *Brain Res, 775*(1-2), 24-29.

Tsikas, D., Sandmann, J., Ikic, M., Fauler, J., Stichtenoth, D. O., & Frolich, J. C. (1998). Analysis of cysteine and N-acetylcysteine in human plasma by high-performance liquid

chromatography at the basal state and after oral administration of N-acetylcysteine. *J Chromatogr B Biomed Sci Appl, 708*(1-2), 55-60.
Twelves, D., Perkins, K. S., & Counsell, C. (2003). Systematic review of incidence studies of Parkinson's disease. *Mov Disord, 18*(1), 19-31. doi: 10.1002/mds.10305
Ubeda-Banon, I., Saiz-Sanchez, D., de la Rosa-Prieto, C., Argandona-Palacios, L., Garcia-Munozguren, S., & Martinez-Marcos, A. (2010). alpha-Synucleinopathy in the human olfactory system in Parkinson's disease: involvement of calcium-binding protein- and substance P-positive cells. *Acta Neuropathol, 119*(6), 723-735. doi: 10.1007/s00401-010-0687-9
Uchihara, T., Giasson, B. I., & Paulus, W. (2016). Propagation of Abeta, tau and alpha-synuclein pathology between experimental models and human reality: prions, propagons and propaganda. *Acta Neuropathol, 131*(1), 1-3. doi: 10.1007/s00401-015-1517-x
Ueda, K., Fukushima, H., Masliah, E., Xia, Y., Iwai, A., Yoshimoto, M., . . . Saitoh, T. (1993). Molecular cloning of cDNA encoding an unrecognized component of amyloid in Alzheimer disease. *Proc Natl Acad Sci U S A, 90*(23), 11282-11286.
Unnithan, A. S., Choi, H. J., Titler, A. M., Posimo, J. M., & Leak, R. K. (2012). Rescue from a two hit, high-throughput model of neurodegeneration with N-acetyl cysteine. *Neurochem Int, 61*(3), 356-368. doi: 10.1016/j.neuint.2012.06.001
Unnithan, A. S., Jiang, Y., Rumble, J. L., Pulugulla, S. H., Posimo, J. M., Gleixner, A. M., & Leak, R. K. (2014). N-acetyl cysteine prevents synergistic, severe toxicity from two hits of oxidative stress. *Neurosci Lett, 560*, 71-76. doi: 10.1016/j.neulet.2013.12.023
Uttara, B., Singh, A. V., Zamboni, P., & Mahajan, R. T. (2009). Oxidative stress and neurodegenerative diseases: a review of upstream and downstream antioxidant therapeutic options. *Curr Neuropharmacol, 7*(1), 65-74. doi: 10.2174/157015909787602823
Uversky, V. N., Li, J., & Fink, A. L. (2001). Metal-triggered structural transformations, aggregation, and fibrillation of human alpha-synuclein. A possible molecular NK between Parkinson's disease and heavy metal exposure. *J Biol Chem, 276*(47), 44284-44296. doi: 10.1074/jbc.M105343200
Valente, E. M., Abou-Sleiman, P. M., Caputo, V., Muqit, M. M., Harvey, K., Gispert, S., . . . Wood, N. W. (2004). Hereditary early-onset Parkinson's disease caused by mutations in PINK1. *Science, 304*(5674), 1158-1160. doi: 10.1126/science.1096284
VanderHorst, V. G., Samardzic, T., Saper, C. B., Anderson, M. P., Nag, S., Schneider, J. A., . . . Buchman, A. S. (2015). alpha-Synuclein pathology accumulates in sacral spinal visceral sensory pathways. *Ann Neurol, 78*(1), 142-149. doi: 10.1002/ana.24430
Vekrellis, K., Xilouri, M., Emmanouilidou, E., Rideout, H. J., & Stefanis, L. (2011). Pathological roles of alpha-synuclein in neurological disorders. *Lancet Neurol, 10*(11), 1015-1025. doi: 10.1016/S1474-4422(11)70213-7
Vezoli, J., Dzahini, K., Costes, N., Wilson, C. R., Fifel, K., Cooper, H. M., . . . Procyk, E. (2014). Increased DAT binding in the early stage of the dopaminergic lesion: a longitudinal [11C]PE2I binding study in the MPTP-monkey. *Neuroimage, 102 Pt 2*, 249-261. doi: 10.1016/j.neuroimage.2014.07.059
Vicente Miranda, H., El-Agnaf, O. M., & Outeiro, T. F. (2016). Glycation in Parkinson's disease and Alzheimer's disease. *Mov Disord, 31*(6), 782-790. doi: 10.1002/mds.26566
Vicente Miranda, H., Szego, E. M., Oliveira, L. M. A., Breda, C., Darendelioglu, E., de Oliveira, R. M., . . . Outeiro, T. F. (2017). Glycation potentiates alpha-synuclein-associated

neurodegeneration in synucleinopathies. *Brain, 140*(5), 1399-1419. doi: 10.1093/brain/awx056
Vijayakumar, D., & Jankovic, J. (2016a). Drug-Induced Dyskinesia, Part 1: Treatment of Levodopa-Induced Dyskinesia. *Drugs, 76*(7), 759-777. doi: 10.1007/s40265-016-0566-3
Vijayakumar, D., & Jankovic, J. (2016b). Drug-Induced Dyskinesia, Part 2: Treatment of Tardive Dyskinesia. *Drugs, 76*(7), 779-787. doi: 10.1007/s40265-016-0568-1
Vjestica, A., Zhang, D., Liu, J., & Oliferenko, S. (2013). Hsp70-Hsp40 chaperone complex functions in controlling polarized growth by repressing Hsf1-driven heat stress-associated transcription. *PLoS Genet, 9*(10), e1003886. doi: 10.1371/journal.pgen.1003886
Voges, D., Zwickl, P., & Baumeister, W. (1999). The 26S proteasome: a molecular machine designed for controlled proteolysis. *Annu Rev Biochem, 68*, 1015-1068. doi: 10.1146/annurev.biochem.68.1.1015
Volpicelli-Daley, L. A. (2017). Effects of alpha-synuclein on axonal transport. *Neurobiol Dis, 105*, 321-327. doi: 10.1016/j.nbd.2016.12.008
Volpicelli-Daley, L. A., Gamble, K. L., Schultheiss, C. E., Riddle, D. M., West, A. B., & Lee, V. M. (2014). Formation of alpha-synuclein Lewy neurite-like aggregates in axons impedes the transport of distinct endosomes. *Mol Biol Cell, 25*(25), 4010-4023. doi: 10.1091/mbc.E14-02-0741
Volpicelli-Daley, L. A., Luk, K. C., & Lee, V. M. (2014). Addition of exogenous alpha-synuclein preformed fibrils to primary neuronal cultures to seed recruitment of endogenous alpha-synuclein to Lewy body and Lewy neurite-like aggregates. *Nat Protoc, 9*(9), 2135-2146. doi: 10.1038/nprot.2014.143
Volpicelli-Daley, L. A., Luk, K. C., Patel, T. P., Tanik, S. A., Riddle, D. M., Stieber, A., . . . Lee, V. M. (2011). Exogenous alpha-synuclein fibrils induce Lewy body pathology leading to synaptic dysfunction and neuron death. *Neuron, 72*(1), 57-71. doi: 10.1016/j.neuron.2011.08.033
Voosen, P. (2016). Deep Space Network glitches worry scientists. *Science, 353*(6307), 1477-1478. doi: 10.1126/science.353.6307.1477
Wales, P., Pinho, R., Lazaro, D. F., & Outeiro, T. F. (2013). Limelight on alpha-synuclein: pathological and mechanistic implications in neurodegeneration. *J Parkinsons Dis, 3*(4), 415-459. doi: 10.3233/JPD-130216
Waxman, E. A., Duda, J. E., & Giasson, B. I. (2008). Characterization of antibodies that selectively detect alpha-synuclein in pathological inclusions. *Acta Neuropathol, 116*(1), 37-46. doi: 10.1007/s00401-008-0375-1
Waxman, E. A., & Giasson, B. I. (2008). Specificity and regulation of casein kinase-mediated phosphorylation of alpha-synuclein. *Journal of neuropathology and experimental neurology, 67*(5), 402-416. doi: 10.1097/NEN.0b013e31816fc995
Werner-Allen, J. W., Levine, R. L., & Bax, A. (2017). Superoxide is the critical driver of DOPAL autoxidation, lysyl adduct formation, and crosslinking of alpha-synuclein. *Biochem Biophys Res Commun, 487*(2), 281-286. doi: 10.1016/j.bbrc.2017.04.050
Wigley, W. C., Fabunmi, R. P., Lee, M. G., Marino, C. R., Muallem, S., DeMartino, G. N., & Thomas, P. J. (1999). Dynamic association of proteasomal machinery with the centrosome. *J Cell Biol, 145*(3), 481-490.
Wilkaniec, A., Lenkiewicz, A. M., Czapski, G. A., Jesko, H. M., Hilgier, W., Brodzik, R., . . . Adamczyk, A. (2018). Extracellular Alpha-Synuclein Oligomers Induce Parkin S-

Nitrosylation: Relevance to Sporadic Parkinson's Disease Etiopathology. *Mol Neurobiol*. doi: 10.1007/s12035-018-1082-0

Wilson, R. S., Yu, L., Schneider, J. A., Arnold, S. E., Buchman, A. S., & Bennett, D. A. (2011). Lewy bodies and olfactory dysfunction in old age. *Chem Senses, 36*(4), 367-373. doi: 10.1093/chemse/bjq139

Winner, B., Jappelli, R., Maji, S. K., Desplats, P. A., Boyer, L., Aigner, S., . . . Riek, R. (2011). In vivo demonstration that alpha-synuclein oligomers are toxic. *Proc Natl Acad Sci U S A, 108*(10), 4194-4199. doi: 10.1073/pnas.1100976108

Winslow, A. R., Chen, C. W., Corrochano, S., Acevedo-Arozena, A., Gordon, D. E., Peden, A. A., . . . Rubinsztein, D. C. (2010). alpha-Synuclein impairs macroautophagy: implications for Parkinson's disease. *J Cell Biol, 190*(6), 1023-1037. doi: 10.1083/jcb.201003122

Wojcik, C. (1997). An inhibitor of the chymotrypsin-like activity of the proteasome (PSI) induces similar morphological changes in various cell lines. *Folia Histochem Cytobiol, 35*(4), 211-214.

Wojcik, C., Schroeter, D., Wilk, S., Lamprecht, J., & Paweletz, N. (1996). Ubiquitin-mediated proteolysis centers in HeLa cells: indication from studies of an inhibitor of the chymotrypsin-like activity of the proteasome. *Eur J Cell Biol, 71*(3), 311-318.

Wong, K. K., Muller, M. L., Kuwabara, H., Studenski, S. A., & Bohnen, N. I. (2012). Gender differences in nigrostriatal dopaminergic innervation are present at young-to-middle but not at older age in normal adults. *J Clin Neurosci, 19*(1), 183-184. doi: 10.1016/j.jocn.2011.05.013

Wu, J. B., Chen, K., Li, Y., Lau, Y. F., & Shih, J. C. (2009). Regulation of monoamine oxidase A by the SRY gene on the Y chromosome. *FASEB J, 23*(11), 4029-4038. doi: 10.1096/fj.09-139097

Xilouri, M., Brekk, O. R., & Stefanis, L. (2013). alpha-Synuclein and protein degradation systems: a reciprocal relationship. *Mol Neurobiol, 47*(2), 537-551. doi: 10.1007/s12035-012-8341-2

Yacoubian, T. A., Cantuti-Castelvetri, I., Bouzou, B., Asteris, G., McLean, P. J., Hyman, B. T., & Standaert, D. G. (2008). Transcriptional dysregulation in a transgenic model of Parkinson disease. *Neurobiol Dis, 29*(3), 515-528. doi: 10.1016/j.nbd.2007.11.008

Yamada, K., & Iwatsubo, T. (2018). Extracellular alpha-synuclein levels are regulated by neuronal activity. *Mol Neurodegener, 13*(1), 9. doi: 10.1186/s13024-018-0241-0

Yang, Z., & Klionsky, D. J. (2010). Mammalian autophagy: core molecular machinery and signaling regulation. *Curr Opin Cell Biol, 22*(2), 124-131. doi: 10.1016/j.ceb.2009.11.014

Yonetani, M., Nonaka, T., Masuda, M., Inukai, Y., Oikawa, T., Hisanaga, S., & Hasegawa, M. (2009). Conversion of wild-type alpha-synuclein into mutant-type fibrils and its propagation in the presence of A30P mutant. *J Biol Chem, 284*(12), 7940-7950. doi: 10.1074/jbc.M807482200

Yoritaka, A., Hattori, N., Uchida, K., Tanaka, M., Stadtman, E. R., & Mizuno, Y. (1996). Immunohistochemical detection of 4-hydroxynonenal protein adducts in Parkinson disease. *Proc Natl Acad Sci U S A, 93*(7), 2696-2701.

Zhai, S., Tanimura, A., Graves, S. M., Shen, W., & Surmeier, D. J. (2018). Striatal synapses, circuits, and Parkinson's disease. *Curr Opin Neurobiol, 48*, 9-16. doi: 10.1016/j.conb.2017.08.004

Zhang, Y., Larcher, K. M., Misic, B., & Dagher, A. (2017). Anatomical and functional organization of the human substantia nigra and its connections. *Elife, 6*. doi: 10.7554/eLife.26653

Zola-Morgan, S., & Squire, L. R. (1993). Neuroanatomy of memory. *Annu Rev Neurosci, 16*, 547-563. doi: 10.1146/annurev.ne.16.030193.002555

Zorzi, E., & Bonvini, P. (2011). Inducible hsp70 in the regulation of cancer cell survival: analysis of chaperone induction, expression and activity. *Cancers (Basel), 3*(4), 3921-3956. doi: 10.3390/cancers3043921

Appendix

Table 2: Primary antibodies

Primary Antibody	Source	Company	Catalog #	Lot #	Dilution
Anti-α-syn 81a (pSer129)	Mouse	Gift from Kelvin Luk (81A) (Waxman & Giasson, 2008)	-	-	1:5000
Anti-α-syn (pSer129)	Rabbit	Abcam	Ab59264	GR52476-25	1:300
Anti α-syn 81a (pSer129)	Mouse	Biolegend	825701	B213120	1:1000
Anti-α-syn EP1536Y (pSer129)	Rabbit	Abcam	Ab51253	GR285618-8	1:1000
Anti-total-α-syn	Rabbit	Abcam	Ab155038	GR117815-9	1:500
Anti-K48-linked poly-ubiquitin	Rabbit	Millipore	05-1307	2299608	1:500
Anti-Tyrosine Hydroxylase	Mouse	Millipore	MAB318	2742733	1:2000
Anti-DAT	Rat	Millipore	MAB369	2701007	1:4000
Anti-NeuN	Guinea pig	Millipore	ABN90	2031353	1:6000
Anti-Glutathione	Rabbit	Millipore	AB5010	2195968	1:500
Anti-Hsp70	Rabbit	Millipore	AB9920	2278553	1:500
Anti-MAP2	Mouse	Sigma Aldrich	M9942	031M4825	1:2000

Table 3: Secondary antibodies

Secondary Antibody	Source	Company	Catalog #	Lot #	Dilution
Anti-mouse @ 488	Donkey	Life Technologies	A21202	1423052	1:800
Anti-mouse @ 555	Goat	Invitrogen	A21424	1141876	1:1000
Anti-mouse @ 647	Donkey	Jackson Laboratories	712-605-150	127706	1:1000
Anti-mouse @680	Donkey	Jackson Laboratories	715-625-151	106244	1:1000
Anti-mouse @ 790	Donkey	Jackson Laboratories	715-655-150	106037	1:1000
Anti-guinea pig @ 488	Donkey	Jackson Laboratories	706-545-148	108077	1:1000
Anti-guinea pig @ 647	Donkey	Jackson Laboratories	706-605-148	123960	1:700
Anti-guinea pig @ 790	Donkey	Jackson Laboratories	706-655-148	106036	1:1000
Anti-rabbit @ 488	Donkey	Jackson Laboratories	711-545-152	120705	1:700
Anti-rabbit @ 555	Goat	Life Technologies	A21429	1562309	1:800
Anti-rabbit @ 647	Donkey	Jackson Laboratories	711-605-152	123104	1:1000
Anti-rabbit @ 790	Donkey	Jackson Laboratories	711-655-152	106035	1:2000
Anti-rat @ 790	Donkey	Jackson Laboratories	712-655-150	106408	1:1000

Table 4: Abbreviations

5N	motor trigeminal nucleus	HP	hippocampus
7n	facial nerve	ic	internal capsule
7N	facial nucleus	IC	inferior colliculus
8n	vestibulocochlear nerve	ILBD	incidental Lewy body disease
A30	cingulate cortex, area 30	LAS	lysosome-autophagy system
AA	anterior amygdaloid area	lfp	longitudinal fasciculus of pons
ac	anterior commissure	LH	lateral habenula
aca	anterior commissure, anterior part	lo	lateral olfactory tract
Acb	nucleus accumbens	LO	lateral orbital cortex
AcbC	nucleus accumbens core	LOT	nucleus of the lateral olfactory tract
AcbSH	nucleus accumbens shell	LPMR	lateral post thalamic nu, mediorostro
aci	anterior commissure, intrabulbar	Lrt	lateral reticular nucleus
acp	anterior commissure, posterior part	LSd	lateral septal nucleus, dorsal part
ADLB	Alzheimer's disease with Lewy bodies	LSv	lateral septal nucleus, ventral part
AHi	amygdalohippocampal area	LTDg	laterodorsal tegmental nucleus
AID	dorsal agranular insular cortex	LV	lateral ventricle
AIV	ventral agranular insular cortex	M2	secondary motor cortex
AMG	amygdala	MD	mediodorsal thalamic nucleus
AOB	accessory olfactory bulb	MDL	mediodorsal thalamic nucleus, lateral
AOD	anterior olfactory area, dorsal	MEA	medial amygdala
AOE	anterior olfactory nucleus, external	MEnt	medial entorhinal cortex
AOL	anterior olfactory nucleus, lateral	ml	medial lemniscus
AOM	anterior olfactory nucleus, medial	mlf	medial longitudinal fasciculus
AON	anterior olfactory nucleus	MoDG	molecular layer of dentate gyrus
AOP	anterior olfactory area, posterior	MVe	medial vestibular nucleus
AOV	anterior olfactory area, ventral	NAC	N-acetyl cysteine
APir	amygdalopiriform transition area	OB	olfactory bulb
AV	anteroventral thalamic nucleus	och	optic chiasm
BLA	basolateral nucleus of amygdala	ot	optic tract
BMA	basomedial nucleus of amygdala	PBS	phosphate buffered saline
BST	bed nucleus of the stria terminalis	PD	Parkinson's disease
CA1	cornu ammonis, field 1	PDD	Parkinson's disease dementia
CA2	cornu ammonis, field 2	PFF	preformed fibril
CA3	cornu ammonis, field 3	Pir	piriform cortex
cc	corpus callosum	PMCo	posteromedial cortical amygdala
CEA	central nucleus of amygdala	Pn	pontine nuclei
CEnt	caudomedial entorhinal cortex	PnO	pontine reticular nucleus, oral part
CNS	central nervous system	Pr5	principal trigeminal nucleus
cp	cerebral peduncle	RBD	REM sleep behavior disorder
CPu	caudoputamen	REM	Rapid eye movement
cst	commissural stria terminalis	rf	rhinal fissure
DA	dopamine	rms	rostral migratory stream
DAT	dopamine transporter	ROS	reactive oxygen species
DG	dentate gyrus	Sub	subiculum
DLB	dementia with Lewy bodies	S1	primary somatosensory cortex
DOPAL	3,4-dihydroxyphenylacetaldehyde	SC	superior colliculus
DS	dorsal subiculum	scp	superior cerebellar peduncle

DTT	dorsal tenia tecta	sm	stria medullaris
Ect	ectorhinal cortex	SN	substantia nigra
Ent	entorhinal cortex	SNpc	substantia nigra, pars compacta
EPl	external plexiform layer, olfactory bulb	SNR	substantia nigra, pars reticulata
FC	frontal cortex	sp	spinal trigeminal tract
fi	fimbria	Sp	spinal trigeminal nucleus
fmi	forceps minor of the corpus callosum	SVZ	subventricular zone
fmj	forceps major of corpus callosum	TeA	temporal association cortex
fr	fasciculus retroflexus	TH	tyrosine hydroxylase
Gl	glomerular layer, olfactory bulb	TT	tenia tecta
GP	globus pallidus	Tub	olfactory tubercle
GrA	granule cell layer of accessory OB	tz	trapezoid body
GrDG	granule cell layer of dentate gyrus	UPS	ubiquitin-proteasome system
GrO	granule cell layer of olfactory bulb	VDB	ventral diagonal band
GSH	glutathione	VM	ventromedial thalamic nucleus
HDB	horizontal limb of the diagonal band	VMH	ventromedial hypothalamic nucleus
hf	hippocampal fissure	VTT	ventral tenia tecta